Analysis of the IgE network: Inhibition of CD23-mediated IgE upregulation and the CD21/C3d interaction

Mohd Norhakim Yahya

Department of Biochemistry

Thesis submitted for the degree of Doctor of Philosophy

at the University of Oxford

Abstract

Analysis of the IgE network: Inhibition of CD23-mediated IgE upregulation and the CD21/C3d interaction.

Mohd Norhakim Yahya
Department of Biochemistry, Somerville College
Submitted for the Degree of Doctor of Philosophy, Hilary Term 2011

Allergic reactions are mainly mediated by the interactions between the IgE and its ligands, amongst them CD23 and CD21 in what is termed the IgE network. CD23 is involved in upregulating IgE expression by forming a trimolecular complex with CD21 and IgE on the B-cell surface, resulting in the specific activation of IgE-positive B cells. CD21 also interacts with C3d and is a bridge between the innate and the immune system. A crystal structure of the interaction has been solved (Szakonyi et al., 2001) but was controversial because it contradicted previous biochemical analyses. The aims of this thesis were to use various biophysical techniques to study the interactions between the molecules in the IgE network and its possible inhibition.

Part 1: Characterisation of a phage display-derived peptide that inhibit IgE binding to CD23

A peptide was previously derived using phage display technology and tested for binding ability to CD23 using SPR and ITC. Subsequent NMR experiments were performed to identify the binding site, followed by characterization of its derivatives. Crystallisation of CD23 with the peptide and soaking with its truncated tripeptide, NWP, were also attempted.

Part 2: Characterisation of CD23 and its interaction with its ligands

X-ray crystallography was undertaken to solve the structure of derCD23 in complex with a phage display-derived peptide (Part1) followed by crystal soaking with a truncated tripeptide, NWP. However, a reproducible, high-resolution wild type derCD23 structure was determined at 1.9 Å. A comparison of the binding behaviour between the monomeric derCD23 and a trimeric CD23 construct was carried out in order to see the effect of oligomerisation upon IgE binding. Using the known interaction map as well as a crystal structure, the possible interacting residues between CD23 and IgE were examined. The characterisation of the CD23/CD21 interaction was continued

from previous efforts in order to confirm that the binding epitope of CD23 for CD21 lies within the C-terminus of CD23. Characterisation of the interactions of CD23/IgE/FcεRI was performed to examine these multimolecular interactions and possible regulatory mechanisms in mast cell degranulation. It was shown that CD23 can form multimeric complexes with IgE-Fc that bind to FcεRI with higher apparent affinity than IgE-Fc alone, which may lead to increases in mast cell degranulation. It was also found that the IgE bound on FcεRI still binds to CD23 although with a lower binding capacity, presumably due allosteric changes. The binding of CD23 with a monoclonal antibody IDEC-152 was also characterised using SPR and NMR spectroscopy. It was proposed that IDEC-152 might interfere with the trimerisation site of CD23 thus reducing its affinity for IgE. A thermofluor assay was developed and optimised for potential screening of compounds that bind to derCD23 using a qPCR machine, which may be useful to screen compounds that bind to CD23 as part of future drug discovery project. Crystallisation of the derCD23/CD21 and IgE/triCD23/CD21 complexes was also attempted as part of ongoing crystallisation projects.

Part 3: The interaction between C3d and CD21

The interaction between C3d and CD21 is believed to be a bridge between the innate and adaptive immune response, and is thought to be pivotal in the initiation of autoimmune disease. Following from previous studies on this interaction, further characterisations were performed using NMR and ITC to confirm the involved sites on CD21 (SCR1-2) in binding to C3d. Several potential salt bridges have been identified so far, allowing a high-resolution docked structure of the C3d/CD21 complex.

Contents

List of Figures

List of Tables

Abbreviations

Chronic lymphocytic leukemia	CLL
Column volume	CV
Collagen induced arthritis	CIA
Complement receptor-2	CD21
Domain 1-2 of CD21	CD21 (SCR1-2)
Soluble CD23 fragment produced by dust mite protease *der P 1*	derCD23
Dithiothreitol	DTT
Fragment antigen binding	Fab
Facilitated antigen presentation	FAP
N-2-hydroxyethylpiperazine-N'-2-ethanesulfonic acid	HEPES
Hepes buffered saline (10 mM Hepes, 150 mM NaCl, 4 mM $CaCl_2$, pH 7.4)	HBS
Heteronuclear single quantum resonance	HSQC
High performance liquid chromatography	HPLC
King's College London	KCL
Kilodalton	KDa
Interleukin	IL
Immunoglobulin E	IgE
the Fc region of IgE consisting of domain Cε2-4	IgE-Fc
the Fc region of IgE consisting of domain Cε3-4	IgE-Fc (Cε3-4)
Isopropyl β-D-1-thiogalactopyranoside	IPTG
Isothermal titration calorimetry	ITC
Luria-Bertani Medium (10 g/L tryptone, 5g/L yeast extract ,10g/L NaCl, pH 7.4)	LB
One dimensional	1-D
Molecular weight cut-off	MWCO
Molecular weight	MW
Nuclear magnetic resonance	NMR
Parts per million	ppm
Phosphate buffered saline (137 mM NaCl, 2.7mM KCl, 8.1 M Na_2HPO_4, 1.76 mM KH_2PO_4, pH 7.4)	PBS
Polyethylene glycol	PEG
Root mean square deviation	RMSD
Short consensus repeat	SCR
Surface plasmon resonance	SPR

Chapter 1

Introduction

1.1 The immune system

The immune system has evolved to provide protective mechanisms against infection. It can be broadly divided into two components: innate and adaptive immunity. The innate immune system consists of protective mechanisms, which are utilised to fight infection in the first exposure to infective agents; it has no immunological memory. Innate immunity is then followed up by the adaptive immune response, which retains memory through memory lymphocytes. Upon exposure by the same infective agent, T cells presented with the same antigen by antigen presenting cells (APC) such as dendritic cells, stimulate B cells through cytokines to exert an antibody-mediated immune response.

The ability of the immune system to differentiate between safe and harmful antigens as well as self and non-self, is central to the homeostasis of the immune system. Failure of such will lead to disorders, such as autoimmune disease, in which the immune system mounts a response towards self-antigens. In allergy, the immune recognition of innocuous allergens results in an inappropriate inflammatory reactions. Studying the interactions between the proteins involved in these reactions can provide insights into the mechanisms of relevant diseases. This work describes some of the structural and biophysical aspects of the interactions of protein involved in two immune disorders, allergy/asthma as well as autoimmune disease such as arthritis. In the former,

experiments were done to further elucidate the interactions of the proteins in the IgE network whilst the latter is mainly concerning the interaction between CD21 and C3d.

1.2 Overview of the IgE network in allergy and asthma

Allergic diseases such as asthma, rhinitis, eczema and food allergies are characterised by hyper-responsiveness and inflammation in skin, nose, lung or the gastrointestinal tract (Gould and Sutton 2008). Although multifactorial in origin, this inflammation process is mainly due to an inappropriate response of the immune system, in predisposed individuals, to otherwise harmless allergens such as house dust mite, pollens or certain types of food. It has also been observed that these predisposed individuals (approximately 30-40% of the population in developed countries) show a tendency, termed atopy, to develop excessive reactions involving a particular class of antibody, immunoglobulin E (IgE) (Devereux, 2006).

IgE is one of five classes of immunoglobulin expressed in mammals and is involved in host defence against parasitic infections (Gould and Sutton, 2008). In allergic responses the expression of IgE is dramatically increased. Binding of antigen-IgE complex to its high affinity receptor, FcεRI, on mast cells leads to the release of preformed mediators of inflammation, such as leukotrienes, histamine and others. This leads to the symptoms of allergy, such as local inflammation, skin rashes and vasoconstriction in the lung (Hogan, 1997). These events are regulated by a set of protein-protein interactions in what is termed the “IgE network” (Figure 1.1).

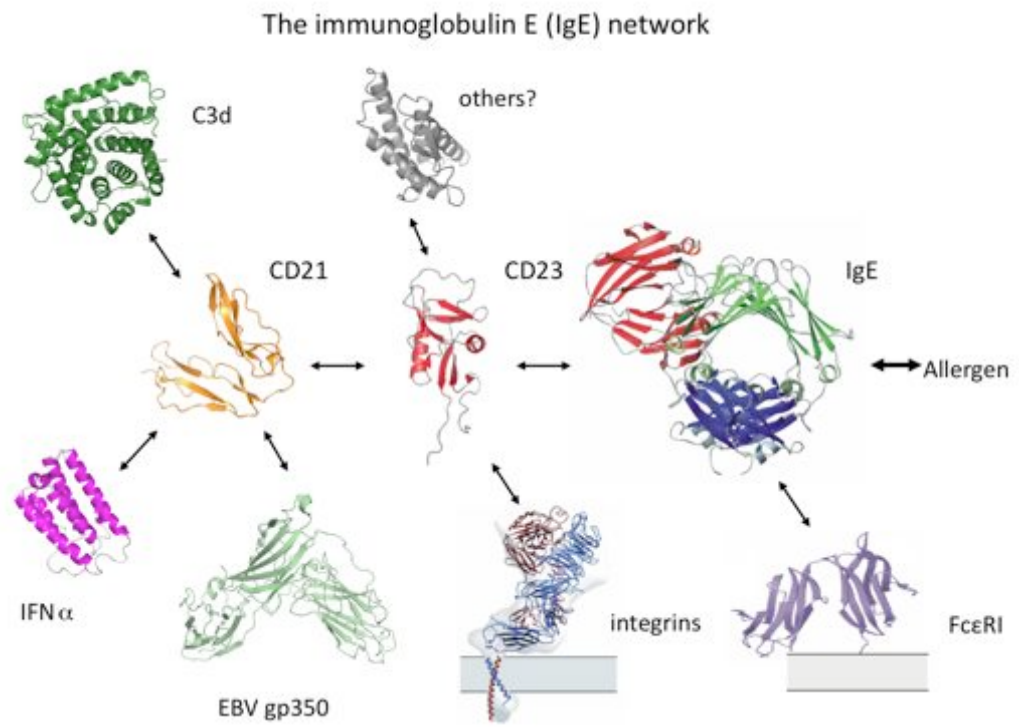

Figure 1.1: The IgE network.
A schematic representation of the known interactions in the IgE network showing the known ligands for each protein. CD23 (centre) binds to CD21 and IgE, and has also been reported to interact with integrins. IgE binds to CD23 and FcεRI, as well as allergens through its Fab region. CD21 (left) also interacts with C3d, IFNα and EBV gp350.

1.2.1 Immunoglobulin E (IgE)

IgE was initially described as 'reagin' in 1922 and was characterised as IgE in 1966 (Stanworth, 1993). In mammals IgE plays an important role as a protective mechanism against parasitic infection (Gould et al., 2003). Parasites such as *Helicobacter pylori* and *Toxoplasma gondii*, which enter the host across epithelial surfaces, trigger a range of IgE-meditated cellular responses that result in the expulsion of the parasite from the body. A correlation between IgE concentration in the serum and protection against helminth worm infections has been noted, as has the protective effect that a specific IgE antibody

had against schistosomiasis (Capron et al., 1999). However, overproduction of specific IgE antibodies in response to common, innocuous antigens underlies allergic reactions (Cookson, 1999). In normal individual the the serum levels of IgE is very low (~0.00015 mg/ml) compared to IgG (~10 mg/ml) and is elevated amongst individuals with predisposition to allergy also known as atopy (Spiegelberg, 1989).

When an atopic individual is exposed to an allergen, the allergen is taken up by antigen presenting cell and the epitope is presented to type 2 helper T cells (T_H2 cells). T_H2 cells secrete IL-4, which recruits more T_H cells into this lineage. T_H2 secrete IL-4, Il-13 and CD40L, which induce class switching in B cells from IgM to IgE. This lead to the production of IgE, which binds to its high affinity receptor, FcεRI, on mast cells priming them for allergen croslinking. Cross-linking of allergen to the IgE/FcεRI complex on mast cells activate the release of preformed mediators of allergy leading to the symptoms of allergy. Mast cells also release IL-4, IL-13 and CD40L, which favour IgE class switching in B cells. These cytokines also induce the production of CD23 on B cells, which modulates IgE synthesis in B cells (Gould and Sutton, 2008) (Figure 1.2).

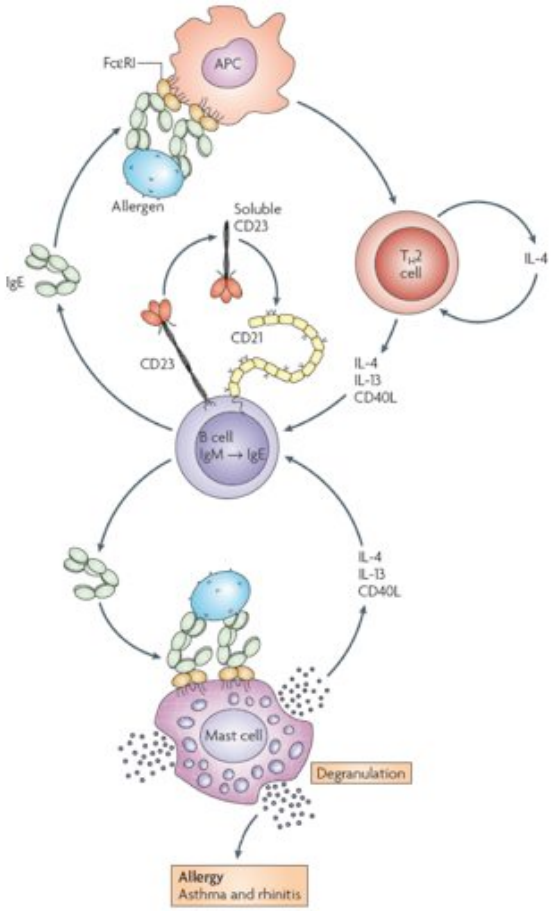

Figure 1.2: Overview of the interactions of the immune cells in IgE-mediated hypersensitivity (Gould and Sutton, 2008)

IgE is very similar in overall structure to other classes of antibodies, with two identical heavy chains and two identical light chains. However, IgE has an additional constant domain (Cε2) rather than the flexible hinge region found in IgG (Figure 1.3). The Cε2 domain plays a role in stabilising the binding of IgE to FcεRI leading to a very slow off-rate, with a $t_{1/2}$ of about 20 hours as measured on SPR and slower still in tissues ($t_{1/2}$ ~2 weeks) (McDonnell et al., 2001). The sites of IgE interactions with its known receptors are located in the Cε3 domain.

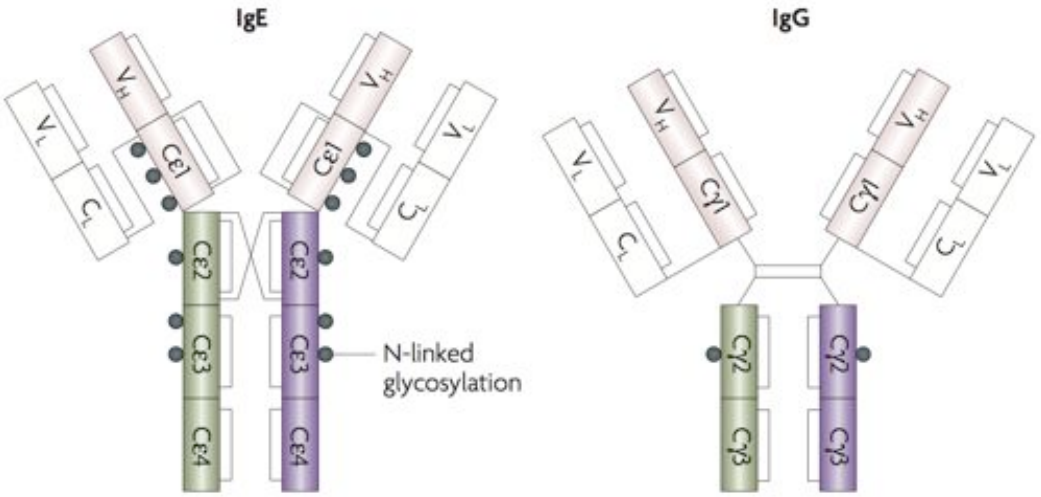

Figure 1.3. The schematic structure of IgE and IgG_1.
The intra- and inter-domain disulphide linkages and the sites of N-linked glycosylation are shown. The Cε2 domain is in place of the flexible hinge region found in IgG. The figure is reproduced from Gould & Sutton (2008).

1.2.2 IgE receptors

Two principal receptors have been discovered for IgE, one being the high affinity receptor FcεRI, and the other called the low affinity receptor FcεRII (CD23). The interaction of IgE with FcεRI has a K_D of 10^{-10} M compared with about 10^{-7} M for CD23 (Gould et al., 2003). Despite of the term "low affinity" the affinity of CD23 for IgE is not particularly low, as it is comparable with the affinity of IgG_1 with its high affinity receptor FcγRIII, characterised by a K_D of about 10^{-7} M. The binding of IgE to FcεRI has an unusually slow off-rate (McDonnell et al., 2001), which is crucial for priming mast cells before allergen binding. The higher affinity receptor is directly involved in the manifestation of allergic symptoms through activation of mast cell degranulation upon cross-linking of bound IgE by allergen.

1.2.2.1 The high affinity receptor FcεRI

FcεRI is expressed as an $\alpha\beta\gamma_2$ tetramer on mast cells and basophils in rodents, and as an $\alpha\beta_2$ trimer in humans. The two extracellular domains of the α-chain (FcεRIα) contain the IgE binding function, whereas the signalling motifs (immunoreceptor tyrosine-based activation motifs (ITAMs)) are located in the intracellular sequences of the β- and γ-chains (Figure 1.4(a)). The high affinity for IgE, combined with slow off-rate of the IgE/FcεRI interaction, primes the complex for antigenic challenge. The crosslinking with allergen results in the activation of signal transduction pathways that lead to the release of cytoplasmic granules to release preformed inflammatory molecules such as histamines, chemokines, proteases as well as cytokines that favour the Th2 response (Kinet, 1999), which cause the symptoms of hypersensitivity. The crystal structure of FcεRI in complex with the dimeric Cε3-Cε4 domains of IgE termed IgE-Fc (Cε3-Cε4) has been solved by Garman et al. (2000). The striking feature of this structure is that the CD23 binding site is exposed, which may allow a possible role for CD23 in the interaction between IgE and FcεRI (Figure 1.4(b)).

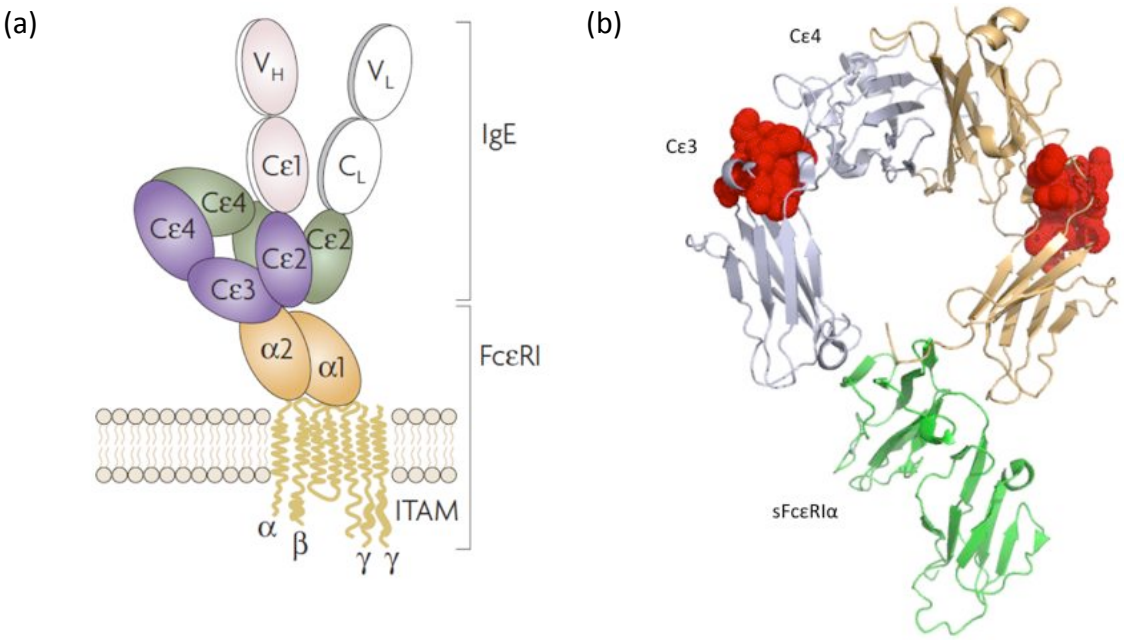

Figure 1.4: The binding of IgE to its high affinity receptor FcεRI.
a) The model of the IgE binding to its high affinity receptor is mediated between its Cε3 domain with α-chain of FcεRI. Figure reproduced from Gould and Sutton (2008). b) The crystal structure of IgE-Fc (Cε3-4) bound to the α-chain domain (termed sFcεRα) solved by Wurzburg et al. (2006) showing CD23 binding sites (red) on Cε3 to be distinct and exposed.

1.2.2.2 The low affinity receptor, CD23

CD23, also known as FcεRII, is the low affinity receptor for IgE. CD23 is a type II transmembrane glycoprotein and C-type lectin expressed in a variety of hematopoietic cells such as B cells, macrophages, eosinophils, natural killer cells as well as T cells, follicular dendritic cells and Langerhan cells (Delespesse et al., 1989). CD23 is also expressed on the surface of intestinal epithelial cells (Kaiserlian et al., 1993) and epithelial cells in the airway (Palaniyandi et al., 2011). CD23 is unique amongst other immunoglobulin receptors, as it is the only antibody receptor identified so far that does not belong to the immunoglobulin superfamily (Kikutani et al., 1986).

1.3 CD23: structure and interactions

1.3.1 CD23 structure

The full length CD23 is a 45 kDa type II membrane protein consisting of a short N-terminal intracellular sequence, an extracellular α-helical coiled-coiled stalk region, a C-type (calcium dependent) lectin head and a short RGD motif, followed by a 30 amino acid tail at the extracellular C-terminus (Figure 1.5). The short N-terminal intracellular sequence of CD23 is present in two splice variants, which differ in their first seven (CD23a) or six (CD23b) amino acid residues. CD23a is constitutively expressed by antigen activated B cells before differentiation into antibody secreting plasma cells, whereas CD23b is expressed upon induction with IL-4 on a variety of inflammatory cells. The alpha helical coiled-coiled stalk region contains heptad repeats of hydrophobic sequence that are shown to be involved in the formation of a trimeric α-helical coiled-coil that is involved in oligomerisation (Beavil et al., 1992; Kilmon et al., 2001) (Figure 1.5). CD23 exist on the membrane mainly as trimer (Kilmon et al., 2004). The oligomerisation states confer different binding behaviour for IgE; in an oligomeric state CD23 has a higher affinity than the monomeric state. Studies using murine CD23 showed that it binds to IgE with biphasic characteristics, with high affinty (K_D ~100 nM) and low affinity (K_D ~1 μM) (Dierks et al., 1993). One explanation of these data would be that trimeric CD23 can bind with high affinity through an avidity effect to two or more separate IgE molecules on the surface of a B cell, whilst monomeric CD23 binds with lower affinity.

The trimeric α-helical coiled-coil is not stable and an antibody directed against the stalk region, mAb 19G5, destabilises the stalk region, which leads to reduction of CD23 binding to IgE (Kilmon et al., 2004). This antibody also makes CD23 more susceptible to

proteolytic cleavage (Ford et al., 2006). Kilmon et al. (2001) showed that polyclonal antibody directed against the stalk region of mouse CD23 leads to the dispersion of the trimer into a monomeric form that binds IgE with lower affinity.

CD23 is cleaved primarily by ADAM-10, a member of the "a disintegrin and metalloprotease" family, to yield an initial soluble fragment of 37 kDa (Weskamp et al., 2006; Lemieux et al., 2007). This fragment can be further cleaved by a cysteine protease, DerP1 from the house dust mite *Dermatophagoides pteronyssinus,* between Ser155-Ser156 and Glu298-Ser299 to generate a 16 kDa fragment. This naturally occurring fragment is called derCD23 and consists of the lectin head domain and 10 amino acids of the C-terminal tail (Schulz et al., 1995). The structure of the lectin head domain was first solved by NMR (Hibbert et al., 2005) (Figure 1.5) and later by crystallography (Wurzburg et al., 2006). Both structures agree on the C-type lectin fold, which has two roughly orthogonal α-helices and two anti-parallel β-sheets consisting of four β-strands each, surrounding a hydrophobic core stabilized by four disulfide bonds. The crystal structure, however, differs from the NMR structure in having two non-silent mutations: H213R and G256S, as well as a different position of calcium occupancy. The NMR structure showed the auxiliary site occupied while the crystal structure showed that calcium is bound to the conserved site.

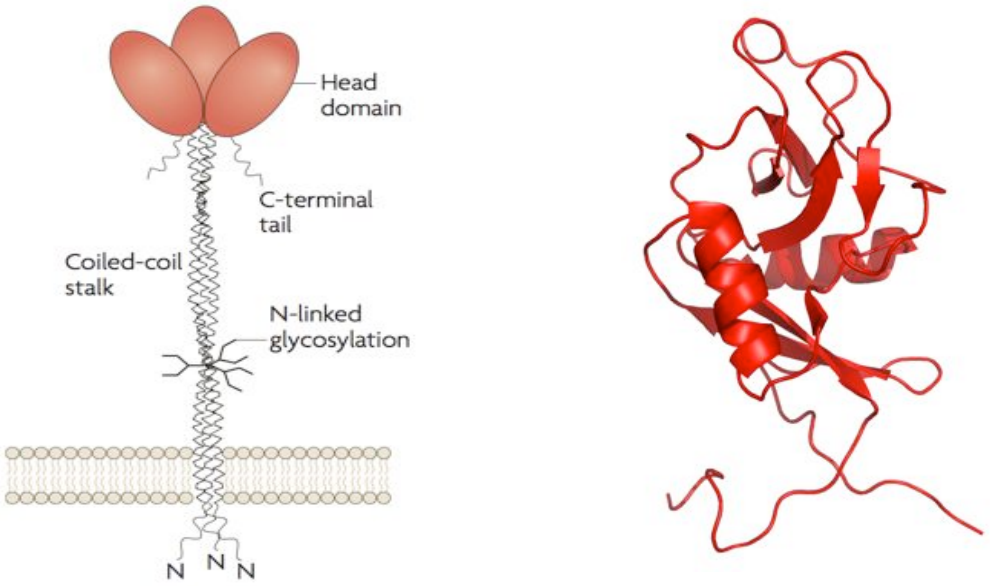

Figure 1.5: Schematic representation of the membrane bound CD23 and structure of soluble derCD23. a) The schematic picture of the membrane bound CD23 showing the three lectin "head" domains, the α-helical coiled-coil 'stalk' and the C- terminal tail. The N-linked glycosylation sites are also highlighted. Figure reproduced from Gould and Sutton (2008). (b) The structure of the lectin head domain of CD23, derCD23 as determined by NMR by Hibbert et al. (2005) (PDB ID: 1T8C).

1.3.2 Interaction of CD23 with its ligands

1.3.2.1 IgE

The binding site of IgE on CD23 has been mapped using NMR chemical shift perturbation mapping and is localised on the lectin head domain (Hibbert et al., 2005). Extensive site-directed mutagenesis studies have indicated that the CD23 binding site on IgE is localised at the Cε3 domain of IgE. The replacement of the residues of AB helix (residues 346-356) of human Cε3 with the homologous murine sequence abolished the binding of CD23 to IgE (Nissim et al., 1993). Indeed the residue Lys352 is deemed to be important for CD23 binding as mutation of this residue led to a complete abrogation of the CD23/IgE interaction (Sayers, 2004). One of the interesting aspects of IgE binding to CD23 is that the CD23 binding sites, including the implicated Lys352 residue are still accessible on the crystal structure of IgE bound to the α-chain of FcεRI, termed sFcεRIα as revealed in the

crystal structure (Garman et al., 2000) (PDB 1F6A) (Figure 1.6). NMR chemical shift mapping of the binding site of CD23 on Cε3 has been performed by Dr Susmita Borthakur (Susmita Borthakur, DPhil thesis, University of Oxford, 2010). When these residues are mapped on the crystal structure of the IgE-Fc (Cε3-4)/sFcεRα complex it shows that the binding site of CD23 on IgE is still exposed when IgE is bound to the its high affinity receptor.

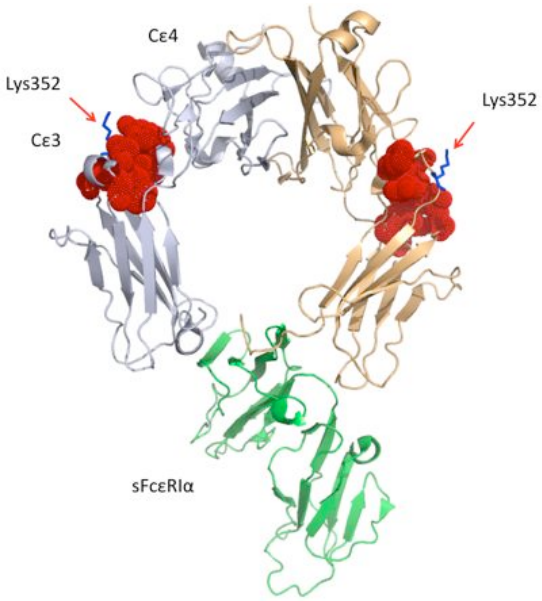

Figure 1.6: Crystal structure of IgE-Fc (Cε3-4) bound to the alpha chain of FcεRI (sFcεRIα). (PDB ID:1F6A (Garman et al., 2000)
Residues implicated in CD23 binding from the work of Dr Susmita Borthakur (DPhil thesis, University of Oxford, 2010) (F346, D347, L348, F349, G406, T407, W410, I411, G413 are shown in red). Lys352 was indicated by Sayers et al. (2004) to also be important in IgE binding. The mapped residues show that CD23 binds to a different site than FcεRI.

The crystal structure of derCD23 with IgE-Fc (Cε3-4) has been solved by Dr Balvinder Dhaliwal at the Randall Division (KCL) (personal communication) and the structure is currently undergoing refinement (Figure 1.7). The structure shows two lectin head domains contacting the Cε3 domain of IgE, consistent with the NMR-defined site. The

structure also confirms that derCD23 binds with a 2:1 stoichiometry with the dimeric IgE-Fc (Cε3-4) region, consistent with the previously determined stoichiometry for this fragment (Shi et al., 1997). This available structure will assist not only in the establishing the main residue to residue contacts but also in designing potential inhibitors of this interaction.

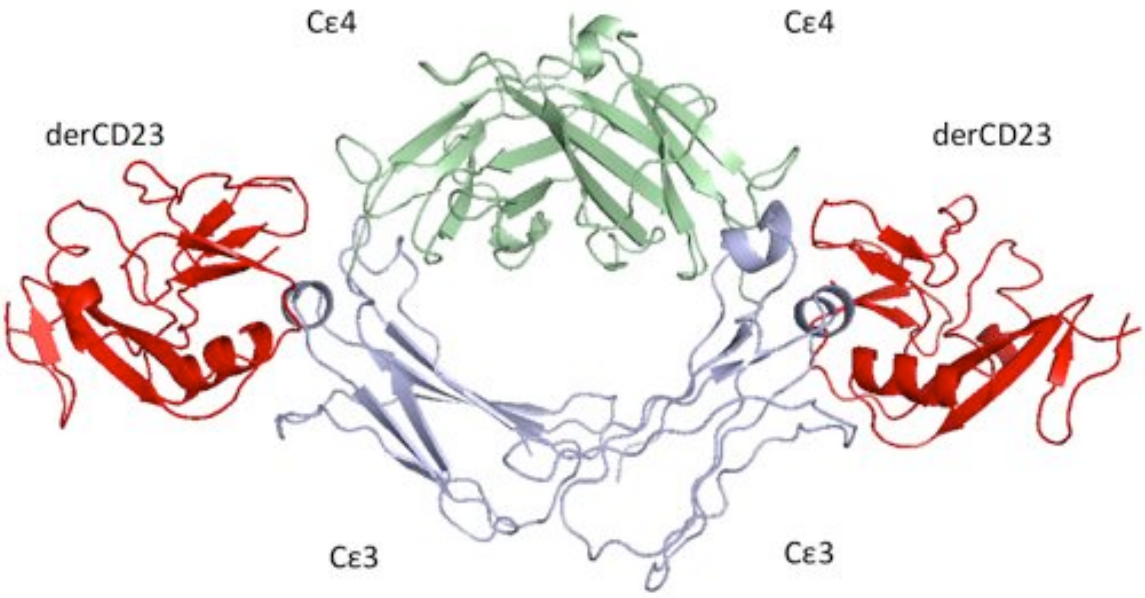

Figure 1.7: The crystal structure of derCD23/IgE-Fc (Cε3-4) complex.
The structure was solved by Dr Balvinder Dhaliwal. The structure shows two derCD23 molecules binding to the Cε3 domains of the IgE-Fc (Cε3-4).

1.3.2.2 CD21

CD21 belongs to a family of complement receptor proteins and is involved in the regulation of IgE synthesis through co-stimulation with IL-4 (Aubry et al., 1992). CD21 is a type 1 membrane protein containing 15 short consensus repeats domains (SCRs). Engagement of CD21 on B cells by some anti-CD21 monoclonal antibodies increased IL-4

induced IgE production, as did treatment with recombinant sCD23 (Aubry et al., 1992). Molecular analysis shows that triggering of CD21 increases the IL-4-induced germline ε transcription levels and has a synergistic effect on the expression of the ε transcript induced by T cells (Henchoz et al., 1994). The first two N-terminal domains of CD21 (SCR1-2) are the main domains involved in the interaction with CD21's known ligands, namely CD23, C3d and the Epstein Barr Virus (EBV) envelope glycoprotein gp350/220. The structure of CD21 (SCR1-2) alone has been determined by X-ray crystallography (Prota et al., 2002) as well as in complex with C3d (Szakonyi et al., 2001). However there is no crystal structure of CD21 in complex with CD23 to date.

CD21 domains SCR5-8 have been implicated in the carbohydrate-dependent binding to CD23. In a work that examined the roles of SCR1-2 and SCR 5-8, Aubrey et al. (1994) showed that when CD21-transfected K562 cells were treated with tunicamycin, which results in the loss of N-linked oligosaccarides, CD23 binding is inhibited to CD21 domains SCR5-8 but not CD21 domains SCR1-2. The glycosylation sites in SCR5-8 were then individually removed by site-directed mutagenesis, and Gln295 and Gln370 were deemed important for the interaction. This study therefore concluded that CD21 binds to CD23 through two sites, a protein-protein mediated interaction through SCR1-2 and a protein-carbohydrate interaction through SCR5-8. The binding site of CD21 (SCR1-2) has been mapped entirely to the C-terminus of derCD23 using NMR chemical shift perturbation studies (Hibbert et al., 2005) (Figure 1.8).

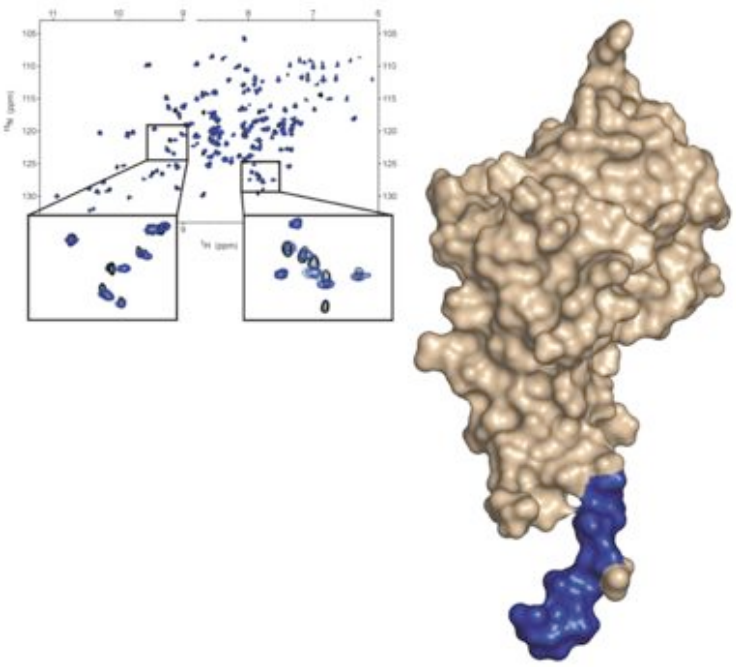

Figure 1.8: The binding site of CD21 on derCD23.
The chemical shift mapping as shown by Hibbert et al. (2005) that localised the binding site of CD21 on the C-terminal tail of CD23, highlighted in blue.

1.3.3 The role of various forms of CD23 on IgE regulation

CD23 is present in both monomer and trimeric forms in solution, whilst mostly a trimer on the membrane. One monomeric form of CD23, termed derCD23, is a cleavage product of the DerP1 enzyme, a proteolytic enzyme found in the faeces of the house dust mite (Schulz et al., 1995). The membrane bound CD23 (mCD23) is mostly a trimer on cell membrane however the trimeric stalk is not stable as it is susceptible to cleavage by endogenous proteases (Kilmon et al., 2004).

Oligomerisation of CD23 is essential for high affinity binding to IgE (Kilmon et al., 2001). McCloskey et al. (2007) later demonstrated using analytical ultra centrifugation that both monomeric and trimeric CD23 have a tendency to self associate upon binding to IgE, forming a high molecular weight aggregate (McCloskey et al., 2007). It was also

established that in monomeric form soluble CD23 inhibits while CD23 oligomers stimulate IgE synthesis in human B cells (Figure 1.9). NMR chemical shift mapping by Hibbert et al. (2005) demonstrated that the lectin head domain of CD23 is able to bind to both the Cε3 domain of IgE and CD21 (SCR1-2) simultaneously, as shown in Figure 1.10. The co-ligation of soluble CD23, presumably in its trimeric form is proposed to upregulate IgE synthesis in B cells (McCloskey et al. 2007).

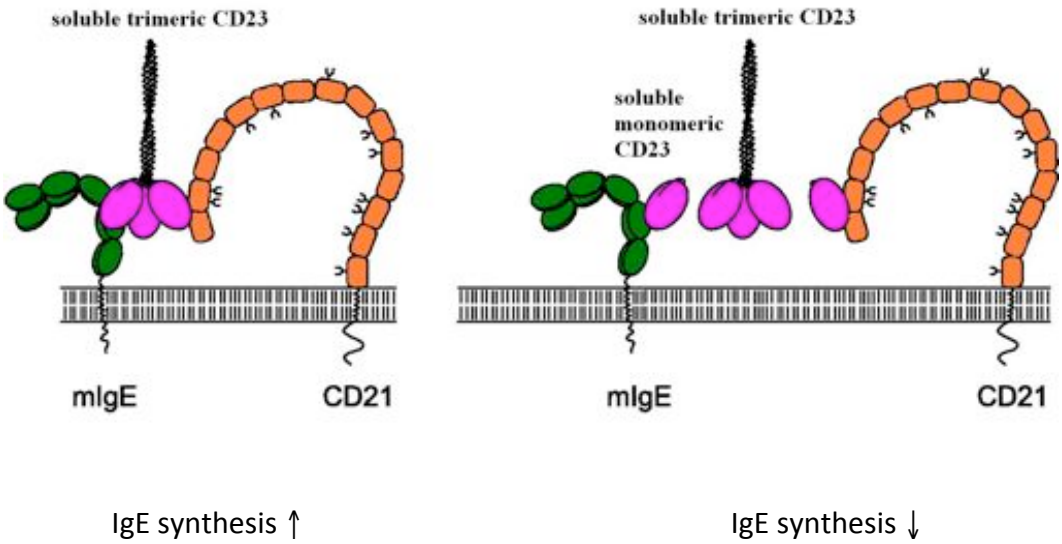

Figure 1.9: Modulation of IgE synthesis in B cells by monomeric and trimeric CD23.
Trimolecular complex formation upregulates IgE levels in B cells (left) while monomeric sCD23 downregulates IgE levels (right). Figure reproduced from McCloskey et al. (2007).

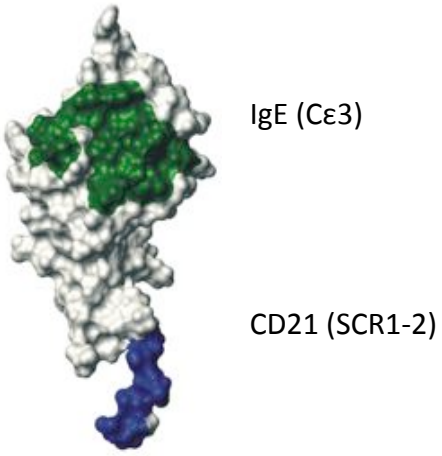

Figure 1.10: Structure of lectin domain of CD23 highlighting the distinct binding sites of IgE and CD21 (SCR1-2).

NMR experiments were previously performed to determine the residues that are involved in trimerisation by examining concentration-dependent changes in NMR chemical shifts. Over a range of different protein concentrations, several contiguous residues were seen to be perturbed in NMR chemical shift perturbation studies, and when these residues are mapped onto the derCD23 structure they reveal a trimerisation interface comprised of oppositely charged residues (Figure 1.11). This oppositely charged interface was proposed to mediate a trimeric structure of the lectin head domain; in this model structure, the binding sites of IgE and CD21 remain solvent exposed for forming ligand interactions.

The formation of the trimer allows for the potential formation of an extended signalling platform for the survival and differentiation of IgE-committed B cells, analogous to the signalling platformed by the co-ligation of antigen/C3d complexes with membrane Ig and CD21/CD19 co-receptor that activate production of antigen specific antibody-mediated responses (Pierce, 2002; Dempsey et al., 1996; Barrington et al., 2009) (Figure 1.12)

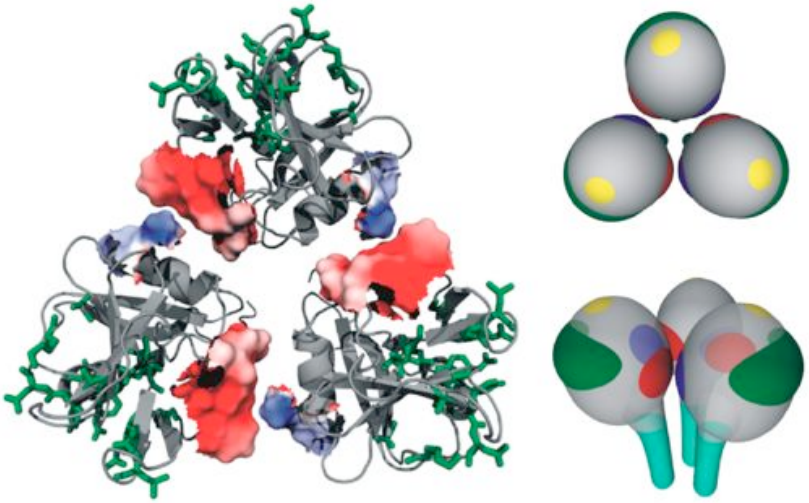

Figure 1.11: The trimerisation model as proposed by Hibbert et al. (2005).
Left: A top view of the proposed CD23 trimer. For each monomer, a backbone ribbon cartoon is shown in grey and residues that show concentration-dependent chemical shift changes are displayed in a surface representation (Residues L198, K212, H213, N225, E231, V240 and Y242) The surfaces are coloured according to electrostatic charge, demonstrating the electrostatic complementarity of the two sites. Side-chains for residues that are part of the IgE interaction site are displayed and coloured in green. Right: Top and side view of the trimerisation model. Calcium binding site is coloured yellow. IgE binding site is coloured green and the oligomerisation sites are coloured red and blue. The CD21 binding site is coloured cyan. Figure reproduced from Hibbert et al. (2005).

Recently, a protease ADAM-10 (a disintegrin and metalloproteinase-10) has been discovered and been identified as the main sheddase of membrane CD23 (Weskamp et al., 2006). ADAM-10 belongs to the ADAM family, which are cell surface proteins with a unique structure possessing both potential adhesion and protease domains. Sheddases, a generic name for ADAM metallopeptidase, function primarily to cleave membrane proteins at the cellular surface. It is proposed that in allergic individuals certain signalling molecules may upregulate ADAM-10's activity, which leads to increases of cleavage and thus the release of CD23 from the cell. Recently a mechanism has been proposed on how ADAM-10 may be regulated. A unique kainate receptor on B cells has been discovered and its activation by glutamate has been correlated with an increase of ADAM-10

expression that leads to shedding of membrane CD23 into soluble CD23. The increased presence of soluble CD23 upregulates IgE synthesis, presumably through binding to membrane IgE and CD21 simultaneously on B cells. It has been proposed that the inhibition of ADAM-10 may be useful in inhibition of IgE synthesis (Weskamp et al., 2006).

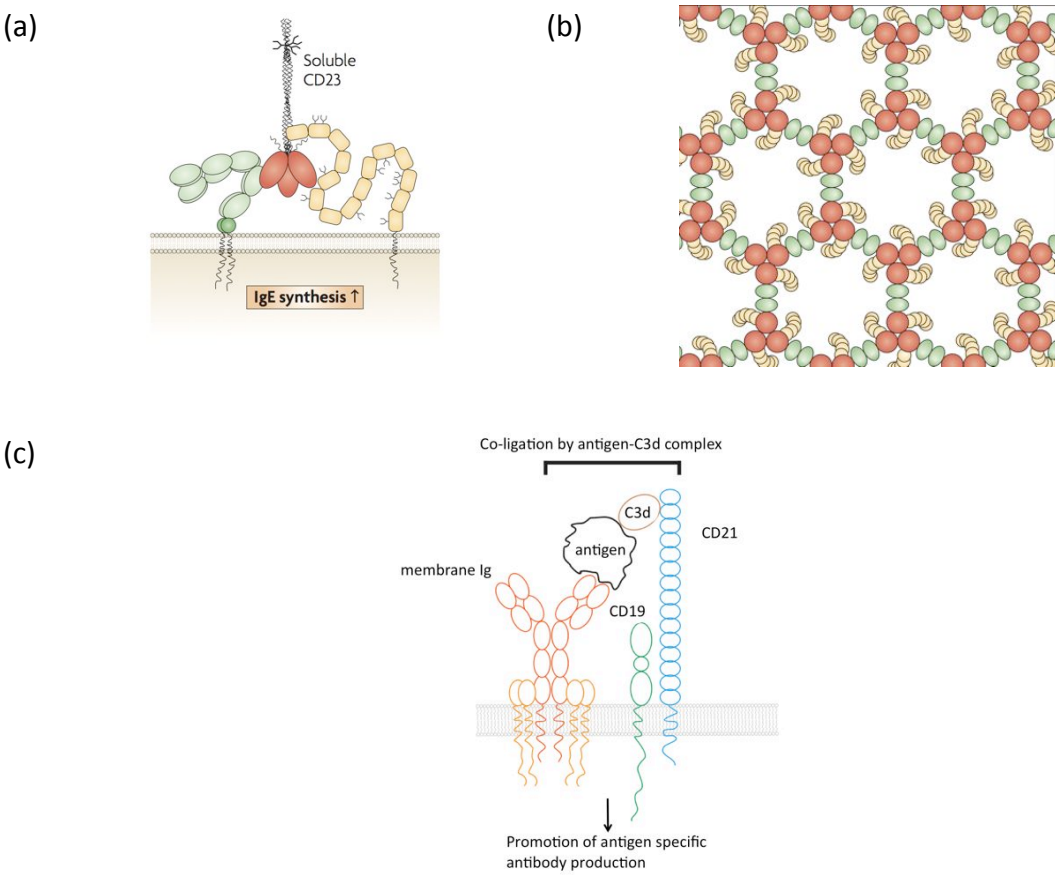

Figure 1.12: The trimolecular membrane IgE/trimeric CD23/ membrane CD21 complex and its proposed role in IgE synthesis.
a) Soluble CD23 forms a trimolecular interaction with IgE and CD21 on IgE committed B cells activating increase of IgE synthesis. B) A possible formation of signaling platform involving the trimolecular complex between soluble trimeric CD23 (red) with membrane IgE (green) and CD21. CD23 binds to the two Cε3 domain of IgE whilst retaining its CD21 binding through the C-terminus. This could lead to the formation of an extended network, creating a signaling platform that leads to the increase of IgE synthesis in an IgE committed B cell. (c) Co-ligation of membrane immunoglobulin and CD21/CD19 coreceptor by antigen-C3d complexes has been shown to lead to the promotion of antigen specific antibody production.

1.3.4 Other effector functions of CD23.

1.3.4.1 CD23 in IgE-mediated antigen presentation and transcytosis

Complexes of IgE and allergen can bind to membrane CD23, which is internalised and antigen is processed and presented to T cells through MHC Class II molecules (Wilcock et al., 2006) (Figure 1.13). This presentation induces T cells to activate IgE committed B-cells to produce IgE, thus amplifying the allergic response (Karagiannis et al., 2001). The presentation of antigen through CD23 lowers the threshold of T-dependent B-cell activation by >100-fold compared to antigen alone (Hjelm et al., 2006). Therefore in atopic individuals, low concentrations of allergen can induce allergic diseases. CD23 acts as a vehicle to increase the uptake of allergen for antigen presentation by antigen presentation cells thus facilitating antigen presentation in a process termed facilitated antigen presentation (FAP). Allergen specific immunotherapy, which involves the immunisation of patients with small doses of the specific allergen, induces production of specific IgG_4 which blocks IgE binding to allergen, thus inhibiting CD23 dependent IgE-mediated facilitated antigen binding (Wilcock et al., 2006). Blocking CD23 binding to IgE can also block FAP regardless of antigen specificity by preventing the binding of IgE/allergen complexes to surface CD23.

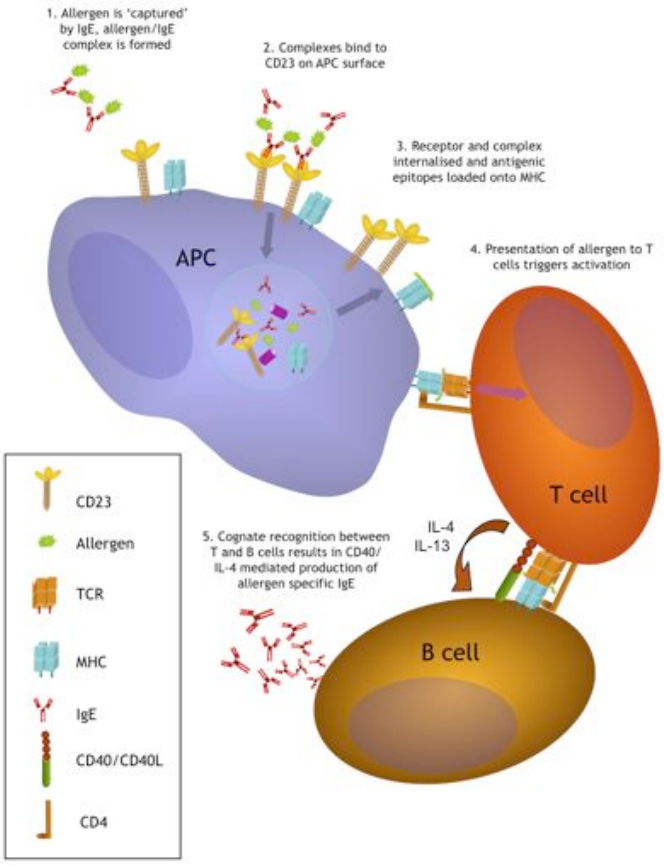

Figure 1.13: The role of CD23 in facilitated antigen presentation.
Allergen is captured by IgE and forms a complex on CD23. The complexes are then internalised and the antigenic epitopes are loaded onto the MHC molecule and presented to T cells which in turn activate B cells to produce IgE thus amplifying the allergic response. Figure adopted from Wilcock et al. (2006).

CD23 present on intestinal epithelial cells facilitates in the trancytosis of IgE-allergen complexes across the gut lumen to the mucosa region, and the antigen is then released. The released allergen then crosslinks and degranulates mast cells. This activates class switching of B cells and IgE synthesis which leads to the initiation and perpetuation of food allergies in murine models (Yang et al., 2000; Tu et al., 2005). In a model of bronchial asthma, complexes of IgE/allergen bound to the CD23 bound to airway epithelia are transcytosised into the sub-epithelial cells. The IgE-allergen complexes are released and

activate mast cell degranulation in the sub-epithelial side of the airway causing inflammatory reactions (Palaniyandi et al., 2011) (Figure 1.14)

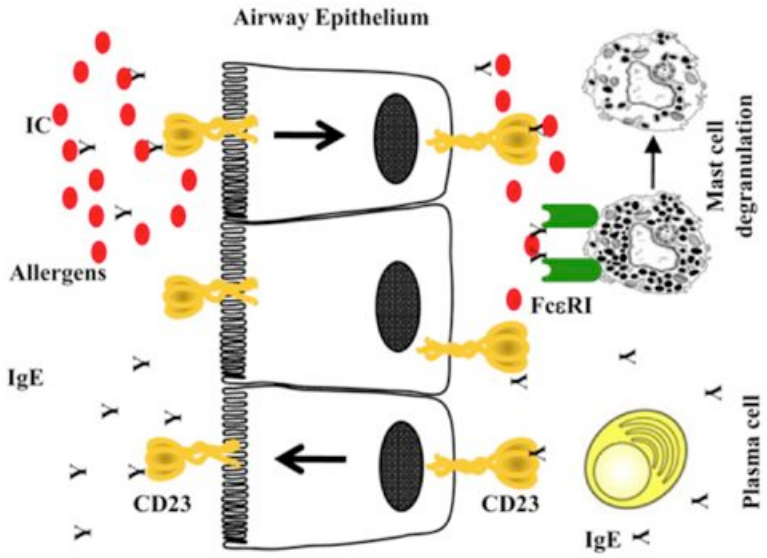

Figure 1.14: The model of CD23 mediated transcytosis of IgE-allergen complex through the airway epithelium as proposed by Palaniyandi et al (2011).
The immune complex (IC) consisting of IgE and allergen may be transported across the airway epithelium through membrane CD23 and released to the subepithelial side (right) and activate mast cell degranulation. This figure is reproduced from Palaniyandi et al. (2011).

1.3.4.2 CD23 in B cell lymphocytic leukaemia

It has been observed that soluble CD23 levels are increased in the sera of patients with chronic lymphocytic leukaemia (CLL) (Schwarzmeier et al., 2005). The increase in soluble CD23 was observed to correlate with the activation of the Notch-2 signalling pathway that promotes B cell survival and apoptosis avoidance by upregulating the anti-apoptotic gene Bcl-2. Cross-linking of membrane CD23 has been shown to induce apoptosis in B cells through intrinsic mechanisms and is inhibited by Bcl-2 (Campbell et al., 1997). An anti-CD23 monoclonal antibody, IDEC-152 (also known as Lumiluximab), has been in

clinical trials for chronic lymphocytic leukaemia; it exerts its clinical efficacy through inducing apoptosis, mainly through an intrinsic mechanism (Byrd et al., 2010).

1.3.4.3 CD23 in rheumatoid arthritis

Arthritis is an autoimmune disease where the immune system has developed a response towards autoantigens. Arthritis can be induced against self-collagen in collagen induced arthritis (CIA) models in mice (Williams, 2004). High levels of soluble CD23 were noted in the sera of patients with rheumatoid arthritis (Chomarat et al., 1993). The treatment with polyclonal antisera against mouse CD23 in the CIA model led to reduction of arthritic symptoms in mice (Plater-Zyberk and Bonnefoy, 1995). Collagen induced arthritis was shown to be delayed and inhibited in CD23 deficient mice (Kleinau et al., 1999). These findings suggest a role of CD23 in disease progression, although its exact mechanism is not clear. IgE/antigen complex-mediated crosslinking of CD23 has been shown to activate a variety of cells to activate proinflammatory events such as the activation of inducible nitric oxide synthase, IL-1 and TNF-α (Vouldoukis et al., 1995; Mossalayi et al., 1997). The administration of a CD23-binding peptide ameliorates symptoms of arthritis in animal and human models as well as suppressing the transcription of inflammatory genes such as TNF-α and IL1- β in macrophages, which further supports a role of CD23 in rheumatoid arthritis (Rambert et al., 2009).

1.4 The interaction between CD21 and C3d and its role in autoimmunity.

On B cells, CD21 forms a co-receptor with membrane immunoglobulin and CD19 thus forming the "B cell receptor" (Carter, 1988). The complement system, which is part of the innate immune system, converges at C3 convertase, which leads to the degradation of C3 into smaller fragments. Its terminal degradation product C3d binds to CD21 and activates the antibody mediated immune response and thus serves as a link between the innate and the adaptive immune system (Fearon and Locksley, 1996; Fearon and Carroll, 2000) (Figure 1.15).

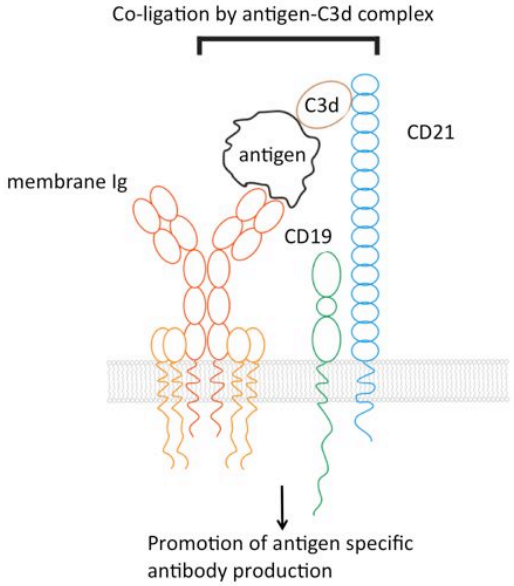

Figure 1.15: The link between innate and adaptive immune system as demonstrated by the co-ligation of antigen/C3d complex to the CD21/CD19/membrane IgE B-cell co-receptor.
The colligation of CD21 and the membrane immunoglobulin by antigen C3d-tagged antigen leads to an amplification of antibody-mediated immune response.

1.4.1 The complement system

The complement pathway is one of the primary responses towards an invading pathogen. Three pathways of activation, namely the classical, alternative and lectin activation pathways, emerge from different activation mechanisms. They are highly regulated

interaction networks consisting of proteins in solution as well as membrane bound receptors that interact to mediate a hierarchical cascade of proteolytic events that converge at the formation of the central C3 convertase (Carroll, 2004). The classical pathway was the first discovered and is activated by attachment of the C1 complex to a target complex. The lectin pathway is homologous to the classical pathway, activated instead by mannose-binding lectin (MBL) and ficolins, instead of C1q (Wallis et al., 2010). The alternative pathway is initiated by spontaneous hydrolysis of C3 and 'ticks over' leading to a continuous generation of transient C3 convertases by spontaneous hydrolysis even in the absence of pathogens. At the point of convergence of these pathways, the C3 convertase cleaves C3 into the small anaphylatoxin C3a (9 kDa) and the larger C3b (177 kDa) molecule (Bokisch et al., 1975). C3b has a reactive moiety that allows attachment to a pathogen's surface (Tack et al., 1980) and forms the basis of further convertase complexes. The plasma protein factor B binds to the C3b molecule on the cell surface and is cleaved to Ba and Bb by factor D with the Bb fragment remaining associated with the surface C3b. This yields the short-lived ($t_{1/2}$ ~90 s) C3bBb complex (Fishelson et al., 1984). This C3 convertase cleaves more C3 molecules into C3a and C3b, causing amplification the complement response. A further molecule of C3b can associate with the bound C3bBb complex to form the $C3b_2Bb$ complex also known as the C5 convertase. The C5 convertase cleaves multiple molecules of C5 into C5a and C5b, initiating the formation of the terminal membrane attack complex (MAC) leading to the destruction of cells and pathogens (Janeway, 2005) (Figure 1.16).

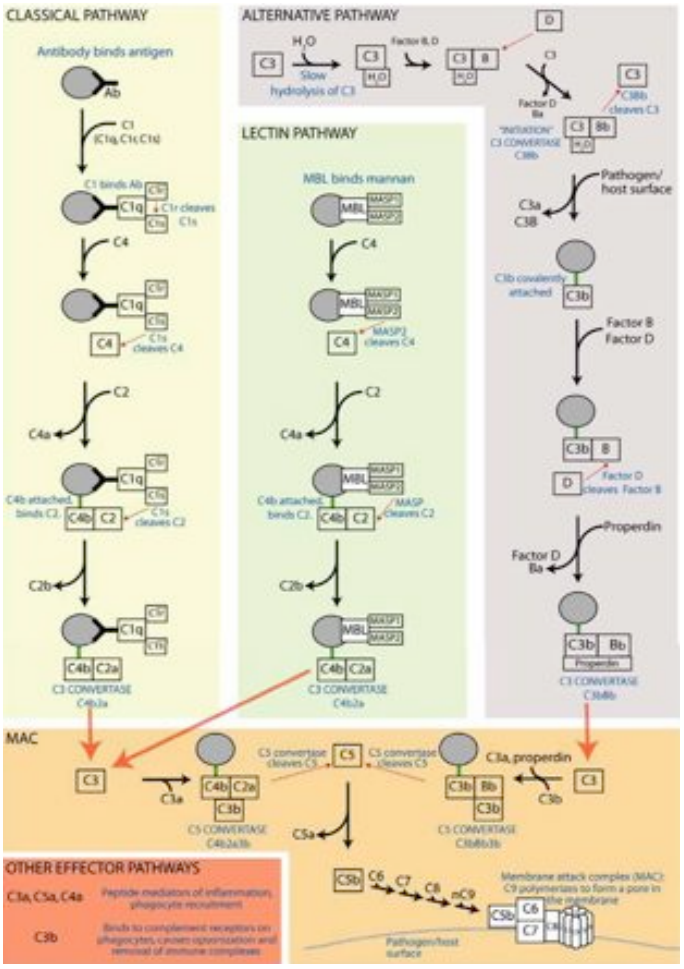

Figure 1.16: Overview of complement activation.
The three pathways converge at the formation of a C3 convertase. C3 convertase cleaves C3 into C3a and C3b which lead to pathogen opsonisation, release of peptide mediators of inflammation, and formation of the terminal membrane attack complex that lyses certain cells and pathogens Green lines corresponds to the covalent bond between pathogen derived antigen (grey) and complement fragments. Figure reproduced from (Volanakis, 1998).

The generation of various anaphylatoxins, such as C3a and C5a, propagate inflammation and mediate the recruitment of phagocytes to the complement activation site. Complement also functions in clearing infections by launching an opsonisation of antigens through some cleavage products of C3 (Figure 1.17), which is followed by phagocytosis.

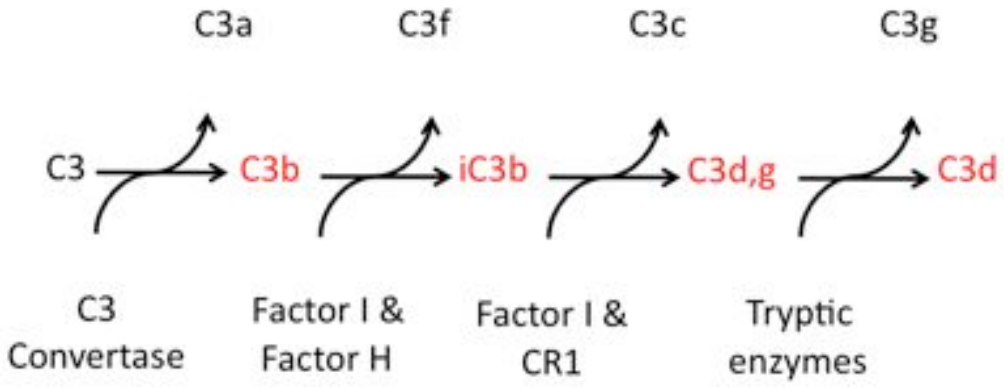

Figure 1.17: Proteolysis of C3.
The C3 convertase cleaves C3 into C3b, which is followed by subsequent proteolytic degradation by various proteases into various opsonins (red). The serine protease Factor I, with Factor H and Complement Receptor 1 participate in the first few degradation reactions. Several tryptic enzymes such as plasmin yield the final degradation product C3d. Attachment of C3b, iC3b, C3d,g and C3d coated pathogens to complement receptors on phagocytes lead to the uptake and phagocytosis of those opsonised particles (Janeway, 2005).

The opsonised particles are recognised by various complement receptors (CR) on phagocytic cells such as CR1 (CD35), CR3 (CD11b/CD18), CR4 (CD11/CD18) (Carroll, 2004), CR1g (Helmy et al., 2006). The proteolytic degradation product of C3, C3b, forms a covalent ester bond with antigen and is then degraded to form C3d which remains covalently bound to antigen and interacts with CR2 (CD21) on B cells to activate the antibody mediated response (Carter et al., 1988; Carter and Fearon, 1992; Dempsey et al., 1996).

C3b leads to a variety of damaging responses and to prevent excessive activation and damage to the host cells, there exist a number of regulators of complement activation (RCA). These are present either as fluid phase or host cell-associated proteins, many of which consist of short domains called short consensus repeat (SCR) domains (Perkins et al., 2002). One of the RCA, complement receptor 2 (also known as CD21), interacts with

the terminal degradation product C3d and is involved in the activation of an antibody mediated immune response thus serving as a link between the innate and adaptive immune response (Dempsey et al., 1996).

1.4.2 Complement receptor 2, CD21

Complement receptor 2, also known as CD21, is a type I integral membrane protein with a C-terminal intracellular region and N-terminal extracellular region that belongs to the family of regulators of complement regulation (RCA) (Hourcade et al., 1989). The extracellular region of CD21 is made up entirely of short consensus repeat (SCR) domains (Moore et al., 1987). The SCR domains typically consist of ~60 amino acids, folded into a β-sheet core stabilised by 2 disulfide bonds. These are formed between 4 invariant cysteines linked in a Cys1-Cys3, Cys2-Cys4 pattern (Liszewski et al., 1991). CD21 consists of 15 (Weis et al., 1988) or 16 (Pochon et al., 1992) SCR domains that have 10 or 11 potential N-glycosylation sites and maintain functionality when expressed as recombinant proteins (Ahearn et al., 1988; Carel et al., 1990).

The structure of CD21 (SCR domains 1-2) itself (Prota et al., 2002) and in complex with C3d (G Szakonyi et al., 2001) has been solved by x-ray crystallography. Both structures showed CD21 (SCR1-2) adopting the typical SCR fold with five short β-strands, a small hydrophobic core and disulfide bonds at either end of each domain (Figure 1.17).

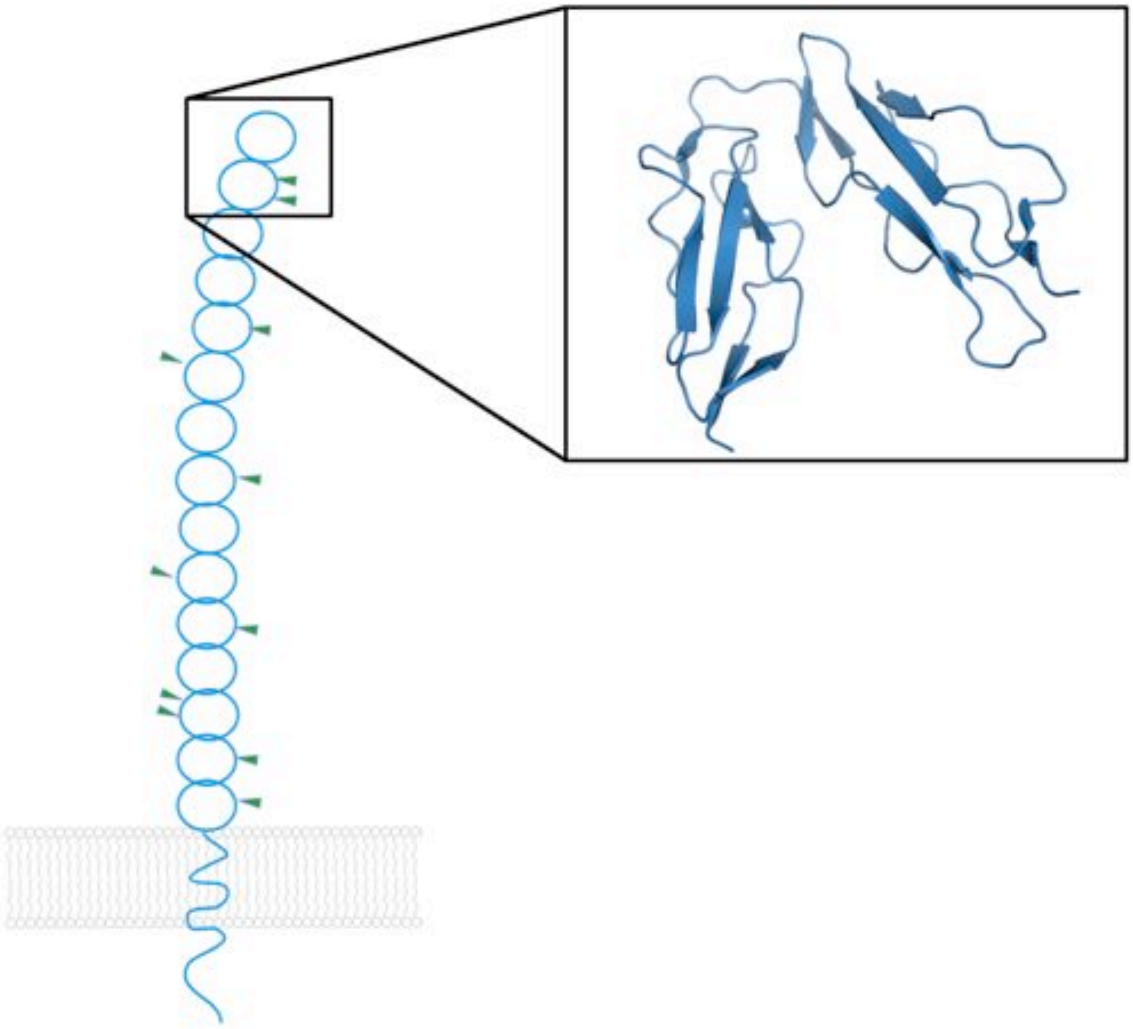

Figure 1.18: The schematic representation of full length CD21 and crystal structure of CD21 (SCR1-2). N-linked glycosylation sites are represented by green triangles. The inset shows the crystal structure of the two N-terminal domains of CD21 (Prota et al., 2002) (PDB ID: 1LY2)

1.4.3 The interaction between CD21 and C3d and its role in autoimmune disease.

Activated C3 forms a covalent bond with antigen and crosslinks CD21/CD19 with membrane bound immunoglobulin. The activated C3 is then degraded to C3d whilst retaining the crosslinking with CD21/CD19 and membrane immunoglobulin. This complex amplifies B cell signalling to elicit antibody mediated immune response at concentrations

10,000-fold lower than antigen alone, thus acting as a molecular adjuvant (Dempsey et al., 1996; Bergmann-Leitner et al., 2006). However, C3d-tagged self-antigen elicits production of autoantibodies resulting in autoimmunity. Exposure of human collagen in a collagen induced arthritis (CIA) transgenic mouse model leads to arthritis (Kato et al., 1996; Rosloniec et al., 1997) suggesting that continuous exposure of collagen to B cell eventually leads to it being recognised as antigen (Verstappen et al., 2006). Mouse models of CIA cannot be induced in mice lacking either CD21 or C3 (Del Nagro et al., 2005). The crosslinking of C3d-tagged self-antigen with CD21 in follicular dendritic cells (FDC) and B cells leads to retention of the self antigen making the response more persistent, as is seen in chronic arthritic disease (Morrow et al., 1983; Del Nagro et al., 2005).

The cause of arthritis is unknown and might involve the inability of the cell to maintain tolerance to self-antigen and the persistence of C3d-tagged self-antigen. Tolerance is the deliberate failure of the immune system to respond to self-antigens, for example by removing any cells that are self-reactive during lymphocyte development. For a B cell to be activated it must bind a T cell with specificity for the same antigen, or else it will be removed from the circulating population.

1.4.4 Controversy regarding the crystal structure of CD21/C3d

The crystal structure of C3d was published by Nagar et al. (1998) showed a defined hydrophobic cleft on a concave site that is surrounded by a ring of negatively charged residues (Figure 1.19). Site-directed mutagenesis and binding studies by Clemenza & Isenman (2000) suggested that CD21 binds to a concave surface of C3d, an area that

consists of mainly negatively charged residues.

(a) (b)

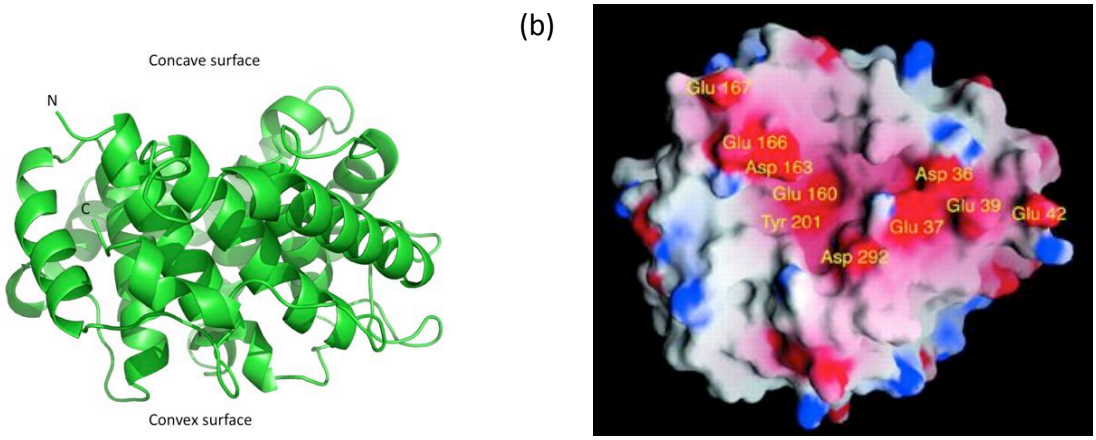

Figure 1.19: The structure of C3d highlighting the surface implicated in ligand binding.
(a) The side view of the crystal structure of C3d indicating the concave and the convex surface b) The main binding site of CD21 on C3d identified by site directed mutagenesis indicating a hydrophobic cleft surrounded by a ring of negatively charged residues. Figures adapted from Nagar et al., (1998) (PDB ID:1C3D) and Clemenza & Isenman (2000).

However, Szakonyi et al. (2001) published a crystal structure of a CD21/C3d complex that was highly controversial (Figure 1.20). The complex seen in the crystal structure contradicts a large body of evidence from site-directed mutagenesis and binding studies. In the crystal structure, the SCR2 domain in CD21 is observed to bind to C3d and a site distinct from the concave site indicated by site-directed mutagenesis is seen in the complex. The dimeric CD21 (SCR1-2) in the crystal structure is not physiologically relevant, as previous biochemical analysis has shown that the interaction has a stoichiometry of 1:1 (Prota et al., 2002).

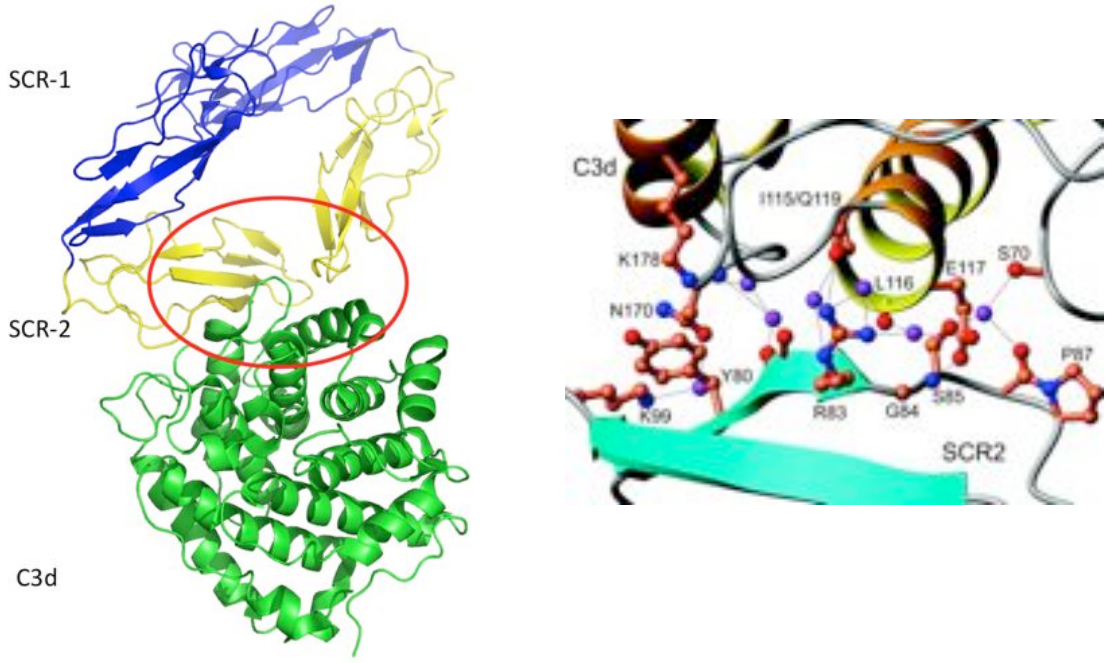

Figure 1.20: The crystal structure CD21 (SCR1-2)/C3d complex as solved by Szakonyi et al. (2001). Left: The crystal structure showed a dimeric CD21 (SCR1-2) binding to C3d, which suggested that the SCR2 domain was implicated in C3d binding and identified a binding site on C3d different from the region previously implicated in site-directed mutagenesis studies. Right: The close up view of the interaction interface between CD21 with C3d from the crystal structure with the SCR2 domain of CD21 mainly implicated involving residues Y80, R83, G84, and S85 as proposed Hannan et al. (2005) (PDB ID: 1GHQ). The dimeric form of CD21 was later shown to be physiologically irrelevant by Prota et al. (2002).

Later in 2005, the same group published a site-directed mutagenesis study implicating SCR1 in binding to C3d; this work showed a putative positively charged patch in SCR1 is involved in binding to C3d (Hannan et al., 2005). They proposed that residues on SCR1 (R13 and K57) were involved merely in pseudospecific interactions with C3d and suggested that SCR2 is the main site of binding to C3d, modeled on a previously published crystal structure (Hannan et al., 2005). Again the same group published a study using NMR chemical shift perturbation mapping that indicated that both domains of CD21 (SCR1-2) are involved in C3d binding (Kovacs et al., 2009). However this experiment was done at low ionic strength, and due to the highly charge mediated interaction (Morikis

and Lambris, 2004) the residues in SCR2 may have shown perturbations in low ionic strength due to non-specific charge mediated interactions. Prota et al. (2002) also pointed out that the non-physiologic zinc present at 200 mM in the crystal structure, that was found bound at the protein-protein interface, may obscure physiological binding from occurring. Isenman et al. (2010) also showed that at such zinc concentrations, the binding between CD21 (SCR1-2) and C3d is completely abolished. Isenman (2010) also performed site-directed mutagenesis binding studies on the C3d site and proposed that the binding site of CD21 on C3d is localized on the concave site, thus contradicting the crystal structure. However these binding experiments were performed using surface plasmon resonance (SPR) using a single concentration of C3d mutants, which is inadequate to provide complete information especially for deriving affinity values and thermodynamic parameters.

1.5 Current therapeutics and design of inhibitors of the IgE network

Omalizumab is an anti-IgE antibody-based drug and has been shown in clinical trials to be very effective against a wide variety of allergic disorders (Strunk and Bloomberg, 2006). However, treatment using this antibody-based therapy is very expensive and given that there are increasing numbers of allergic incidents, this treatment will not be feasible for large populations. Omalizumab only functions by binding to free IgE and directly reduces levels of IgE expression, and therefore continuous administration is required. Consequently CD23 has emerged as target because it is involved in the regulation of IgE synthesis.

Several *in vitro* studies showed that cross-linking of CD23 leads to reduction of IgE synthesis (Campbell et al. 1992; Nakamura et al. 2000a; Sherr et al. 1989). IDEC-152, an anti-CD23 monoclonal antibody, has been shown to reduce IgE levels and allergic symptoms in humans (Poole et al., 2005). Crosslinking of CD23 leads to the abrogation of CD23-mediated IgE-dependent antigen presentation to T_H2 cells, which leads to a decrease the immunological response to allergens and impairs IgE synthesis by inhibiting IgE class switching in B cells.

Treatment with anti-CD23 could inhibit CD23 positive B cells, macrophages, and dendritic cells from producing cytokines. The administration of anti-CD23 mAbs in murine asthma models results in the suppression of lung eosinophil infiltration and reduction of airway hyper-responsiveness (Cernadas et al., 1999). From these observations, it is thought that CD23 inhibitors such as an anti-CD23 antibody could be a potential therapeutic strategy for the treatment of allergy. Again however, the administration of antibodies may be expensive and complicated to administer. The further understanding of the antibody's mechanism may inform the design of small molecule inhibitors that may function by mimicking the antibody's mode of action.

As indicated, soluble CD23 is involved in upregulating IgE synthesis by co-ligating with both membrane IgE and CD21 on the surface of B cells. One way to prevent this co-ligation is to inhibit the interaction of IgE/CD23 itself. A recent study also showed that a CD23-binding phage display derived peptide (FHENWPS) could alleviate symptoms of IgE mediated arthritis in human and animal models (Rambert et al., 2009), which provides another example of the clinical relevance of this inhibition. It is hoped that the further

understanding of this interaction, aided by the detailed information of the interaction from the derCD23/IgE-Fc (Cε3-4) crystal structure may help to design of molecules to disrupt this interaction.

1.6 Aims of the thesis

The aim of this thesis is to increase the understanding of various interactions within the IgE network. Firstly, several phage display derived peptides were selected, and the biophysical characterisation of the strongest binding peptide was performed. This was followed by functional assays to elucidate its effect on the inhibition of IgE synthesis and IgE binding on CD23 expressing cells. Co-crystallisation was also attempted and, although not successful, a high-resolution structure of the non-mutated derCD23 was derived which may be important in future crystallographic drug discovery efforts.

A comparison in binding affinity between the monomeric and trimeric CD23 was performed using biophysical techniques, primarily using surface plasmon resonance. Additionally the oligomerisation phenomenon of CD23 was examined, which may provide insights on potential inhibition targets. NMR chemical shift perturbation mapping and the crystal structure of derCD23/IgE-Fc- (Cε3-4) were used to direct and assess various site-directed mutagenesis studies done previously as well as in this work. The binding site of CD21 (SCR1-2) on derCD23 has been shown to involve CD23's C-terminal tail by NMR chemical shift mapping experiments (Hibbert et al., 2005). A truncated construct lacking the C-terminus was made to confirm that no other residues are involved in CD21 (SCR1-2) binding. The anti-CD23 monoclonal antibody IDEC-152 has been established to be effective in reducing IgE levels in clinical trials. Biophysical analyses were performed to

provide insights into the mechanism of this antibody. The intermolecular interactions between CD23, IgE and FcεRI were also examined and their potential biological implications explored. The interaction between CD21 (SCR1-2) and C3d was examined, following up from previous work done in our lab. NMR chemical shift mapping experiments performed at different ionic strengths were performed to delineate the specific binding region of C3d on CD21 (SCR1-2). Identification of salt bridges was performed through double mutant cycles and analysed using isothermal titration calorimetry (ITC) in order to provide insights into the nature of this interaction. It is hoped that the increase of the understanding of this interaction between these proteins in the IgE network will not only increase our understanding of the relationship between these molecules but may assist in the development of potential therapeutics.

Chapter 2

Materials and Methods

All enzymes were purchased from New England Biolabs unless otherwise stated

2.1 Buffers and solutions

DNA stain solution: 0.2 μg/ml ethidium bromide in 1 x TAE buffer

EDC: 0.4 M 1-ethyl-3-(3-dimethylaminopropyl)-carbodiimide

M9 minimal medium: 43 mM Na_2HPO_4, 22 mM KH_2PO_4, 8.5 mM NaCl, 0.03 mM $CaCl_2$, 19 mM NH_4Cl, 1 mM $MgSO_4$, 1 mM vitamin B1 (Thiamine-HCl), 0.3 % (w/v) glucose, pH 7.2

NHS: 100 mM N-hydroxysuccinimide

NZY$^+$ broth: 1 % (w/v) NZ-amine^{TM}, 0.5 % (w/v) yeast extract, 86 mM NaCl, 12.5 mM $MgCl_2$, 12.5 mM $MgSO_4$, 20 mM glucose

PBS: 10 mM Na_2HPO_4, 137 mM NaCl, 2.7 mM KCl, pH 7.4

PDEA: 80 mM 2-(2-pyridinyldithio)ethaneamine in 100 mM sodium borate, pH 8.5

SDS-PAGE destain solution: 10 % acetic acid, 40 % methanol, 50 % H_2O

SDS-PAGE loading buffer (reducing): 100 mM Tris-HCl, 200 mM DTT, 4 % (w/v) SDS, 20 % (v/v) glycerol, 0.2 % bromophenol blue

SDS-PAGE loading buffer (non-reducing): 100 mM Tris-HCl, 4 % (w/v) SDS, 20 % (v/v) glycerol, 0.2 % bromophenol blue

SDS-PAGE resolving gel: 12.5 %: 0.4 mM Tris, 12.5 % (w/v) acrylamide, 0.01 % (w/v) SDS, pH 8.8, polymerised with 0.01 % (w/v) APS and 0.5 % (v/v) TEMED

SDS-PAGE resolving gel: 15 %: 0.4 mM Tris, 15 % (v/v) acrylamide, 0.01 % (w/v) SDS, pH

8.8, polymerised with 0.01 % (w/v) APS and 0.5 % (v/v) TEMED

SDS-PAGE running buffer: 25 mM Tris, 250 mM glycine, 3.5 mM SDS, pH 8.3

SDS-PAGE stacking gel: 0.43 mM Tris, 4 % (v/v) acrylamide, 0.01 % (w/v) SDS, pH 6.8, polymerised with 0.025 % (w/v) APS and 1.25 % (w/w) TEMED

SOC buffer: 2 % (w/v) tryptone, 0.5 % (w/v) yeast extract, 10 mM NaCl, 2.5 mM KCl, 10 mM $MgCl_2$, 10 mM $MgSO_4$, 20 mM glucose.

TAE buffer (50 x): 2 M Tris-acetate, 50 mM EDTA, pH 8.5

2.2 Molecular Biology

2.2.1 Site directed mutagenesis

Site-directed mutagenesis was carried out using a QuikChange II site-directed mutagenesis kit (Stratagene) according to the manufacturer's instructions. Briefly, 5 µl of 10X reaction buffer, 125 ng of forward and reverse primer, 5–50 ng of DNA template, 1 µl of deoxynucleoside triphosphate (dNTP) mix were combined and the volume made up to 50 µl with ddH_2O. 2.5 U of PfU®Ultra HF polymerase were then added and a thermal cycler used to generate 12 (for point mutations) or 16 (for single amino acid changes) cycles of 95^{o}C (30 seconds), 55^{o}C (1 minute) and 68^{o}C (7 minutes). The reaction mixture was then cooled to 4^{o}C and 10 U of DpnI restriction enzyme was added. The solution was thoroughly mixed and incubated at 37^{o}C for 1 hour. 1 µl of the reaction mixture was then used to transform XL-1 blue cells as described in Section 2.2.4. The list of primers for the introduction of mutations in derCD23 and CD21 (SCR1-2) are as follows:

Table 2.1: List of primers for mutations introduced in derCD23

R188A	5’-cagtgggtccacgccgcttatgcctgtgacgac-3’
R188A_antisense	3’-gtcgtcacaggcataagcggcgtggacccactg-5’
D192	5’-cggtatgcctgtgctgacatggaagggcag-3’
D192A_antisense	3’-ctgcccttccatgtcagcacaggcataccg-5’
E257A	5’-cggagccagggcgctgactgcgtgatgatg-3’
E257A_antisense	3’-catcatcacgcagtcagcgccctggctccg-5’
E227A	5’-gccttcggaacttggctctgaagggagag-3’
E227A_antisense	3’-ctctcccttcagagccaagttccgaaggc-5’
CD23minus7 (to truncate the C terminus)	5’-gggaattccatatgagcggctttgtgtgcaaca-3’
CD23minus7_antisense	3’-cgcggatccttatcatggcggcgtgcatgtggcca-5’

Table 2.2: List of primers for mutations introduced in CD21 (SCR1-2)

R13A	5'-tccgcctatcctaaatggcgcgattagttattattctaccc-3’
R13A_antisense	5'-gggtagaataataactaatcgcgccatttaggataggcgga-3'
R28A	5'-cattgctgttggtaccgtgatagcgtacagttgttcaggt-3'
R28A_antisense	3'-gtaacgacaaccatggcactatcgcatgtcaacaagtcca-5'
K41A	5'-ggtaccttccgcctcattggagaagcaagtctattatgcataact-3'
K41A_antisense	3'-ccatggaaggcggagtaacctcttcgttcagataatacgtattga-5'
K57A	5'-aaagtggatggaacctgggatgcacctgctcctaaatgtga-3'
K57A_antisense	3'-tttcacctaccttggaccctacgtggacgaggatttacact-5'
R83A	5'-agcccatagtaccaggaggatacaaaattgagggctctacaccctac-3’
R83A_antisense	3'-tcgggtatcatggtcctcctatgttttaactcccgagatgtgggatg-5

2.2.2 DNA vectors

2.2.2.1 DerCD23

DerCD23 comprises the amino acids Ser156 to Glu298 using the numbering from the Swiss-Prot Accession code P06734. A pET5a expression construct of derCD23 generated as previously described (Hibbert et al., 2005) was kindly donated by Dr Martine Bomb (Department of Biochemistry, University of Oxford). The vector was propagated in the *E. coli* DH5α strain (Invitrogen) and selected by resistance to ampicillin (Melford).

2.2.2.2 CD21 (SCR1-2)

The N-terminal domains of CD21 consisting of the first two domains SCR1 and SCR2 (CD21 (SCR1-2)) comprise the amino acids Ser2 to Ser128 using the numbering from the experimentally determined N-terminal sequence of the mature protein (Fingeroth et al., 1988). A pET41b expression construct of CD21 generated as previously described and kindly donated by Dr Martine Bomb. The vector was propagated in the *E. coli* DH5α strain (Invitrogen) and selected by resistance to kanamycin (Melford).

2.2.2.3 C3d

C3d comprises the amino acids Asp996 to Arg1303 of mature C3 using the numbering from the Swiss-Prot Accession code P01024. C3d contains three cysteine residues at positions 1010, 1101 and 1158. Cys1010 forms part of the reactive thioester moiety in C3. This was mutated to an alanine residue to ensure that only one disulfide linkage could form between Cys1101 and Cys1158 in recombinant C3d. A pET15b expression construct of C3d (Cys1010Ala), generated as previously described (Nagar et al., 1998) was kindly

donated by Professor David Isenman, University of Toronto. The expressed protein contains an additional 8 amino acids (MLDAERLK) as compared to enzymatically produced C3d. Whereas the first 2 amino acids (ML) are vector derived, the other 6 (D996 – K1001) correspond to the C-terminal fragment of C3dg. The amino acid numbering used forthwith in this thesis corresponds to the C3d residue numbers (Met1–Arg 310) for consistency with published literature. The vector was transformed and propagated into the *E. coli* DH5α strain (Invitrogen) and selected by resistance to ampicillin (Melford).

2.2.3 Agarose gel electrophorosis

1% agarose was melted in TAE buffer, cooled and set in a gel tray with a plastic lane comb. Once set, the gel was placed into electrophoresis equipment and submerged in 1 x TAE buffer. 3-50 µl samples in DNA loading buffer were placed in the wells alongside appropriate DNA molecular weight markers (Promega). A voltage of 90 V was applied across the gel for 50 minutes or until the fragments were separated. The gel was stained with DNA stain solution containing ethidium bromide for 30 minutes and DNA fragments visualised under a UV lamp. To purify the DNA fragments, bands were cut out from the gel under UV illumination and purified using the Qiagen gel extraction kit (Qiagen).

2.2.4 Transformation

50 µl frozen aliquots of chemically competent cells DH5α *E. coli* (Invitrogen) for vector propagation, BL21 (DE3) *E. coli* for protein expression (Invitrogen) and XL1-blue supercompetent *E. coli* (Stratagene) for mutagenesis reactions were thawed on ice. 1-5 µl of DNA was added to the competent cells and mixed by gently swirling. The mixtures were incubated on ice for 30 minutes. A heat shock was performed at 42^{o}C for 20 seconds

(for DH5α cells), 30 seconds (for all BL21 (DE3) cells) and 45 seconds (for XL1- blue cells). Cells were then immediately placed on ice for 2 minutes before adding 450 µl of SOC medium for DH5α and BL21 (DE3) cells or 500 µl of NZY^+ broth for XL1-blue cells. The samples were then incubated at 37^{o}C for 30–60 minutes with shaking at 225–250 rpm before being plated on selective agar and incubated overnight at 37^{o}C.

2.2.5 Plasmid purification

Single colonies from agar plates were picked into 5–100 ml LB containing the appropriate antibiotic (30 µg/ml kanamycin or 100 µg/ml ampicillin (Melford)) and incubated overnight at 37^{o}C with shaking at 225–250 rpm. The cells were spun down by centrifugation at 6000 x g for 15–30 minutes at 4^{o}C. DNA was purified from the cell pellet using the DNA Mini- and Midiprep kits (Qiagen) according to the manufacturer's instructions. DNA concentration was estimated by UV spectroscopy where an absorbance at 260 nm of 1 corresponds to 50 µg/ml. The purity of the DNA was determined using the sample's absorbance at 260 and 280 nm. A 260/280 ratio of 1.8 corresponds to a pure DNA sample.

2.2.6 DNA sequencing

Purified DNA constructs were sequenced to ensure no sequence errors were present. DNA sequencing was performed in-house by Geneservice Ltd. or MWG Operon using appropriate primers.

2.3 Protein production and purification

2.3.1 Production of human CD23

2.3.1.1 Expression of human derCD23

BL21 (DE3) cells were transformed with PET5a containing the sequence of derCD23 comprising the amino acid Ser156 to Glu298 based on Swiss Prot accession number P06734. BL21 (DE3) *E.coli* cells were grown overnight in 5 ml LB medium containing 100 µg/ml ampicillin at 37^{o}C. The culture was then diluted ten-fold into 500 ml LB and incubated at 37^{o}C in an orbital shaker until OD 0.6-1.0 was reached. A final concentration of 1mM IPTG was then added to induce protein expression for 3-4 hours. Cells were then harvested by centrifugation at 4000 g and 4^{o}C for 40 minutes. Pellets from 500 ml cultured were resuspended in 30 ml 25 mM Tris-HCl, pH 7.5 and stored at -20^{o}C. In the case of ^{15}N labelling of derCD23, cultures were grown using the M9 minimal medium with addition of 0.7 g/L $^{15}NH_4Cl$ (Spectra media).

2.3.1.2 Washing of derCD23 inclusion bodies.

Cell pellets in resuspension buffer were thawed and Triton-X100 was added to a final concentration of 1% (v/v). The suspension was homogenised using the Avestin French press at 18-20 MPa. Samples were centrifuged at 17000 x g at 4^{o}C for 10 minutes. Pellets were resuspended in 20 mL Tris-HCl pH 7.5 and centrifuged again under the same conditions and repeated once more. A hand held homogenizer was used to solubilise spun down pellets. Pellets were resuspended in 20 ml 25 mM Tris-HCl pH 7.5, 0.5M guanidine hydrochloride and centrifuged under the same conditions. Finally the pellets were resuspended in 15 mL 25 mM Tris-HCl pH 7.5, 6M guanidine hydrochloride and

solubilised overnight with orbital shaker. The sample was centrifuged at 17000 g at 4^{o}C for an hour. Supernatant containing protein was kept at -20^{o}C before the refolding step.

2.3.1.3 Refolding of derCD23

3.5 ml of protein sample in solubilisation buffer was diluted with solubilisation buffer to a total volume of 15 ml with the final concentration of 0.7 mg/ml to 1.0 mg/ml protein. 0.5 mM DTT was added and the solution was then diluted tenfold into ice cold refolding buffer (1M pyridinio propanesulfonate (Sigma), 10 mM Tris-HCl pH 8.0, 1mM $CaCl_2$ with 0.98 mM oxidized glutathione, 0.65 mM reduced glutathione) at 0.25 ml/min with rapid stirring. The sample solution was left static at 4^{o}C for 2-3 hours. NaCl was added from 2 M stock to a final concentration of 50 mM and the mixture was left at 4^{o}C for another 2-3 hours. The solution was then dialysed into 2 L of 25mM Tris-HCl pH 7.5 using prepared dialysis membrane (Visking) or Snakeskin 3500 MWCO dialysis membrane for 16 hours at 4°C with three buffer changes.

2.3.1.4 derCD23 purification

The pH of the refolded protein sample was adjusted to 7.5 if it had not been achieved after buffer exchange. The protein sample was filtered with 0.45 µM filter (Millipore, MA, USA) and degassed. Sample was then loaded onto a 20ml HiPrep Heparin column (Amersham Biosciences, Buckingham, UK) previously equilibrated with loading buffer (25 mM Tris pH 7.5) at 2.5 ml/min using a peristaltic pump. The column was then placed onto the AKTA FPLC system and then washed with 2 column volumes (CV) of the loading buffer. Correctly folded CD23 folded protein was eluted at 3 ml/min with 3 CV of loading buffer containing 250 mM NaCl and fractions were collected and concentrations

measured using a spectophotometer. After use the column was sequentially washed with water, 2M NaCl, water and stored in 20% ethanol. Collected fractions from heparin column purification were then loaded onto a Superdex 200 or Superdex 75 gel filtration column (GE Healthcare) previously equilibrated with 20 mM Tris HCl, 400 mM NaCl, pH 6.8 over one column volume and eluted. Gel filtration was done to separate out incorrectly folded or aggregated protein as well as to remove impurities that might cause aggregation.

2.3.2 Peptide preparation

2.3.2.1 Refolding of peptides

The peptide sequence (CHSWHKNTNWPWRTLGGC) was ordered from Genscript (New Jersey, USA). Peptides containing cysteines were refolded to form disulfide bonds according to the methods by (Woo et al. 1989) with slight modification in that a volatile buffer, ammonium carbonate pH 8.5, was used. Peptide was reduced in a buffer containing DTT when necessary and diluted a hundred-fold from the reducing buffer into the refolding buffer and left stirring for 25 hours at 25^{o}C with exposure to air. At the end of refolding, the pH was slowly lowered to pH 4.0 with glacial acetic acid to prevent further disulfide exchange. Any precipitates were removed by centrifugation. The solution was then frozen at -80^{o}C and lyophilised overnight until a dry powder was obtained. When salt needed to be removed, lyophilised sample was resuspended and dialysed against water overnight using 500 Da molecular weight cut-off dialysis tubing (Spectrum Float-A-Lyzer).

2.3.3 Expression and purification of CD21 (SCR 1-2)

2.3.3.1 Expression of CD21 (SCR1-2)

BL21 (DE3) *E.coli* cells were transformed with a pET41b expression vector (Novagen) expressing the residues 2-128 of CD21. Transformed BL21 (DE3) *E.coli* cells were grown overnight at 37^0C in 5 ml LB medium containing 30 μg/ml kanamycin and diluted into 500 ml LB (30 μg/ml kanamycin), incubated at 37^oC in orbital shakers until OD_{600} = 0.6–1.0 was reached. A final concentration of 1mM IPTG was added to induce protein expression for 4-14 hours. Cells were then harvested by centrifugation at 4000 g and 4^oC for 40 minutes. The pellets were resuspended in 20 ml PBS, transferred into 50 ml Falcon tubes, centrifuged at 4500 x g for 15 minutes, the supernatant discarded and the pellets stored at –20^oC. In the case of ^{15}N-labelling of CD21 (SCR1-2), cultures were grown using the M9 minimal media with addition of 0.7 g/L $^{15}NH_4Cl$ (Spectra Media).

2.3.3.2 Washing of CD21 (SCR1-2) insoluble inclusion bodies

Frozen pellets of unlabelled or labelled CD21 (SCR1-2) were resuspended in 20 ml PBS before being homogenised at 19 kpsi (Emulsiflex-C5, Avestin). The homogenous suspension was spun at 15000 x g for 30 minutes at 4^oC. The pellet containing the inclusion bodies was washed 3–4 times in PBS 0.05 % Tween 20 (Sigma), centrifuged at 15000 x g for 30 minutes at 4^oC and the supernatant discarded. The pellet was then resuspended in 8 M urea, 1 mM EDTA, 100 mM Tris-HCl, 25 mM DTT (pH 8) and left on a roller shaker for 2 - 4 hours at room temperature. The solubilised inclusion bodies were rapidly acidified to pH 4 by adding concentrated HCl and centrifuged at 15000xg for 30 minutes at 4^oC. The supernatant, containing fully solubilised and reduced protein, was

dialysed three times against 1 L of 6 M urea, 10 mM HCl, pH 3.5 using a dialysis membrane with a 3500 Dalton molecular weight cut-off (Pierce) to remove the DTT. The dialysed protein sample was then centrifuged at 15000 x g for 30 minutes at 4^{o}C to remove any remaining insoluble matter.

2.3.3.3 Refolding of CD21 (SCR1-2)

Refolding of solubilised CD21 (SCR1-2) was carried out by drop-wise 50-fold dilution of the supernatant from the last centrifugation step into ice-cold refolding buffer (0.02 M ethanolamine, 1 mM EDTA, 0.5 M arginine, 1 mM cysteine, 2 mM cystine, pH 11) with stirring. The mixture was kept static at 4^{o}C overnight.

2.3.3.4 Purification of CD21 (SCR1-2)

The CD21 (SCR1-2) construct contains a hexahistidine tag at the C-terminus, which allows purification to be performed using a nickel-chelating column followed by a gel filtration column. Refolded protein was concentrated to approximately 50-100 ml using a Vivaflow 200, 5000 Dalton molecular weight-cut off membrane (Sartorius) and dialysed 3 times against 1 L of 20 mM sodium phosphate, 500 mM NaCl, pH 7.4, This was followed by a centrifugation step at 10000 x g for 30 minutes at 4^{o}C. The pH of the sample was checked and adjusted to 7.4 with HCl if required. The sample was then filtered through a 0.45 µm filter (Whatman) before being applied to the Nickel Chelating Sepharos Fast Flow column (GE Healthcare) , previously charged with 0.1 M $NiSO_4$ and equilibrated in 20 mM sodium phosphate, 500 mM NaCl, pH 7.4. Bound protein was eluted in a gradient over 5 CV of 0-0.5M imidazole. Fractions containing protein were pooled and dialysed 3 times against 1 L of required buffer (20 mM phosphate, 150 mM NaCl, 0.01 % NaN_3, pH 6.8 or 10 mM

HEPES, 150 mM NaCl, 4 mM $CaCl_2$, 0.01 % NaN_3, pH 6.8). Dialysed protein was further concentrated to ≤ 5 ml in a 20 ml centrifugal concentrator with a 3500 or 5000 kDa molecular weight cut-off (Sartorius) and applied to a HiLoad 26/60 Superdex 75 gel filtration column (GE Healthcare) to separate correctly folded CD21 (SCR1-2) from misfolded aggregates. Fractions containing monomeric CD21 (SCR1-2) were pooled and further concentrated.

2.3.4 Production of human C3d

2.3.4.1 Expression of C3d

BL21 (DE3) cells were transformed with the pET15b plasmid containing the C3d residues 995-1303 of human C3 with a Cys1010Ala mutation. Thus the C3d construct used contains the annotated residues 1-308 and is used throughout this thesis. For immobilisation of C3d through thiol coupling, a C3d construct was backmutated to Ala1010Cys (A17C) and purified in the same way (Martine Bomb, DPhil thesis, University of Oxford, 2008). Overnight cultures were grown in 5 ml LB with 100 µg/ml ampicillin. Then the culture was diluted 500-fold into LB in a shaker flask with 100 µg/ml ampicillin and grown until an optical density at 600 nm of 0.8-1.0 is achieved at 37^{o}C at 200 rpm agitation. Protein expression was induced with IPTG at a concentration 0.25 mM, at 16^{o}C for 20 hours for soluble cytoplasmic expression. Cells were harvested by centrifugation at 400 g for 40 minutes. Cells pellets were then resuspended in 10 mM sodium phosphate, 100 mM NaCl, and 2mM EDTA pH 7.1 and washed twice in the same buffer before storage at -20^{o}C.

2.3.4.2 Purification of recombinant C3d.

C3d purification was performed according to Nagar et al. (1998) with slight modifications. Pellets were thawed, resuspended in 10 mM sodium phosphate, 100 mM NaCl, 2 mM EDTA, pH 7.1, containing 10 X protease inhibitors (Sigma, catalogue number: P8340) before being homogenised at 19 kpsi (Emulsiflex-C5, Avestin). The homogenous suspension was spun at 15000xg for 30-60 minutes at 4^{o}C. The supernatant containing soluble C3d was collected and dialysed three times against 1 L of 20 mM sodium acetate, 20 mM NaCl, 1 mM EDTA pH 5.5 for purification by ion exchange chromatography. The dialysed protein solution was loaded onto a 20 ml CM agarose Fastflow column (GE Healthcare) previously equilibrated in dialysis buffer and washed until the absorbance at 280 nm was negligible. C3d was eluted in 100% 20 mM sodium acetate, 300 mM NaCl, 1 mM EDTA, pH 5.5. Protein fractions were pooled and dialysed three times against 1 L of 10 mM sodium phosphate, 40 mM NaCl, 2 mM EDTA, pH 7.1 and loaded onto a 20 ml Mono Q column (GE Healthcare) equilibrated in this same buffer. C3d was eluted in a 0.04–0.35 M NaCl gradient over 6 column volumes. Fractions containing protein were pooled and dialysed against 3 x 1 L 10 mM PIPES, 150 mM NaCl, pH 6.0. The dialysed sample was then concentrated to ≤ 13 ml in a 20 ml centrifugal concentrator with a 5000 or 10000 kDa molecular weight cut-off (Sartorius) and applied to a HiLoad 26/60 Superdex 75 gel filtration column (GE Healthcare). Fractions containing monomeric C3d were pooled and further concentrated and dialysed into the required buffer (20 mM phosphate, 50 mM NaCl, pH 6.8).

2.3.5 Other materials

2.3.5.1 IgE and biotinylated IgE

IgE-Fc was kindly donated by Dr Balvinder Dhaliwal and Dr Nyssa Drinkwater (King's College London (KCL)). Biotinylated IgE-Fc was kindly donated by Dr Susmita Borthakur (KCL).

2.3.5.2 Trimeric CD23

Trimeric CD23 (triCD23) was kindly donated by Wen Pin Kao at the Randall Division (KCL). TriCD23 contains an engineered, isoleucine-zipper stalk at the N-terminus of the full length CD23 (sequence: IAAIESKIAAIESKIAAIESKIAAIESKRN), which holds the three molecules together. Wen Pin Kao performed biophysical characterisation of the molecule and confirmed that the integrity of trimeric structure is stable at various pH and salt conditions (Wen Pin Kao, KCL, personal communication).

2.3.5.3 FcεRI

IgG_4 antibody fusion protein containing two α-chains of FcεRI in place of the light variable regions of the Fab was kindly donated by Dr. Balvinder Dhaliwal and Dr. Mary Holborn at the Randall Division (KCL). The α-chain of FcεRI containing a free thiol at the N-terminus was kindly donated by Dr Anthony Keeble at the Randall Division (KCL).

2.3.5.4 IDEC-152 Fab

The IDEC-152 antibody was kindly donated by Biogen IDEC (UK). Papain digestion and purification of the monomeric antigen binding fragment (Fab) was performed by Lin Dao Peng at the Randall Division (KCL).

2.4 Protein Characterisation techniques

2.4.1 Protein concentration

Protein concentration was derived by spectroscopy using a NanoDrop ND-1000 instrument (Fisher), measuring UV/visible absorption from wavelengths of 200–700 nm. Peaks at ~ 215 nm (absorption from the peptide bond) and 280 nm (absorption from tryptophan, phenylalanine and tyrosine residues) were observed. The absorption at 280 nm gives a measure of protein concentration, based on a calculated molar extinction coefficient, derived with typically 5% error, from the amino acid composition of a protein (Gill and von Hippel, 1989).

Predicted extinction coefficients, calculated using

http://us.expasy.org/tools/protparam.html, were as follows:

CD21 (SCR1-2): 27430 M^{-1} cm^{-1}
derCD23: 45430 M^{-1} cm^{-1}
triCD23: 46710 M^{-1} cm^{-1}
C3d: 45505 M^{-1} cm^{-1}.
IgE-Fc: 95,700 M^{-1} cm^{-1}

2.4.2 SDS-PAGE

Protein purity was assessed using standard SDS-PAGE techniques (Sambrook and Russell 2001). Briefly, protein samples were boiled for 5–10 minutes at 100^{o}C in SDS-PAGE loading buffer, containing 200 mM DTT for reduced samples or DTT free for non-reduced samples. They were loaded onto homemade 12.5 % or 15 % polyacrylamide gels (BioRad Mini Gel system). Low-molecular weight markers (GE Healthcare) were run alongside protein samples. Typically 5-10 µg of protein sample was loaded in a total volume of 20 µl. The gels were run in 1 x SDS-PAGE running buffer at 130 V until the dye front had passed the bottom of the stacking gel and the voltage was then increased to 150 V for

separation on the resolving gel. When the dye front reached the bottom of the plate, the gels were removed from the tank and placed into SDS PAGE gel staining solution for 3–24 hours. Gels were destained in SDS-PAGE destain solution and dried using the DryEase Mini-Gel Drying System (Invitrogen).

2.5 Biophysical experiments

2.5.1 Nuclear Magnetic Resonance

2.5.1.1 Basic Principles

NMR spectroscopy is a powerful technique that allows the determination of protein structure and dynamics in solution, at atomic resolution. NMR results from the absorption of energy by reorienting nuclei in the presence of a magnetic field. In order to be amenable to NMR studies, nuclei must be magnetically active with a non-zero spin number (I). Applying a magnetic field to these nuclei results in a splitting of the energy states of the nuclei into (2I + 1) separate energy levels. The nuclei most commonly used in biological applications of NMR, such as ^{1}H, ^{15}N, ^{13}C and ^{31}P all have a spin of I = 1⁄2, and will thus be split into 2 energy levels. At equilibrium, the populations in each state will be nearly equal. Application of an appropriate radiofrequency pulse will cause transitions between these energy levels and it is both the excitation and the subsequent relaxation to equilibrium that are exploited in the NMR experiment. In order to remove the field strength dependence from the absorption frequency, the latter is often represented as the chemical shift, expressed in parts per million (ppm). The energy difference, and consequently the population difference, between the excited and relaxed states of nuclear spins are very small, making NMR a relatively insensitive technique. Recent advances in the development of cryogenic probes, which can give a signal enhancement

of 4–16 fold over standard probes, have extended the concentration limits to the low µM rang (Medek et al., 2000). The power of NMR comes from the fact that the energy transitions between the separate states are highly sensitive to the chemical environment of the nuclei. Changes in the chemical environment of a residue in a protein, due for example to ligand binding, oligomerisation, degradation, aggregation or misfolding will lead to an alteration in the chemical shifts which can easily be monitored by NMR.

2.5.1.2 ^{1}H NMR spectroscopy to determine protein foldedness

^{1}H spectra were recorded on the refolded and purified protein samples, to check for correct folding. Typically folded proteins show good signal dispersion downfield of 8.5 ppm, indicative of amide backbone folding. Well-resolved resonances in the upfield shifted methyl peak region (between 0 and -1.0 ppm) are characteristics of a well-folded protein (Rehm et al., 2002). An unfolded protein will show poorly resolved resonances around 8.5 ppm, as this region denotes the random coiled configuration of the backbone amides (Wüthrich, 1986). NMR spectra of *E. coli* expressed and refolded derCD23 and CD21 (SCR1-2) as well as C3d are shown in Figure 2.1.

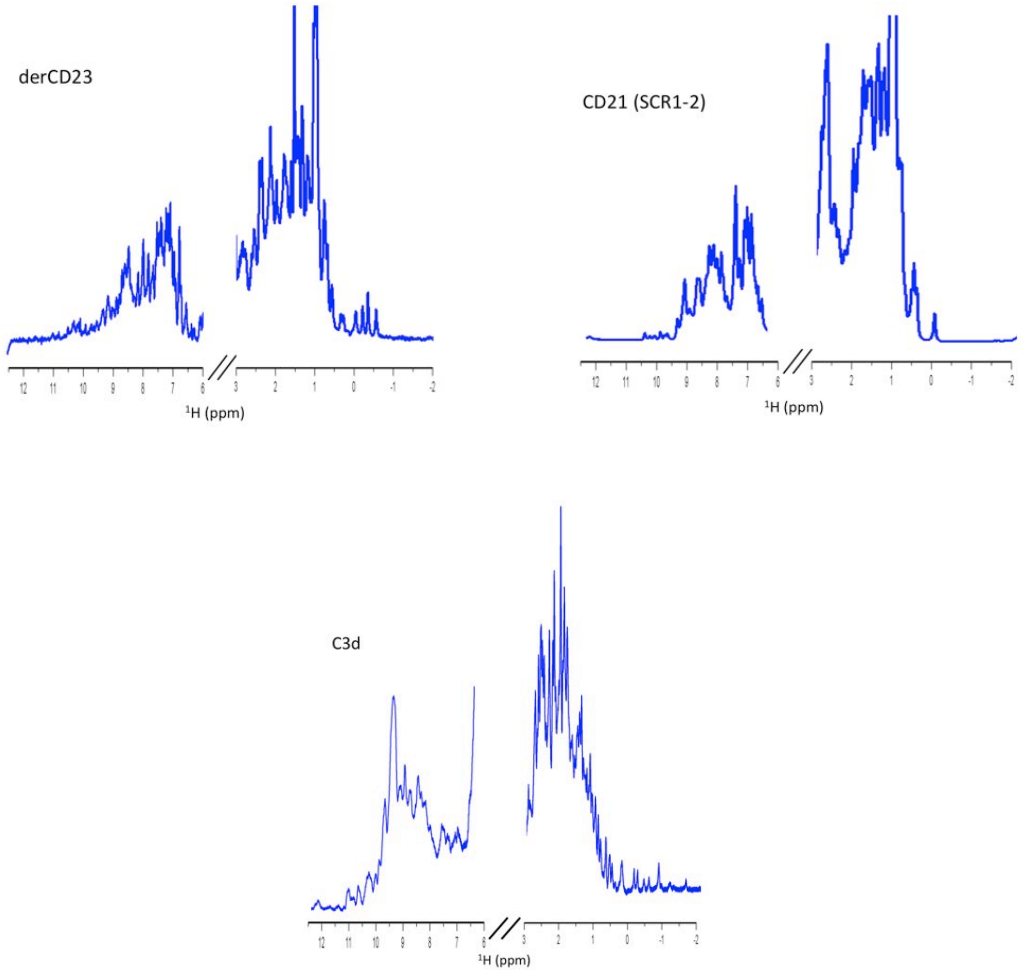

Figure 2.1: ^{1}H proton NMR spectra of refolded derCD23 and SCR (1-2) as well as C3d.
1D NMR spetrum of derCD23, CD21 (SCR 1-2) and C3d show well-dispersed resonance with distinct differences in methyl signals indicating foldedness.

2.5.1.3 NMR chemical shift perturbation mapping

To map ligand-binding interfaces by NMR, the chemical shift perturbation method is most commonly used (Clarkson and Campbell, 2003). Previously, the backbone assignments of CD21 (SCR1-2) and derCD23 have been completed by Dr Martine Bomb (Martine Bomb, DPhil Thesis, 2008) and Dr Rick Hibbert (Hibbert et al., 2005), respectively. The ^{1}H,^{15}N- Heteronuclear Single Quantum Correlation (HSQC) spectrum can be monitored for perturbation in resonance position of specific amino acids in

response to addition of unlabelled ligand. The resonances may either shift or broaden selectively upon ligand binding and these can be used to elucidate the location of the binding sites. Chemical shifts are generally represented in a weighted plot, $\sqrt{(\delta_N/5)^2 + \delta_H^2}$ where δN and δH are the induced shifts in the nitrogen and proton dimensions respectively (Clarkson and Campbell, 2003). Residues involved in binding can then be mapped onto a known protein structure. NMR titrations can also yield information about the kinetics and affinities of the monitored protein–ligand interaction. An assigned two dimensional ^{1}H,^{15}N-HSQC NMR spectrum can provide insights of the interactions of a ligand to a protein. In an HSQC spectrum, each peak is a crosspeak belonging to the hydrogen and nitrogen atom in a amide group (NH) arising from backbone amides as well as side chain amides. When the protein and ligand bind in low affinity, the bound and free states exchange quickly leading to small chemical shift differences that are averaged into a single signal and thus termed “fast exchange” and is easily traceable upon increasing concentration and hence helpful in ascertaining the sites of interactions (Figure 2.2(a))**.** In “slow exchange” where the binding affinity is high, separate signals from both states are observed which lead to a signal appearing later elsewhere on the HSQC spectrum upon the saturation of the binding site (Figure 2.2(b)). In the intermediate exchange regime, the rate of exchange occurs between the two states leading to coalescence hence no signal. The three broad kinetics observed during an NMR titration are summarised in Table 2.3.

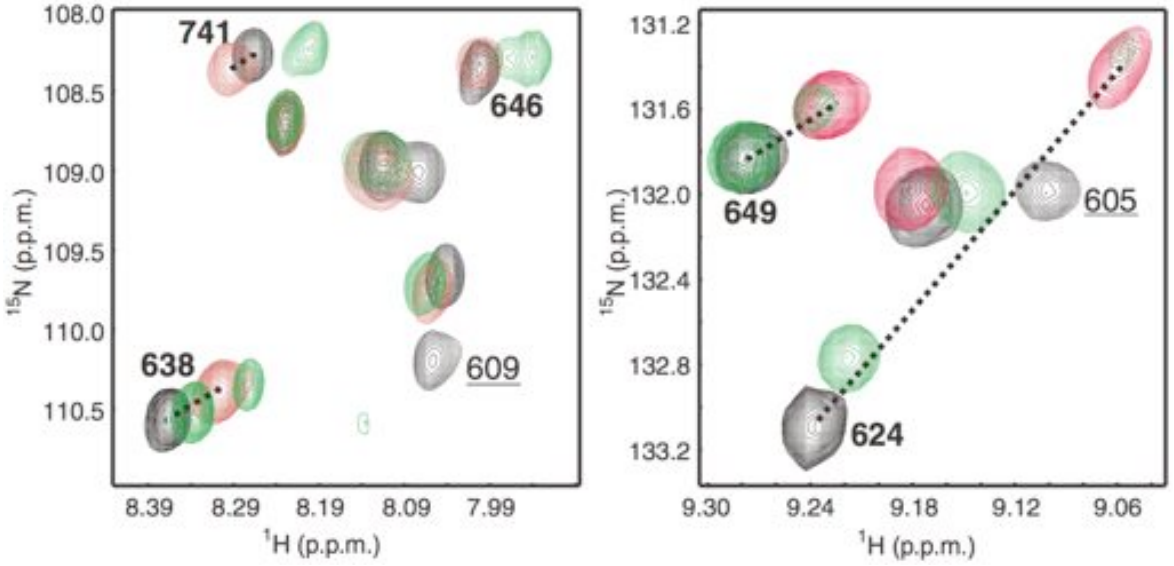

a) b)

Figure 2.2: Changes of peaks in the ^{1}H,^{15}N HSQC spectra in a titration
a) ^{1}H,^{15}N-HSQC spectrum of peaks under the "fast exchange" regime whereby peaks can be traced in a titration. b) ^{1}H,^{15}N-HSQC spectrum of peaks under the "slow exchange" regime whereby peaks appeared later and at a different position at the end of titration (black: first point, red: last point) (Figures reproduced from (Wiesner et al., 2006)).

Table 2.3: Summary of NMR kinetics and peak characteristics.

Affinity of interaction	Typically observed exchange regime	Observed shift characteristics
Weak (K_D > 10 μM)	fast	• Single set of resonances; weighted average of free and bounds shifts • Easily trackable during titration
Intermediate (100nM < K_D < 10 μM)	intermediate	• Extensive line broadening • Peaks may disappear completely • Difficult to track
Strong (K_D < 100 nM)	slow	• One set of resonances each for the free and bound state throughout titrations • Replaced by bound set • Not easily trackable

2.5.1.4 Sample preparation

Protein samples were concentrated to volumes of ~ 400 µl, supplemented with 5 % D_2O and transferred into Shigemi (Shigemi Inc.) or standard NMR tubes (Sigma). All spectra were recorded on the Bruker Cryoprobe system (Bruker) with an Oxford Instruments magnet operating at a proton frequency of 500 MHz or 700 MHz at 35^{o}C for derCD23 and 25^{o}C for CD21. The proton carrier frequency was set on water (between 7.4 and 7.8 ppm).

2.5.1.5 Data Processing

Spectra were processed using the inbuilt Bruker processing software (Bruker TopSpin). Spectral analysis was carried out using Sparky (Goddard & Kneller, UCSF).

2.5.1.6 NMR titration experiments

2.5.1.6.1 NMR titration of 12_3C peptide

^{15}N-labelled derCD23 sample samples were prepared in 25 mM Tris, 125 mM NaCl, and 4 mM $CaCl_2$, pH 6.8 with 5% D_20 at concentration of 100µM. The peptide was prepared in the same buffer and concentrated to minimise dilution effects and was titrated into a derCD23 sample in a standard NMR tube at 0:1, 0.25:1. 0.5:1, 0.75:1, 1:1 molar ratios (12_3C:^{15}N-derCD23). NMR data were collected at 35^{o}C at proton frequencies on 500 MHz Bruker instrument with cryoprobe. DerCD23 has previously been assigned by Hibbert et al. (2005) and the chemical shifts are available from the Biological Magnetic Resonance Data Bank, University of Wisconsin, USA (BioMagResBank) under the accession number 6732.

2.5.1.6.2 NMR titration of NWP tripeptide into CD23

The NWP tripeptide was obtained from Genscript and cleaned through repeated lyophilisation in water to remove trace amounts of TFA from previous HPLC purification. The peptide was then dried to powder and solubilised to 20 mM concentration in buffer to minimised dilution effect. NWP was then titrated at a concentrations of 0 μM, 100 μM, 200 μM, 300 μM, 500 μM into 200 μM ^{15}N-labelled derCD23 sample in 25 mM Tris, 125 mM NaCl, and 4 mM $CaCl_2$, pH 6.8 with 5% D_20. NMR data were collected at 35^{o}C on a 700 MHz Bruker spectrometer with cryoprobe.

2.5.1.6.3 NMR titration of IDEC-152 Fab

The IDEC-152 Fab was dialysed in 25 mM Tris, 125 mM NaCl, and 4 mM $CaCl_2$, pH 6.8 and concentrated to minimise dilution effects. IDEC-152 FAB was then titrated at a concentration of 0:1, 0.25:1. 0.5:1, 0.75:1, 1:1 molar ratio (IDEC-152 Fab: ^{15}N-derCD23) into a 100 μM ^{15}N labelled derCD23 sample. NMR data were collected at 35^{o}C on a 500 MHz Bruker spectrometer with cryoprobe.

2.5.1.6.4 NMR titrations of C3d into ^{15}N-labelled CD21

C3d samples were dialysed in 20 mM sodium phosphate at 50 mM/150/400 mM NaCl pH 7.1 and concentrated to minimise dilution effects. C3d was then titrated at 0:1, 0.25:1. 0.5:1, 0.75:1, 1:1 molar ratio (C3d:^{15}N-CD21 (SCR1-2)) into a 50 μM ^{15}N labelled CD21 sample. NMR data were collected at 25^{o}C on a 500 MHz Bruker spectrometer with cryoprobe.

2.5.2 X-ray crystallography

2.5.2.1 Basic principles of X-ray crystallography

Macromolecular X-ray crystallography is the primary technique used to solve the structures of macromolecules such as proteins. In order for a structure to be determined, a protein crystal is required. Protein crystals are required to amplify the diffraction from each individual molecule in order for data to be collected above the noise level. The requirement of protein crystal for structure determination dictates that a crystallising condition is to be found for a particular protein. Crystallisation of protein molecules occurs as a result of a controlled precipitation process, which involves an equilibration of a drop of purified protein solution with precipitating agents such as polyethylene glycol as well as other chemical component that may drive crystallisation. The conditions from which protein crystals form are unique and therefore a screening of various conditions is required. Once a condition that provides initial crystals is achieved, further optimisation is carried out by varying the components of the initially obtained condition such as pH as well as concentration of precipitants and additives. Once single or separable crystals are obtained, the crystals are then added with a cryoprotectant, typically containing small molecular weight PEGs or glycerol to prevent ice formation. The crystals were then harvested and mounted on a loop, which is then cryocooled in liquid nitrogen, and taken to a synchrontron. The crystal samples are then placed in an X-ray beam from an X-ray source at a synchrotron with appropriate wavelength to obtain diffraction patterns that can then be computationally integrated and processed to generate an electron density map using a variety of computation tools (Potterton et al., 2004). In cases where sequentially homologous structure is available, the electron density map can be fitted

into a model of the studied molecule using a molecular replacement technique which uses the phase information obtained from a previously solved homologous structure (Evans and McCoy 2007). The modelled structure is therefore visualised, refined and tested using several crystallographic computational tools available (Emsley and Cowtan, 2004). Data collection and processing were performed with the help of Dr Balvinder Dhaliwal (KCL).

2.5.2.2 Crystallisation experiments

2.5.2.2.1 Crystallisation of the derCD23/12-3C complex.

5 mg/ml (0.3mM) derCD23 was mixed with 0.75 mM 12_3C peptide in 25 mM Tris pH 6.8, 125 mM NaCl, 4 mM $CaCl_2$. A robotic pipetting instrument, the Mosquito Robot (TTP Labtech), was used to aliquot into crystallisation trays with 500 nL reservoir solution from the main commercial plates into the main subwell followed in 1:1 ratio of protein solution and reservoir solution. The commercial screening plates were SaltRx (Hampton Research), ProComplex (Qiagen), PACT suite (Qiagen), JCSG+ (Qiagen). The plates were then sealed with a clear seal and incubated at 18^{o}C.

2.5.2.2.2 Crystallisation trials of of triCD23

5 mg/ml (0.3mM) triCD23 was dialysed in 25 mM Tris pH 6.8,125 mM NaCl, 4 mM $CaCl_2$. A Mosquito Robot was used to aliquot into crystallisation trays as stated above (Section 2.5.2.2.1).

2.5.2.2.3 Crystallisation trials of the derCD23/CD21 (SCR1-2) complex

An equimolar mixture of derCD23: CD21 (0.3 mM:0.3 mM) was made in 25mM Tris, 150 mM NaCl, pH 6.8 . The Mosquito robot was used to aliquot into crystallisation trays as stated above (Section 2.5.2.2.1).

2.5.2.2.4 Crystallisation trials of the triCD23/CD21 complex

A 1: 3 molar ratio of triCD23: CD21 was made in an equimolar mixture of derCD23: CD21 (0.3 mM: 0.9 mM) was made in 25mM Tris, 150 mM NaCl, pH 6.8. The Mosquito robot was used to aliquot into crystallisation trays as stated above (Section 2.5.2.2.1).

2.5.2.2.5 Crystallisation trial for the triCD23/IgE-Fc complex

A 1:3 molar ratio of triCD23:IgE-Fc was made in an equimolar mixture of derCD23: CD21 (0.3 mM : 0.9 mM) was made in 25mM Tris, 150 mM NaCl, pH 6.8 . The Mosquito robot was used to aliquot into crystallisation trays as stated above (Section 2.5.2.2.1).

2.5.2.2.6 Crystallisation trial for triCD23/IgE-Fc/CD21 (SCR1-2) complex

A 1:3:3 molar ratio of triCD23:IgE-Fc:CD21 (SCR1-2) (0.3 mM:0.9 mM:0.9 mM) was made in 25mM Tris, 150 mM NaCl, pH 6.8. The Mosquito robot was used to aliquot into crystallisation trays as stated above (Section 2.5.2.2.1).

2.5.2.2.7 DerCD23 crystal soaking with NWP

DerCD23 crystals were grown in a crystallising solution containing 16% PEG 6000, 2% 1,6-Hexanediol, 0.1 M sodium acetate, pH 5 and 0.05 M $(NH_4)_2SO_4$. The crystal drops were soaked with 24 mM NWP in 25mM Tris, 125 mM NaCl, 4 mM $CaCl_2$ at a dilution of 1:1.

The cryoprotectant used was 32 % PEG 6000, 2% 1,6-hexanediol, 0.1 M sodium acetate pH5. 0.05 M $(NH_4)_2SO_4$ with 15% glycerol, and NWP peptide at 24 mM.

2.5.2.3 Data collection and processing

X-ray diffraction data were collected at beamline I03 at the Diamond Light Source, 360 1° oscillation images were collected with the help of Dr Balvinder Dhaliwal (King's College London). Indexing, integration and merging of data were carried out with the *HKL*2000 suite of programs (Otwinowski and Minor, 1997).

A molecular-replacement solution was found using *Phaser* (McCoy et al., 2007) part of the CCP4 suite of programs using the DerCD23 structure previously determined by Dr. Stella Fabiane (KCL) (unpublished results) as a search model with 100% sequence identity. The initial model underwent two rounds of rigid-body refinement followed by iterative cycles of refinement in *REFMAC5* (Murshudov et al., 1997) and *AutoBuster* (Bricogne et al., 2010). Manual model rebuilding with *COOT* (Emsley and Cowtan, 2004) was then performed. These steps were carried out with the help of Dr Balvinder Dhaliwal (KCL).

2.5.3 Surface Plasmon Resonance (SPR)

2.5.3.1 Basic principles of SPR

SPR is an optical technology that detects refractive index changes at the surface of a sensor chip, which consists of a thin gold film on the flat surface of a prism. The refractive index is dependent on the sample concentration at the interface, allowing binding interactions to be monitored in real time (Schasfoort, 2008). Figure 2.3 shows a schematic representation of an SPR system.

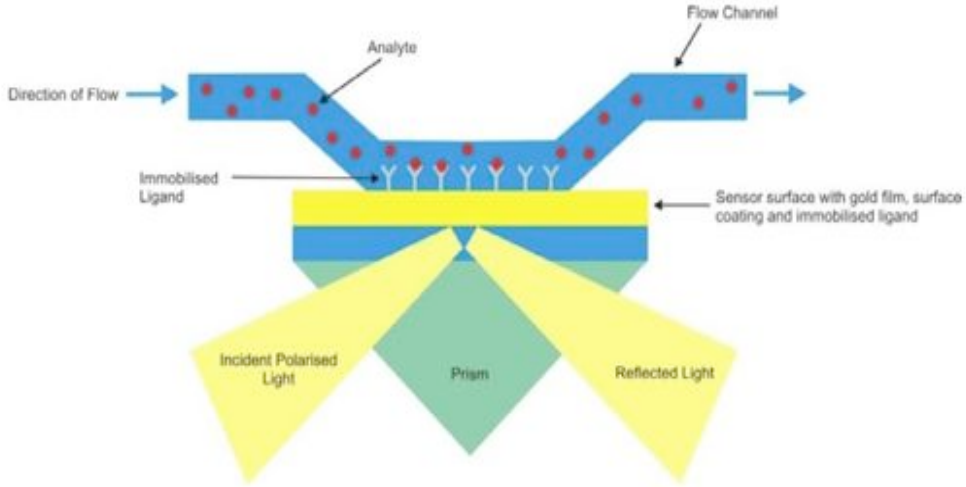

Figure 2.3: Schematic representation of an SPR system.
Ligand is immobilized on the sensor chip and the binding molecule (analyte) is flowed over the sensor in solution. The binding of the analyte to the immobilized ligand results in the refrective index which is measured in real time. Adapted from (Schasfoort, 2008)

When a beam of plane polarised light passes from material with a high refractive index into a material with a low refractive index, some light is reflected from the interface. If the angle at which the beam strikes the gold film on the surface of the prism is greater than a critical angle, the light will be totally internally reflected. However, the reflection will not be total as some of the energy is lost through interaction with oscillating plasma waves (surface plasmons) at the surface of the metal film. When the wave vector of the incident light matches the wavelength of the surface plasmons, the electrons resonate, resulting in a loss of energy and therefore a reduction in the intensity of the reflected light. Since the amplitude of the wave vector in the plane of the metallic film depends on the angle at which it strikes the interface, a surface plasmon resonance angle (θ_{spr}) exists at which the energy loss is greatest. This results in a dip in the intensity of reflected light and changes in the angle of the dip are measured in the SPR experiment. An evanescent

(decaying) electrical field associated with the plasma wave travels for a short distance (approximately 300 nm) into the medium from the metallic film. Therefore, the resonant frequency of the surface plasmon wave (and thus θ_{spr}) depends on the refractive index of the medium close to the chip surface. If the surface is immersed in an aqueous buffer (refractive index of approximately 1.0) and protein (refractive index of approximately 1.33) binds to the surface, this results in an increase in refractive index, which is detected by a shift in the θ_{spr}. The instrument uses a photo-detector array to measure very small changes in θ_{spr}. The change is quantified in resonance units or response units (RUs) with 1 RU equivalent to a shift of 10^{-4} degrees (Schasfoort 2008). The increase of signal is proportionate to the molecular weight as well as the concentration of the analyte being flowed.

2.5.3.2 Immobilisation of protein on SPR chips

2.5.3.2.1 Amine coupling of derCD23

Standard amine coupling techniques were employed (Schasfoort 2008) using an amine coupling kit provided by the manufacturer (Biacore, GE Healthcare). All immobilisation steps were carried out at a flow rate of 10 µl/min. CM4 or CM5 sensor surfaces were activated with a 50 µl pulse of EDC/NHS. Purified derCD23 was diluted to a concentration of 1 µM in 10 mM sodium acetate pH 5.0 and immobilised to the activated CM4 or CM5 sensor chip to immobilisation densities of 200–400 RU. This was followed by a 90µl pulse of ethanolamine to block all remaining activated carboxymethyl groups.

2.5.3.2.2 Streptavidin capture of biotinylated IgE-Fc

Biotinylated IgE-Fc was a kind gift from Susmita Borthakur (Department of Biochemistry, University of Oxford). Steptavidin surfaces on CM4 or CM5 sensor chips (Biacore, GE Healthcare) were prepared by standard amine coupling techniques (Section 2.8.2.1). Briefly, after EDC/NHS activation, 25 µl of streptavidin (Sigma) diluted to 1 mg/ml in 10 mM sodium acetate pH 5.0 was flowed over the sensor surfaces at 10 µl/min followed by a 90 µl pulse of ethanolamine. Biotinylated IgE-Fc in PBS was immobilised onto the avidin coated flow cell surfaces to immobilization densities of 100–800 RU (resonance units).

2.5.3.3 FcεRI capture of IgE-Fc

An IgG_4 antibody fusion protein containing two α-chains of FcεRI in place of the light variable regions (Section 2.3.5.3) was immobilized through standard amine coupling. IgE-Fc was then flowed over the surface to the desired immobilization level.

2.5.3.2.4 Immobilisation of α-Chain of FcεRI

The α-chain of FcεRI containing a free thiol group at the N-terminus was kindly donated by Dr. Anthony Keeble (KCL) and was immobilised through standard thiol coupling. Briefly, the sensor surface was activated with a 50 µl pulse of EDC/NHS and reactive disulfide groups were introduced with a 50 µl pulse of 80 mM 2-(2-pyridinyldithio)ethaneamine (PDEA) in 0.1 M sodium borate pH 8.5. The α-chain in PBS was immobilised to densities of 100–800 RU. Excess reactive groups were then deactivated with a 40 µl pulse of 50 mM cysteine, 100 mM NaCl, pH 4.0. All steps were carried out at a flow rate of 10 µl/min or the appropriate flow rate depending on the amount of sample available for each experiment.

2.5.3.2.5 Immobilisation of C3d (A17C)

C3d (A17C) contains a free thiol and was immobilised through standard thiol coupling. Briefly, the sensor surface was activated with a 50 µl pulse of EDC/NHS and reactive disulfide groups were introduced with a 50 µl pulse of 80 mM 2-(2-pyridinyldithio)ethaneamine (PDEA) in 0.1 M sodium borate pH 8.5. The C3d (A17C) was immobilised to densities of 100–800 RU. Excess reactive groups were then deactivated with a 40 µl pulse of 50 mM cysteine, 100 mM NaCl, pH 4.0.

2.5.3.3 SPR experimental set up.

All SPR experiments were carried out at 25^{o}C and a flow rate of between 15-25 µl/min based on amount and volume of protein available. The ligand contact and dissociation time varies according to the amount of material available, which is detailed in each of the results from the experiments described in the ensuing chapters.

The running buffer for the CD21 (SCR1-2)/derCD23 interaction as well as CD23/IgE-Fc and CD23/IgE-Fc/FcεRI interactions was 10 mM HEPES, 150 mM NaCl, 4 mM $CaCl_2$, 0.005 % Tween-20, pH 6.8 and 20 mM sodium phosphate, 150 mM NaCl, pH 6.8 for CD21 (SCR1-2)/C3d interactions.

Regeneration buffer used is detailed in Table 2.4. Regeneration buffer is not needed in cases where protein dissociates completely from the surface. Surface regeneration was achieved by a 30 second contact time injection of regeneration buffer, followed by a stabilisation period of 120 seconds or longer, after each analyte injection. When necessary, the injection of regeneration buffer was done twice to completely remove the bound analyte from the surface.

Analyte concentrations were injected in duplicate when sample was in sufficient amount, generally involving a titration series of "low to high" analyte concentration series. Buffer blanks were also included. SPR data was processed with the BIAevalution T100 software (Biacore, GE Healthcare) for subtracting reference curves. Curve fitting and other analysis was performed using MicroCal Origin 7.0 (OriginLab).

Table 2.4: The regeneration buffer and control surface used in SPR experiments

Analyte	Immobilised protein	Regeneration buffer	Control surface
derCD23	Biotinylated IgE-Fc through streptavidin	-	Streptavidin captured biotin
CD21	C3d A17C mutant containing a free sulfhydryl	1M NaCl	Blank flow cell (EDC/NHS activated, ethanolamine blocked)
IgE-Fc 12_3C, and NWP tripeptide IDEC-152 Fab	derCD23 /triCD23	-	Blank flow cell (EDC/NHS activated, ethanolamine blocked)
CD23 and IgE-Fc mix	IgE bound to FcεRI	20 mM glycine/HCl, pH 2.5	Amine coupled FcεRI
	IgE bound to the α-chain immobilized through thiol coupling	20 mM glycine/HCl, pH 2.5	α-chain immobilized through thiol coupling
IDEC-152-Fab	derCD23	4M $MgCl_2$	Blank flow cell (EDC/NHS activated, ethanoloamine blocked)

2.5.4 Isothermal Titration Calorimetry (ITC)

2.5.4.1 Basic principles of ITC

ITC is a calorimetric technique that measures the heat changes associated with a molecular interaction such as a protein-protein interaction. An ITC instrument consists of two identical cells, the sample and reference cells, both composed of a highly efficient

thermal conducting material. These are surrounded by an adiabatic jacket and cooled by a surrounding water bath (Figure 2.4). The system measures the time dependent input of power required to maintain equal temperatures in the sample and reference cell. Upon ligand binding, heat is either absorbed or given out by the molecules in the sample cell. The ITC instrument accordingly heats or cools the sample cell back to the reference temperature. ITC provides a direct measure of heat evolved in binding of a ligand to a target molecule. This heat is directly proportional to the amount of ligand that binds to the protein in a given injection and the binding enthalpy for the reaction (ΔH) (Van der Merwe, 2001). This technique powerful as it provides the direct measurement of the association constant, K_A, the stoichiometry, n, and the binding enthalpy, ΔH. Analysis of the data then yields values for ΔG using the following equation:

$$\Delta G = -R\,T\,\ln K_A$$

Where ΔG is the free energy of the reaction, R is the gas constant and T is the temperature of the reaction in Kelvin (K).

The entropy change ΔS of the reaction is then calculated using the standard thermodynamic expression described in the following equation:

$$\Delta G = \Delta H - T\Delta S$$

ITC provides a definite way to determine the different entropic and enthalpic contributions to the binding affinity based on equation above. These can yield important information about a given protein–protein interaction. ΔH reflects the thermal contributions of the bond formation for ligand-protein interactions relative to those existing with the solvent. On the other hand, ΔS is predominantly governed by changes in solvation entropy upon ligand binding, when water is released from the binding interface,

but also changes in conformational entropy upon binding as both interaction partners lose some degrees of freedom in the bound complex. In a typical experiment, small additions of ligand (5–15 μl) are titrated into the sample cell containing 200μl of the binding partner. The first few injections lead to a large heat signal as all ligands can be bound by the molecules in the cell. As the protein in the cell becomes saturated with ligand, the heat signal diminishes until only the background heat of dilution of the ligand is observed. To establish the heat of the dilution, an identical control experiment in which ligand is titrated into the cell containing only buffer is performed. This background heat of dilution is then subtracted from the actual ligand–protein interaction experiment.

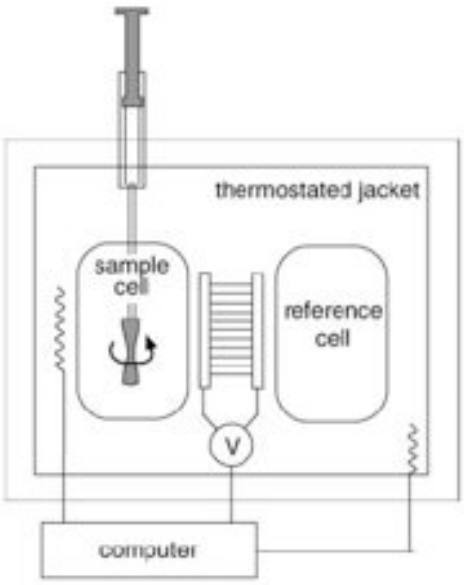

Figure 2.4: Schematic representation of an ITC instrument.

The reference cell serves as a temperature reference only and is filled with degassed ddH2O for all experiments. The injection syringe contains a small paddle at the bottom, which acts as a stirrer to ensure correct mixing of the ligand and analyte. Figure adapted from (Velázquez-Campoy et al., 2004)

The heat evolved and the binding affinity of the interaction is directly linked to the concentrations of both interaction partners used, which must therefore be established

accurately.

2.5.4.2 Experimental set up

Experiments were carried out on a VP-ITC microcalorimeter (MicroCal) at 25^{o}C. All buffers and samples were degassed at 20^{o}C for 10–20 minutes under vacuum before use. Results were analysed using the proprietary MicroCal Origin 7.0 (OriginLab) software.

2.5.5 Differential Scanning Fluorimetry (DSF)

2.5.5.1 Basic principle

Differential scanning fluorimetry is a fluorescence-based techniqued primarily developed to screen compounds and conditions that promote stabilisation of proteins for crystallisation (Niesen et al., 2007).

A dye, Sypro Orange^{TM}, that changes its chemical configuration and only fluoresces upon binding to the hydrophobic portion of a denaturing protein, provides a thermal denaturation signal measured using a quantitative PCR instrument.

Compounds or conditions that promote stabilisation of a protein will cause it to denature at a slightly higher temperature, which is shown by a shift of the melting temperature, T_m (Niesen et al., 2007). Fluorescence intensity is plotted as a function of temperature that generates a sigmoidal curve that can be described by a two-state transition (Figure 2.5) The mid-point of the transition curve T_m, is calculated using the Boltzmann equation,

$$y = \mathrm{LL} + \frac{(\mathrm{UL} - \mathrm{LL})}{1 + \exp\left(\frac{T\mathrm{m} - x}{a}\right)}$$

LL – Minumum intensity
UL – Maximum intensity
a- slope of the curve within Tm

This principle could then be exploited in screening for compounds that bind to the target protein and stabilise the protein by forming a complex and causing a shift or increase of T_m.

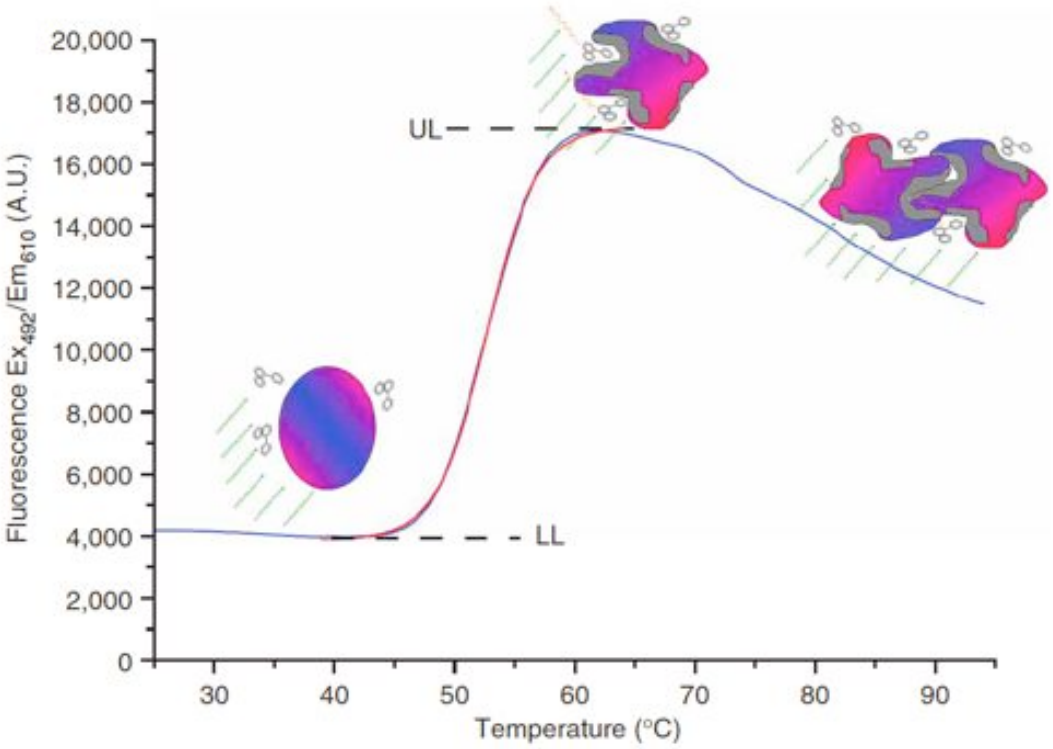

Figure 2.5: Recording of fluorescence intensity in a DSF experiment.
Typical recording of fluorescence intensity versus temperature for the unfolding of protein (citrate synthase) in the presence of SYPRO orange. The dye is symbolised as a three-ring aromatic molecule. In the presence of a folded protein, basic fluorescence intensity is excited by light of 492 nm (green arrows pointing towards the protein molecule). As the temperature increases, protein molecules begin to unfold, exposing hydrophobic patches. The dye molecules begin to bind to exposed hydrophobic patches and emit strong fluorescent light at 610 nM. The signal then begins to be reduced due to protein precipitation or aggregation. The upper and lower levels of fluorescence intensity, LL and UL as defined in the Boltzmann equation, are shown on the figure. The figure is reproduced from Niesen et al. (2007).

2.5.5.2 Experimental set up

A typical DSF experiment is performed using a 96 well PCR plates (Sigma). Individual wells were aliquoted with 15 μL protein solution containing a 1:1000 dilution of the Sypro Orange dye. For each condition or concentration a triplicate measurement is done. The plate is sealed using a clear plastic seal and centrifuged for one minute. The plate was then inserted into an Mx3005p (Stratagene) real time PCR machine using a Sypro Orange filter set up at 492 nM. Experiments were performed with a 10-minute incubation period at 25^{o}C followed by 74 cycles of temperature increment of 1^{o}C each for 90 seconds each until the maximum temperature of 99^{o}C is achieved. Data were collected from the end points of each of the cycles and plotted in Origin 7.0 (Originlab) and the data fitted using the Boltzmann equation stated above.

2.5.6 Cell culture studies

2.5.6.1 Isolation and Culture of Human B Cells

Human B cells were isolated from tonsillar tissue from donors undergoing routine tonsillectomies as described by McCloskey et al. (2007) with ethical approval from Guy's, King's and St. Thomas Hospital Trust. Tonsillar mononuclear cells were separated by density on a Ficoll gradient. B cells were then isolated using 2-aminoethylisothiouronium bromide (AET) treated sheep red blood cells. B cells were routinely >98% CD20-positive and <2% CD3-positive as determined by flow cytometry. B cells were cultured in 24-well plates (Nunc) at 0.5 × 10^6 cells/ml in RPMI 1640 (Sigma, catalogue number: R6504) which contains a defined composition of amino acids and vitamins supplemented with penicillin (100 IU/ml), streptomycin (100 μg/ml), 2 mM glutamine (Invitrogen) 10% fetal bovine serum (Hyclone, Perbio Biosciences Ltd.), transferrin (35 μg/ml), and insulin (5 μg/ml)

(Sigma). Cells were activated with 1 μg/ml anti-CD40 antibody (G28.5; ATCC) and 200 IU/ml IL-4 (R&D Systems) for up to 10 days.

2.5.6.2 Culture of 8866 cells.

The 8866 cell line expresses CD23 on the membrane and was chosen to study the inhibition of IgE binding by the peptide described in Chapter 3. The growth of 8866 cells in culture was kindly done by Clare Harper at the Randall Division (KCL). The 8866 cells were cultured from a frozen stock with RPMI-1640 supplemented with 2 mM L-glutamine (Invitrogen), 10% Fetal Calf Serum (Hyclone, Perbio Biosciences Ltd.) and penicillin (100 IU/ml), streptomycin (100 μg/ml). Cells were grown to about 10 x 10^3 cells/ml at 37^{o}C and 5% CO_2. 1ml of the cells were aliquoted into FACS tube and washed twice with PBS and centrifuged at 4000 rpm for 5 minutes and resuspended with 0.5 ml PBS into five separate tubes with one of them as the negative control with no IgE-GFP staining.

2.5.6.3 Enzyme linked immunoassay (ELISA)

An ELISA was performed to measure the quantity of IgE expressed by IgE-positive B-cells treated with the peptide described in Chapter 3. Maxisorp plates (Nalge Europe Ltd.) were coated with polyclonal mouse anti-human IgE (DakoCytomation) diluted 1:7000 in carbonate buffer, pH 9.8, for 16 h at 4^{o}C. Unbound sites were then blocked with 2% (w/v) Marvel skimmed milk powder in PBS with 0.05%, Tween (PBS-T) for 30 min at room temperature. Samples were added at appropriate dilutions to ensure that at least three readings were within the linear portion of the standard curve, and the plates were incubated for 16 h at 4^{o}C; NIP-IgE (JW8/5/13; ECACC, UK) was used to construct a standard curve. IgE binding was detected by mouse anti-human IgE conjugated to

horseradish peroxidase (DakoCytomation) diluted 1:1000 in 1% Marvel PBS-T for 4 h at room temperature. The colour reaction was developed with OPD (Sigma). The sensitivity of the assay was 10 ng/ml.

Chapter 3

Characterisation of a peptide that binds to CD23 and inhibits IgE binding discovered through phage display.

3.1 Introduction

Blocking IgE binding to CD23 is a potential target for inhibiting CD23-mediated IgE dependent allergy, and inhibitors such as Lumiluximab, an anti-CD23 monoclonal antibody, has been shown to be effective in clinical trials for chronic lymphocytic leukemia (Rosenwasser and Meng 2005) as well as in allergy (Rosenwasser et al. 2003).

A recent work also showed that a CD23-binding phage display derived peptide (FHENWPS) could alleviate symptoms of CD23 mediated arthritis in humans and in animal models (Rambert et al., 2009). Inhibition of the interaction between CD23 and IgE is a potential target for therapeutic intervention because it is involved in the modulation of IgE levels as well as other processes including facilitated antigen presentation as well as CD23 mediated transcytosis. This chapter describes the efforts to analyse a CD23-binding peptide and characterise its structural and biophysical properties and its therapeutic potential.

3.2 Phage display derivation of derCD23 binding peptides

Previously, Dr. Ho An Chen (Department of Biochemistry, University of Oxford) performed a screening of phage display libraries (Pasqualini et al., 1995) for peptides binding to derCD23. DerCD23 protein was immobilized on an ELISA plate surface and a library of phage, each displaying a single and different peptide sequence, was exposed to the surface. A biopanning and clonal amplification procedure was repeated several times and the final individual clones were then sequenced. Several peptide sequences were excluded due to high level of calculated hydrophobicity which would not be soluble under physiological conditions out of which five were selected and share a consensus 'NWP' motif (Table 3.1).

Table 3.1: Phage display derived peptide sequence

7_1	FHENWPS
7_1 C	CHSFHENWPSGGC
C7C_conc	ACWHTNWPSC
C7C_1	CWHPWHKKC
12_3C	CHSWHKNTNWPWRTLGGC

3.3 Confirmation of disulfide folding through mass spectroscopy

Circularisation of peptides is a method that has been established to increase stability and solubility of therapeutic peptides (Gallop et al., 1994). The 12_3C peptide was therefore subjected to refolding through oxidation as described in Chapter 2. Mass spectrometry was used to confirm that the peptide had been refolded properly through formation of a disulfide bond between the cysteine residues at the termini. The calculated size of a linear peptide from the Protparam program on ExPASY is 2183.4. Mass spectrometry performed on the circularised peptide indicates a dominant population of the molecule

with the size of 2181.3 Da; this is 2 Da less than the theoretical mass, and is consistent with the loss of two hydrogens resulting from the formation of a disulfide bond (Figure 3.1).

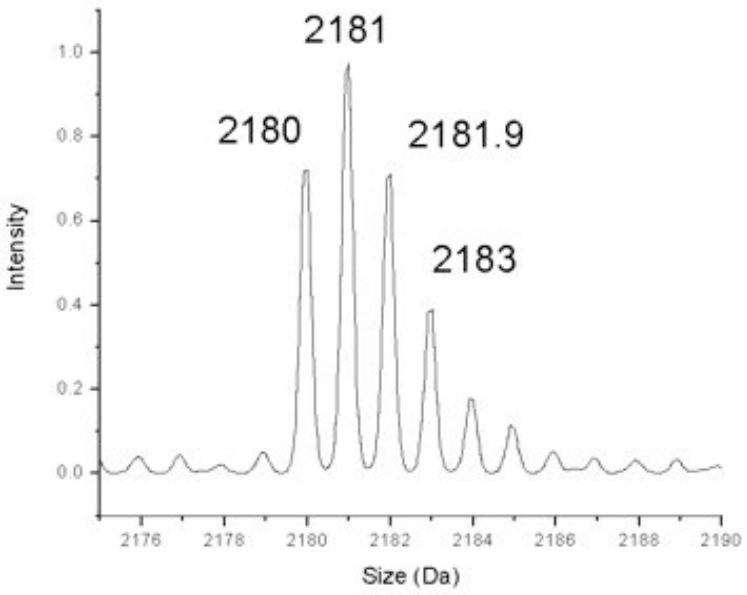

Figure 3.1. Mass spectrum indicating size of the refolded 12_3C peptide.
The chromatogram indicates that the circular peptide is the predominant species and the mass has been reduced by 2 Da to 2181.3 compared to the theoretical mass of linear 12_3C at 2183.4 Da.

3.4 Biophysical analysis

3.4.1 Binding of 12_3C on derCD23

DerCD23 was first immobilized onto a CM4 SPR chip to a density of 100RU. As a positive control, IgE was injected over the sensor chip to check the activity of derCD23 on the chip (Figure 3.3 (a)), confirming the immobilised CD23 is active. A binding experiment was performed over a range of 12_3C concentrations (Figure 4.3 (b)). The binding sensorgram shows fast on-rates and fast off-rates. The binding curves were then fitted to a Langmuir plot assuming a 1:1 binding model (Figure 3.2 (c)) and a K_D of 7.0 ± 0.1 µM was obtained

using Origin 7.0 software. The K_D obtained for this peptide is close to those obtained previously for CD23 binding to IgE and CD21 at 1.3 ± 0.3 µM and 0.87 ± 0.09 µM, respectively (Hibbert et al., 2005).

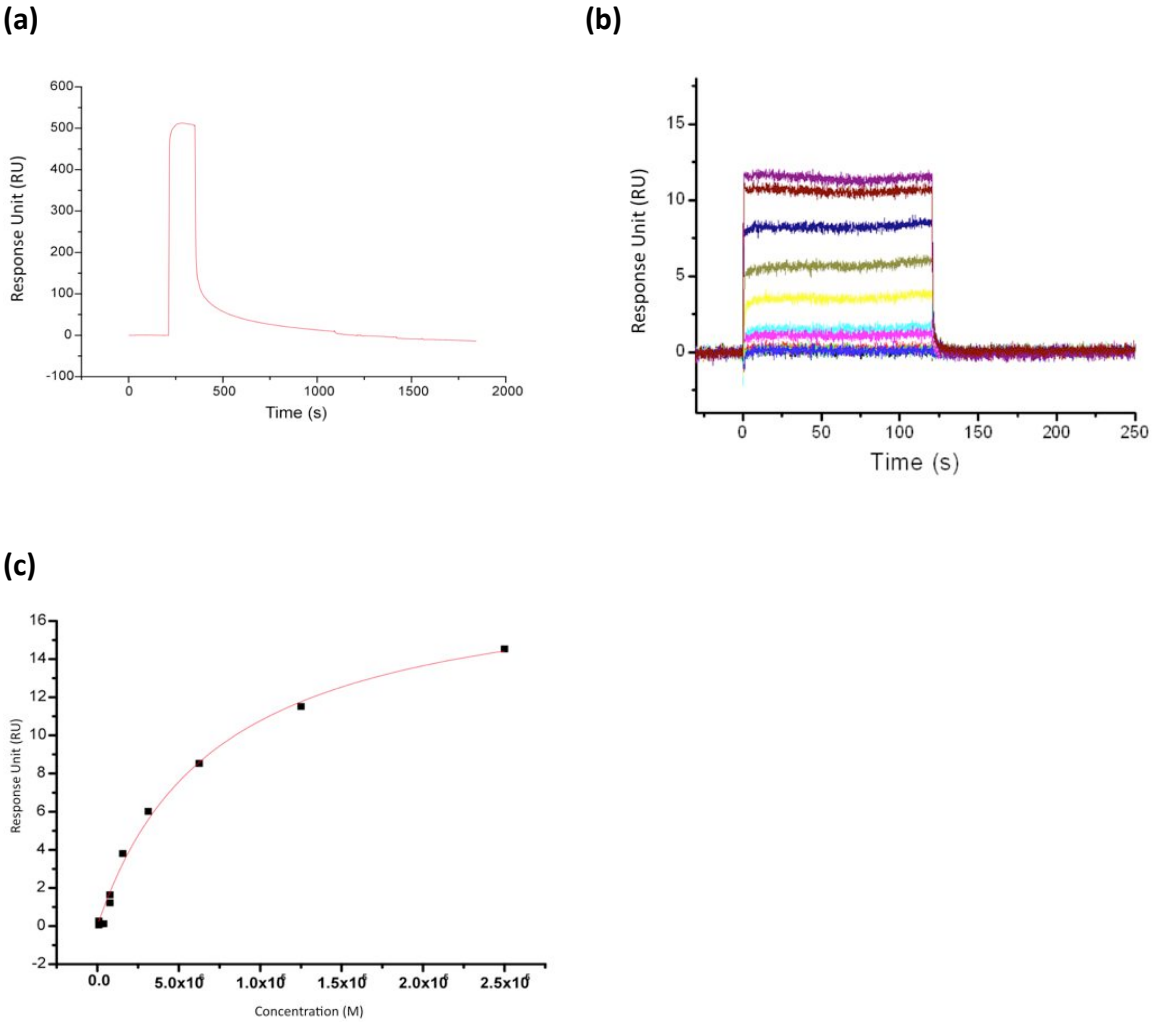

Figure 3.2: The binding of 12_3C peptide to derCD23
(a) IgE binding to CD23 as control, (b) sensorgram of 12_3C at concentrations 0.0977 µM, 0.0195 µM, 0.39µM, 0.78µM, 1.5625µM, 3.125µM, 6.25µM, 12.5µM and 25µM binding to CD23 (c) 1:1 fit of 12_3C binding to CD23.

3.4.2 Thermodynamic analysis of 12_3C binding to derCD23

An SPR thermodynamic experiment was done over a range of temperatures (5°C, 15°C, 25°C and 35°C) in order to derive the thermodynamic parameters of binding. The binding

energy calculated shows a favourable reaction with a negative enthalpy, ΔG value of –29.4. The enthalpy ΔH is –36.5 ± 7 kJ/mol indicating an exothermic reaction, while the TΔS is –11.4 kJ/mol, indicating an unfavourable entropic contribution toward binding (Figure 3.3).

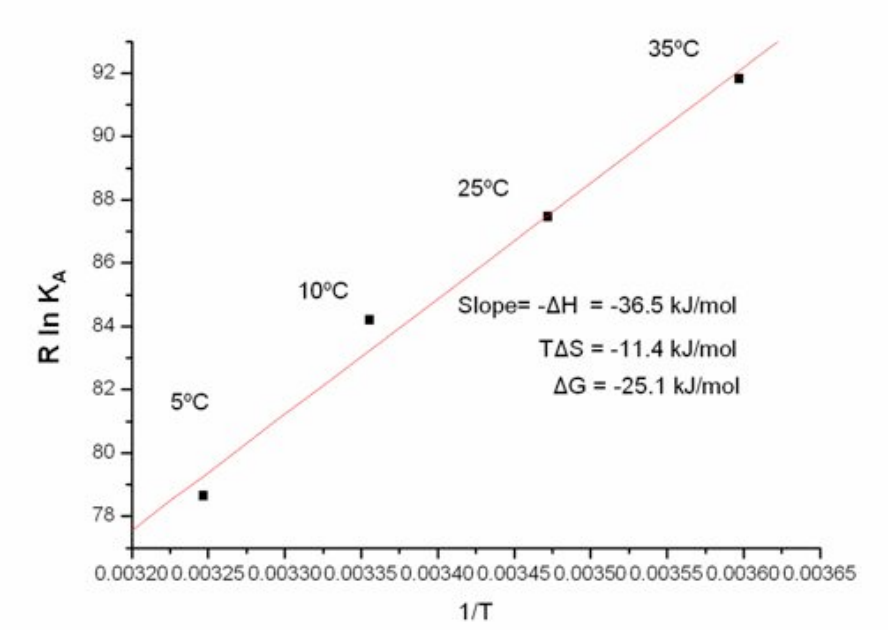

Figure 3.3: Sensorgram of 12-3C binding to CD23 chip at different temperatures: 5°C, 10°C, 25°C and 35°C. The thermodynamic values obtained were ΔG= -29.4 kJ/mol, ΔH = -36.5 kJ/mol and TΔS= -11.4 kJ/mol.

3.4.3 Inhibition of IgE binding to CD23

To test for Inhibition of IgE binding, a mixture of IgE-Fc (at constant concentration of 1 μM) and increasing concentrations of 12_3C was flowed over the CD23 surface. The sensorgram shows that the peptide reduces the amount of IgE-Fc binding. The data was then fitted into a Langmuir curve and a K_i of about 20 μM was obtained (Figure 3.4). This therefore confirms that 12_3C is a competitive inhibitor of the CD23/IgE interaction.

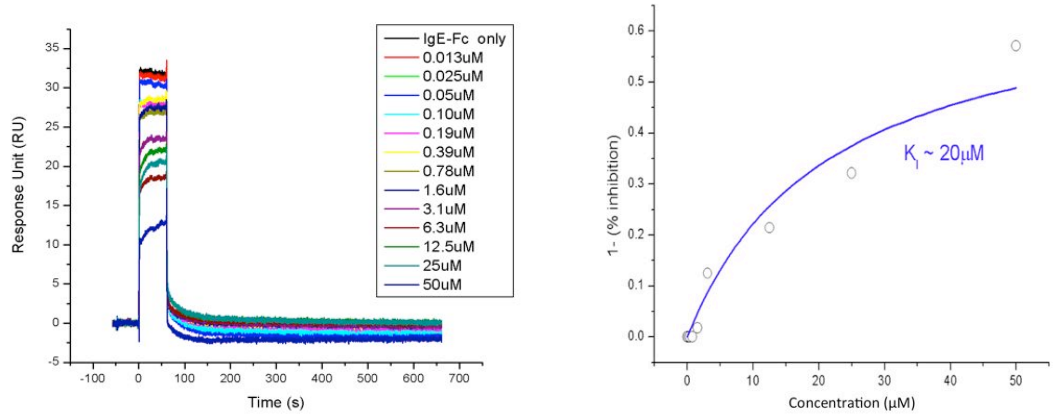

Figure 3.4: Competitive inhibition of IgE binding to CD23 by 12_3C.
Increasing concentrations of peptide (0-50 μM) with constant IgE (1 μM) concentration was flowed over the CD23 surface and binding of IgE was reduced with a K_i of approximately 20 μM.

3.4.4 Comparison of binding with linear 12_3C and NWP

3.4.4.1 Binding of the linear 12_3Cx

To determine whether cyclisation of the peptide improved binding, a linear version of 12_3C was obtained termed 12_3Cx. A slight modification is included in that cysteines residues at both N- and C-terminus of the peptide are replaced with alanine residues to prevent spontaneous disulfide bond formation (sequence=AHSWHKNTNWPWRTLGGA). 12_3Cx was then flowed onto the CD23 surface and a K_D of 560 μM was obtained (Figure 3.5); this is an affinity about 80 times lower than the K_D of 12_3C (7.0 μM). One explanation for this would be that a linear peptide may have a substantial entropic penalty in its binding, given that it would be more flexible during binding compared to a more rigid cyclic peptide.

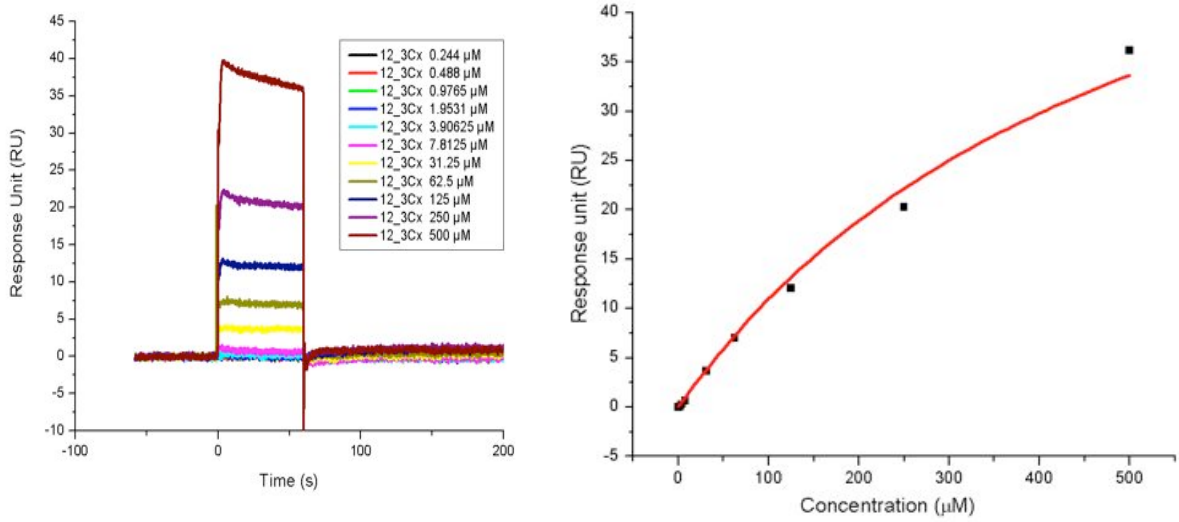

Figure 3.5: The sensorgram of 12_3Cx binding to immobilised derCD23.
The data was fitted into a Langmuir Curve using Origin 7.0 and a K_D of 560µM was obtained.

3.4.4.2 Binding of the NWP tripeptide

Most of the peptides derived through phage display in this study share the similar consensus sequence "NWP". Therefore it was speculated that this motif was the minimal sequence that still retains binding to derCD23 and could be used a basis for the development of small molecules that bind to CD23. To test for binding, an NWP tripeptide was flowed at increasing concentrations (0-4mM) over the immobilised derCD23 on an SPR chip (Figure 3.6). A K_D of 1.2 mM is obtained which is much weaker binding than either 12_3C or 12_3Cx. However this confirms that NWP retains CD23-binding activity and the extension of the tripeptide within the flanking sequence may be required for the higher affinity binding seen in 12_3C.

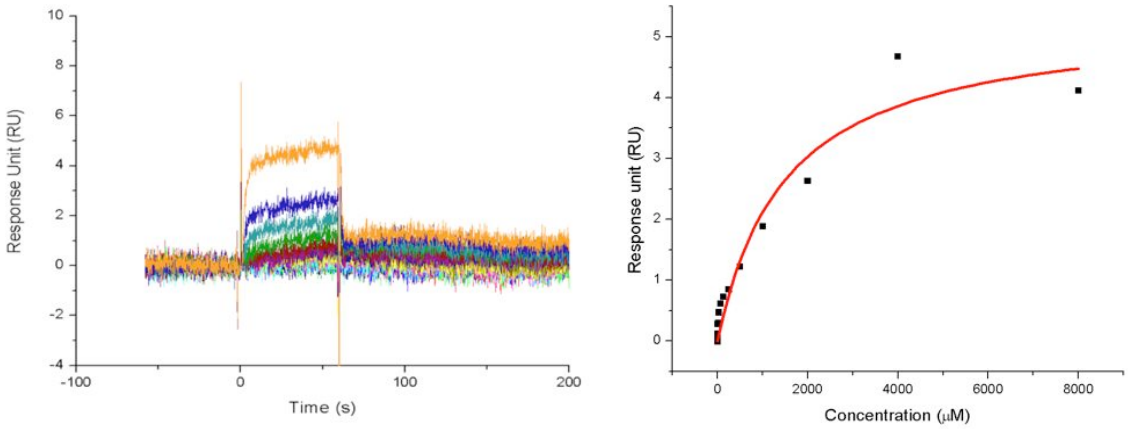

Figure 3.6: Binding of NWP tripeptide to derCD23.
Data was fitted into a Langmuir Curve using Origin 7.0 and a K_D of 1.2 mM was obtained.

3.4.4.4 Binding of NWP to CD23 as shown by DSF

Differential scanning fluorimetry is a useful method that was developed to identify buffer conditions and additives that lead to a stabilisation of protein molecules, especially in crystallisation efforts (Niesen et al., 2007). However this assay can also be used to screen for potential compounds that bind to a protein target (Lo, 2004). The basis is that compounds that bind to a protein will stabilise it and therefore will lead to an increase of melting temperature, $T_{m,}$ of a target protein. As discussed in Chapter 3, a condition by which derCD23 can be observed in DSF experiments had been established. These conditions take into consideration the minimal of amount of derCD23 required to give an observable signal. In this experiment 10 μM derCD23 was added to 1 mM DTT and a 1:1000 dilution of Sypro Orange and aliquoted in triplicates into a 96 well PCR plate. The NWP tripeptide at concentration of 1mm and 2mM was added to another two sets of triplicates as well as a triplicate containing NWP and Sypro Orange dye only. As shown in Figure 3.7, derCD23 gives a considerable dye signal and Tm of 65^{o}C. Addition of 1mM NWP and 2 mm NWP increases the T_m of derCD23 to 71^{o}C and 80^{o}C whereas NWP and

the Sypro Orange alone itself did not give any signal, signifying that NWP does not interact with the Sypro Orange dye to give any detectable signal. The reduction of signal intensity with the addition of NWP may be perhaps be explained by the possibility of NWP competing for derCD23 binding with Sypro Orange and thus leading to reduction of signal. However it can be seen that the derCD23 melting temperature is increased, which leads to the higher temperature required for the denaturation of derCD23 in the presence of NWP. One of the applications of this result is that NWP can be used a positive control in future drug screening for derCD23 binders using this assay.

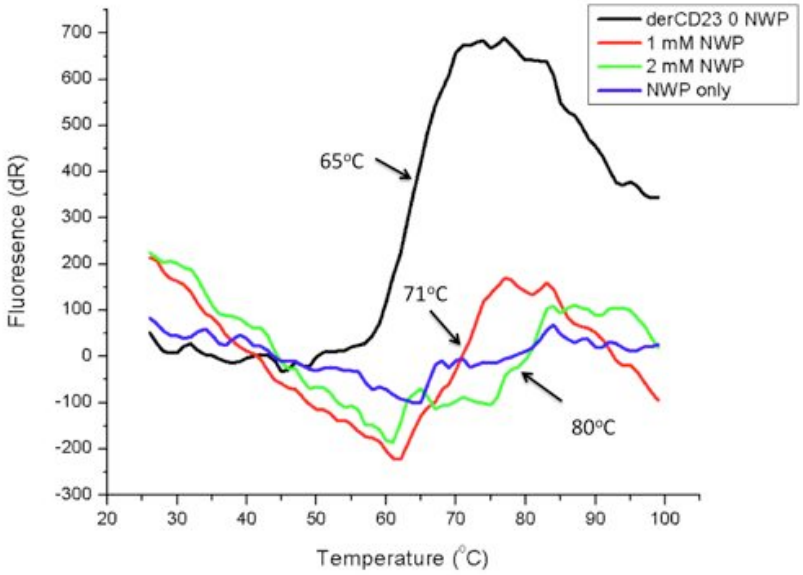

Figure 3.7: DSF profile shows the signal obtained for derCD23, derCD23 + 1mM NWP, derCD23+ 2mM NWP and NWP only.
The T_m values were 65°C, 71°C and 80°C each. Determination of Tm was done by fitting the curve using a fit of a Boltzmann function on the Origin 7.0 software (Originlab Corporation, Northampton MA, USA).

3.4.5 Binding sites of 12_3C and NWP on CD23 as shown by NMR spectroscopy

3.4.5.1 NMR titration of 12_3C binding to ^{15}N-labelled derCD23

The NMR spectrum of derCD23 used in this study has been previously assigned by Hibbert et al. (2005). In the two dimensional ^{1}H,^{15}N-HSQC spectrum each peak corresponds to a single residue. The assignment of these peaks facilitate tracking of residues on derCD23 affected by the binding of an added ligand. This is a very powerful technique to ascertain specific interaction sites on a protein in solution.

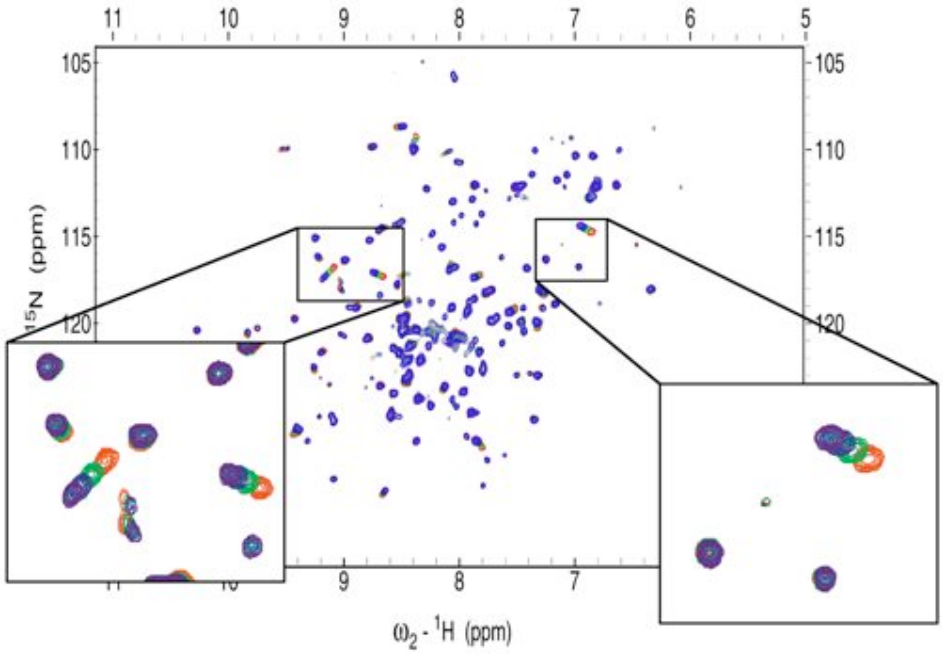

Figure 3.8: ^{1}H,^{15}N-HSQC spectrum of derCD23 titrated with 12_3C peptide.
Insets show specific perturbations on involved residues.

Figure 3.8 shows significant perturbations in a small number of specific peaks upon addition of 12_3C, which indicates that the peptide did not lead to overall structure changes of CD23 but affected only certain specific residues in derCD23. Perturbations were categorised as “fast exchange”. In the “fast exchange” interaction regime, the

association and dissociation events occur quickly relative to the NMR timescale and when both signals are averaged only a single average signal can be detected, which is indicated by a single peak. Upon titration of increasing concentrations of ligand, the affected residue will experience more changes in chemical shift, reflecting the degree of saturation of the bound state.

12_3C was titrated at increasing concentrations of 0 µM, 41.5µM, 83µM, 124.5µM and 166µM (0:1,0.25:1,0.5:1,0.75:1,1:1 molar ratio) into the obtained concentration amount of ^{15}N-labelled derCD23. Two distinctive categories of peak perturbations were identified. A group of perturbed peaks corresponding to the residues Val235, Leu226, Glu231, Lys229, Gly230, Asp344, and Leu277 showed significant chemical shift perturbations upon addition of 12_3C. When mapped on to the surface of the derCD23 structure they revealed a pattern, which defines the site of interaction of the 12_3C peptide on derCD23; this binding site overlaps with the IgE binding site (Figure 3.9).

Additionally, a group of chemical shift perturbations are mapped and were identical to the pattern of peaks previously identified as being involved in derCD23 trimerisation, as defined by Hibbert et al. (2005). These areas are the negative and positively charged patches on the opposite sides of the lectin domain that form the trimeric structure through electrostatic interactions. Perturbed residues Gln225, Val310, Tyr242 are close to the negatively charged patch residues on derCD23, whereas the positively charged residues Phe209, Lys212 and His213 that perturbed overlap with the positively charged patch on derCD23 previously implicated in trimerisation (Figure 3.10).

(a)

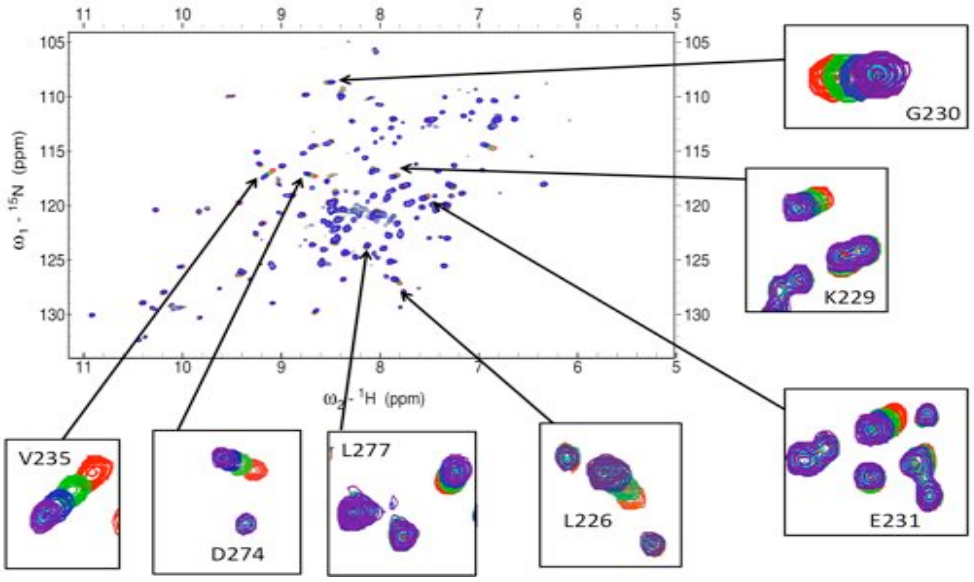

(b)

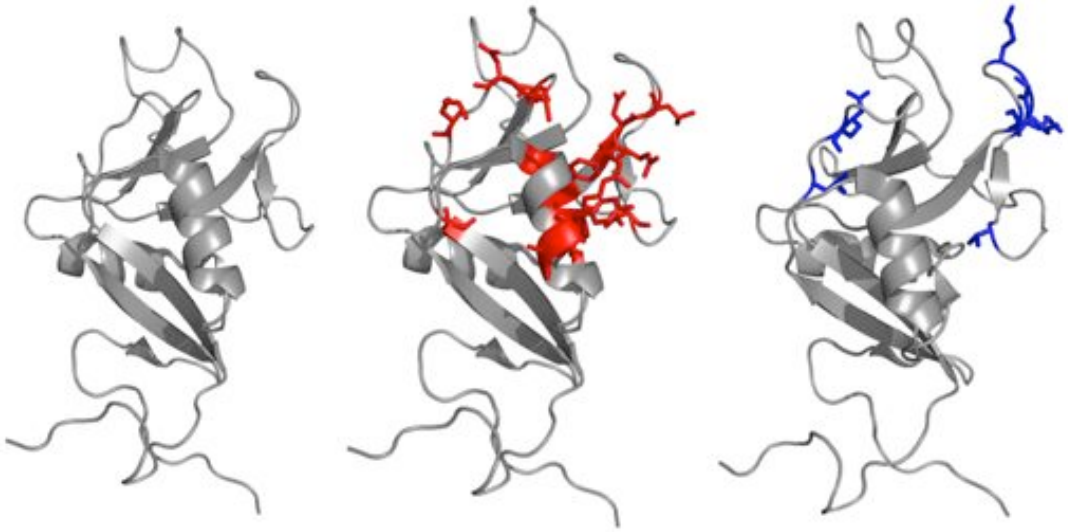

derCD23 | IgE binding sites on derCD23 (as defined by Hibbert et al. (2005)) | Residues that show perturbations upon addition of 12_3C

Figure 3.9: NMR-based mapping of 12_3C binding site.
The ^{1}H,^{15}N-HSQC spectra show perturbations in residues Val235, Leu226, Glu231, Lys229, Gly230, Asp274, Leu277 (a) that overlap with the IgE binding site (b). The previously determined IgE binding site by Hibbert et al. (2005) is highlighted in red and the binding site of the 12_3C peptide is highlighted in blue.

(a)

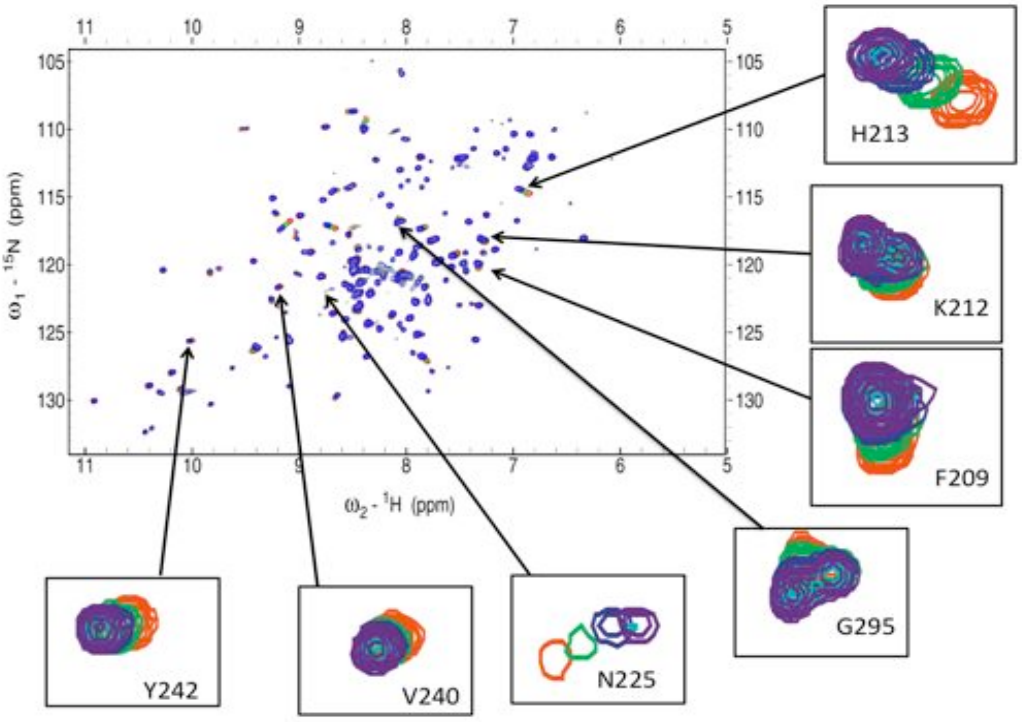

(b)

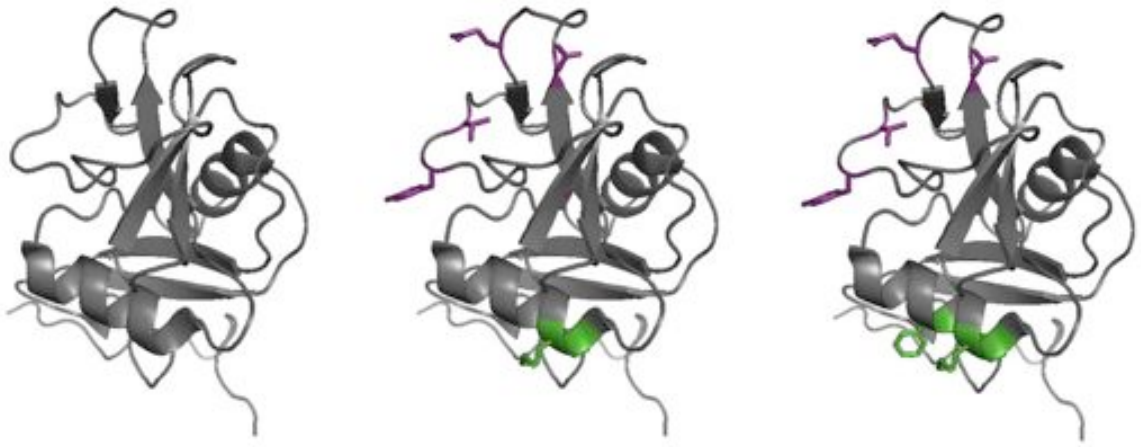

Top view of derCD23

Residues involved in trimerisation (as defined by Hibbert et al. (2005))

Residues that show perturbation upon addition of 12_3C

Figure 3.10: Residues involved in CD23 trimerisation.
The ^{1}H,^{15}N-HSQC spectra show affected residues Phe209, Lys212, His213, Gln225, Val240, Tyr242, and Gly295 (a). Residues F209, K212 and H213 overlapped with the positively charged residues previously implicated in trimerisation. When all these residues are mapped on the CD23 surface it reveals a pattern almost similar to the trimerisation peaks as shown in the far right picture of panel (b). Positively and negatively charged residues are highlighted in green and purple respectively.

3.4.5.2 NMR titration of NWP tripeptide to ^{15}N-labelled CD23

A sample of ^{15}N-labelled derCD23 at a concentration of 200 µM was titrated with the NWP tripeptide to determine whether NWP binds to similar residues as the full-length 12_3C peptide. From the experimental data, the residues implicated are similar (Figure 3.11 and 3.12). These indicate that the NWP motif is the main site for binding to derCD23 and the remaining flanking sequence in the 12_3C may be required for stabilising the interaction and increasing the affinity of the interaction.

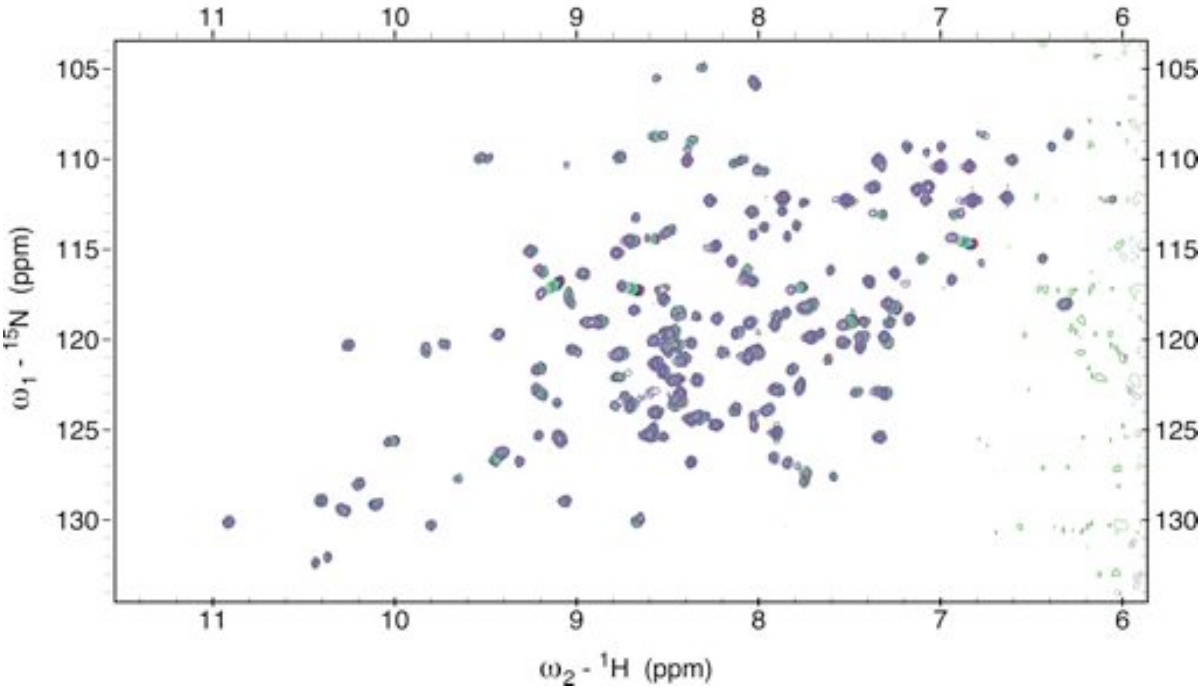

Figure 3.11: The NMR spectrum of ^{15}N-labelled derCD23 titrated with NWP tripeptide.

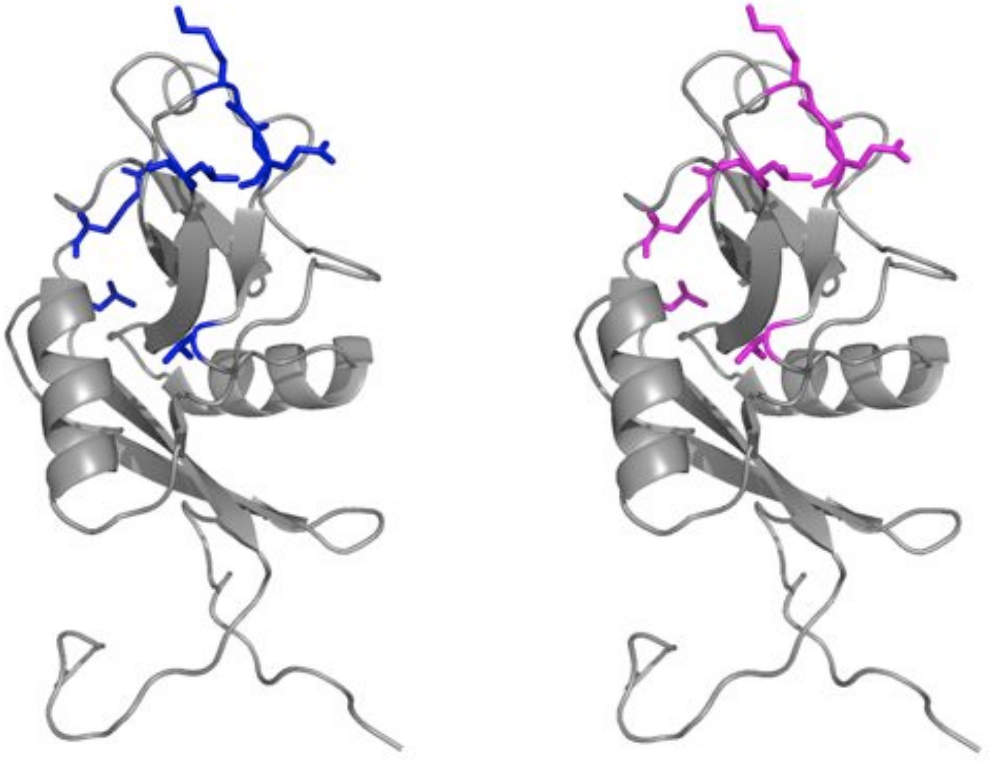

12_3C binding site NWP binding site

Figure 3.12: Comparison between the binding sites of 12_3C and NWP on derCD23.
The NWP peptide (right) binds to derCD23 to a similar site as the full-length 12_3C with essentially identical implicated residues Val235, Leu226, Glu231, Lys229, Gly230, Asp274 and Leu277.

3.5 Reduction of IgE expression by 12_3C in primary B cell culture

Primary B cells were obtained with consent from tonsils of children that underwent tonsillectomies at Evelina Children's Hospital at St Thomas'. B-cells were purified and cultured with IL-10, IL4 and anti-CD40 to induce IgE class switching. 12_3C was added at concentration of 0 μM 1μM, 10 μM and 100μM. Supernatants were collected at days 2, 7 and 14. ELISA measurements were done on the supernatant. The data below shows a reduction in IgE levels in the supernatant sample at day 7 and day 14 in a manner dependent on 12_3C concentration.

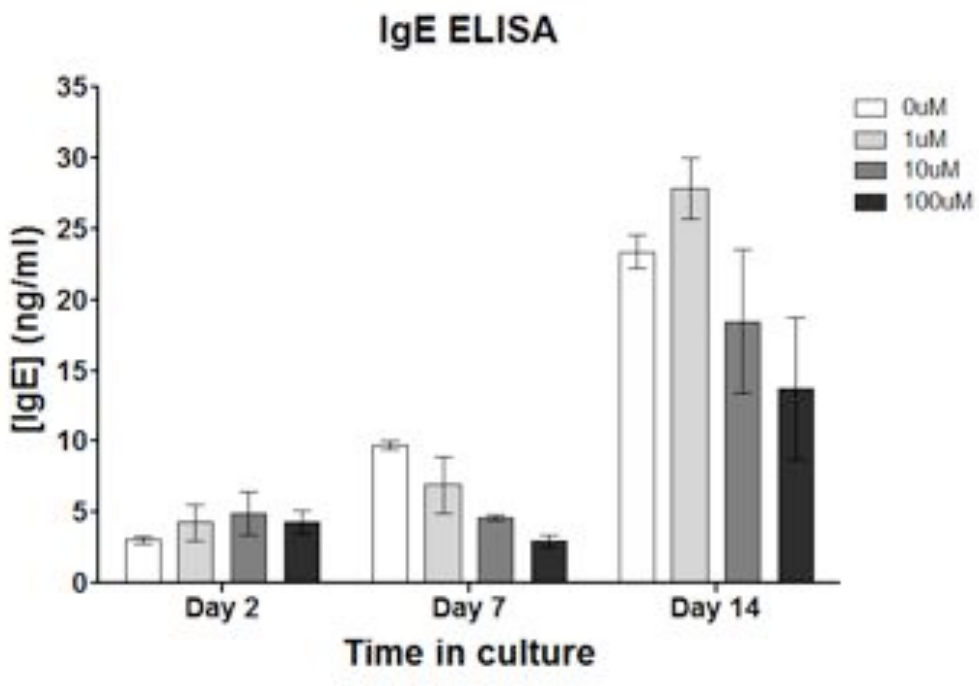

Figure 3.13: Measurement of IgE level in B cell culture with addition of the 12_3C peptide.
ELISA experiments indicate that the 12_3C peptide led to a reduction of IgE levels. In Day 7, B cells begin switch to produce IgE. Reduction of IgE levels is seen in Day 7 as well as Day 14 in a concentration dependent manner.

3.6 Inhibition of IgE binding on CD23 expressing 8866 cells

8866 cells were originally isolated from the peripheral blood of a 51-year-old American woman with chronic myelogenous leukemia (Rogentine and Gerber, 1969). The B-lymphoid cell line expresses a relatively high amount of calcitonin receptors, membrane bound immunoglobulin and CD23 (Sarfati et al., 1984).

The interaction between CD23 and IgE has been established by SPR to have the "fast-on/fast-off" kinetics. Therefore an IgE-GFP fusion protein also is likely to bind to CD23 on the surface of 8866 cells with the same kinetics. IgE-GFP was kindly donated by Wen Pin Kao (KCL). The two groups of samples were prepared as described in Section 2.5.6.2. To both groups, a final concentration of 2 µM of IgE-GFP and a final concentration of 10 µM of 12_3C were added and incubated for an hour on ice. The first group of samples was not washed while the second group of samples was washed with PBS twice, centrifuged and resuspended in 0.5 ml PBS. A negative control containing only cells was also incorporated in the experiment. All the samples were then subjected to flow cytometry measurements using a Beckton Dickinson FACScalibur instrument and data were analysed using the software FloJo with the help of Dr Phillip Hobson at the Randall Division (KCL).

All the sample cells were evenly distributed to ~10,000 cells in each tube. From the flow cytometry analysis it is shown that IgE-GFP can be used to detect binding to surface CD23 on the 8866 cells. It was initially a matter of concern that IgE-GFP may dissociate too fast from the cells which would otherwise make 8866 cell staining unfeasible using IgE-GFP. However it was shown that 8866 cells can be stained with IgE-GFP, although a final washing step reduced the amount of IgE-GFP intensity on the cells. Previously, it was

established that the affinity of CD23-12_3C to be ~7 µM. Therefore a single concentration slightly higher than the K_D value at 10 µM was chosen to test for the ability of the peptide to inhibit IgE from binding to membrane CD23. Figures 3.14 (a) and 3.14 (b) show that 12_3C reduces IgE-GFP staining by an order of magnitude, which indicates the ability of 12_3C to inhibit IgE binding to cell surface CD23.

(a) Unwashed

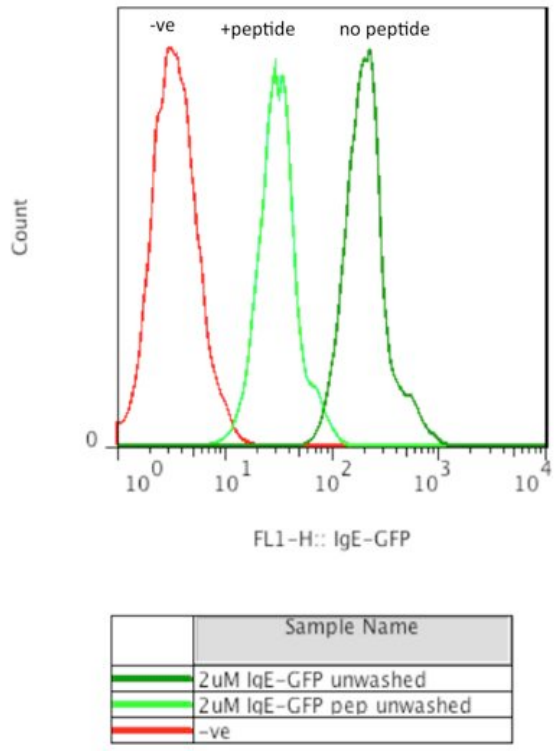

Histogram of cell counts of negative staining, and cells with and without and 10 µM 12_3C added with 2 µM IgE-GFP each without washing.

(b) Washed with 2x PBS

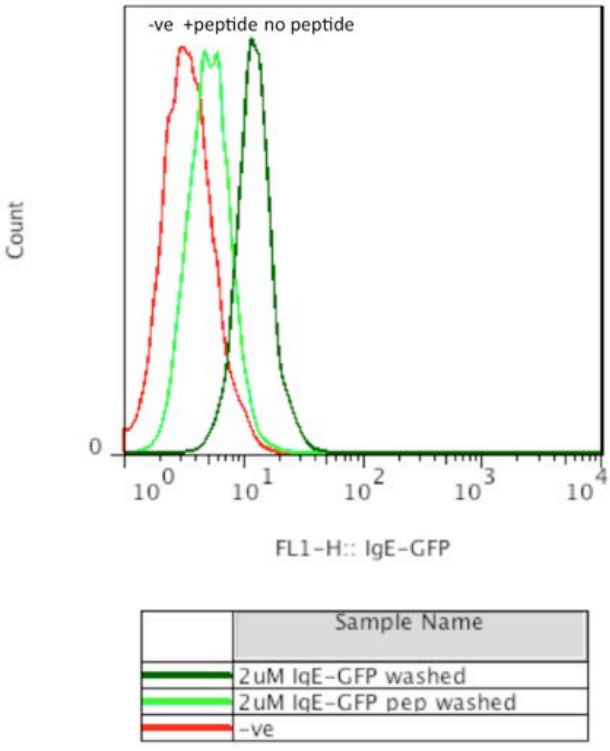

Histogram of cell counts of negative staining, and cells with and without 10 µM 12_3C added with 2 µM IgE-GFP each with washing.

Figure 3.14: The inhibition of IgE-GFP binding to CD23 expressing 8866 cells.

3.7 Crystallisation of derCD23- 12_3C and its derivatives

Crystallisation of derCD23 in complex with the 12_3C peptide was attempted. However initial analysis indicated that the peptide is not present in the structure. Therefore crystallisation efforts with the truncated NWP tripeptide were pursued through crystal soaking methods. The soaking experiments were not successful as the NWP tripeptide was not present in the crystal structure. However, the data collected gave us the highest resolution crystal structure of native derCD23 recorded to date; this is described in detail in Chapter 4.

3.8 Discussion

Mechanism of 12_3C inhibition of IgE

NMR experiments reveal a competitive inhibition of IgE binding to derCD23 by the 12_3C peptide, as indicated by the chemical shift perturbations that overlap with the IgE binding site. The 12_3C peptide also appeared affect the trimerisation of derCD23, possibly by an allosteric mechanism. This may be similar to the oligomerisation of CD23 induced by IgE binding, which is required for high affinity binding and leads to the upregulation of IgE (Kilmon et al., 2001). SPR analysis also indicates that the peptide can directly inhibit IgE binding to CD23. Subsequent FACS analysis also showed that the peptide could inhibit IgE-GFP from binding to CD23-overexpressing 8866 cells, demonstrating the IgE blocking ability of the peptide on cells. The observation of peptide inhibition of IgE binding to CD23 on cells may indicate a potential application in inhibiting facilitated antigen presentation by blocking antigen-IgE complexes from binding to $CD23^{+}$ cells. The peptide could also be be useful in preventing trancytosis as described by Palaniyandi et al. (2011), where it could prevent the uptake of IgE-allergen complexes on the airway epithelium. Primary B-

cell culture experiments also indicate that the peptide has an effect in reducing IgE expression in B cells, presumably by inhibiting the activation of IgE^+ B cells mediated by trimeric CD23 binding to membrane IgE; this needs to be further investigated.

Inhibiting the interaction between CD23 and IgE is a potential therapeutic target and therefore inhibitors are sought. Phage display derived peptides are emerging as an alternative to antibody-based treatments (Ladner, 2004). There are several issues related phage display derived peptides. One major disadvantage of peptide based therapies is the very poor bioavailability of peptides compared with antibodies, due to protease degradation and kidney filtration. It has been suggested that natural peptides have gone through natural selection for bioavailability and stability against degradation by housekeeping proteases (Watt, 2006). However, there are several strategies to prevent destabilisation and degradation as well as increasing bioavailability of peptides. Chemical modifications such as addition of polyethylene glycol (PEG), for example, have been shown not only to increase solubility and stability of therapeutic peptides in plasma but also to lower immunogenicity. It is hoped that future work on this peptide and its eventual derivatives can bring about the production of more potent inhibitors of the IgE/CD23 interaction. The NWP tripeptide, which retains binding, albeit at lower affinity, can be a starting point for further drug design, perhaps by applying structurally guided chemical modification to improve structural complementarity with CD23. CD23 is relatively a flat surface protein molecule, with no obvious deep pocket for inhibition. However, recently it has been shown that flat protein-protein interactions can be exploited as target for inhibitors (Arkin and Wells, 2004). Technology such as disulfide trapping, for example, can be used to probe for molecules that can bind to flat protein

surfaces and be improved to obtain high affinity compounds that eventually disrupt such protein-protein interactions (Buck and Wells, 2005). It is hoped that possibly this and other approaches can be used towards the discovery of compounds that inhibit IgE/CD23 interactions and eventually be of therapeutic application.

Chapter 4

CD23: structure and interactions.

4.1 Introduction

This chapter describes various studies concerning CD23:

1. The production of derCD23.
2. The crystal structure of derCD23 at 1.9 Å.
3. The interaction between derCD23 and IgE.
4. The interaction between CD23 and CD21 (SCR1-2)
5. The interaction between CD23 and the anti-CD23 monoclonal antibody IDEC-152
6. Multimolecular interactions between CD23, IgE-Fc and FcεRI
7. Development and optimisation of a differential scanning fluorimetry assay for screening for compounds binding to derCD23.

The structure of the lectin head domain of CD23 has been solved previously using NMR spectroscopy and X-ray crystallography. The X-ray structure previously determined (Wurzburg et al., 2006) contains two non-silent mutations: H213R and G256S. It was not revealed, however, whether these mutations were engineered to help in crystallization or were a result of spontaneous mutation. It is also noted that Wurzburg et al. (2006) initially attempted to crystallize derCD23 in complex with IgE-Fc (Cε3-4) but the crystallisation condition was subsequently reproduced to obtain crystals of CD23 alone. CD23 is expressed, mostly as a trimer, on the membrane of B cells and in soluble forms, and cleaved by proteolytic enzymes to various sizes (Kilmon et al. 2001; Kilmon et al., 2004). A protease enzyme ADAM-10 has been discovered and characterised recently, and

its involvement in upregulation of IgE through cleavage of membrane CD23 into soluble form has been demonstrated (Weskamp et al., 2006; Sturgill et al., 2011; Conrad et al., 2010). CD23 is also cleaved into a smaller form at both the N- and C-terminus by a cysteine protease enzyme called Der p1, from the house dust mite, *Dermatophagoides pteronyssinus,* into a 16 kDa size molecule consisting only the lectin head domain and 10 amino acids of the C-terminus; this fragment is termed derCD23 (Schulz et al., 1995). DerCD23 was shown to retain binding to IgE and CD21 (SCR1-2) (Hibbert et al., 2005). McCloskey et al. (2007) demonstrated that the soluble trimeric CD23 upregulates IgE synthesis in B cells and the monomeric derCD23 inhibits IgE synthesis. It was proposed that the soluble trimeric CD23 upregulates IgE regulation by co-ligating with both membrane IgE and CD21 leading to the activation of a downstream signaling cascade that leads to an increase in IgE synthesis. Monomeric CD23, on the other hand, blocks this trimolecular complex, thus inhibiting IgE synthesis (Figure 4.1).

The characterisation of the monomeric CD23 (derCD23) and the trimeric CD23 were performed to compare the binding events of these two fragments to IgE. The interaction between IgE and CD23 has now been mapped on each protein using NMR chemical shift mapping, and site-directed mutagenesis studies by Susmita Borthakur (personal communication) and X-ray crystallography by Balvinder Dhaliwal (personal communication). These data confirm the Cε3 domain as the primary binding site of CD23. Sayers et al. (2004) showed that residue Lys352 of IgE is of primary importance in binding of CD23. The interaction between CD23 and CD21 involves the C-terminus of CD23 (Hibbert et al., 2005).

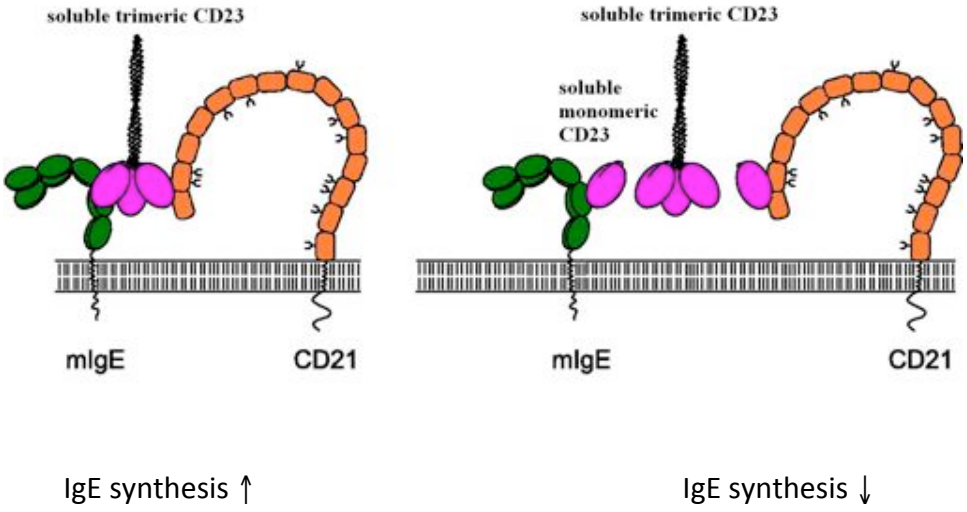

Figure 4.1: Regulation of IgE synthesis by monomeric and trimeric CD23.
Trimolecular complex formation upregulates IgE levels in B cells (left) while monomeric sCD23 downregulates IgE levels (right). Figure adapted from McCloskey et al. (2007).

Studies using a version of derCD23 truncated at the C terminus were done to confirm the role of the C-terminus in CD21 binding. The anti-CD23 monoclonal antibody Lumiluximab, also known as IDEC-152, has been shown to be effective in Phase II clinical trials for allergy and asthma (Rosenwasser, 2003). However in the absence of structural information of the antibody's interaction with CD23, the exact mechanism of its action is unknown. Biophysical characterisations were performed to provide more information on this interaction. From the crystal structure of IgE-Fc (Cε3-4) in complex with its high affinity receptor FcεRI (Garman et al., 2000), it is clear that the binding site of CD23 is still exposed in the bound structure as shown in Figure 1.6. Therefore biophysical experiments were performed to study the intermolecular interactions between CD23, IgE and FcεRI and their potential biological implications. Keeping in view of the long-term goal of discovering inhibitors for CD23, a differential scanning fluorimetry (DSF) assay was

developed and optimised for derCD23 for use in screening of binding compounds. This DSF assay also was used to show that calcium has a role in stabilisation of the CD23 lectin head domain.

4.2 Production of derCD23

CD23 contains four disulfide bonds and the reducing environment of bacterial cytoplasm leads to difficulty in obtaining soluble protein from bacterial expression systems. Therefore this construct is over-expressed into inclusion bodies (Stewart, 1998). Extensive washing of inclusion bodies is needed to obtain a more purified protein sample to remove impurities that may lead to the aggregation of the protein (Maachupalli-Reddy et al., 1997). After solubilisation of inclusion bodies with denaturing agent, the protein is refolded in a buffer containing a mixture of oxidising and reducing agents that facilitate in folding.

Due to the nature the refolding method, some proteins will be incorrectly folded and this commonly leads to aggregation. In order to remove misfolded protein and contaminants that might lead to aggregation, size exclusion purification using a gel filtration column has been added to a previously established protocol (Hibbert et al., 2005) to distinguish the misfolded and aggregated protein from the monomeric and correctly folded CD23. The gel filtration chromatogram (Figure 4.2(b)) shows two distinct peaks that correspond to derCD23 of different sizes, the first being the larger aggregate complex whereas the second corresponds to the correctly folded monomeric derCD23 indicated by a band size of 16kDa by gel electrophoresis, and confirmed by NMR spectroscopy.

Gel electrophoresis was performed on both fractions in both reducing and non-reducing conditions. It was confirmed that most of the aggregated protein was misfolded CD23 indicated by size, whereas the second fraction indicated a pure soluble CD23 sample.

(a)

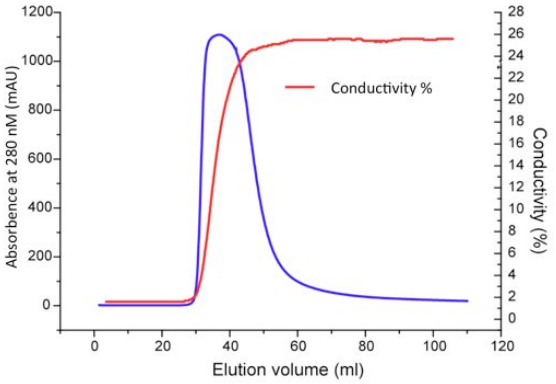

(b)

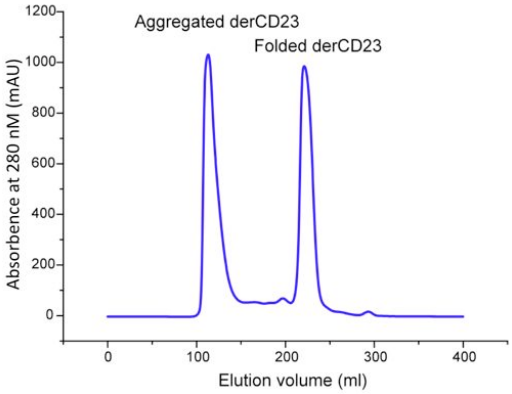

(c)

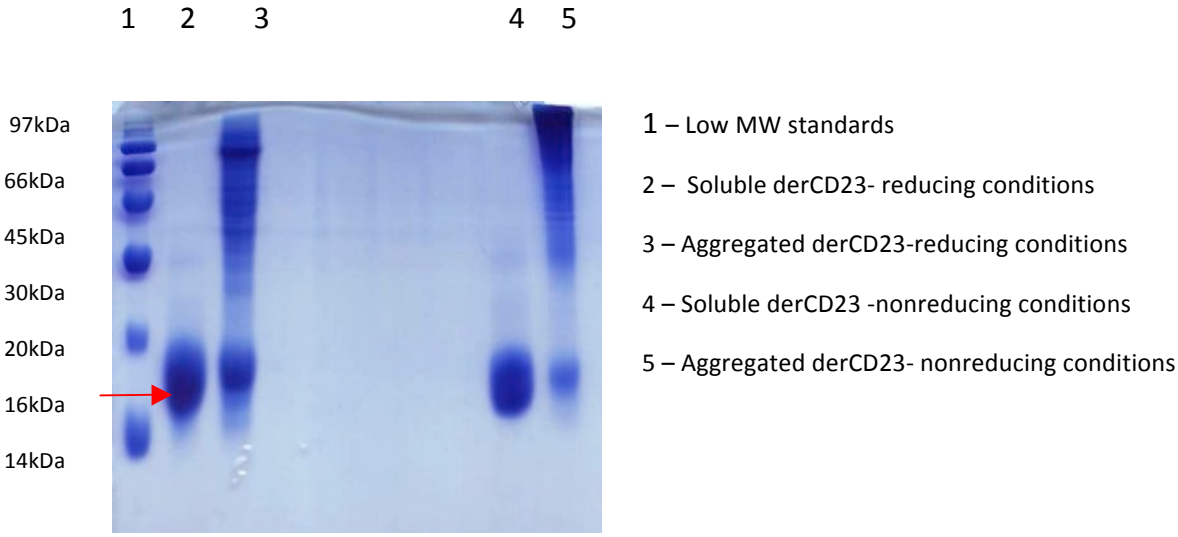

Figure 4.2: Purification of derCD23
(a) Heparin column purification showed a single eluted peak (b) Size exclusion purification using a gel filtration column indicates two distinct peaks belonging to aggregated derCD23 and the second being monomeric folded derCD23 and (c) Gel electrophoresis indicate the purity of the folded peak compared to the aggregated peak in reducing and non reducing condition.

4.2.1 ^{1}H- NMR of CD23 to ascertain foldedness

One-dimensional proton NMR is extremely useful for determining the foldedness and viability of a protein sample before subsequent use in experiments (Rehm et al., 2002). A correctly folded CD23 shows well-dispersed proton spectrum with four characteristic upfield shifted methyls seen in a ^{1}H-NMR spectrum (Figure 4.3). The one-dimensional ^{1}H-NMR experiments were routinely done with derCD23 sample to confirm foldedness.

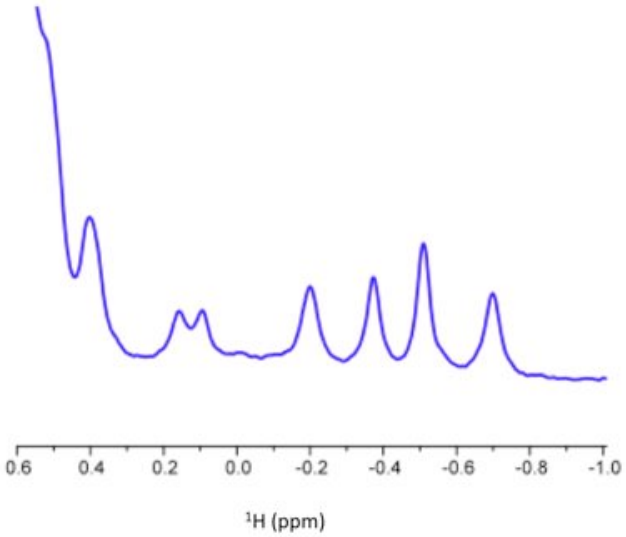

Figure 4.3: A distinct pattern of upfield-shifted methyls indicated a correctly folded CD23.

4.3 Crystal structure of derCD23 at 1.9 Å

4.3.1 Introduction

The structure of the monomeric CD23 was first solved using NMR (Hibbert et al., 2005) followed by a crystal structure (Wurzburg et al., 2006). Both structures are very similar with slight difference on the calcium-binding site.

The construct used by Wurzburg et al. (2006) contains two non-silent mutations: H213R and G256S. It was not revealed whether these mutations were engineered to help in crystallisation. It is known that a mutation can introduce subtle energetic changes that may require a different crystallisation conditions to that of the wild type protein (McElroy et al., 1992). In many cases, a complete re-screen or even further genetic engineering may be necessary (Derewenda, 2010). As in the case of derCD23, a reproducible crystallisation condition that yields a high-resolution structure of the mutation-free CD23 molecule will be useful for routine crystallography-based drug discovery project.

The initial objective of the crystallographic effort was to crystallize derCD23 with a CD23 binding peptide, 12_3C (characterized in Chapter 3). The crystallisation trials were performed (Section 4.3.2) and conditions obtained were optimised, however the best crystal obtained only showed an apo structure, without the peptide. Therefore the effort shifted to the soaking of derCD23 crystals with a truncated version of the peptide, the NWP tripeptide, which retains binding albeit at a lower affinity. The structure was solved but the NWP tripeptide was not observed. However this crystal sample provided us with the highest resolution structure of derCD23 obtained so far. This protein structure is therefore described in this chapter. In addition to this, other crystallisation efforts were

also undertaken, including the CD23/CD21 complex, trimeric CD23, trimeric CD23 in complex with CD21 and IgE-Fc, none of which yielded suitable crystals at the time of this thesis submission.

4.3.2 Crystal growth

As previously mentioned, crystallisation of derCD23 with the 12_3C peptide was attempted. 12_3C has an affinity of 7.0 ± 0.1 μM, as described in Section 3.4.1. A two-fold molar excess of 12_3C to derCD23 (600 μM:300 μM) was subjected to crystallisation trials. A two-fold molar ratio was used to ensure a saturation of binding site on CD23 by the peptide. Crystals were found under a condition C10 from the commercial screen ProComplex (Qiagen) (25% PEG 4000 0.15 M ammonium sulfate, $(NH_4)_2SO_4$, 0.1 M MES pH 5.5) and was further optimised by varying the concentration of PEG as well as pH. Bigger and single crystals were obtained in 12.5% PEG 4000, 0.15 M MES pH 6.0, 0.15 M $(NH_4)_2SO_4$ (Figure 4.4). The crystals were taken to the Diamond Synchrotron and data were collected at beamline IO3. Initial analysis of the structure obtained revealed that the peptide was not present in the crystal structure (Dr Balvinder Dhaliwal, KCL, personal communication).

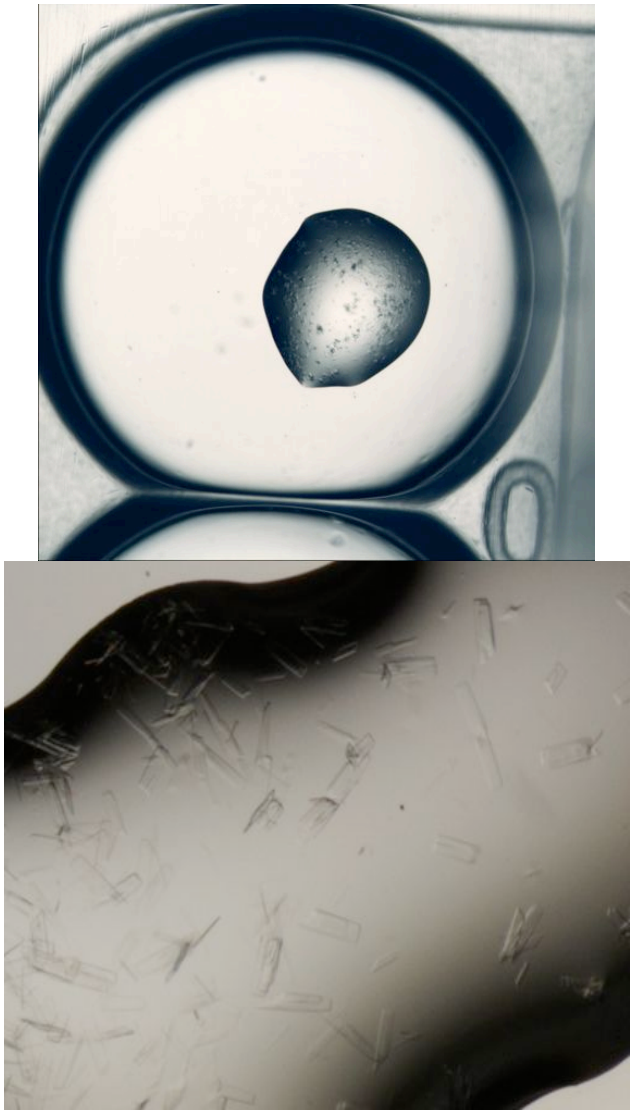

Figure 4.4: Crystals obtained after optimisation of crystallisation conditions of derCD23/12_3C peptide complex.
(Top) The condition Procomplex condition C10 (25% PEG 4000 0.15 M $(NH_4)_2SO_4$, 0.1 M MES pH 5.5. (Bottom) 12.5% PEG 4000, 0.15 M MES pH 6.0, 0.15 M NH_4SO_4.

The truncated version of the 12_3C peptide, NWP, which is the consensus sequence from a number of peptides derived as described in Chapter 3, was shown to retain binding to derCD23 albeit at a much lower binding affinity of 1.2 mM (Section 3.4.4.2). This tripeptide was then used for soaking experiments of derCD23 crystals.

Previously, a condition was established to grow derCD23 crystals reproducibly (25% (w/v) polyethylene glycol monomethyl ether (PEG MME) 5000, 0.1 M sodium acetate pH 4.7, 2% 1-6 Hexanediol, 0.05 M $(NH_4)_2SO_4$) (Dr Stella Fabianne, unpublished results). This condition was then optimised further with different molecular weight polyethylene glycols (PEGs). The best crystals judged by size and morphology were obtained in 16% PEG 6000, 2% (v/v) 1,6- hexanediol, 0.1 M sodium acetate, pH5 and 0.05 M $(NH_4)_2SO_4$ (Figure 4.5). The crystals were subsequently soaked in NWP tripeptide by slowly exchanging the drop solution for 24 mM NWP, 18% (w/v) PEG6000, 2% (v/v) 1,6-hexanediol, 0.1 pH 5.0, and 0.05 M $(NH_4)_2SO_4$. Higher NWP tripeptide concentrations at 50 mM and higher, led to the changes of morphology of the soaked crystals, which became rounder and produced no diffraction when tested at the beamline possibly by changing the internal order of the crystal lattice.

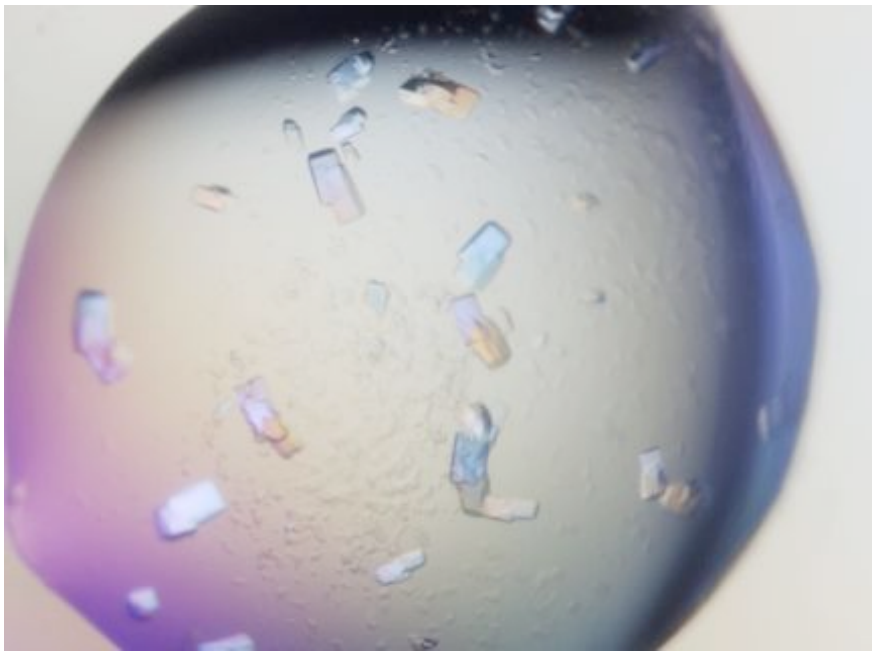

Figure 4.5: DerCD23 crystals were obtained in 2 weeks with 16% PEG 6000, 2% 1,6-hexanediol , 0.1 M sodium acetate pH 5 and 0.05 M $(NH_4)_2SO_4$.

4.3.3 Data collection and structure determination.

After 3 days, crystals of derCD23 were transferred to a cryoprotectant solution consisting of 24mM NWP, 32% (w/v) PEG 6000, 2% (v/v) 1,6-hexanediol, 0.1M sodium acetate pH 5.0, 0.05M $(NH_4)_2SO_4$, 15% (v/v) glycerol, and then flash-cooled to 100K (Figure 4.6).

Figure 4.6: The soaked derCD23 crystal in a nylon loop.
The crystal is approximately 80µm in length. The crystal was transferred into cryoprotectant solution, mounted in a nylon loop and subsequently cryo-cooled to 100K. The crystal was translated and the X-ray beam size optimised such that diffraction data were only collected from the single lattice part of the crystal.

X-ray diffraction data were collected at beamline I03 at the Diamond Light Source. Indexing, integration and merging of data were carried out with the *HKL*2000 suite of programs (Otwinowski and Minor, 1997). Statistics for data collection and processing are shown in Table 4.1.

Table 4.1: Statistics for data collection and processing

Beamline	I03, Diamond Light Source
Wavelength (Å)	0.9763
Space group	P1
Unit-cell parameters (Å)	a = 52.69, b = 56.86, c = 62.49 α = 68.45 β = 87.83 γ = 73.56
Resolution range (Å)	60.0 – 1.90 (1.97 –1.90)
Observations	189032
Unique reflections	48564
Average redundancy	3.9 (3.9)
Completeness (%)	96.1 (96.3)
I/σ(I)	24.7(2.7)
R_{merge}	0.055 (0.395)

Values in parentheses are for the outer resolution shell.

4.3.4 Determination of number of molecules in the asymmetric unit

In order to estimate the number of molecules in the asymmetric unit the Matthew's coefficient probability tool available on http://www.ruppweb.org/Mattprob/ was used (Matthews, 1968; Kantardjieff & Rupp, 2003). The crystal volume per unit of protein molecular weight, V_m, known as the Matthew's Coefficient is given:

V_m (matthews coefficient) = Volume of unit cell/ (MW of macromolecule*Z *X)

where Z is number of asymmetric units and X is number of molecules. The V_m value is usually found to have values between 1.6 and 3.5 $Å^3$ Da. In this case, derCD23 crystallised in space group P_1, which contains one asymmetric unit in each unit cell. Given the molecular weight (MW) of derCD23 of 16500, and the unit cell with a parameter of a = 52.69 Å, b = 56.86 Å, c =62.49 Å , α = 68.45° , β = 87.83° , γ = 73.56°, the Matthew's coefficient was

calculated to give the highest probability of having 4 molecules with Vm value of 2.52 $Å^3$ Da with a solvent content of 51.26%.

4.3.5 Structure solution and refinement

A molecular replacement solution was found using *Phaser* (AJ McCoy et al., 2007) part of the CCP4 suite of programs using the structure of derCD23 previously determined by Dr. Stella Fabiane (unpublished results) as a search model with 100% sequence identity. Four molecules were located. The initial model underwent two rounds of rigid-body refinement followed by iterative cycles of refinement in *REFMAC5* (G.N. Murshudov et al., 1997) and *AutoBuster* (Bricogne et al., 2010) and manual model rebuilding with *COOT* (Emsley and Cowtan, 2004) was then performed. The data obtained showed excellent electron density map, which favours the manual rebuilding with *COOT* (Figure 4.7). Several key features in *COOT* include “auto-fit rotamer” and “rigid body zone”. “Auto-fit rotamer” is used to fit the rotamer side chain into the electron density map. “Rigid body zone” is used to fit the backbone chain between two defined points into the electron density map. The quality of the model undergoing refinement and model building was monitored using the R factors R_{work} and R_{free} values:

$$R_{work} = \frac{\sum ||F_{obs}| - |F_{calc}||}{\sum |F_{obs}|}$$

$$R_{free} = \frac{\sum_{test} ||F_{obs}| - |F_{calc}||}{\sum_{test} |F_{obs}|}$$

F are structures factor amplitudes, observed or calculated, from the model. R_{work} takes into consideration the structure factors used during refinement, while R_{free} is the 5% test set of reflections excluded from refinement to avoid overfitting of the data and is used as cross-validation (Brünger, 1992). Refinement statistics are shown in Table 4.2.

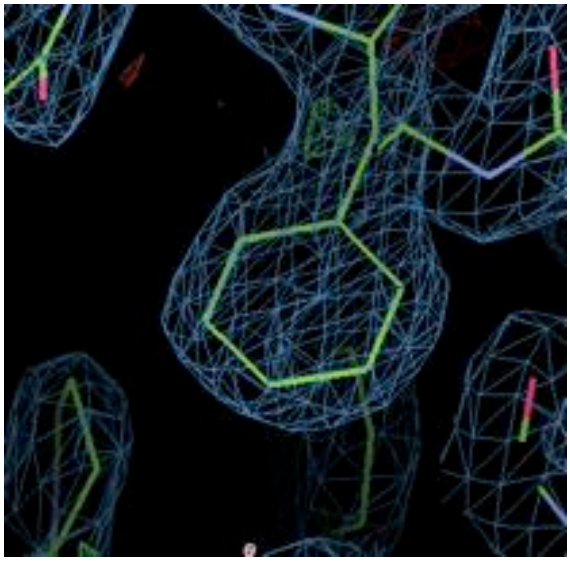

Figure 4.7: Electron density seen on the $2F_0$-Fc map set at 1σ showed excellent electron density that favours the manual rebuilding.

Table 4.2: Refinement statistics

Resolution range (Å)	21.9-1.90
Total No. of reflections	48535
No. of working reflections	46068
No. of test reflections	2467
R factor	
R_{work}	0.174
R_{free}	0.209
No. of atoms	
Protein	4445
Water	252
Others	4 (glycerol: 2, SO_4^{-2}: 2)
R.m.s. bond-length deviation (Å)	0.009
R.m.s. bond-angle deviation (°)	1.00
Mean B factor ($Å^2$)	
Main chain	35.52
Side chain	43.89
Waters	44.19
Others (glycerol and SO_4^{-2})	37.22
R.m.s. backbone B-factor deviation[¶]	2.12

[¶]R.m.s. deviation between *B* factors for bonded main-chain atoms.

4.3.6 Validation of the structure

Molprobity (Davis et al., 2007) was used as a validation tool for assessing the backbone torsion angles (phi ϕ and psi ψ) of each of the residues in the molecule based on the Ramachandran plot (Ramachandran et al., 1963). 95.2% of all residues were in the favoured region whilst all residues (100%) were in the allowed regions of the Ramachandran plots thus confirming the validity of the structure (Figure 4.8).

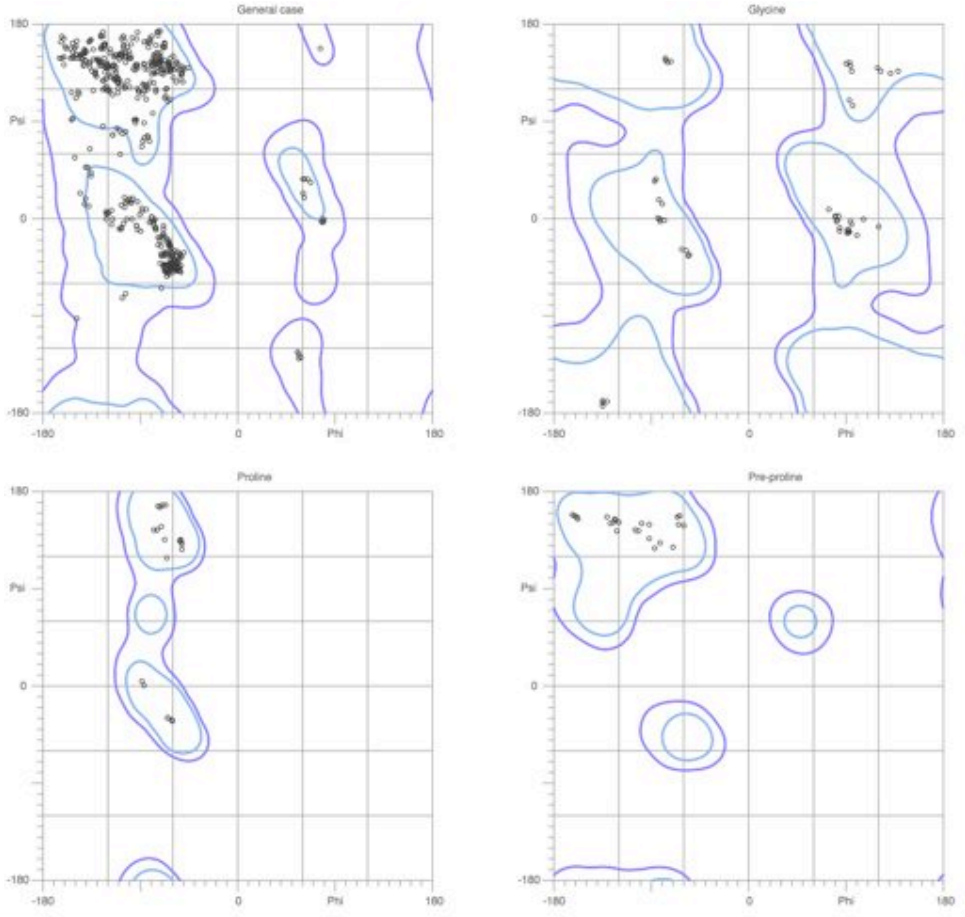

Figure 4.8: Ramachandran plots for the final model.
The phi (ϕ) and psi (ψ) angles for the residues of the structure were plotted using Molprobity. The allowed regions are shown for each case, clockwise from top left: for general case, glycine, proline and pre-proline residues. All the residues, indicated by small circles, are included in the favoured (light blue) or allowed (dark blue) regions of the plot.

4.3.7 Disulfide bonds

During data collection at a synchrotron, radiation damage can result in chemical changes of a biological molecule including breakage of disulfide bonds (Ravelli and Garman, 2006). Most of the disulfide bonds in all four chains are present in partial occupancy. Partial occupancy of disulfide bonds results from a mixture of complete and broken disulfide bonds in the summation of all the molecules within the crystal. Only Cys160-Cys288 in Chain B was found to be unbroken. In Chain C the disulfide bonds for Cys160-Cys288 and Cys163-Cys174 were found to be broken.

4.3.8 Structure analysis

4.3.8.1 Overall structure

Overall, all the derCD23 molecules are very similar in structure with the previously solved NMR and crystal structure of the lectin head domain of CD23 (Hibbert et al., 2005; Wurzburg et al., 2006). The three-dimensional structure of derCD23 consists of two roughly orthogonal α-helices and eight β-strands, forming two anti-parallel β-sheets (Figure 4.9 (a)). Four disulfide bonds contribute to the tertiary structure, while seven tryptophan residues and other conserved side chains form a hydrophobic core within the domain. There are four molecules in the asymmetric unit termed Chains A, B, C and D. Glycerol and sulfate ions were found to be bound between the molecules. Sulfate ions were found to be situated between Arg263 and Arg267 on Chain A and B with Lys 229 in Chain C and D, respectively. Glycerol molecules were found between the α-1 helix of chain A and C, and between α-1 helix of chain B and D (Figure 4.9(b)).

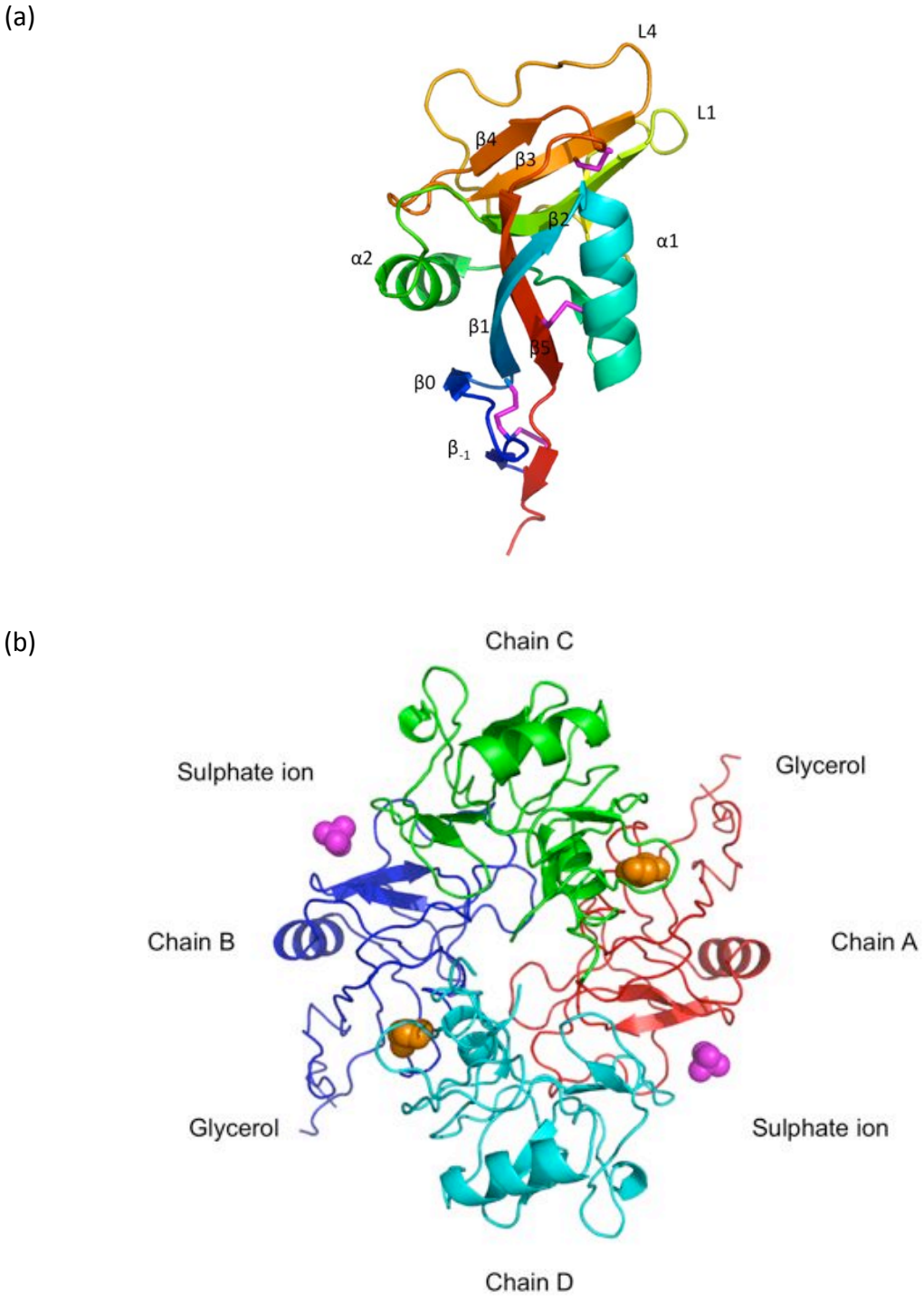

Figure 4.9: The structure of derCD23 obtained.
(a) The rainbow coloured structure of one of the derCD23 molecule highlighting secondary structure elements. (b) The structure of the four derCD23 molecules found in the asymmetric unit with sulfate ions and glycerol molecules highlighted. Chains A, B, C and D were coloured red, blue, green and cyan respectively. Glycerol molecules were coloured in orange and sulfate ions in purple.

4.3.8.2 Identification of sulfate and glycerol ions

4.3.8.2.1 Sulfate ions

There are two sulfate ions (SO_4^{2-}) and two glycerol molecules found in the asymmetric unit. Sulfate ions were situated to be bound between Chain A and D, and Chain B and C in similar locations. A sulfate ion is situated between Arg263 and Arg267 on Chain A with Lys229 in Chain D. A sulfate ion was also found between Arg263 and Arg267 on Chain B with Lys229 of Chain C (Figure 4.10).

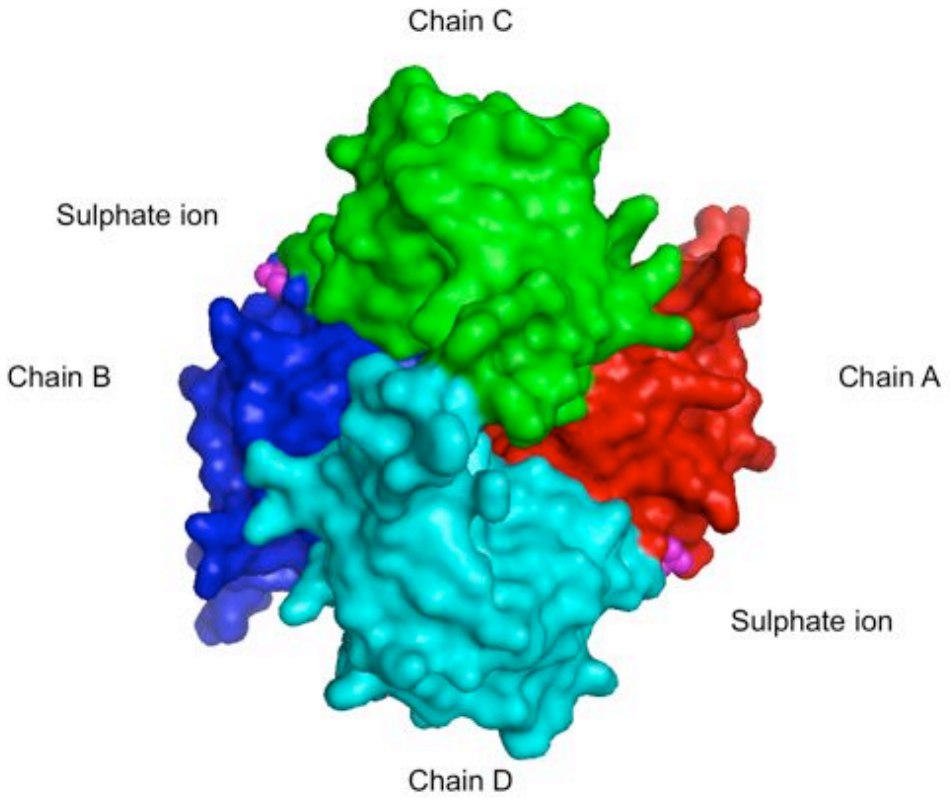

Figure 4.10: Surface representation to highlight the position of sulfate ions in the crystal structure.
A sulfate ion is found between chain A and D, and Chain B and C.

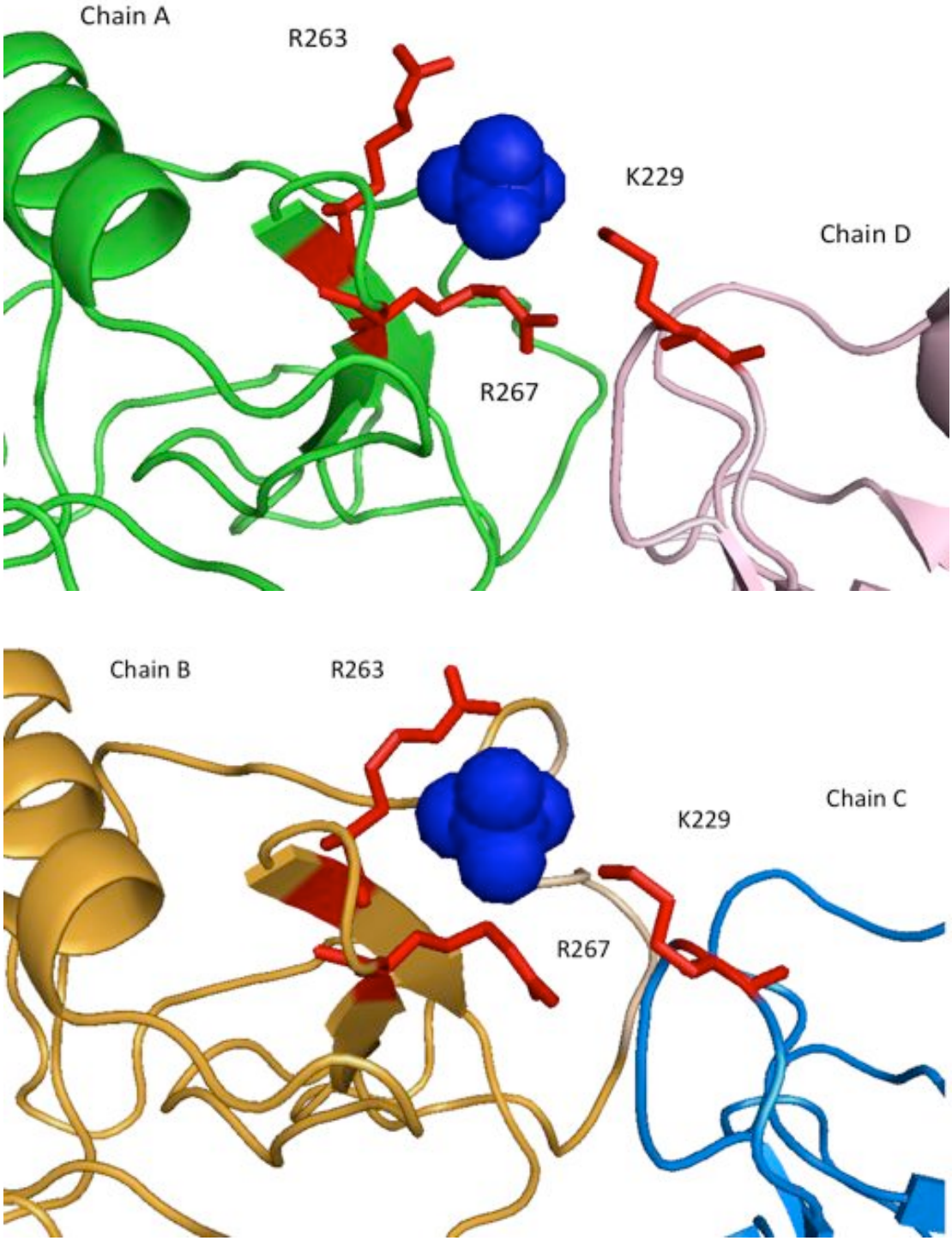

Figure 4.11: The location of sulfate ion in the crystal structure.
The sulfate ion location between Chains A and D (top) and Chains B and C (bottom). A sulfate is situated between Arg263 and Arg267 in Chain A and D with Lys229 in Chains C and D.

The presence of sulfate ion may be explained by the crystallisation condition used in the crystallisation (0.05 M $(NH_4)_2SO_4$). Sulfate was also present in conditions used to grow crystals of CD23 in the previously solved structure by Wurzburg et al. (2006) in which 0.2 M lithium sulfate was present as a component in the crystallisation buffer used. In other cases the addition of ions such as cadmium in sulfate solutions has been known to induce the crystallisation of horse spleen ferritin (Trakhanov et al., 1998). It would be interesting to see whether varying sulfate contents and types would be beneficial in crystallising other types of CD23-related molecules such as triCD23.

4.3.8.2.2 Glycerol molecules

Glycerol molecules were found between the α-1 helix of chain A and C, and between α-1 helix of chain B and D. The protein crystal was grown at pH 5. It is unlikely that the oxygen atom attached to C2 carbon of the glycerol molecule forms a hydrogen bond with the nitrogen atom on the histidine side chain, as it would have been protonated at this pH. The location of the glycerol, which is present in the cryoprotectant, is possibly a crystallographic artefact, which can be observed at such resolution.

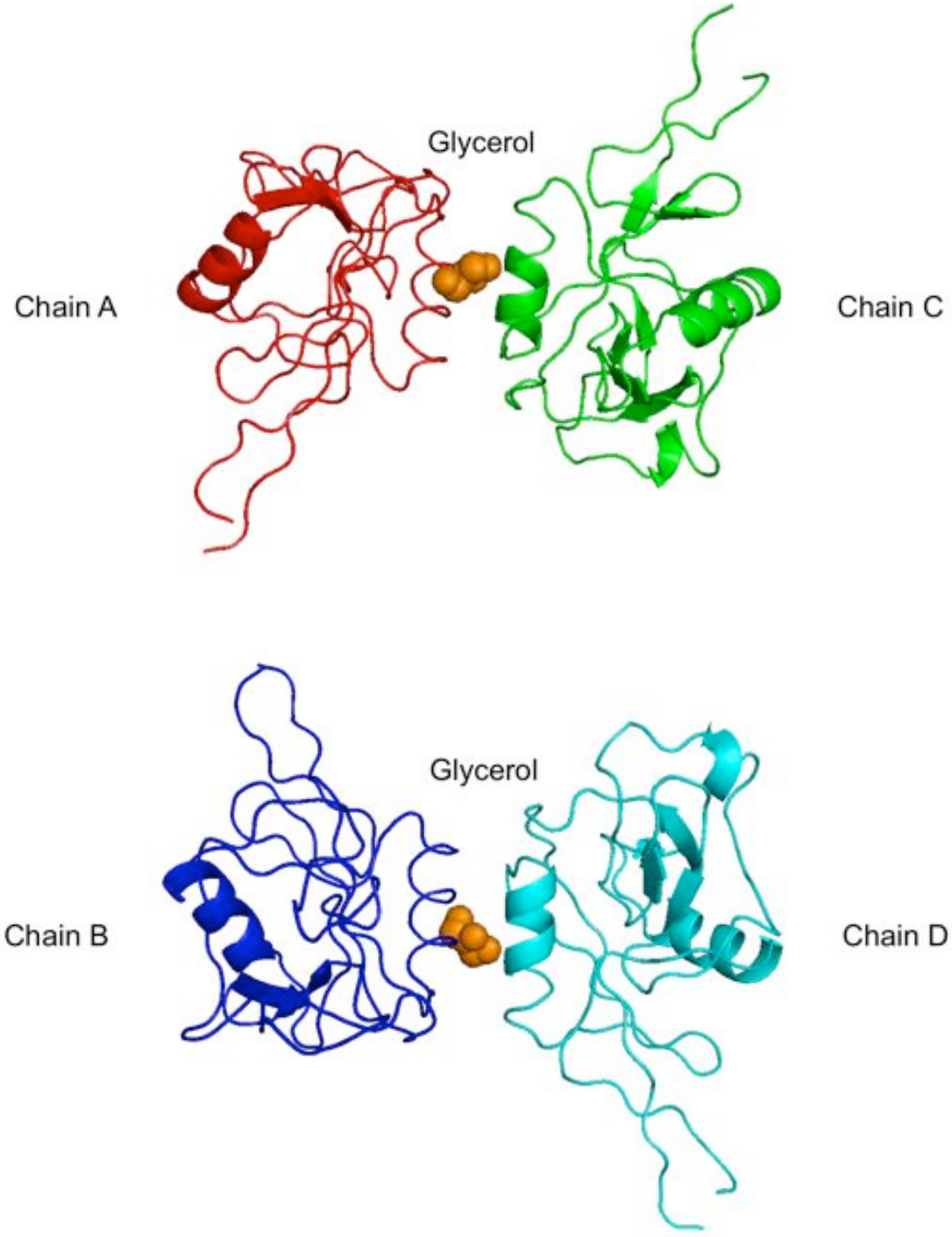

Figure 4.12: Glycerol molecules are found between the α-1 helix of Chains A and C, and Chains B and D.

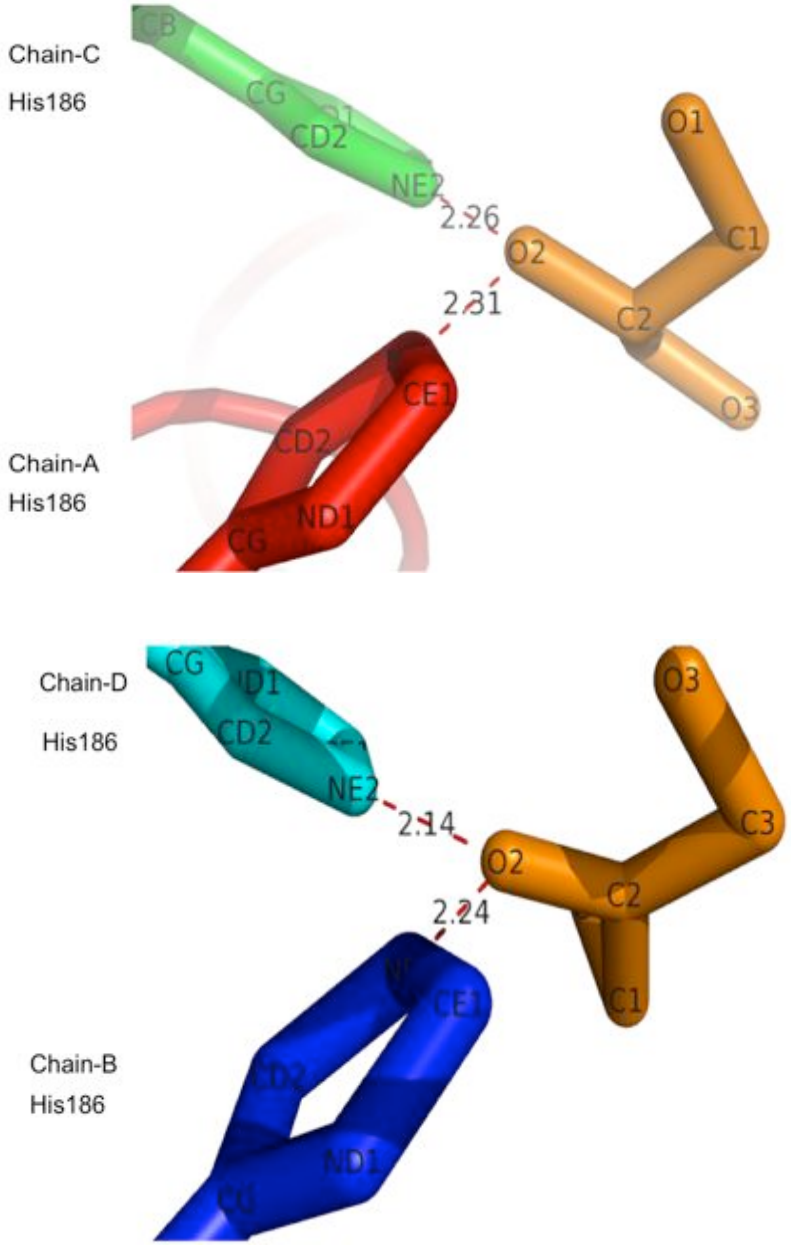

Figure 4.13: Distance measurement between glycerol molecule to the nearest side chain (His186) on the α-helix 1 of between Chain A-C and B-D.
The measurements showed a distance between 2.14 and 2.31 Å.

4.3.8.3 Inherent flexibility of derCD23 molecules in the absence of calcium

The superposition of all the four derCD23 molecules using PyMol revealed that the four Chains A, B, C and D showed a RMSD range between 0.17-0.67 Å (Figure 4.14). These four chains could be grouped to two highly homologous pairs, Chain A/B and Chain C/D.

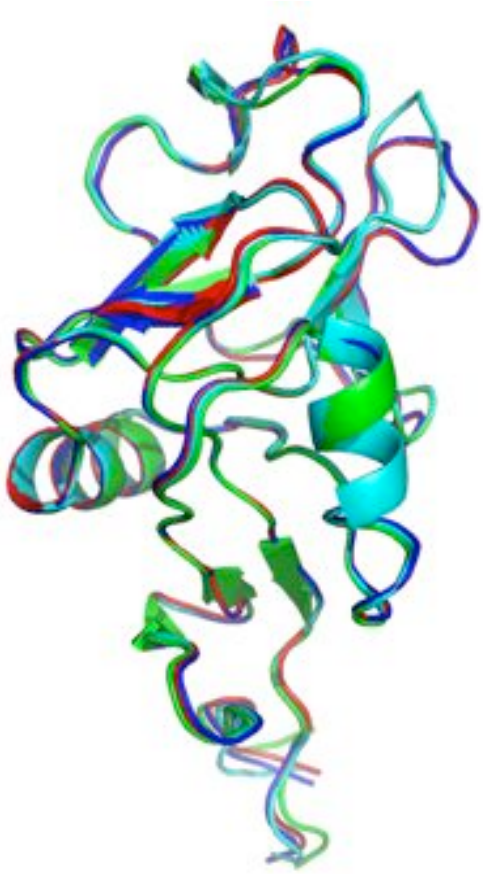

Figure 4.14: Superposition of all derCD23 molecules found in the asymmetric unit.
Superposition of Chains A, B, C, D revealed a RMSD between 0.17-0.67 Å. Chains are coloured as follows: Chain A (Red), Chain B (blue), Chain C (green) and Chain D (cyan).

The RMSD resulting from superposition of Chain A and B has a value of 0.17 Å indicating a high degree of similarity. Superposition of Chain C and D revealed a RMSD value of 0.23 Å also indicating high similarity (Figure 4.15).

(a) (b)

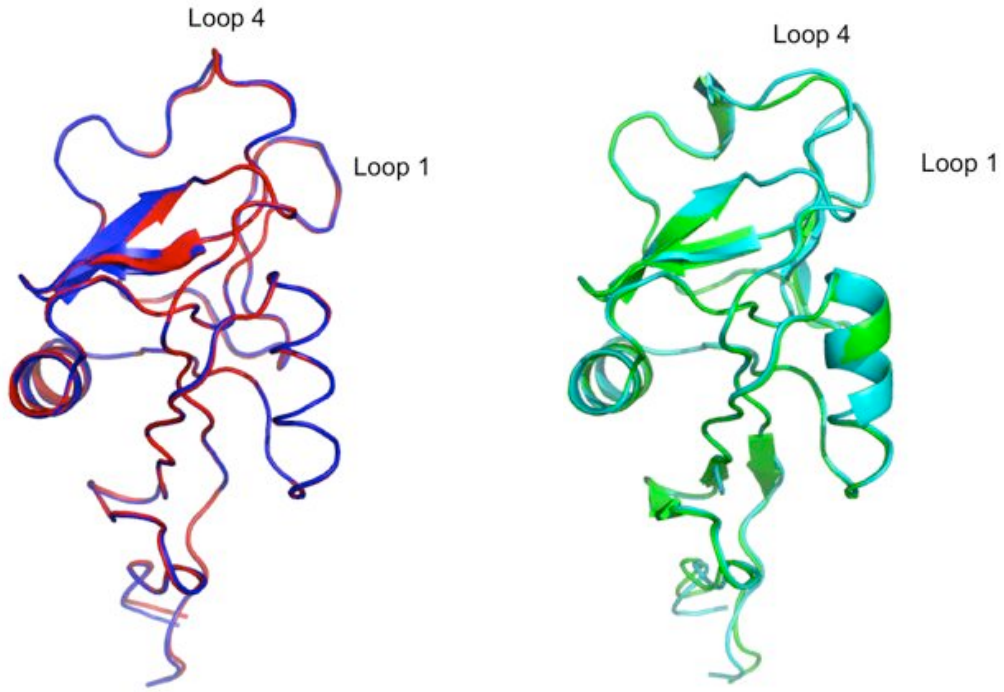

Figure 4.15: Superposition of the pairs of highly homologous chains in the structure.
a) Superposition of Chain A and B showed a RMSD of 0.17 Å b) Superposition of Chain C and D showed a RMSD of 0.23 Å.

Superposition of Chains A/C and B/D

Contrasting the similarity in A/B and C/D, is the superposition of A/C and B/D. Superposition of molecules A/C showed an RMSD value of 0.67 Å while B/D showed an RMSD value of 0.55 Å. From this superposition, it is evident that the Loop 1 and Loop 4 have an inherent flexibility between derCD23 molecules (Figure 4.16).

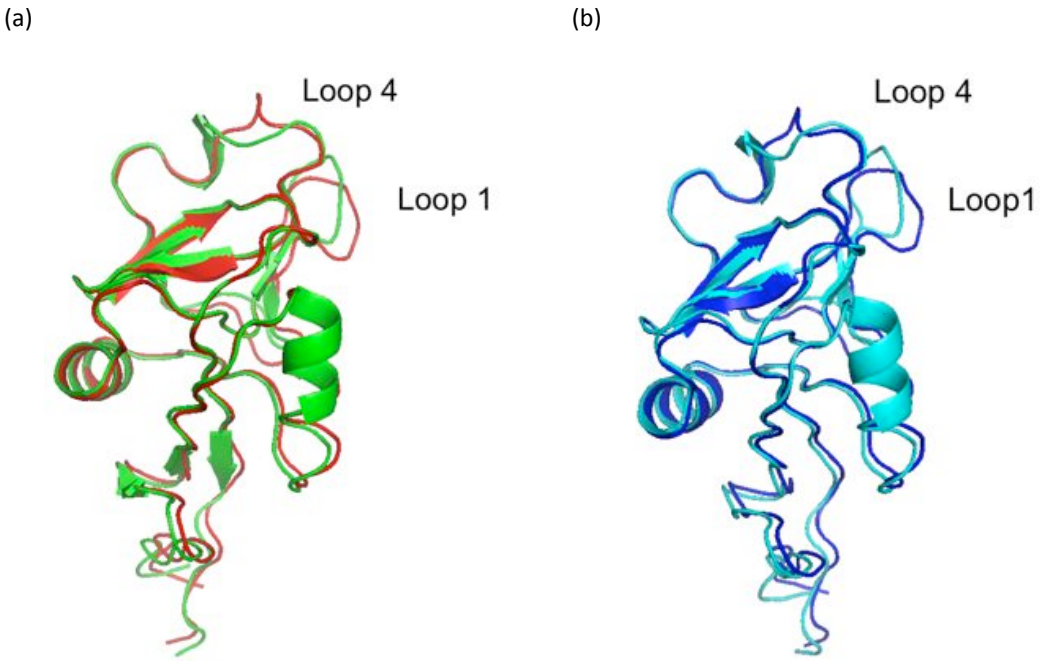

Figure 4.16: Superposition of Chain A/C and B/D.
(a) The superpostiion of Chain A-C showed an RMSD vlaue of 0.670 Å. Loop 1-4 (residue 230-259) showed significant conformational difference. (b) Superpositionof Chain B-D showed an RMSD value of 0.55 Å. Loop 1 and Loop 4 also showed conformational diffferences.

Comparison with the previous crystal structure from Wurzburg et al. (2006)

The 1.9 Å overall structure agrees very well with the previously determined crystal structure by Wurzburgh et al. (2006). The two non-silent mutations did not seem to show much difference between the structures although the region comprising Loop1 and Loop4 in this structure differs to the previously solved structure.

The apo crystal structure PDB ID 2H2R was compared with the Chain A and B from this study. The other structure in the same paper PDB ID: 2H2T contains calcium ions and was therefore not chosen for comparison with the structure obtained in this study. 2H2R

contains two chains in the asymmetric unit, Chain 2H2R_A and 2H2R_B, and when superposed revealed a RMSD of 0.34 Å.

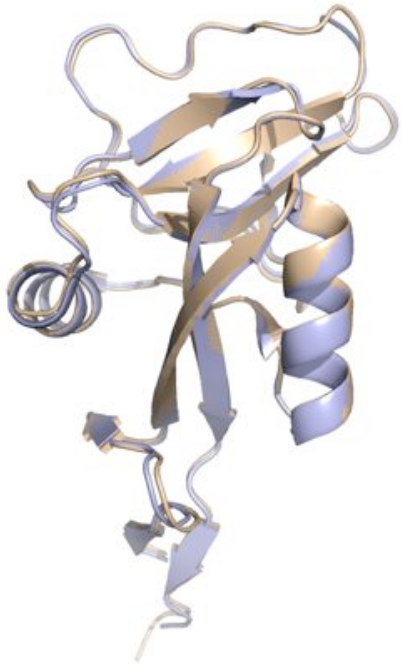

Figure 4.17: Superposition of Chain A and B in PDB ID: 2H2R (Wurzburg et al., 2006) with an RMSD of 0.34 Å.

The superposition of all the derCD23 molecules in the study with the crystal structure of Apo CD23 from Wurzburg et al. (2006) revealed a range of RMSD values from 0.71 to 0.81 Å showing that in the absence of calcium ions, the region comprising Loop1 and Loop 4 have an inherent flexibility. The presence of calcium ions led to conformational changes in these loops (Wurzburg et al. 2006). Previous SPR analysis has shown that the absence of calcium reduced the affinity of CD23 to IgE by seven-fold (Hibbert et al., 2005).

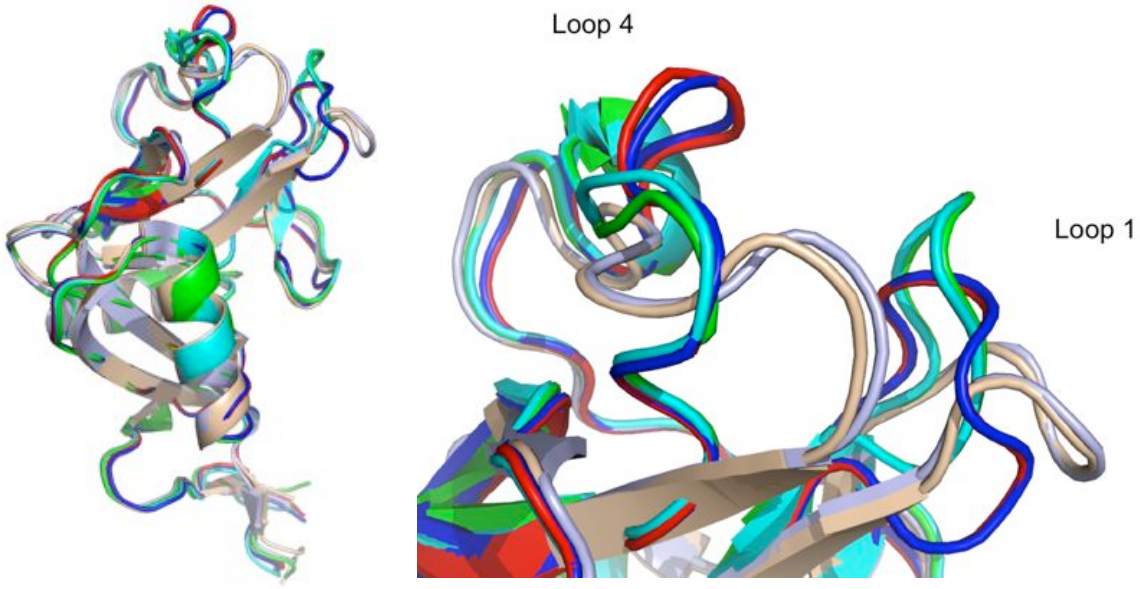

Figure 4.18: The superposition of all the derCD23 structures in this study with the crystal structures obtained by Wurzburg et al. (2000).
It was revealed that the loop 1 and Loop 4 region have an inherent flexibility in the absence of calcium.

4.3.8.4 The H213R and G256S mutations in the crystal structure by Wurzburg et al. (2006)

In the previous crystal structure two mutations were found: H213R and G256S. His213 was previously implicated as one of the residues involved in trimerisation of CD23 as shown by Hibbert et al. (2005). The non-silent mutation from a positively charged residue histidine to another positively charged residue arginine may not affect the propensity of the CD23 head lectin domain to oligomerise, although this can only be confirmed through further mutational studies. However, if future drug discovery efforts targeting the trimerisation sites are to be performed then wild-type structure must be used. The other mutation occurring on the residue Gly256 occurs in Loop4, which is a region of considerable flexibility. This residue is within to the area of IgE binding as previously mapped using NMR chemical shift mapping by Hibbert et al. (2005). Indeed in the crystal

structure of the derCD23/IgE-Fc (Cε3-4) complex solved by Dr Balvinder Dhaliwal (to be discussed in Section 4.4.4) this residue is in the region of 253-257, which is in the area of lost electron density and may be involved in IgE binding. This may explain the failure of co-crystallisation effort of CD23/IgE Fc (Cε3-4) complex initially performed by Wurzburg et al. (2006) as this residue is within the region that may be important in IgE binding.

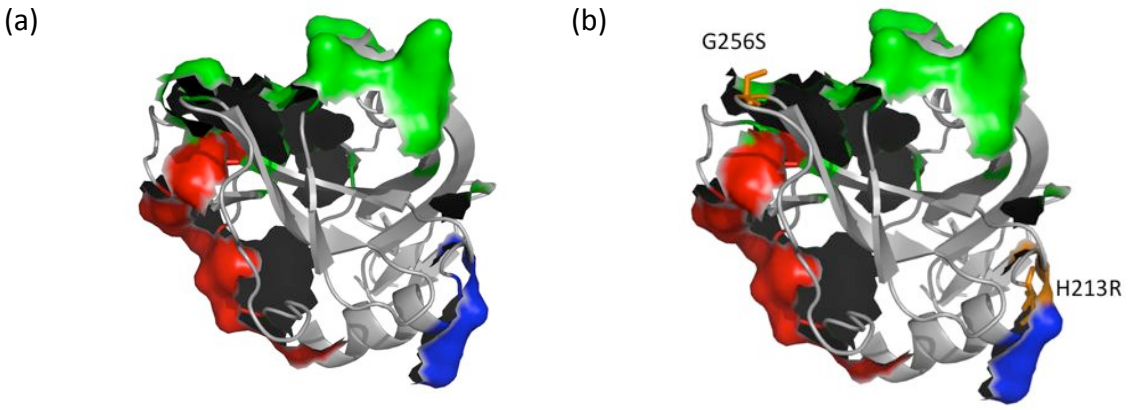

Figure 4.19: The mapping of the two mutations His213R and Gly256S in the CD23 structure from Wurzburg et al. (2006).
a) The IgE binding site (green) and the trimerisation interface (red-negatively charged, blue-positively charged). b) The location of G256S is within the IgE binding site and H213R is at one of the trimerisation interfaces.

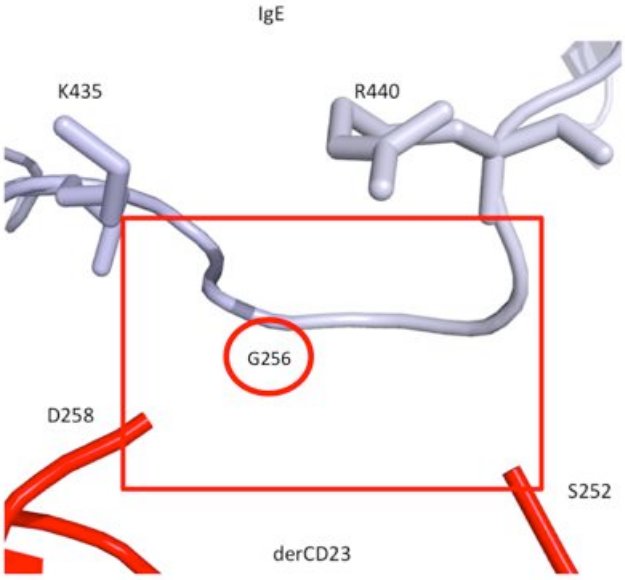

Figure 4.20: The location of Gly256 in the region 253-257 of lost electron density in the derCD23/IgE-Fc (Cε3-4) complex structure.
The mutation G256S from Wurzburg et al. (2006) is in the region that may be involved in IgE binding in the derCD23/IgE-Fc complex solved by Dr Balvinder Dhaliwal (personal communication). The potential contact between derCD23 residues in this region with Arg440 of IgE is discussed in Section 4.4.4.

4.3.9 Other crystallisation efforts

As mentioned in Chapter 2, other crystallisation trials were also done namely triCD23, and complexes of triCD23/IgE-Fc/CD21 (SCR1-2), triCD23/CD21 (SCR1-2). However, at the time of writing, no good crystals were obtained. Crystallisation of the derCD23/CD21 complex will be described in Section 4.5.6. Further crystallisation efforts are now being carried out by Lin Dao Peng and Wen Pin Kao. The crystallisation of the triCD23/IgE/CD21 complex is of particular interest, as it would shed insight on the detailed interaction of the trimolecular complex. It was proposed by Sutton and Gould (2008) that the trimolecular complex formed between triCD23 and membrane IgE and CD21 would form a signalling complex that activates B cells to increase IgE synthesis (Figure 4.21 (a)). This is analogous to the signalling platform formed by co-ligation of the antigen/C3d complex with

membrane Ig and CD21/CD19 co-receptor that activates production of antigen specific antibody-mediated response (Pierce, 2002; Dempsey et al., 1996; Barrington et al., 2009) (Figure 4.21(c)).

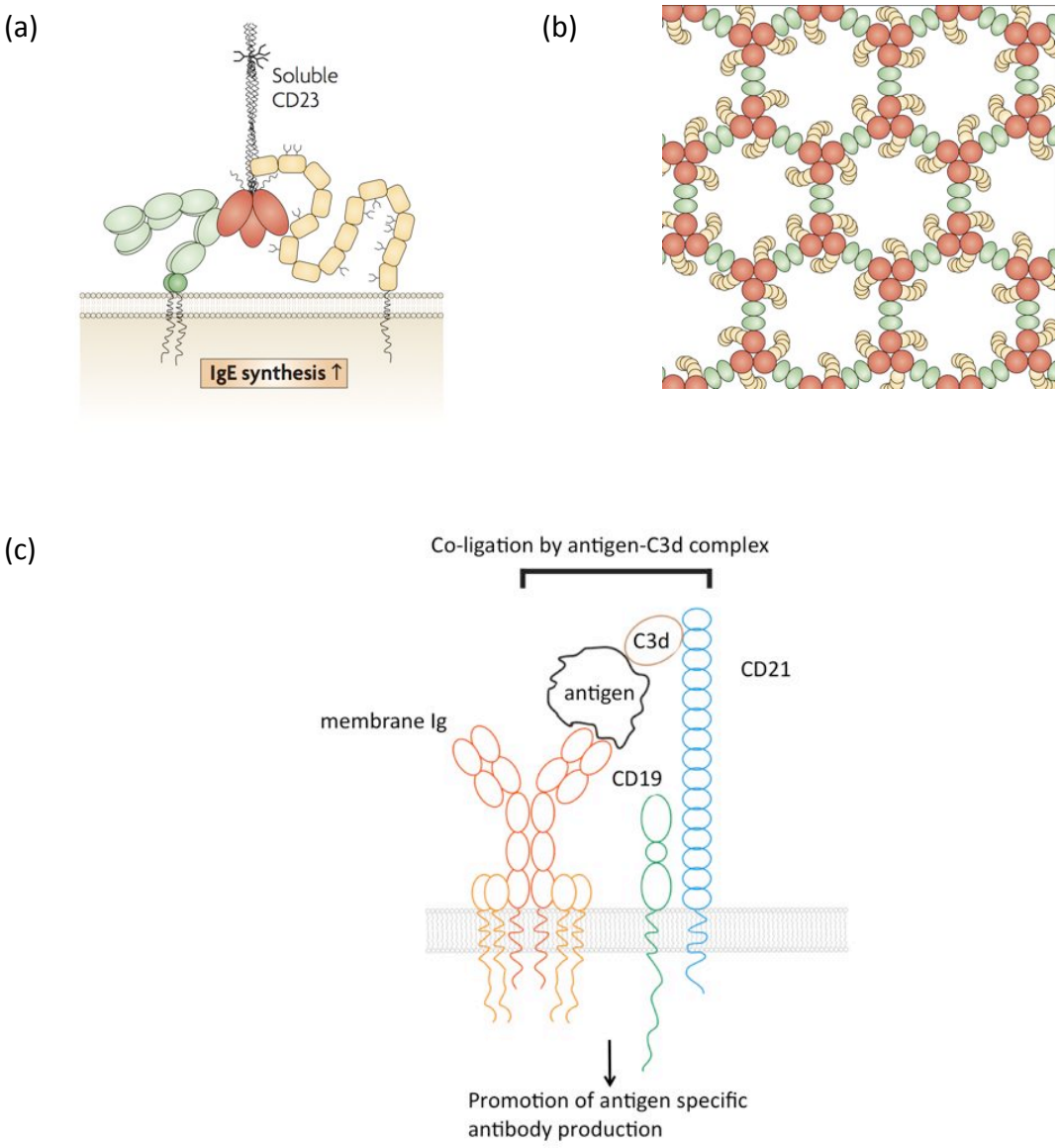

Figure 4.21: The trimolecular complex formation and its proposed role in IgE synthesis.
a) Soluble CD23 forms a trimolecular interaction with IgE and CD21 on IgE committed B cells activating increase of IgE synthesis. b) The formation of a postulated signaling platform involving the trimolecular complex between soluble trimeric CD23 (red) with membrane IgE green) and CD21. It is known that CD23 binds to the two Cε3 domain of IgE whilst retaining its CD21 binding through the C-terminus. This could lead to the formation of an extended network of signaling platform that leads to the increase of IgE synthesis in IgE committed B cells. c) Coligation of membrane immunoglobulin and CD21/CD19 co receptor by antigen-C3d complexes has been shown to lead to the promotion of antigen specific antibody production.

4.3.10 Discussion

A high-resolution crystal structure of derCD23 has been obtained which resulted from several attempts at co-crystallisation as well as crystal soaking of derCD23 with its binding peptides and derivatives. The structural alignment studies on CD23 show that there is an inherent flexibility that was observed in the crystal structures in Loop1 and Loop 4. Despite the failure of co-crystallisation and soaking experiments, a high-resolution crystal structure of derCD23 has been obtained. Future drug discovery efforts involving high throughput crystallisation will require conditions that produce high quality and reproducible protein crystals. As noted, the mutations H213R and G256S from Wurzburg et al. (2006) occurred in sites involved in trimerisation and IgE binding, respectively. The conditions that provide high quality structure of non-mutated CD23 are important if crystallographic-based drug discovery efforts such as compounds and fragment-soaking targeting these sites are to be undertaken. Other crystallisation efforts were undertaken although they were not successful. These efforts are now being continued by others and will help in elucidating the detailed interactions between CD23 and its binding partners.

4.4 The interaction between CD23 and IgE

4.4.1 Introduction

CD23 exists on the membrane and in solution in different forms. On the membrane it exists mostly as a trimer (Kilmon et al., 2004). However the membrane CD23 can be proteolytically cleaved by ADAM-10 into soluble forms (Weskamp et al., 2006). The trimeric version of the soluble form is thought to upregulate IgE synthesis on B cells, by binding to both membrane IgE and CD21 forming a trimolecular complex and activating a signalling cascade which leads to the increase of IgE synthesis (McCloskey et al., 2007). The monomeric version of CD23, termed derCD23, is thought to prevent upregulation of IgE expression by inhibiting the trimeric CD23 from crosslinking membrane IgE and membrane CD21 (McCloskey et al., 2007).

NMR chemical shift mapping of CD23 has been previously performed in our lab (Hibbert et al., 2005) that showed a contiguous surface of IgE binding site on the lectin head domain. The binding site of CD23 on IgE is localised on the Cε3 domain of IgE (Bettler et al., 1989; Chrétien et al., 1988; Nissim et al., 1993). The NMR resonances of the Cε3 domain of IgE have been assigned by Dr Susmita Borthakur (KCL) and the CD23 binding site has been defined. A crystal structure of the derCD23/IgE-Fc (Cε3-4) complex has also been determined by Dr Balvinder Dhaliwal at the Randall Division (KCL) and is used to assist in the analysis of CD23/IgE interactions. This section discusses the various interaction analyses of CD23/IgE interactions.

4.4.2 Binding of derCD23 and trimeric CD23 to IgE

Surface plasmon resonance (SPR) was used to determine the dissociation constant for the interaction between derCD23 and the Fc fragment of IgE (domains Cε2-4) termed IgE-Fc (Cε2-4). Biotinylated IgE-Fc (Cε2-4) (Section 2.3.5.1) was immobilised to streptavidin coated CM5 sensor chip at 80 RU and derCD23 was flowed over the surface. DerCD23 shows fast-on/fast-off kinetics with a calculated K_D of 1.4 μM. A similar experiment was also done for the trimeric CD23 (triCD23) and a K_D of 600 nM was obtained. The difference in the affinity is thought to be due avidity effect in triCD23 (Figure 4.22). The triCD23 construct has an engineered alpha-helical coiled-coil stalk region that holds the three-lectin head together (Section 2.3.5.2).

(a) derCD23 binding to immobilised IgE-Fc

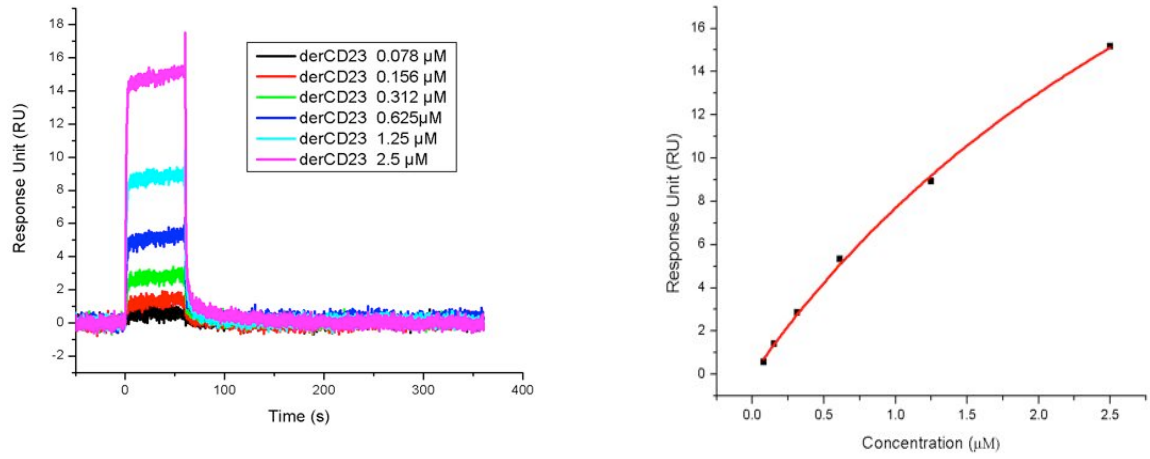

b) triCD23 binding to immobilised IgE-Fc

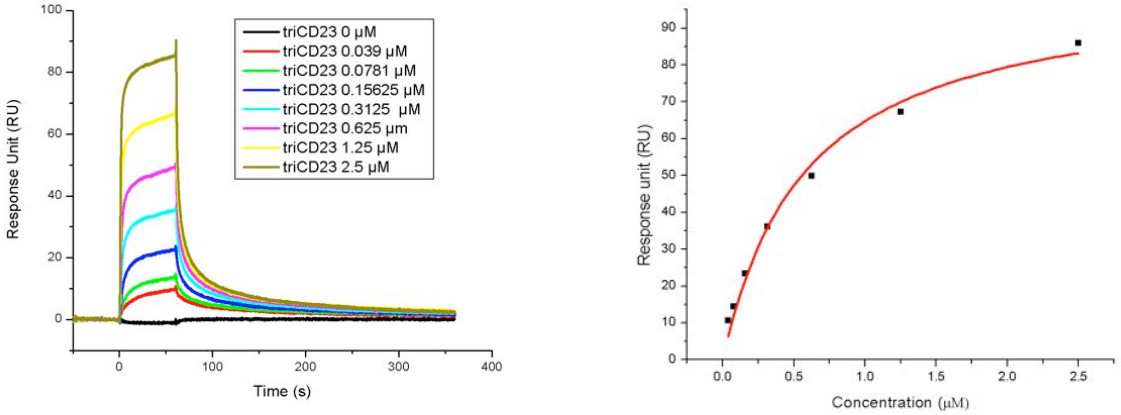

Figure 4.22: SPR data and Langmuir curve of derCD23 and triCD23 binding to IgE-Fc.
Both experiments were done with similar concentration range (0-2.5 µM). a) The interaction of derCD23 with IgE-Fc shows a fast-on/fast-off kinetics with a calculated K_D of 1.4 µM. b) The interaction of triCD23 with IgE-Fc shows two component dissociation kinetics with both fast and slower dissociation. The K_D calculated for this interaction was 600 nM. Data fitting was performed using Origin 7.0. (OriginLab Corporation, Northampton, MA).

4.4.3 Oligomerisation of derCD23 and trimeric CD23 to IgE

4.4.3.1 Oligomerisation of derCD23 upon binding to IgE

To test for the propensity of derCD23 to oligomerise upon binding to IgE, a CM4 sensor SPR chip was coated with biotinylated IgE-Fc at two different immobilisation levels, at 100 RU and 600 RU on separate flow cells. DerCD23 was then flowed over the surfaces simultaneously. From the sensorgram (Figure 4.23 (a)), it can be seen that at lower immobilisation level of IgE-Fc derCD23 shows a fast-on/fast-off kinetics, and the binding is consistent with a 1:1 stoichiometry. This suggests that monomeric derCD23 in solution binds to a single immobilised IgE molecule thus explaining the 1:1 stoichiometry. NMR experiments previously performed by Hibbert et al. (2005) showed that derCD23 is monomeric in solution but has a tendency to oligomerise at higher concentrations, with an affinity, K_D for itself of about 2 mM. The concentration range used in the SPR experiment, however, is low enough to keep derCD23 in the monomeric state. At the higher immobilisation level of IgE-Fc, derCD23 starts to show a slower dissociation rate (Figure 4.23 (b)). This is due to an avidity effect of the (now) oligomeric derCD23. Although the concentration of derCD23 in solution is well below its K_D for itself, as derCD23 binds to the surface of a high-immobilisation density SPR chip, the local concentration of derCD23 becomes high enough to drive derCD23 oligomerisation.

(a) DerCD23 binding to 100 RU IgE-Fc

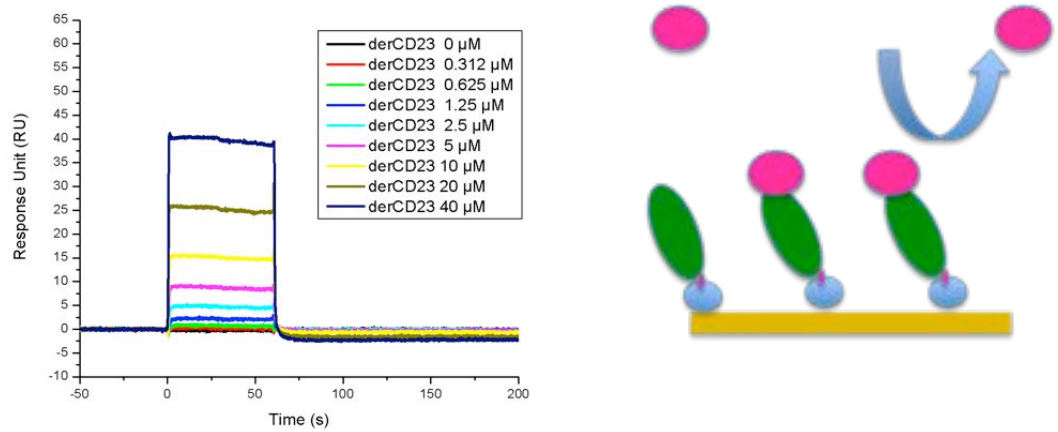

(b) DerCD23 binding to 600 RU IgE-Fc

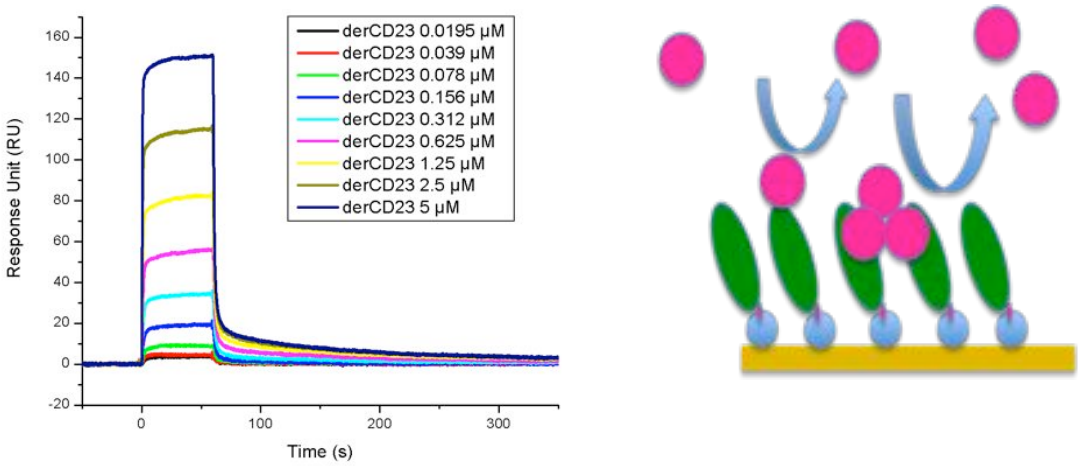

Figure 4.23: Binding of derCD23 on lower and higher immobilisation levels of IgE-Fc.
(a) derCD23 in concentration range of 0-40 µM flowed on lower immobilisation surface at 100 RU showed a fast-on/fast-off kinetics with IgE Fc. (b) derCD23 in concentration range (0-5 µM) flowed on higher immobilisation level surface at 600 RU showed a tendency to oligomerise. Data fitting was performed using Origin 7.0 (OriginLab Corporation, Northampton, MA).

4.4.3.2 Interaction of trimeric CD23 at different immobilisation levels of IgE

Trimeric CD23 (triCD23) showed evidence of avidity effects at lower immobilisation densities than the derCD23 molecule (Section 4.4.2). To test for further oligomerisation at higher density, a streptavidin coated CM4 sensor chip was coated with a high (1000 RU), intermediate (500 RU) and low (100 RU) immobilisation levels of biotinylated IgE-Fc on separate flow cells. Trimeric CD23 has a tendency to bind to the negatively charged dextran matrix surface on the CM5 chip possibly due to the extra engineered alpha-helical coiled-coil region (sequence: IAAIESKIAAIESKIAAIESKIAAIESKRN), which contains several positively charged residues and therefore the CM4 sensor chip was chosen as its dextran matrix has a lower degree of carboxylation and is less negatively charged.

A constant concentration of triCD23 at 10 μM was then flowed over the surface. As shown in Figure 4.24, triCD23 shows a much slower dissociation rate at higher immobilisation levels. The dissociation constant, k_{off} obtained for the interaction at 1000RU, 500 RU and 100 RU are 0.05 s^{-1}, 0.15 s^{-1} and 0.2 s^{-1}. These values suggest that at higher density of IgE-Fc immobilisation the dissociation rate becomes slower which suggests avidity, mediated by an oligomeric CD23 structure.

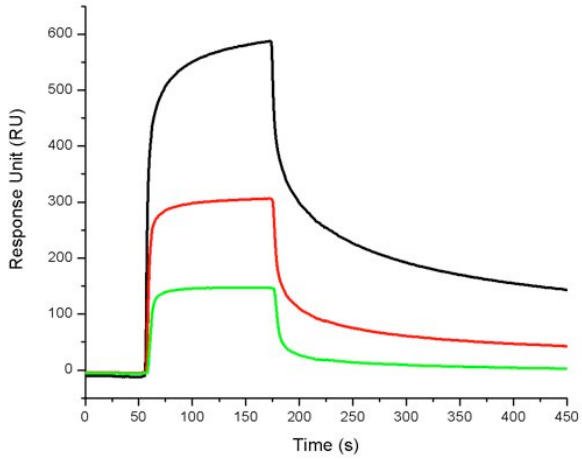

Figure 4.24: TriCD23 binding to different immobilisation levels of IgE-Fc.
A constant concentration of triCD23 at 10 μM was flowed over on three different immobilisation levels of IgE-Fc at 1000 RU (black), 500 RU (red) and 100 RU (green).

4.4.3.3 Inherent propensity for oligomerisation of CD23 upon IgE binding: implications for IgE inhibition

From the observations above it can be shown that both derCD23, containing only the lectin head domain, as well as the trimeric CD23 can form high molecular weight aggregates upon binding to IgE-Fc. This suggests that the lectin head domain has an inherent propensity to oligomerise, supported by the trimeric model of CD23 proposed by Hibbert et al. (2005). The role of the stalk region is therefore to stabilise the trimer formation on the membrane and perhaps in solution. The destabilisation of the CD23 stalk by the antibody 19G5 (Ford et al., 2006) and EBVCS1 (Munoz, 1998) lead to the release of soluble CD23 and subsequent increase in IgE synthesis. ADAM-10 has been identified as the principal CD23 cleavage enzyme (Weskamp et al., 2006) and its inhibition also leads to the reduction of soluble CD23 release and subsequent reduction in IgE levels (Sturgill et al., 2011). The stabilisation of trimeric CD23 therefore, has been suggested as a

therapeutic target (Conrad et al., 2007). This would prevent the cleavage of membrane bound CD23 into its soluble forms thus inhibiting IgE synthesis. However stabilization of trimerisation through its stalk would be difficult as most antibodies designed against the stalk region lead to destabilization (Ford et al., 2006; Munoz, 1998). The inhibition of the CD23 metalloprotease, ADAM-10 is also an attractive target but it is involved in many functions including Notch-dependent lymphocyte development and therefore inhibition may lead to adverse effects. Taken together, the stalk region of CD23 is an attractive target for IgE inhibition. The lectin head is perhaps a potential target for trimerisation disruption of soluble CD23. It has been shown that the oligomeric form of CD23 is required for the high affinity binding to IgE exemplified by the higher affinity binding of trimeric CD23, and disrupting it may be one of potential mechanism to inhibit the binding of CD23 to membrane IgE which could inhibit IgE synthesis as proposed in the trimolecular interaction model of IgE upregulation (McCloskey et al., 2007).

4.4.4 Identification of potential contact residues between CD23 and IgE

The binding site of IgE on CD23 has been previously defined using NMR chemical shift perturbation experiments (Hibbert et al., 2005). On IgE, the binding epitope of CD23 has been defined to be within the Cε3 domain (residue 328-437) (Vercelli et al., 1989; Chrétien et al., 1988; Nissim et al., 1993). The NMR resonances of the Cε3 domain of IgE have been assigned recently by Dr Susmita Borthakur (KCL), and were used to map the binding site of CD23 on Cε3 (unpublished data). The residues implicated were found to be clustered in the AB and EF helices of Cε3 forming a contiguous binding surface (Figure 4.25).

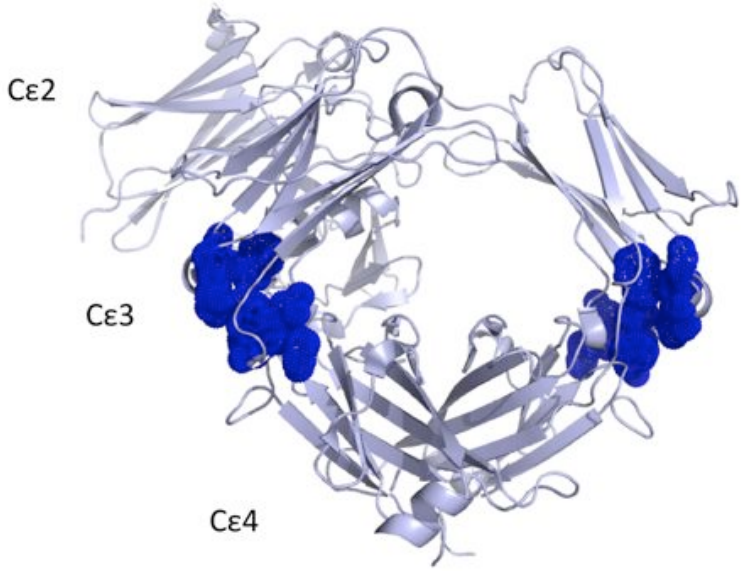

Figure 4.25: The NMR chemical shift mapping of CD23 on Cε3 mapped on Fc fragment of IgE, IgE-Fc (Cε2-4).
PDB ID: 1O0V (Wan et al., 2002) showing a contiguous surface as previously determined by Dr Susmita Borthakur (unpublished data).

Previously, Dr Rick Hibbert performed site-directed mutagenesis on derCD23. The following mutations were made: R224A, K276A, Y189A, D236A, L226A and D265A (unpublished data). Mutations were tested for their effect on the interaction with IgE-Fc (Cε2-4). Four further mutations on derCD23 were made in this study, namely R188A, D192A, D257A and D227A (Figure 4.26). On the IgE side, several mutations were performed on the Cε3 domain of IgE-Fc (Cε3-4), namely K380A, R351A, K435A, D347A, E412A and F439A; the binding analysis using SPR was performed by Dr Susmita Borthakur (unpublished data) (Figure 4.27b). The binding affinity values of all the tested mutants so far are as presented in Table 4.3.

Table 4.3: List of derCD23 and IgE-Fcmutants generated and affinity values obtained.

The binding affinities for mutants of derCD23 and IgE-Fc IgE-Fc (Cε2-4). a) The binding affinity values of derCD23 mutants with IgE-Fc (Cε2-4). The values highlighted in bold are those performed in this study. b) the affinity values for IgE-Fc (Cε2-4) binding to derCD23 as performed by Dr Susmita Borthakur.

(a)

CD23	Affinity, K_D (μM)
WT	1.3
R188A	**25.0**
D192A	**4.3**
E257A	**26.0**
D227A	**31.0**
R224A	25.0
K276A	19.5
Y189A	15.6
D236A	9.0
L226A	6.8
E265A	2.7

(b)

IgE-Fc (Cε2-4)	Affinity, K_D (μM)
WT	1.3
E412A	22
K380A	13
R351A	2.6
K435A	5.0
D347A	2.5
F439A	2.5

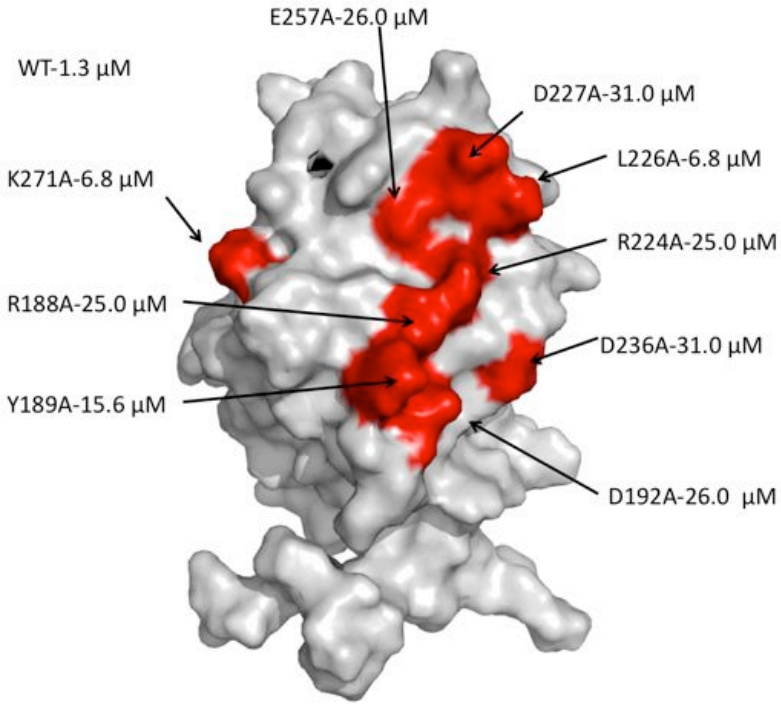

Figure 4.26: The effect of CD23 mutations on the affinity values for IgE-Fc (Cε2-4) binding.

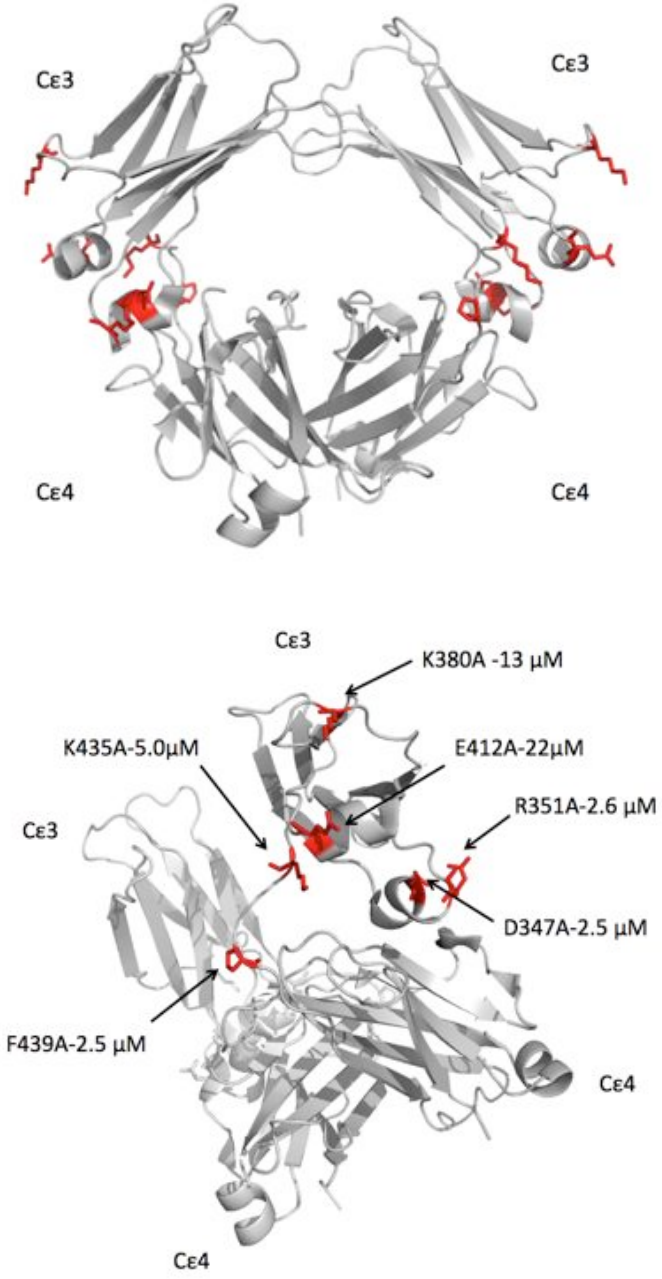

Figure 4.27: Effects of IgE-Fc (Cε2-4) mutations on derCD23 binding.
The effects of mutations on IgE-Fc (Cε2-4) binding to derCD23 mapped on a structure of IgE-Fc (3-4) PDB ID: 3H9Z. (Top) Front face of IgE-Fc (Cε3-4) highlighting the reidues mutated. (Bottom) A tilted view of IgE-Fc (Cε3-4).

A crystal structure of the derCD23/IgE-Fc (Cε3-4) complex has recently been solved by Dr Balvinder Dhaliwal at the Randall Division (KCL) and is currently being refined (Figure 4.28). The interaction surfaces defined by the NMR and site-directed mutagenesis studies agree well with the crystal structure. However in the crystal structure there is an area of lost density between residues 253 and 257 in derCD23, which is not modeled into the structure and may be caused by flexibility in this region. By using the crystal structure of derCD23/IgE-Fc (Cε3-4) as well as the NMR mapping and SPR binding data, several possible residue-residue contacts, including salt bridges, can be identified.

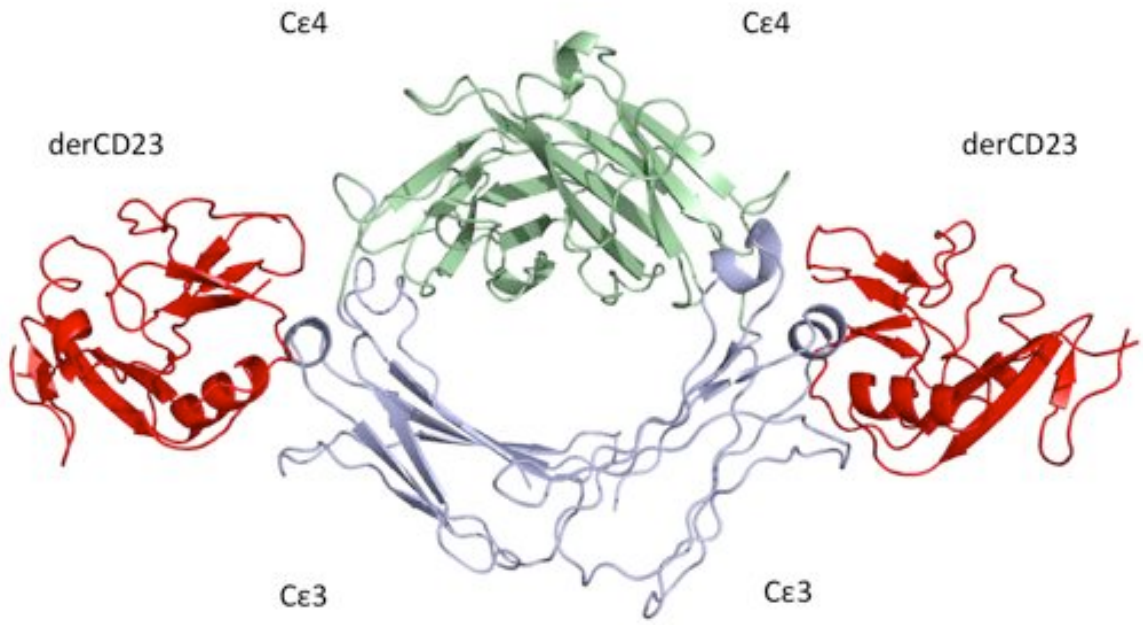

Figure 4.28: The crystal structure of CD23/IgE-Fc (Cε3-4) complex.
The structure was solved by Dr Balvinder Dhaliwal**.** The structure shows two derCD23 molecules binding to the Cε3 domains of the IgE-Fc (Cε3-4).

E412 may form interchangeable salt bridge with R188 and R224

The interaction between the derCD23 mutations: R188A and R224A with wildype IgE-Fc showed a K_D of 25.0μM and 24.9 μM, respectively, which is a reduction of ~20-fold compared to the wildtype interactions. The interation between the IgE-Fc (Cε2-4) E412A mutation with wildtype derCD23 showed a K_D of 22 μM, which is a reduction of ~19-fold compared to the wildtype interactions. These reductions in affinity indicate a stronge energetic contribution to binding to IgE. In the crystal structure, the side chain of the negatively charged E412 is close to the positively charged R188A with a distance of 3.5 Å. The side chain of R224 is also in close contact to E412 with a distance of 4.6 Å. This may suggest that E412 could form salt bridges with R224 and R188 in CD23 (Figure 4.29).

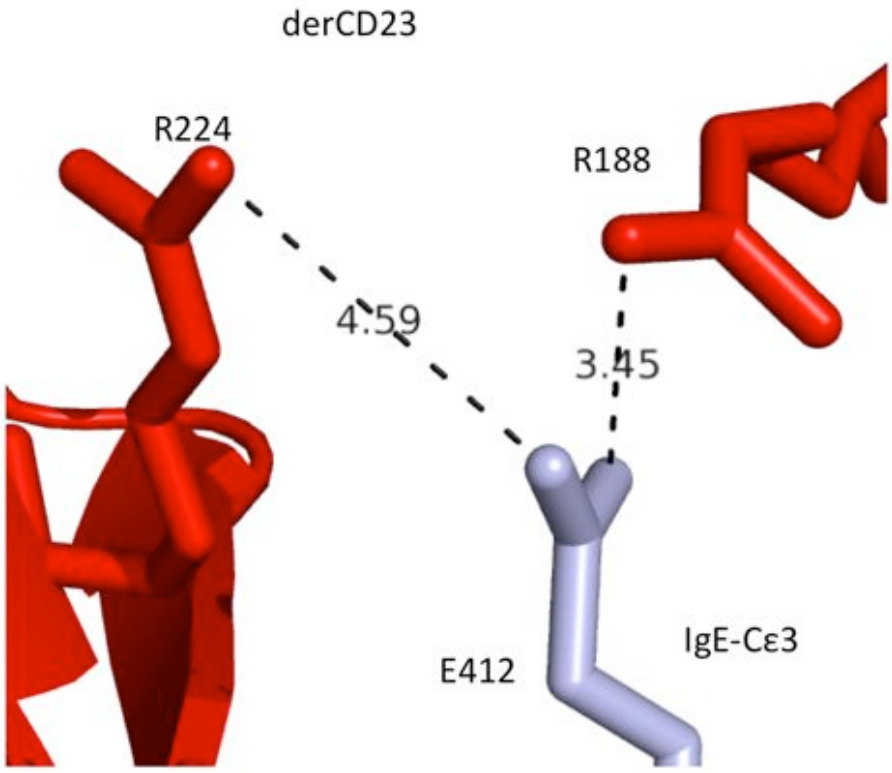

Figure 4.29: Potential interchangeable salt bridges between IgE-Fc (Cε2-4)-Glu412 and residues Arg224 and Arg188 in derCD23.

Salt bridges between CD23 D192 and IgE K380

The derCD23 D192A mutant showed an affinity of 4.3 μM with wild type IgE-Fc (Cε2-4). The affinity obtained for IgE-Fc (Cε2-4) K380A with wildtype derCD23 was 13 μM, which is a ten-fold reduction compared to the wildtype interactions. The distance between the side chains is measured to be 3.9 Å (Figure 4.30).

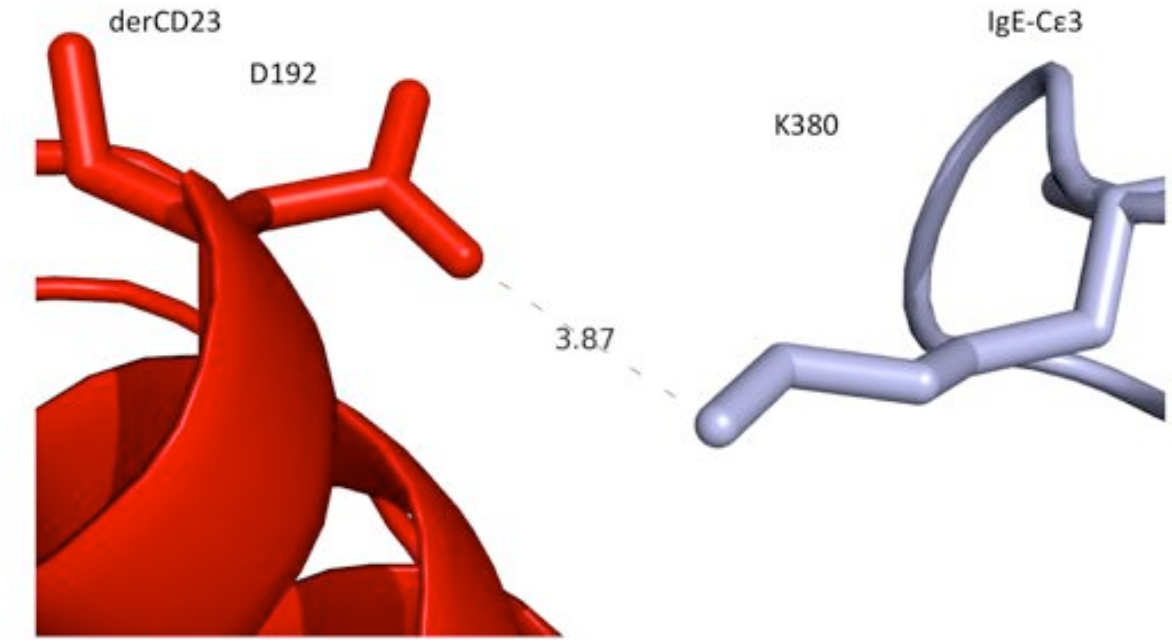

Figure 4.30: Potential salt bridge between derCD23-D192 and IgE-Fc (Cε2-4) K380.

Potential salt bridges within the lost density area 253-257 in IgE

The CD23 mutant E257A showed a ~20-fold reduction of affinity (K_D of 26 μM) with the wild type IgE-Fc (Cε2-4). However in the crystal structure the density is lost around this region between residues 253 and 257 and not modeled into the crystal structure. This missing segment is close to the positively charged residues K435 and R440 from IgE (Figure 4.31). The IgE mutant K435A showed a ~4-fold reduction of affinity (K_D of 5.0 μM) also indicating its involvement in binding to derCD23.

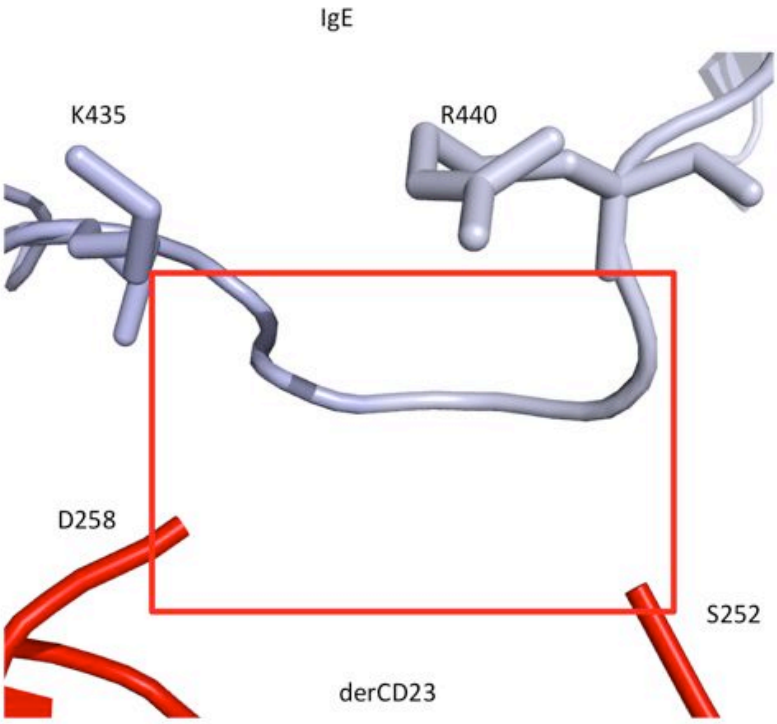

Figure 4.31: The lost electron density area between residues 253-257.
Residue Glu257, which is within the area of lost density showed a reduction of affinity.

Residue contacts between Tyr189 with Asp 409

The derCD23 mutation Y189A showed a reduction of affinity ~12-fold (K_D of 26 μM) with the wild type IgE-Fc (Cε2-4). Upon inspection of the crystal structure, it was shown that a hydrogen bond may be formed between the hydroxyl of derCD23 Y189 and the carboxylic acid oxygen of IgE-Fc D409 with a measured distance of 2.56 Å (Figure 4.32).

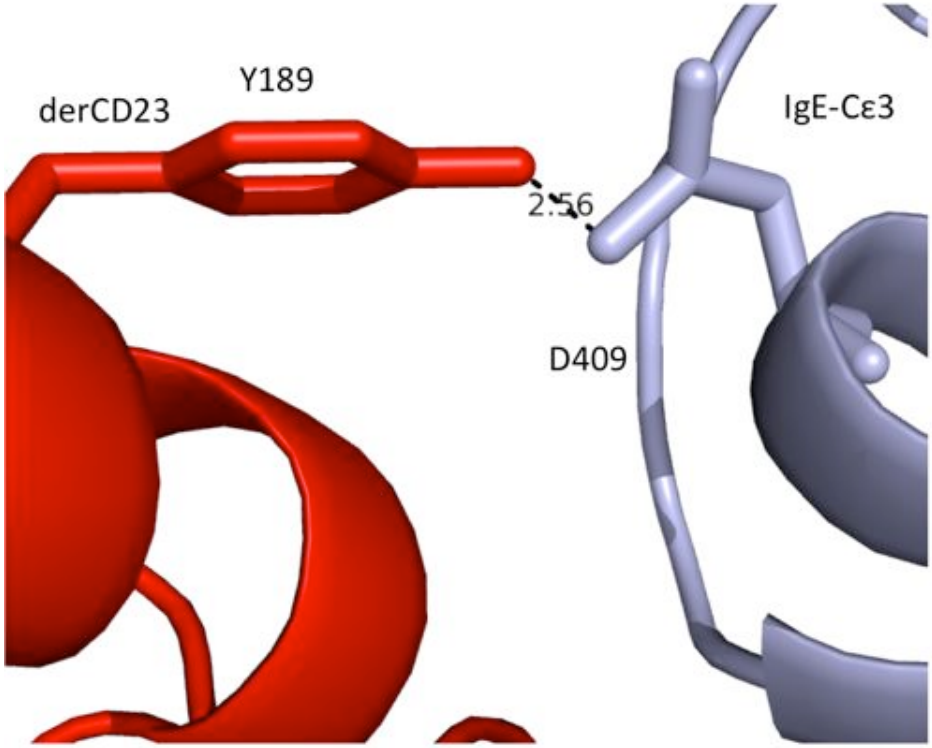

Figure 4.32: Potential hydrogen bond contact between the –OH group of Tyr 189 and the =0 group of Asp 409.

4.4.5 Generation of mutants with possible biological consequences

A double mutant derCD23 (R188A, D227A) leads to a >150-fold reduction of IgE binding affinity. The double mutant markedly reduced IgE binding to CD23, with an estimated K_D of ~350 μM (Richard Hibbert, DPhil Thesis, University of Oxford, 2005) . As noted earlier, it was proposed that trimeric CD23 binds to both membrane IgE and membrane CD21 to upregulate IgE synthesis in activated B cells. A comparison can be done on the effect on IgE synthesis between the trimeric CD23, which crosslinks membrane IgE and membrane CD21, with the CD23 double mutant that binds only to CD21. The double mutant can also be tested for inhibiting the trimolecular interaction by binding to membrane CD21, thus

blocking trimeric CD23 from crosslinking membrane IgE and CD21 simultaneously (Alison Cooper, KCL, experiments in progress).

4.4.6 Discussion

The differences seen in the behaviour of binding between derCD23 and the trimeric CD23, which contains the engineered stalk region, indicate that the trimeric version of CD23 binds to IgE with higher affinity. Monomeric derCD23 has a tendency to oligomerise upon binding to high-density immobilised IgE-Fc indicating oligomerisation upon binding. Trimeric CD23 also shows the same tendency to oligomerise upon binding to high immobilisation level of IgE-Fc.

Several mutations were made on CD23 to identify specific residues that are involved in IgE binding. These mutations alongside others previously made were analysed using the available crystal structure of the derCD23/IgE-Fc (Cε3-4) complex. The analysis so far has showed that the region previously defined as CD23 binding site is largely confined to the Cε3 domain, consistent with previous site-directed mutagenesis studies. However, it was also noticed that part of the Cε4 domain might be implicated in binding as the CD23 mutant E257A, which resides within the area of lost electron density near to Arg440 at the Cε3/Cε4 linker region, led to a significant reduction in affinity in the SPR analysis. These contact residues identified so far are mapped onto the crystal structure of derCD23/IgE-Fc (Cε3-4) as shown in Figure 4.33 and magnified in Figure 4.34. Further mutagenesis studies will be needed to establish the important binding interface in the CD23/IgE interaction. Upon refinement of the crystal structure, a potential inhibitor could

perhaps be designed using the combined knowledge together with the NMR titration data as well as the site-directed mutagenesis studies.

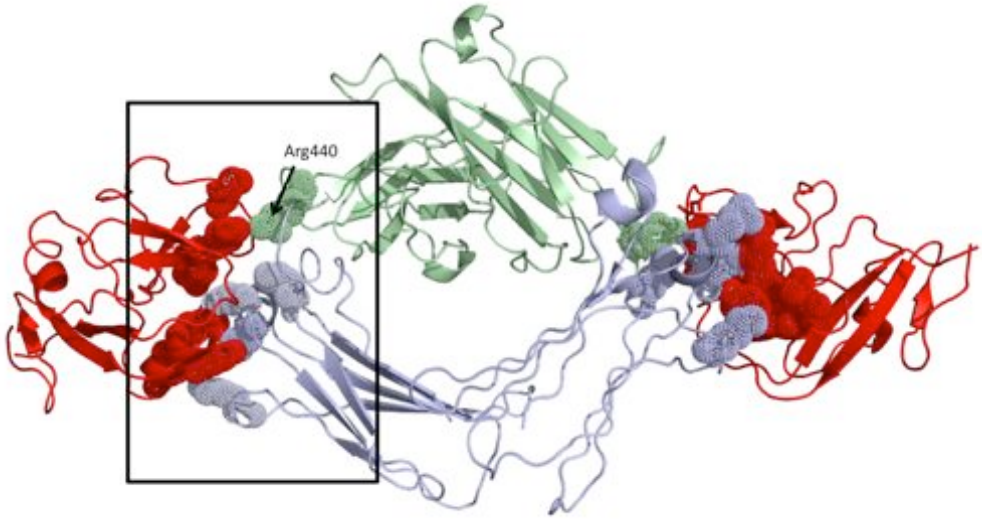

Figure 4.33: The structure of CD23-IgE with the potential residue contacts highlighted including Arg440 in the linker region between Cε3 and Cε4 of IgE-Fc (Cε3-4).

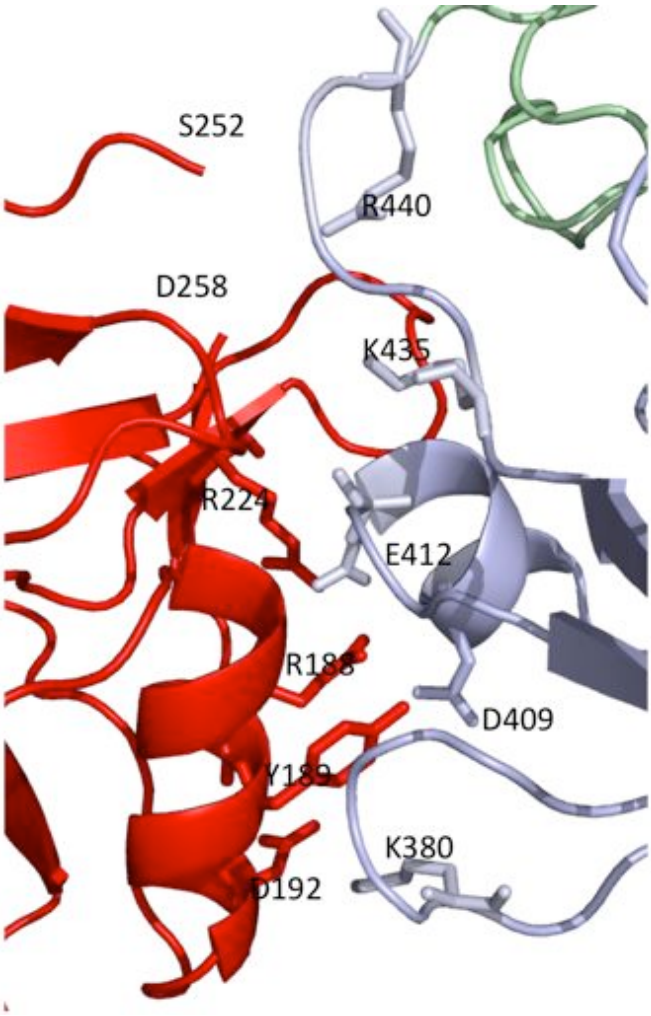

Figure 4.34: The magnified view of the contact residues identified.
The possible interactions identified so far which can be grouped into four possible pairings. A) The interaction between the area of missing density in derCD23 (S252-D258) with IgE R440 and K345 B) Interaction between derCD23 R224/R188A with IgE-E412 C) The interaction between derCD23-R189 and IgE-D409 and D) The interaction between derCD23-D192 with K380.

4.5 The Interaction between CD23 and CD21

4.5.1 Introduction

The binding site of CD21 (SCR1-2) on derCD23 has been determined by NMR chemical shift perturbation studies and found to be the last seven amino acids of the C-terminal tail (Figure 4.35). This section discusses the generation of CD23 mutants lacking the C-terminal region to confirm the binding site of CD21.

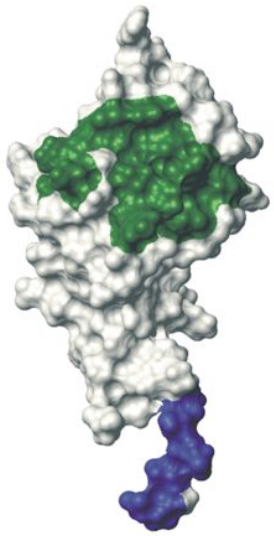

Figure 4.35: The binding sites of IgE (green) and CD21 (SCR 1-2) on derCD23as previously mapped using NMR chemical shift perturbation experiments by Hibbert et al. (2005).

4.5.2 Generation of mutant CD23 with diminished binding to CD21

A construct of derCD23 lacking the seven C-terminal residues, termed derCD23minus7, was expressed and purified using the same protocol previously established for derCD23 (Hibbert et al., 2005). The correct folding of this mutant protein was confirmed by one-dimensional ^{1}H-NMR spectroscopy. The mutant showed the same characteristic pattern of upfield-shifted methyl peaks expected for a correctly folded derCD23 (Figure 4.36). Purification of CD21 (SCR1-2) is described in Section 2.3.3.

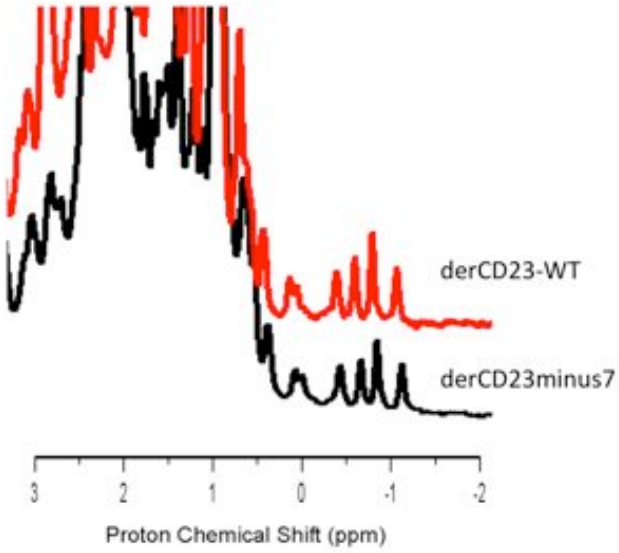

Figure 4.36: ^{1}H-NMR spectra of the wildtype derCD23 and the truncated derCD23minus7.
The characteristic pattern of the upfield methyl peak indicate that derCD23 and CD23minus7 are folded.

4.5.3 SPR immobilisation attempts with CD21 (SCR1-2)

In order to do a side-by-side comparison of the binding of different derCD23 constructs to CD21, the immobilisation of CD21 onto an SPR sensor chip is required. Two approaches were attempted. Firstly is the immobilisation of CD21 through streptavidin using a biotinylated CD21 (SCR1-2) and secondly, the use of an anti-histag antibody (Qiagen) to immobilise CD21 (SCR1-2) through its hexahistidinte tag in its C-terminus is present in the construct.

4.5.3.1 Biotinylation of CD21 (SCR1-2)

CD21 was biotinylated by mixing with NHS-biotin (Sigma) with 3:1 molar ratio (CD21: NHS-biotin) in PBS, pH 7.3 and incubated at room temperature for 2 hours or overnight at 4^{o}C. A molar ratio 3:1 of CD21: NHS-biotin was used to ensure that no CD21 molecule is biotinylated at more than one site and single biotinylation was confirmed by mass

spectrometry. NHS attached to biotin forms a spontaneous amide bond with primary amines on the side chain of lysine residues (Hermanson, 2008).

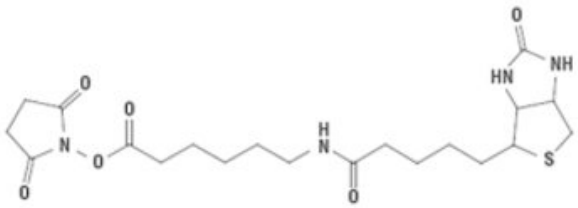

Figure 4.37: Structure of EZ™ Link NHS-LC-Biotin.

Streptavidin (Sigma) was then immobilised on a CM5 sensor chip using amine-coupling methods. Biotinylated CD21 was then bound to streptavidin surface to a density 400 RU. However, when the derCD23 was flowed over the binding surface, the binding was observed to be very weak as it did not reach saturation, B_{max}, as expected at such density level (Figure 4.38). As a positive control, a test with a mutant C3d construct E160A showed an affinity of 10 uM which is much lower than the previously measured value at 700 nM (Martine Bomb, DPhil thesis, 2008) (Figure 4.39). It is clear that the immobilisation of the CD21 (SCR1-2) protein through biotinylation results in a substantial loss in its capacity to bind to either derCD23 or C3d. It is possible that the heterogeneity of CD21 biotinylation (Figure 4.40) may also lead heterogeneity in the immobilization that may obscure the binding sites. In an alternative strategy, a specific biotinylation peptide sequence may be placed at the C-terminus of the CD21 (SCR1-2) construct, which can in turn be enzymatically biotinylated in a specific manner using commercially available kits (Ashraf et al., 2004) and enable immobilization with a uniform orientation (with SCR-2 tethered to streptavidin).

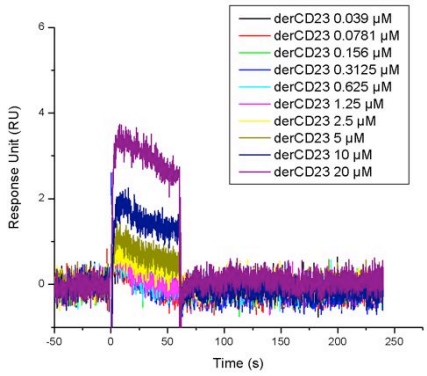

Figure 4.38: DerCD23 binding to CD21 surface immobilised through biotinylation.
DerCD23 was flowed over a range of concentrations (0-20 µM) to the biotinylated CD21 (SCR1-2) bound to the streptavidin surface.

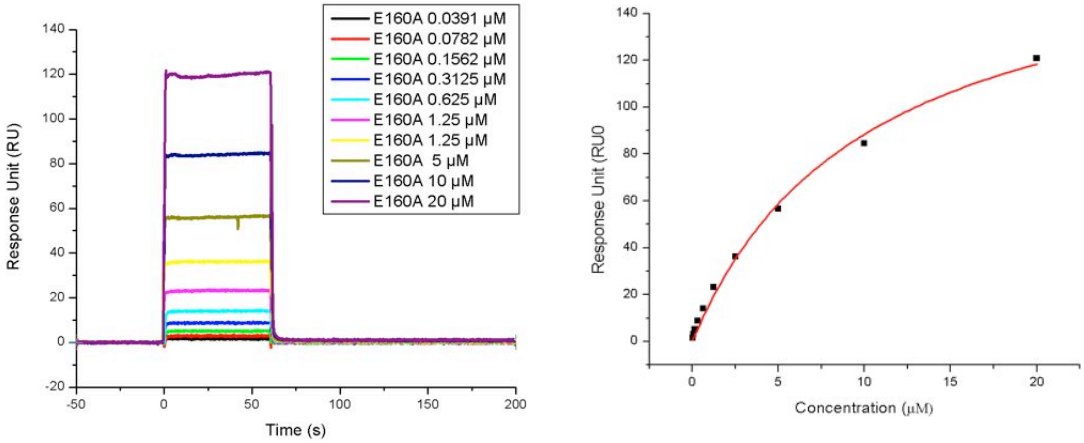

Figure 4.39: C3d mutant binding to CD21 surface immobilised through biotinylation.
Binding of a C3d mutant E160 over a range of concentrations (0-20 µM) to the same CD21 (SCR1-2) surface. The K_D obtained was 10 µM, which is signifcantly lower than the ITC-derived value of 700 nM.

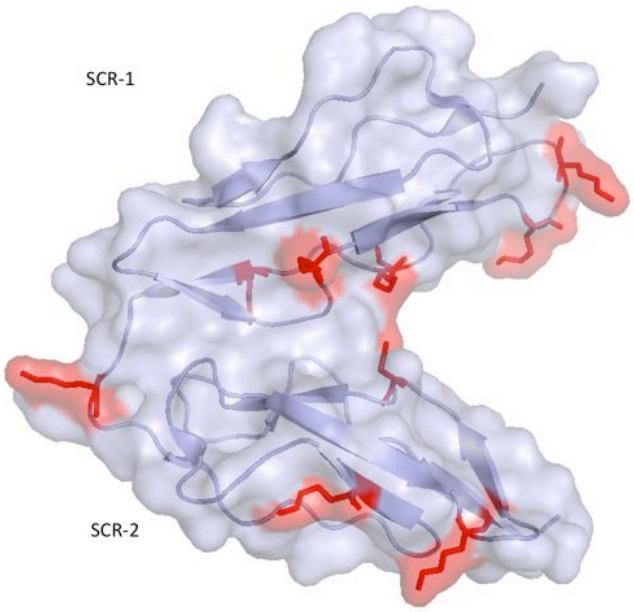

Figure 4.40: Lysine residues highlighted on CD21 (SCR1-2) showing dispersed positions of the lysine residues that may have led to a heterogeneity of biotinylation.

4.5.3.2 Immobilisation through an anti-his tag antibody

The CD21 (SCR1-2) construct contains a hexahistidine tag (Section 2.3.3.4), which can be exploited for immobilization using an anti-His tag antibody. The anti-his tag antibody, Penta-His Antibody (Qiagen) was chosen for immobilization through binding to the His-tag (Müller et al., 1998). The anti-his tag antibody was immobilized on a CM4 chip to a density of 400 RU through the amine coupling procedure (Schasfoort, 2008). 10 μM CD21 (SCR-1-2) was then flowed over the anti-His tag surface. However, it was found that CD21 dissociated gradually from the surface (Figure 4.41). DerCD23 was flowed over a range of concentration (0-20 μM) and showed concentration dependent binding as shown in Figure 4.41. The dissociation of CD21 (SCR1-2) from the anti-his tag antibody led to difficulty in obtaining an affinity value for derCD23 binding. The regeneration of the

surface with 1M $MgCl_2$ in each cycle followed by CD21 (SCR-1-2) immobilisation was attempted but resulted in reduced antibody binding capacity for CD21 (SCR1-2).

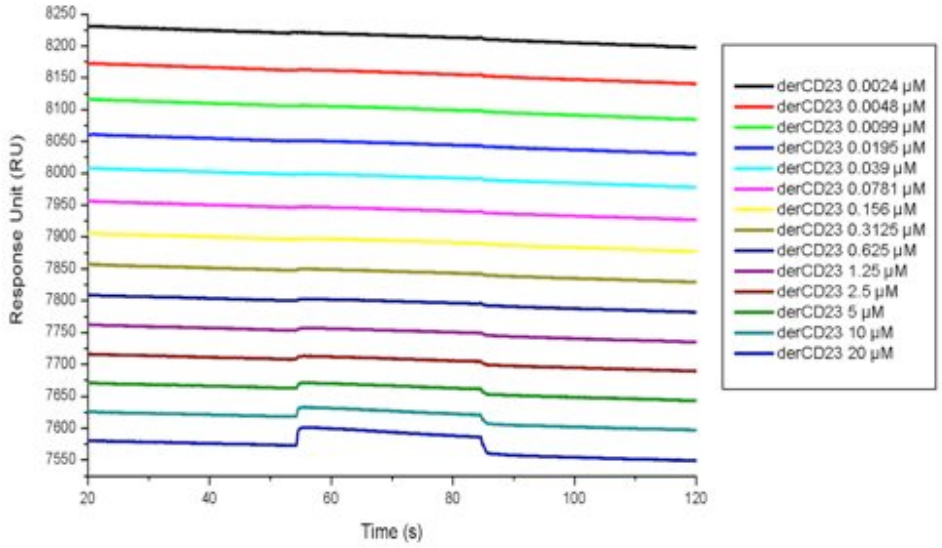

Figure 4.41: The binding of derCD23 over a range of concentration from (0-20 µM) to the anti-his tag immobilised CD21 surface showing the change in baseline levels.

DerCD23minus7 was also flowed over similarly regenerated surface using the same concentration range. DerCD23minus7 binds more to the control surface resulting in a concentration dependent negative signal (Figure 4.42).

(a)

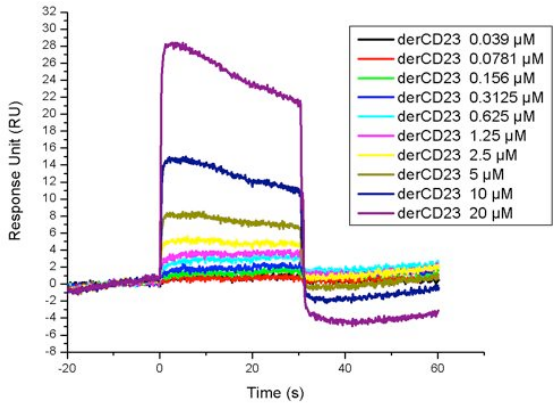

(b)

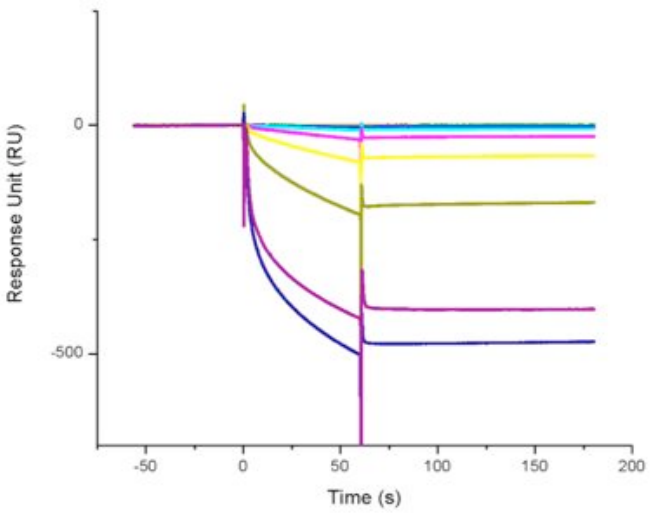

Figure 4.42: Binding of derCD23 and derCD23minus7 on CD21 immobilised through anti-histag antibody.
a) DerCD23 was flowed over the anti-his tag bound CD21 surface at concentrations 0-20 µM. The dissociation of CD21 from anti-his tag antibody leads to unstable baselines, which led to problems in interpretting the data. b) The surface was regenerated and CD21 was immobilised to the same resonance unit. DerCD23minus7 was flowed over the anti-histag immobilised CD21 surface. At increasing concentrations, CD23minus7 starts to bind non-specifically to the control surface leading to a negative resonance signal.

4.5.4 NMR titration of ^{15}N-labelled CD23minus7 with unlabelled CD21

In order to establish whether other residues on derCD23 apart from the C-terminus could be involved in CD21 (SCR1-2) binding, an NMR chemical shift titration experiment was performed using the ^{15}N-labelled derCD23minus7 titrated with unlabelled CD21 (SCR1-2).

BL21 (DE3) cells were transformed with the derCD23minus7 construct and in grown in minimal media containing ^{15}N-labelled NH_4Cl and the protein expressed, refolded and purified. CD21 (SCR1-2) was refolded, purified, dialysed into the appropriate buffer and concentrated to minimise dilution effects.

A sample of 100 μM ^{15}N-labelled CD23minus7 was titrated with an increasing final concentration of CD21 at molar ratios of 0:1, 0.25:1, 0.5:1, 0.75:1, 1:1 and 1.25:1 (CD21 (SCR1-2): derCD23minus7. Inspection of the ^{1}H-^{15}N HSQC spectra reveals that no chemical shift perturbations were seen in the overlaid spectra (Figure 4.43). To confirm that the two proteins are not precipitated or unfolded which could otherwise lead to spectral changes, the one-dimensional ^{1}H-NMR spectra were collected for each point of the titration (Figure 4.44). The characteristics peaks for both CD23 and CD21 are visible at each point of the titration with signals from the latter becoming more dominant towards oversaturation at 125%. The absence of chemical shift perturbations in the CD23minus7 spectrum even when saturated with CD21 confirms that the CD21 binding site is localised on the C-terminal tail of CD23.

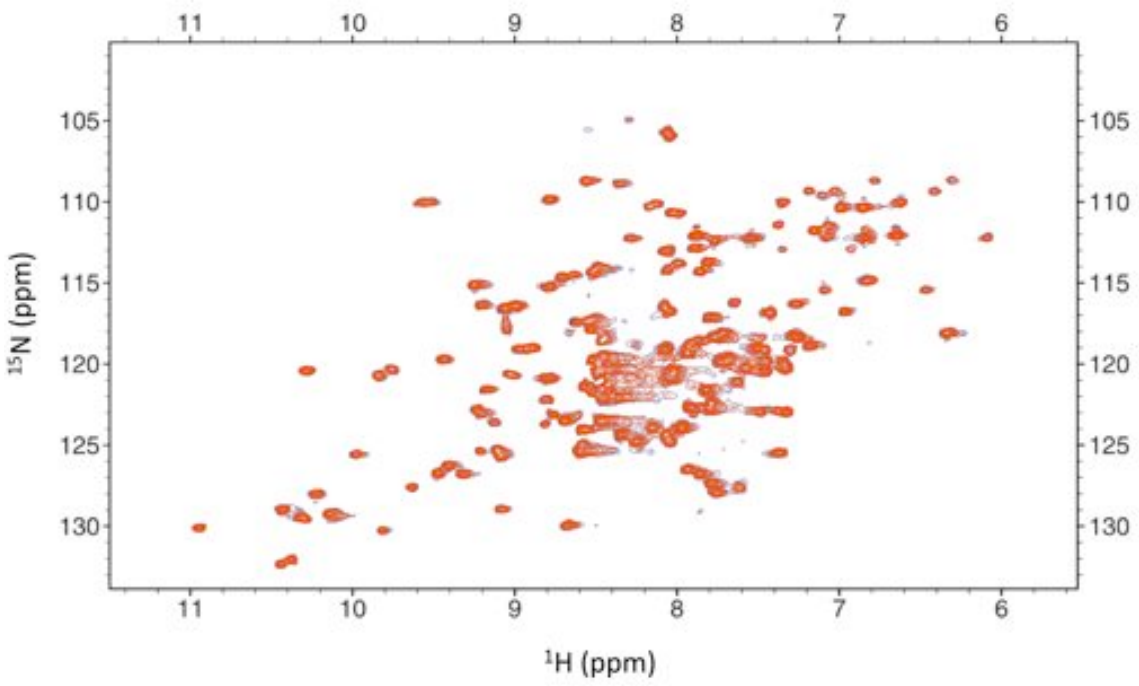

Figure 4.43: ^{1}H,^{15}N- HSQC spectrum of derCD23minus7 titrated with CD21 (SCR1-2).
The spectra of the titration at 0:0 CD21 (SCR1-2): derCD23minus7 (red) and 1.25:1 CD2 (SCR 1:2): derCD23minus7 (blue) are overlaid. No perturbations are seen from the spectra.

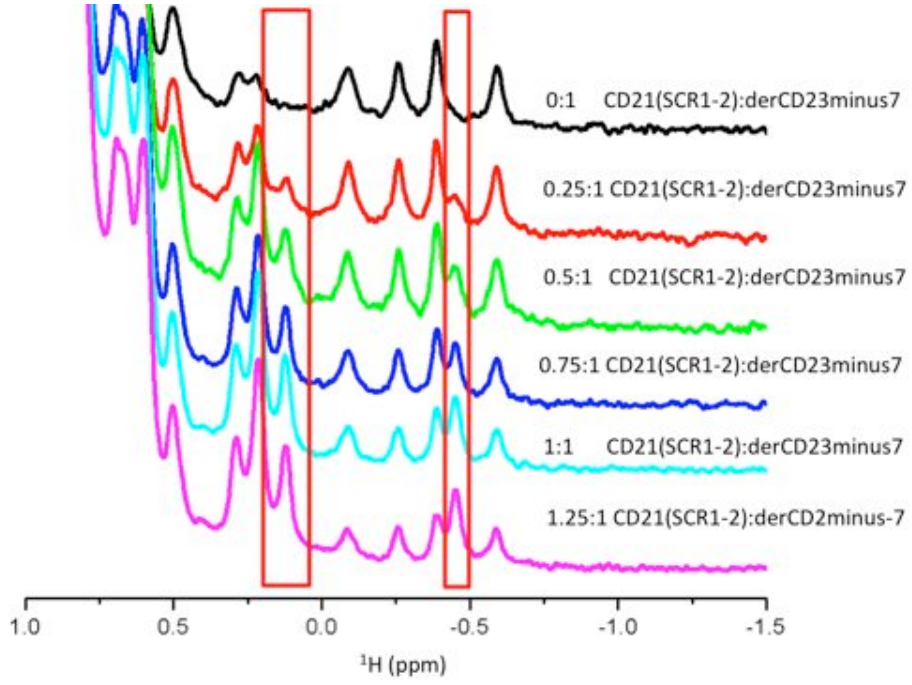

Figure 4.44: ^{1}H-NMR spectrum of ^{15}N-labelled derCD23minus7 titrated with CD21 (SCR1-2).
Unlabelled CD21 (SCR1-2) was titrated into ^{15}N-labelled derCD23minus7 titrated at molar ratios of 0:1, 0.25:1, 0.5:1, 0.75:1, 1:1 and 1.25:1 (CD21 (SCR1-2): ^{15}N-labelled derCD23minus7). Boxes highlighting the characteristic upfield methyl shifts of folded CD21 emerging during the titration.

4.5.5 Peptide inhibition of the CD23-CD21 interaction

The previously performed NMR chemical shift perturbation (Hibbert et al., 2005) as well as the studies presented in this work showed that the C-terminal seven residues of CD23 (ASEGSAE) is the CD21 binding site. A synthetic peptide comprised of this sequence was ordered (Genscript, NJ, USA) and used to further investigate the interaction of derCD23 with CD21 (SCR 1-2). Two different sets of experiments were done using an SPR sensor chip with immobilized derCD23. Firstly, a range of concentration of this peptide was mixed with a constant concentration of IgE-Fc and flowed over the CD23 surface. It can be seen that binding of IgE to CD23 is not affected. The peptide was then tested for its inhibitory effect on CD21 (SCR 1-2) binding to CD23. Similarly a range of concentration of this peptide was mixed with a constant concentration of CD21 (SCR-2). It can be seen that CD21 (SCR 1-2) binding was inhibited with the calculated a K_I of ~31 µM. The observed selective inhibition of CD21 binding, but not IgE binding, confirms that the C-terminus of CD23 is the site for CD21 binding. However this peptide binds to CD21 (SCR1-2) with a lower affinity compared to the previously determined K_D of the derCD23/CD21 (SCR1-2) interaction at ~1 µM (Hibbert et al., 2005). It is possible that there is an additional electrostatic attraction between CD21 (SCR1-2) and derCD23 that may account for the difference between the K_D of the derCD23/CD21 (SCR 1-2) interaction and K_I of the peptide.

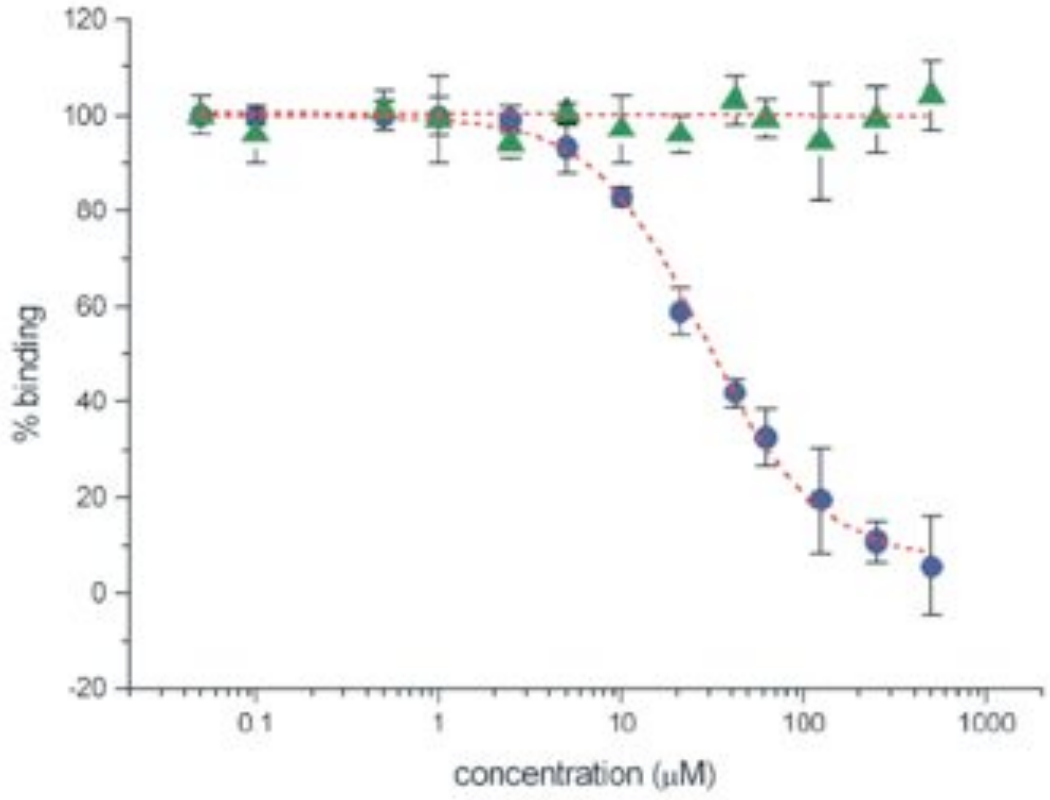

Figure 4.45: Selective inhibition of the CD21 (D1D2)/derCD23 interaction by the ASEGSAE peptide.
The peptide selectively inhibited the CD21 (D1D2)/derCD23 interaction (blue circles) without significant effect on the IgE-Fc/derCD23 interaction (green triangles). Identical experiments were performed twice and errors are the difference between the two experiments.

4.5.6 Crystallisation attempts of the derCD23/CD21 complex

Co-crystallisation of derCD23 in complex with CD21 was attempted. Firstly, the main subwells of 96 well crystallisation plates were aliquoted with commercially available crystallisation screen solution using a Mosquito robot. The commercial crystallisation conditions used were SaltRx (Hampton Research), ProComplex (Qiagen), PACT suite (Qiagen), JCSG+ (Qiagen). An equimolar mixture of derCD23:CD21 in 25mM Tris, 150 mM NaCl, pH 6.8 was then aliquoted into the secondary subwell accompanying the main subwells and sealed and incubated at 18^{o}C.

After a month, a few crystals were found in one condition in the PACT (Qiagen) screen (0.1 M MMT buffer pH 4, 25% (w/v) PEG 1500) (Figure 4.46). MMT buffer is a commercially made buffer (Qiagen) made with DL-malic acid, MES and Tris base in the molar ratios of 1:2:2. A test using the PX Scanner confirmed that those crystals were not salt. Salt crystals typically have large unit cells, which lead to high intensity spots on the diffraction pattern. Further optimization was done around this condition and crystals were also seen in 22.5% PEG 1500, 0.1 M MMT, pH 4.25 (Figure 4.47).

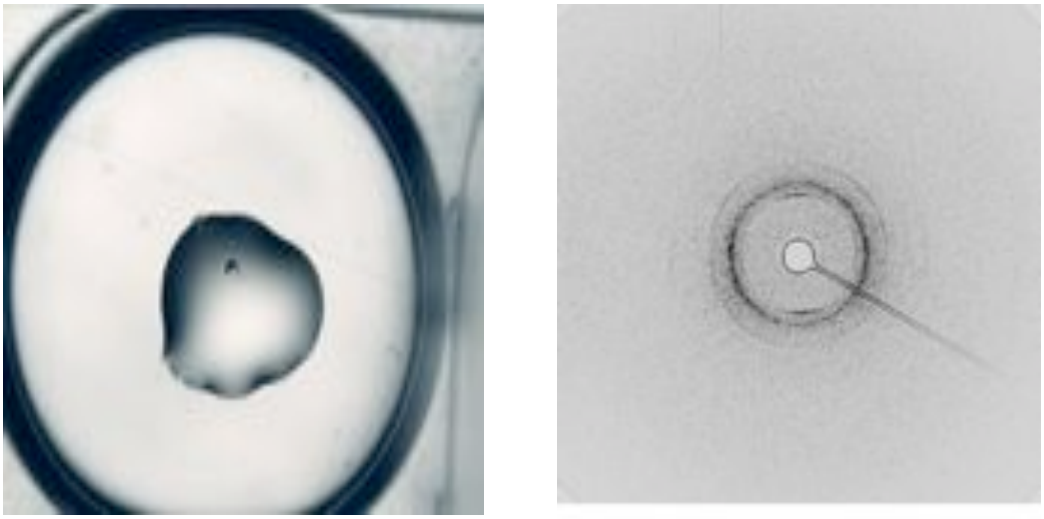

Figure 4.46: The crystal found in the PACT commercial screen condition (0.1 M MMT buffer pH 4, 25% (w/v) PEG 1500).
A test using the PXscan confirmed that the crystal was not a salt crystal.

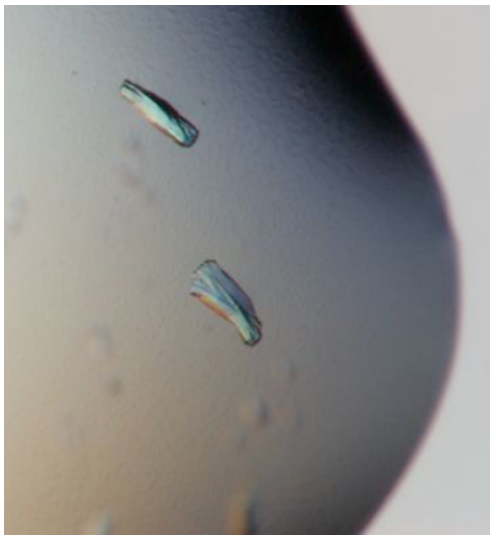

Figure 4.47: Crystals obtained with further optimisation 22.5% PEG 1500, 0.1 M MMT, pH 4.25.

30% PEG 1500, 0.1 MMT buffer, pH 2.5 solution with the same pH was tested as a cryprotectant at the same pH and prevented ice formation when tested with an in-house cryostream. These crystals could not be broken up into big single crystals and the data collected at the Diamond Synchrotron showed multiplicity within the crystal lattice and therefore could not be solved (Dr Balvinder Dhaliwal, personal communication). Crystals grown under this condition can be crushed into smaller crystals and used in a microseeding experiment to obtain bigger and single crystals (Oswald et al., 2008). Currently Lin Dao Peng and Wen Pin Kao at the Randall Division (KCL) are continuing the efforts in crystallisation of the derCD23/CD21 complex. The crystal structure of the complex would reveal the detailed interaction between derCD23 and CD21, which may assist the design of potential inhibitors of this interaction.

4.5.7 Future use of derCD23minus7 in functional studies.

The generation of CD23minus7 will be useful in future functional studies. CD23minus7 retains binding to IgE and therefore is a useful reagent to ascertain whether the CD21

binding is required for IgE upregulation in B cells. It could also be useful as a competitive inhibitor of CD23 binding to IgE and CD21 on the B cell surface by binding to IgE on the surface but not crosslinking IgE with CD21. Alison Cooper at the Randall Division (KCL) is now performing some of the biological aspects of this study by examining the effect on IgE synthesis in primary B cell culture by the additon of this mutant protein.

4.5.8 Discussion

The binding site of CD21 on derCD23 has been previously established through NMR chemical shift perturbation mapping to be localised on the C-terminus. A version of derCD23 truncated at the C-terminus was produced. The immobilisation of CD21 (SCR1-2) was attempted both through biotinylation and anti-his tag antibody. However the immobilisation conditions achieved did not behave well enough to derive an affinity constant for derCD23 binding. Having CD21 (SCR1-2) as the immobilised component would be ideal compared to having different CD23 mutants immobilised if a comparison between the different derCD23 versions is to be made. The NMR titration of ^{15}N-labelled derCD23minus7 with CD21 (SCR1-2) was performed. No perturbations were seen in the ^{1}H,^{15}N-HSQC indicating that in the absence of the C-terminus, no other interaction can be be detected. In full-length CD23 there are an additional 23 residues extended from the C-terminus of derCD23. Further studies are in progress to examine contributions of the rest of the residues of the C-terminus to CD21 binding.

4.6 The interaction between CD23 and the anti-CD23 monoclonal antibody IDEC-152

4.6.1 Introduction

IDEC-152 (also known as lumiluximab) is a primatized, IgG_1, anti-CD23 monoclonal antibody consisting of primate (cynomolgus macaque) variable regions and human constant regions (Nakamura et al., 2000). A Phase I clinical trial was conducted that established not only the safety of administration of this antibody but also its efficacy in reducing IgE levels in a concentration dependent manner (Rosenwasser et al., 2003). IDEC-152 has also been shown to be effective in treating chronic lymphocytic lymphoma (Byrd et al., 2010). Studies have shown that IDEC-152 kills CLL B cells predominantly through apoptosis-mediated through intrinsic pathways. Lumiluximab also led to the down-regulation of antiapoptotic proteins Bcl-2, Bcl-X(L) and XIAP, activation of Bax and the mitochondrial release of cytochrome C, all which are hallmarks of apoptosis (Pathan et al., 2008). However, antibody-based treatment, despite being clinically effective, is expensive and complicated to administer. Therefore it is hoped that biophysical studies of the IDEC-152/CD23 interaction may assist in the design of smaller molecules, potentially by mimicking the antibody's mode of action.

4.6.2 Binding of IDEC-152 Fab to derCD23

The anti-CD23 antibody IDEC-152 was kindly donated by Biogen-IDEC. Lin Dao Peng at the Randall Division, KCL, performed a papain digestion (Andrew, 2002) to obtain a monomeric antigen-binding fragment of IDEC-152 (IDEC-152 Fab).

An SPR experiment was performed to meaure the binding affinity. An increasing concentration of IDEC-152 from 0 to 100 nM was flowed over the surface of a derCD23

immobilised SPR chip for 120 seconds with flow a rate of 10 μl/min. Dissociation was then monitored for 5 minutes before dissociation of the bound IDEC-152 Fab-CD23 by two injections of 4M $MgCl_2$.

Association kinetics can be difficult to fit if the binding curve is close to linear, which is seen at lower concentrations of the IDEC-152 Fab titration (Figure 4.48). The Biacore T100 evaluation software (GE Healthcare) was used to fit the data for the measurements of the three highest concentrations at 50 nM, 75 nM and 100 nM which gave the average association constant, k_{on}=3.09 x 10^{-5} (± 7.78 x10^{-4}) $M^{-1}s^{-1}$, dissociation constant, k_{off}= 2.54x10^{-4} (± 1.93x10^{-5}) s^{-1}, and affinity, K_D= 8.63x10^{-10} (±2.45x10^{-10}) M.

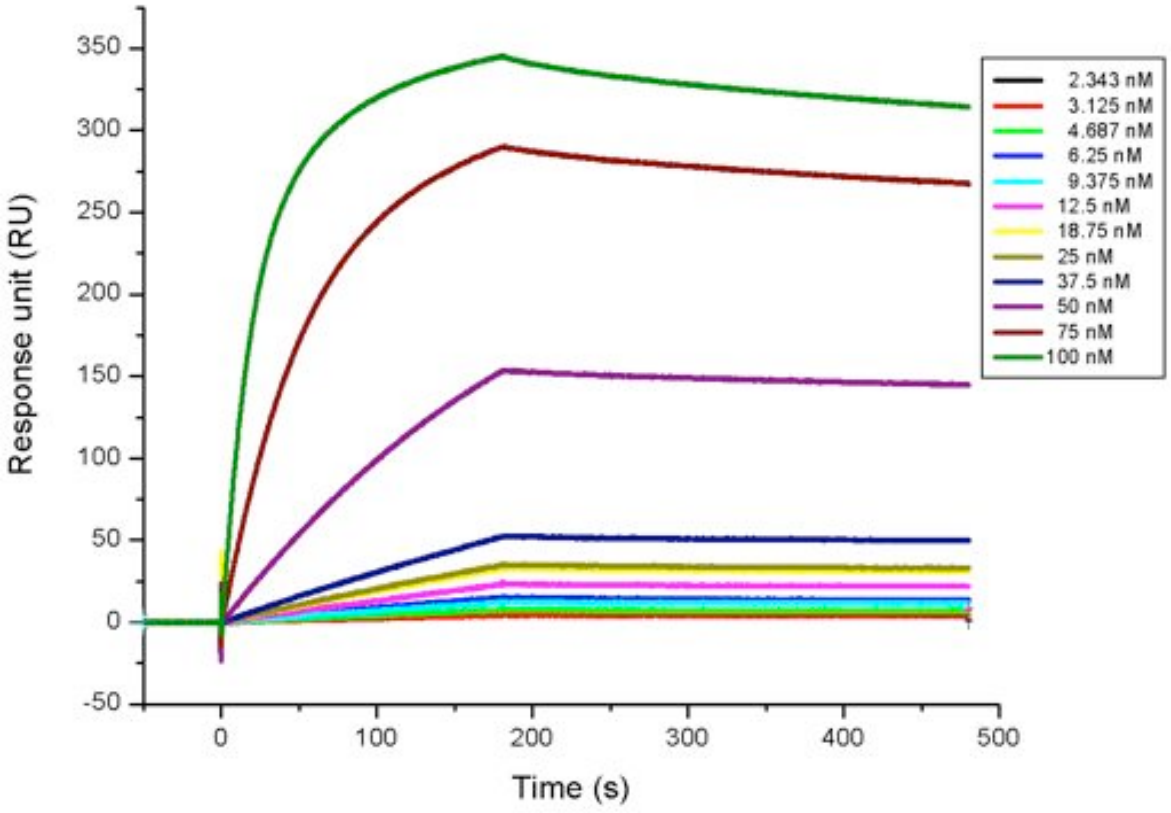

Figure 4.48: The binding of IDEC-152-Fab at increasing concentration (0-100 nM) on a derCD23 SPR surface.

4.6.3 IDEC-152 binding effects on IgE binding to derCD23.

To investigate whether IDEC-152 has an effect in IgE binding to CD23, SPR experiments were performed. A CM5 sensor chip was coated with 250 RU of derCD23 through amine coupling. IgE-Fc was flowed over at a concentration range of 0 to 20 μM at a flow rate of 20 μl/minute for 60 seconds. In the second experiment IDEC-152 Fab at a concentration of 1 μM was flowed over the surface until a saturation of binding was achieved. The saturation of binding was calculated to be 625 RU and the level of saturation was achieved to the expected level. The IDEC-152 forms a complex, which dissociates slowly on the derCD23 surface; this allows the binding of IgE-Fc to the IDEC-152 bound derCD23

complex to be performed. IgE-Fc was then flowed over the surface at an identical concentration range of 0 to 20 μM and a flow rate of 20 μl/minute for 60 seconds.

The two sets of binding curves showed high similarity when overlaid (Figure 4.49). This indicates that there is no discernible difference in terms of association and dissociation kinetics between the two binding curves. The calculated affinities are also identical, with both interactions having a K_D of ~1.4 μM. This observation therefore suggests that the binding of IDEC-152 does not affect the direct binding of IgE to derCD23.

a)

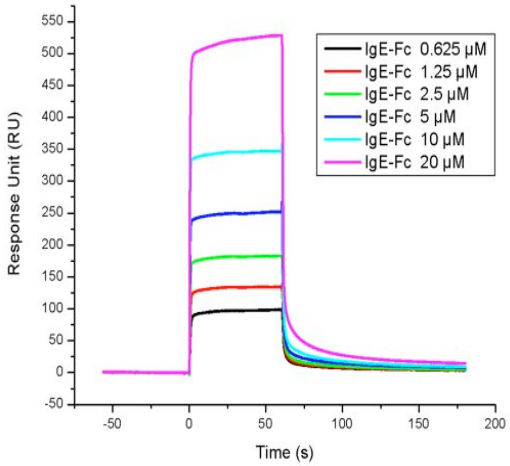

b)

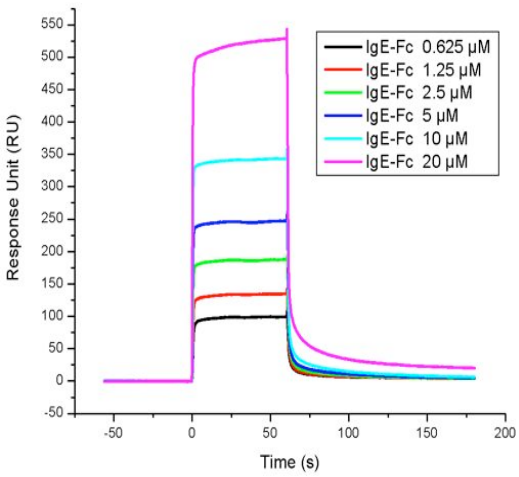

c)

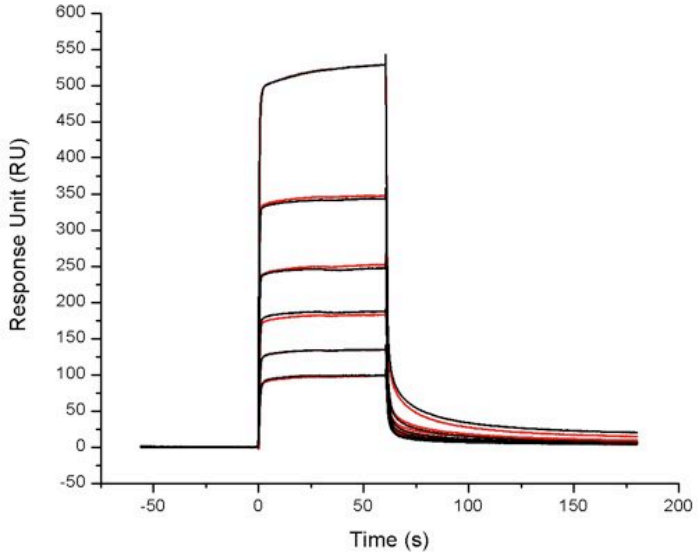

Figure 4.49: The binding of IgE-Fc to CD23 and CD23 with immobilised IDEC-152
a) IgE-Fc binding derCD23 showed a fast-on/fast-off kinetics with the exception of the highest concentration (20 µM). b) IgE-Fc binding to CD23 saturated with IDEC-152 Fab also showed a fast-on/fast-off kinetics. c) The overlay of both sensorgram reveals that the binding kinetics of IgE-Fc does not change when CD23 is presaturated with IDEC-152 (black: IgE-Fc binding to CD23; red: IgE-Fc binding to derCD23 saturated with IDEC-152 Fab)

4.6.4 NMR titration of ^{15}N-labelled derCD23 with IDEC-152 Fab

A crystal structure of the IDEC-152 Fab/derCD23 complex has been solved and is currently under refinement by Dr Balvinder Dhaliwal, but the coordinates of the complex were kindly provided to assist in the analysis of the NMR titration data as shown in Figure 4.50.

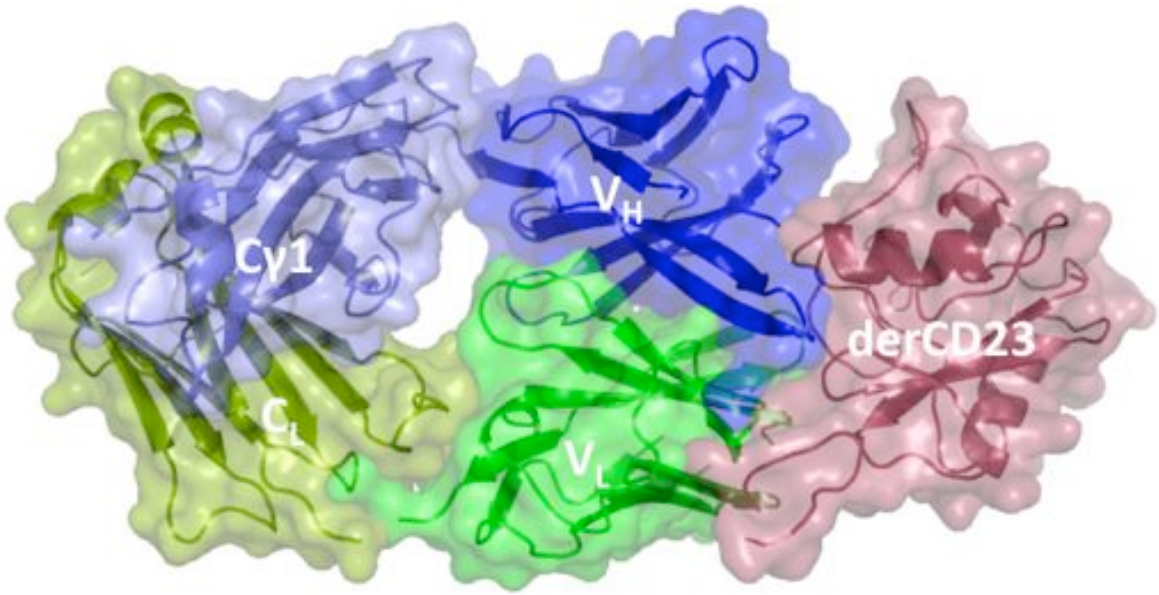

Figure 4.50: The putative crystal structure of IDEC-152 152/derCD23 complex showing the light and heavy variable region (V_L and V_H) binding to derCD23.

4.6.4.1 NMR titration experiment set up

An NMR titration was performed using a 100 μM sample of ^{15}N-labelled derCD23 and a concentrated sample IDEC-152-Fab dialysed in an identical buffer was titrated into the sample, and data were collected on a Bruker 500MHz NMR instrument. The comparison of the ^{1}H,^{15}N-HSQC spectrum of pre-titrated derCD23 with the spectra collected during the IDEC-152 Fab titration showed changes in a small number of peaks.

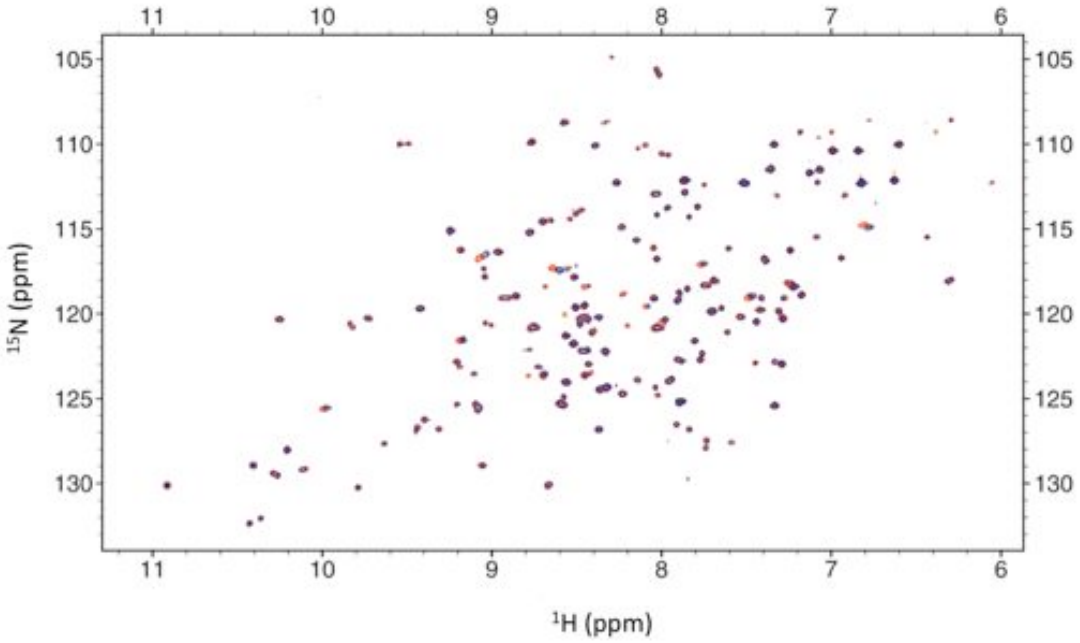

Figure 4.51: Titration of ^{15}N-labelled derCD23 with IDEC-152 Fab.
IDEC-152 Fab was titrated into a sample of ^{15}N-labelled derCD23 at concentration of 100 uM from 0:1 (red) to 1:1 (blue) molar ratios of IDEC-152 Fab: derCD23.

4.6.4.2 Chemical shift mapping of IDEC-152 Fab on derCD23

From the chemical shift plot 13 peaks showed significant chemical shift changes Δδ (see Section 2.5.1.3) which are defined as Δδ> above 0.15 ppm (Figure 4.52). These residues namely Lys166, Gln197, Phe209, Lys212, His213, Lys229, Glu231, Val240, Asp241, Tyr242, Asp270, Ala271 and Asp274 are mapped onto the crystal structure of the IDEC-152 Fab/derCD23 complex (Figure 4.53).

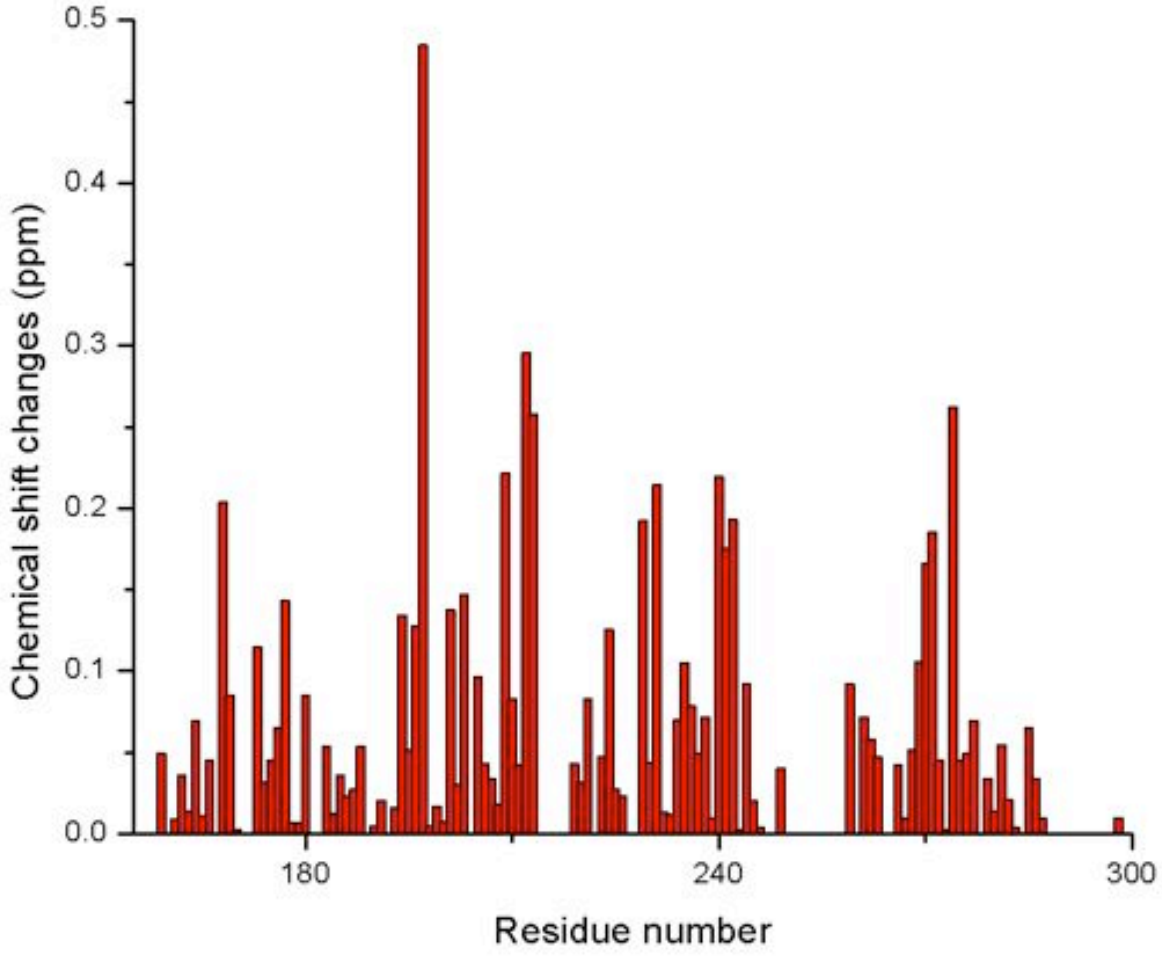

Figure 4.52: Chemical shift differences between 0% IDEC-152-Fab and 100% equimolar of IDEC-152.
Plotting of the combined chemical shift $(\sqrt{(\delta_N/5)^2 + \delta_H^2})$ after 1:1 molar ratio of IDEC-152-Fab allows the identification of residues that are significantly perturbed in the titration. Significant chemical shifts are defined to be those above 0.15 ppm.

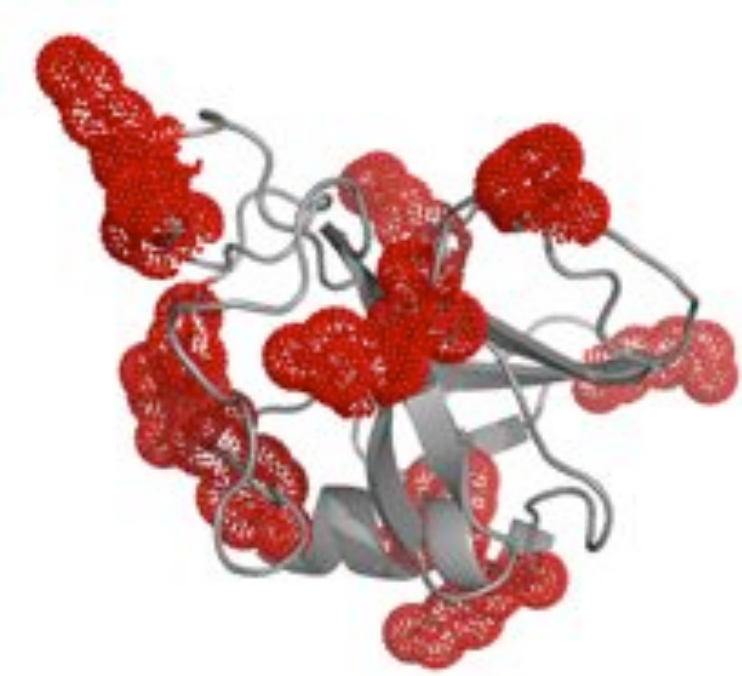

Figure 4.53: Mapping of the derCD23 residues perturbed in the IDEC-152 Fab titration onto the derCD23 structure.

4.6.4.3 Changes in the residues involved in trimerisation

The chemical shift changes plot also showed trimerisation residues being involved namely Phe209, Lys212, His213, Lys229, Glu231, Val240, Asp241, and Tyr242. These residues were then mapped onto the derCD23 structure (Figure 4.54).

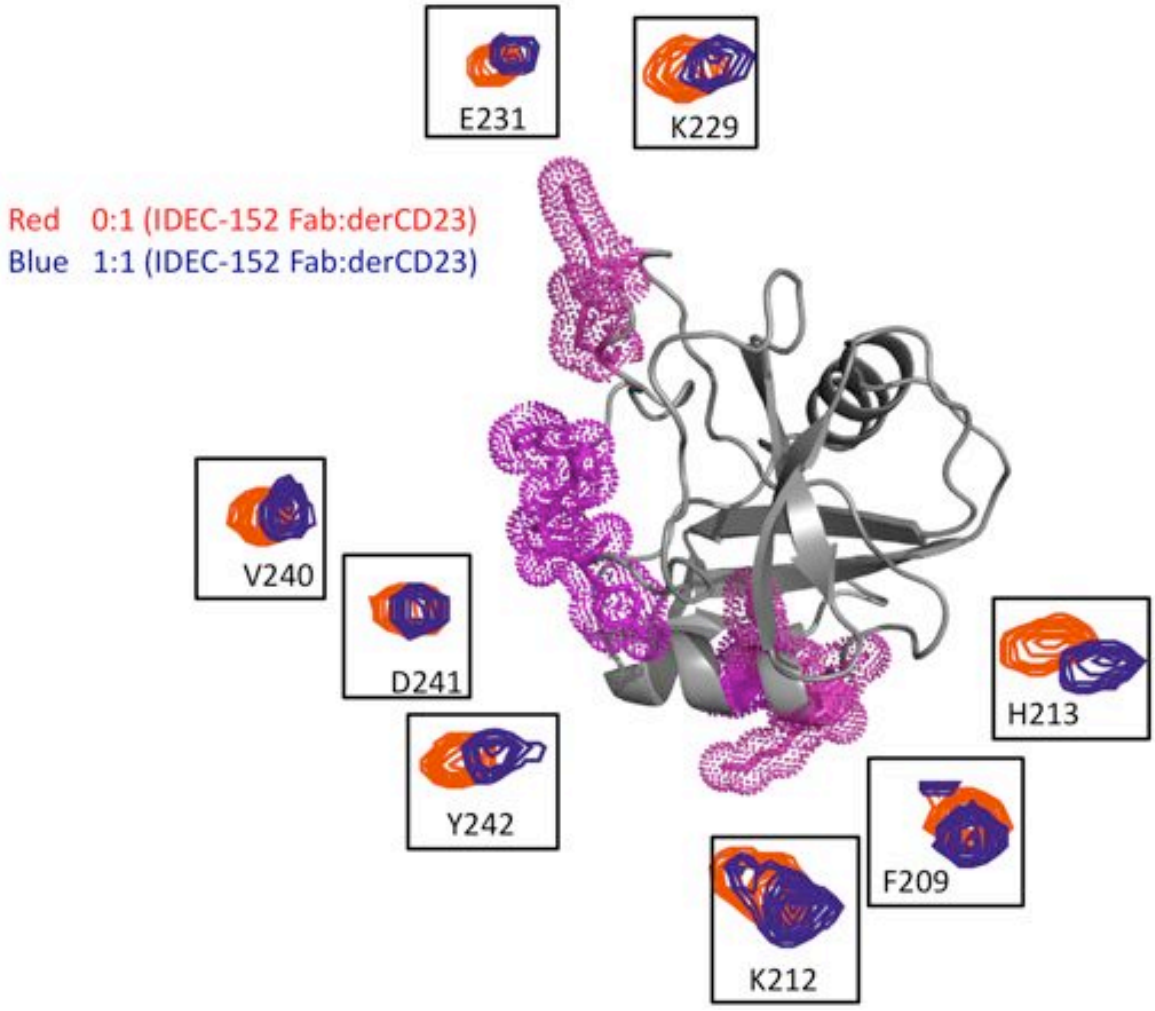

Figure 4.54: The peaks implicated in trimerisation that showed chemical shift change in the NMR titration of IDEC-152 Fab.
The insets show the peaks of the residues implicated in the ^{1}H-^{15}N-HSQC in the titration. Red and blue peaks indicate molar ratio of 0:1 and 1:1 of IDEC-152:derCD23 respectively.

4.6.4.4 Mapping of residues implicated onto the IDEC -152 Fab-derCD23 complex crystal structure

Mapping of the residues involved in the NMR titration onto the IDEC-152 Fab/derCD23 complex showed that some of the trimerisation residues that are perturbed in the NMR titration are situated at the interface of the IDEC-152 Fab/derCD23 complex in the crystal structure as shown in Figure 4.56. Residues Gln197, Val240, Asp241 and Tyr242 are close

to the IDEC-152 Fab. Residue His239 is also implicated and showed broadening in the $^{1}H,^{15}N$-HSQC (Figure 4.55).

In the crystal structure, residue Gln171 is in close contact with IDEC-152 Fab. The backbone amide peak in the $^{1}H,^{15}N$-HSQC however, showed no chemical shift perturbation (Figure 4.55). The interaction between the side chains of Gln171 may cause chemical shift change in the side chain only, leaving the backbone unperturbed.

Perturbations on the side chain amides can also be observed in the $^{1}H,^{15}N$-HSQC. The peaks of the NH_2 group of a side chain belonging to asparagine and glutamine are mainly seen as pairs of NH peaks each belong to the same nitrogen dimension around 110-115 ppm, with distict peaks for each proton around 8.0-6.5 ppm (Cavanagh et al., 2006) (Figure 4.56 (a)). As shown in the magnified view, there are two pairs of peaks that were perturbed in the IDEC-152 Fab titration that can be tentatively attributed to either side chain amides of Gln197 and Gln171 (Figure 4.56 (b)).

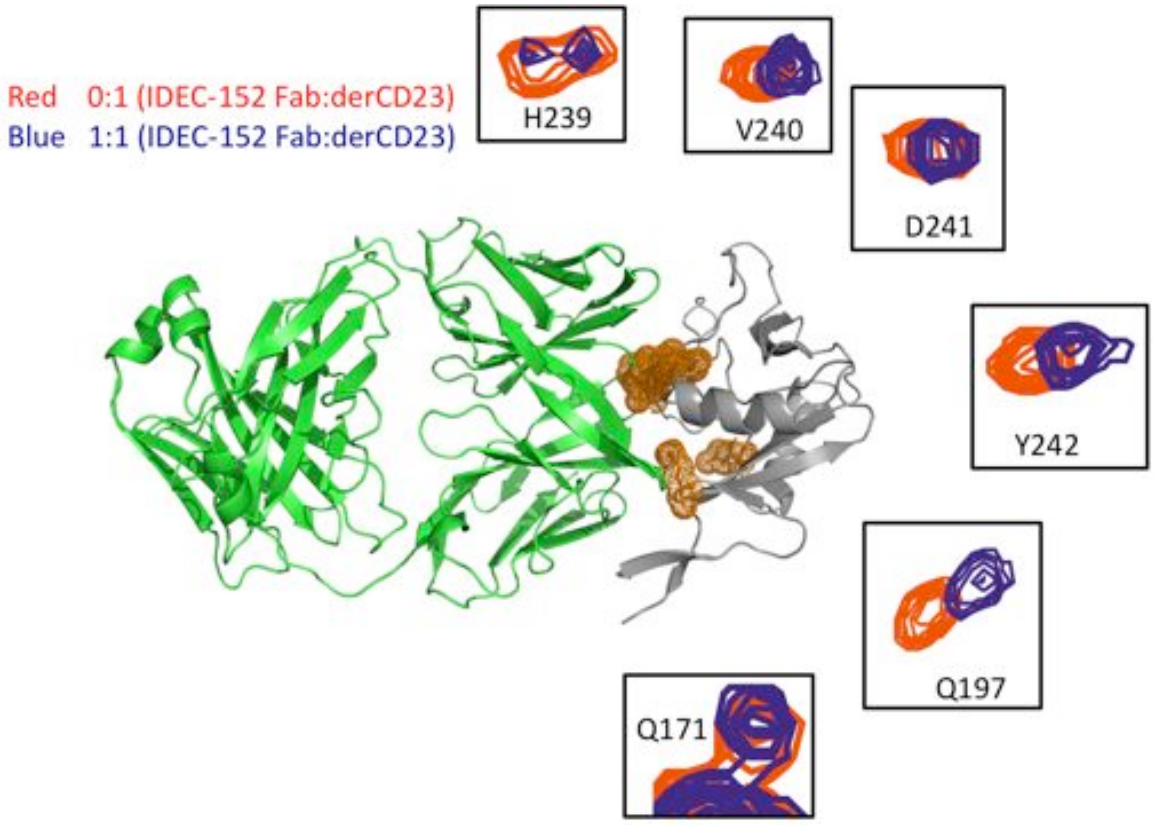

Figure 4.55: The direct interface residues residues in the NMR titration mapped onto the crystal structure of IDEC-152 Fab/derCD23 complex.
The $^{1}H,^{15}N$-HSQC of derCD23 titrated with IDEC-152 Fab shows the derCD23 residues closely in contact with the Fab region of IDEC-152 Gln107, His239, Val240, Ap241 and Tyr242. Gln171 did not show perturbation in the backbone amide but may be implicated with possible perturbation in the side chain region (red and blue indicate molar ratio of 0:1 and 1:1 of IDEC-152:derCD23 respectively).

(a)

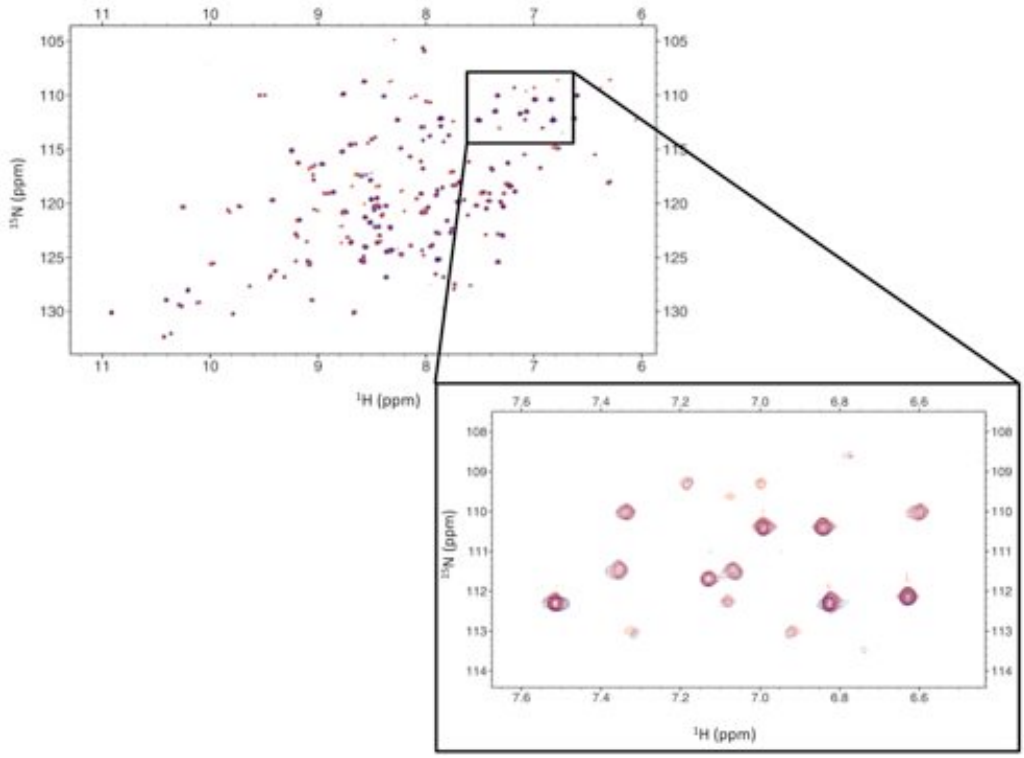

(b)

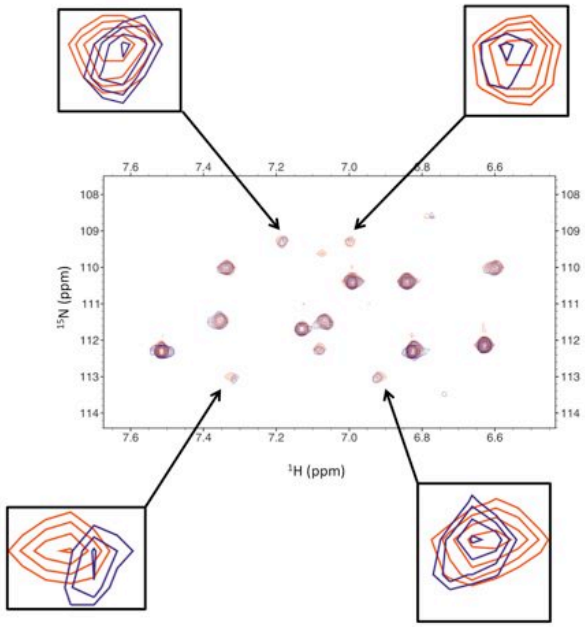

Figure 4.56: Perturbations in the side chain of residues Gln197 or Gln171 in the NMR titration.
a) The area of group peaks for the NH_2 side chains amides of asparagine and glutamine usually appears around this region of the ^{1}H,^{15}N-HSQC spectrum (Cavanagh et al., 2006). b) A magnified view showed possible pairs amide sidechain peaks that show perturbations which could be attributed to either Gln197 or Gln171 (red and blue indicate molar ratio of 0:1 and 1:1 of IDEC-152:derCD23 respectively).

4.6.4.5 Allosteric changes caused by IDEC-152 Fab binding as observed by NMR.

4.6.4.5.1 Analysis of the methyls perturbed in the ^{1}H-NMR spectra of the titration

Methyl groups that pack against the aromatic rings of residues in the core of a protein molecule typically show changes in shifts in the ^{1}H NMR spectrum. A ligand may bind to a protein and induce a conformational change, which changes the position of the aromatic rings in relation to the methyl groups. This could then lead to changes seen in the ^{1}H NMR spectrum where the methyl peaks are observed.

The methyl peak of Leu223 (HD1) gradually shifts and broadens during the IDEC-152 Fab titration, whilst the other Leu (HD2) showed only slight broadening (Figure 4.57). In the derCD23 structure the methyl group of Leu223 packs against the aromatic ring of Trp234 (Figure 4.58). The assignments of these peaks were obtained from the previously deposited assignment of derCD23 on BioMagResBank under the accession number 6732.

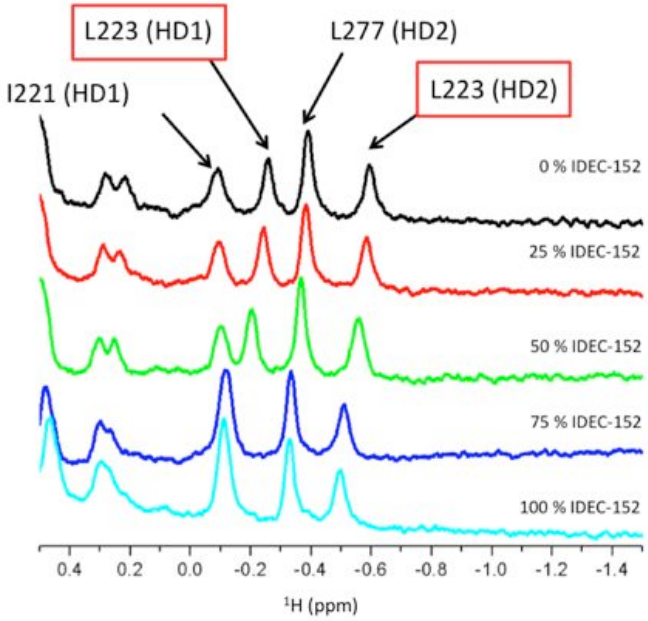

Figure 4.57: The ^{1}H-NMR spectra of derCD23 during the IDEC-152 Fab titration showing changes in the signals of upfield methyl peaks.

The methyl peaks for Leu223 (HD1) and Leu23 (HD2) showed changes. Leu223(HD1) gradually broadens out and integrated into the Ile221 methyl peak at increasing IDEC-152-Fab concentration. Leu223 (HD1) also showed downfield shifting.

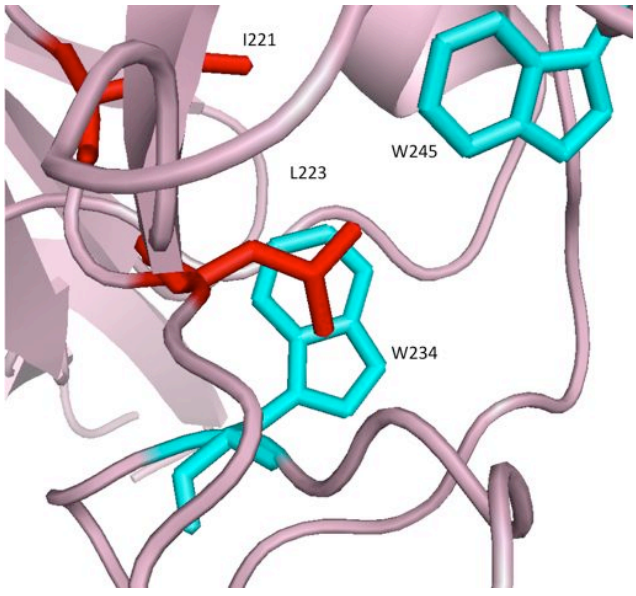

Figure 4.58: The position of residue Leu223 in the derCD23 structure.

The methyl groups from the side chain of L223 (red) are packed against the aromatic rings of Trp234, which led to changes in the chemical environment of the methyl groups.

4.6.4.5.2 Changes in the IgE binding sites

Out of the IgE binding residues, only three residues Asp270, Ala271 and Asp274 showed chemical shift perturbations, all of which are probably due to subtle conformational changes, and appear not to affect IgE binding as demonstrated by the SPR analysis (Section 4.6.3).

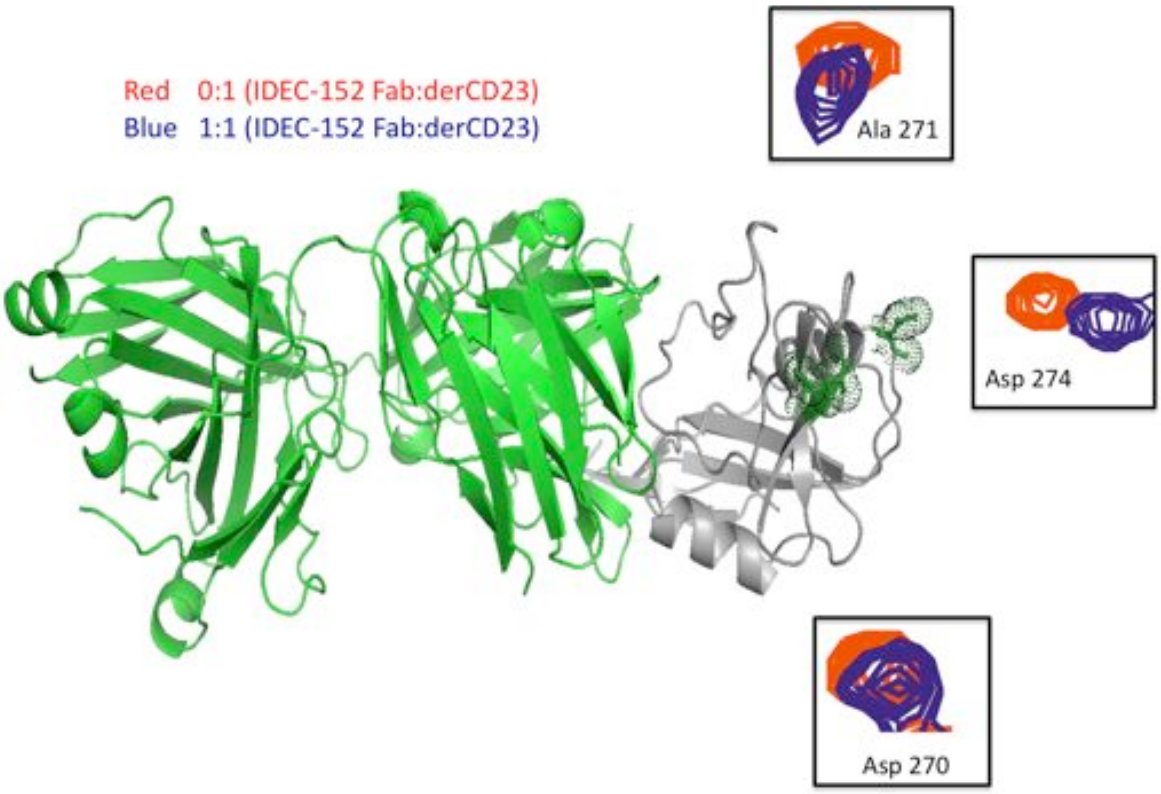

Figure 4.59: IgE-binding site residues perturbed by the addition of IDEC-152 Fab to derCD23.
(red and blue indicate molar ratios of 0:1 and 1:1 of IDEC-152:derCD23, respectively)

4.6.5 Discussion

The SPR analysis performed in this study demonstrated that the binding of IDEC-152 to derCD23 does not inhibit IgE binding as the binding site IDEC-152 Fab and IgE are distinct from each other on CD23. The mapping of the IDEC-152 Fab binding site on the trimeric model of CD23 by Hibert et al. (2005) indicates that it overlaps with one of the trimerisation regions (Figure 4.60).

The other intriguing observation is that trimerisation sites, away from the crystallographic binding interface, also showed perturbations and when mapped onto the IDEC-152 Fab/derCD23 complex crystal structure show that those residues are situated in the direct interface between IDEC-152 Fab and derCD23. In the ^{1}H NMR spectra changes were seen in some of the core methyls, which demonstrates that CD23 experiences subtle allosteric changes as a result of IDEC-152 fab binding. These data also suggest that the trimerisation site of CD23 may be a potential target for inhibition, and upon the refinement of the crystal structure, an inhibitor may perhaps be designed to disrupt the trimerisation of CD23. Several preliminary experiments being conducted by Wen Pin Kao and Lin Dao Peng at the Randall Division (KCL) showed some indication that IDEC-152 Fab may dissociate the trimeric CD23 into monomers. Marie Pang at the Randall Division (KCL) also performed some cell binding assay using $CD23^{+}$ 8866 cells that IDEC-152 Fab reduces IgE binding to CD23 on cells. Our data suggest that IDEC-152 may possibly act by disrupting the trimeric CD23 through steric hindrance in the implicated trimerisation interface, hence reducing its affinity for IgE, as the monomeric CD23 binds to IgE with a lower affinity. More importantly, IDEC-152 may disperse the trimeric CD23 into monomers,

which will not crosslink membrane IgE, and membrane CD21 in the same was as the trimeric CD23 does.

(a)

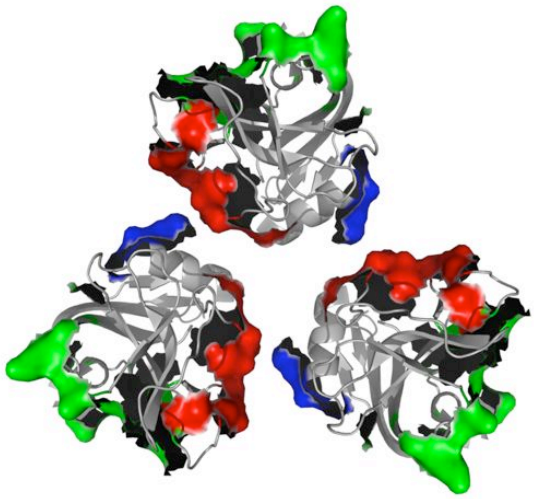

(b)

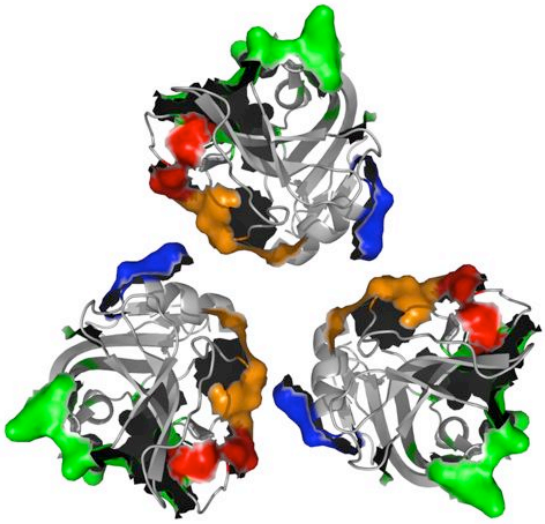

Figure 4.60: The binding site of IDEC-152 Fab on the trimeric CD23.
a) The trimeric model of CD23 as proposed in Hibbert et al. (2005). The oppositely charged trimerisation interfaces are shown red (negatively charged) and blue (positively charged) and IgE binding site is highlighted in green. b) IDEC-152 binding site is highlighted as orange in the trimeric model indicating clashes with the oppositely charged trimerisation interface.

4.7 Multimolecular interactions between CD23, IgE-Fc and FcεRI

4.7.1 Introduction

The cross-linking of IgE bound to its high affinity receptor, FcεRI, by the specific allergen activates the cascade of signalling events that lead to the release of preformed mediators of inflammation (Liu et al., 2011).

A crystal structure of IgE-Fc (Cε3-4) bound to the alpha chain of FcεRI (sFcεRIα) has been solved (Garman et al., 2000) and showed FcεRI binds to the Cε3. Site directed mutagenesis studies showed that the binding site of CD23 is situated away from the FcεRI binding site on IgE with residues 346-356 implicated (Nissim et al., 1993). Residue Lys352 in the Cε3 domain has also been implicated as important for CD23 binding (Sayers, 2004). The NMR chemical shift mapping of the binding site of CD23 on Cε3 performed by Dr Susmita Borthakur from our group (unpublished results) included the region indicated by these previous observations. When mapped onto the crystal structure of the IgE-Fc (Cε3-4)/sFcεRα complex, the CD23 binding site is clearly distinct from that of sFcεRα (Figure 4.61). This suggests that CD23 may still be able to bind to the IgE/FcεRI complex. This section discusses the binding events of two possible phenomena: i) the effect of CD23 on IgE binding to FcεRI and ii) the binding of CD23 on IgE bound to FcεRI.

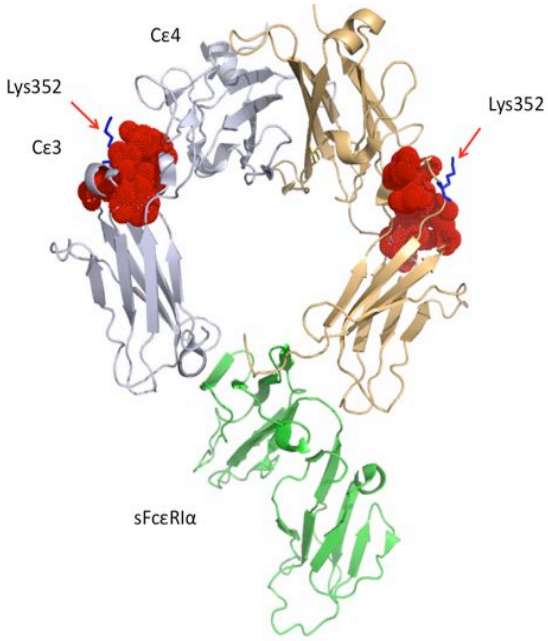

Figure 4.61: Crystal structure of IgE-Cε3-Cε4 bound to the alpha chain of FcεRI (sFcεRα).
PDB ID 1F6A: (Garman et al., 2000) Residues implicated in CD34 binding from the work of Dr Susmita Borthakur (DPhil thesis, 2010) (Phe346, Asp347, Leu348, Phe349, Gly406, Tyr407, Trp410, Ile411, Gly413). Lys352 was indicated by Sayers et al. (2004) to be important in IgE binding. The mapped residues show that CD23 essentially binds to a different site than FcεRI.

4.7.2 Binding of CD23-IgE complexes on FcεRI shows an avidity effect

An SPR experiment was done to investigate the effect of the derCD23/IgE-Fc complex on binding to FcεRI. A CM4 sensor chip was coated with an IgG_4 fusion protein containing two alpha chains of FcεRI replacing the V_H domain of IgG_4, through amine coupling. A series of protein mixtures containing a constant concentration of IgE-Fc at 50 nM and an increasing concentration of derCD23 was flowed over the surface. It was observed that as the derCD23 concentration increases, more binding signal is observed (Figure 4.62). This is possibly due to the formation of high molecular weigh complexes of derCD23 and IgE-Fc which provide an avidity effect for the complexes' binding to FcεRI Previous analytical

centrifugation analysis demonstrated that derCD23 has a tendency to form a high molecular weight complex with IgE (McCloskey et al., 2007).

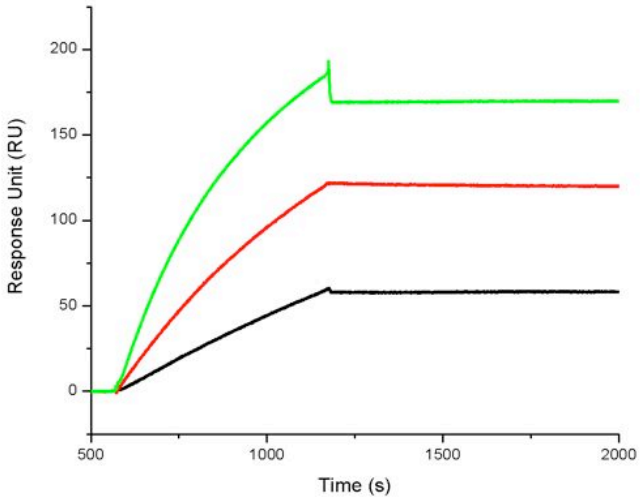

Figure 4.62: A constant concentration of 50 nM IgE-Fc mixed with increasing concentrations of CD23 (0-20 µM) showed increased binding of IgE to FcεRI.
Only CD23 concentrations of 0 µM (black), 10 µM (red) and 20 µM (green) are shown for clarity.

4.7.3 Binding of CD23 on IgE bound to FcεRI

A parallel experiment was performed on a CM5 sensor chip. In one surface streptavidin was first immobilised through amine coupling. In the second surface the alpha chain of FcεRI containing a free thiol group was immobilised through thiol coupling. Both surfaces were then immobilised with biotinylated IgE-Fc and IgE-Fc respectively to similar density of 120 RU. IgE-Fc has a slow dissociation to FcεRI (McDonnell et al, 2001) and did not dissociate during the experiment. The expected calculated B_{max} value for a 16KDa protein (derCD23) binding to a 75 KDa (IgE-Fc) at 120 RU immobilisation level is calculated to be 25.6 RU.

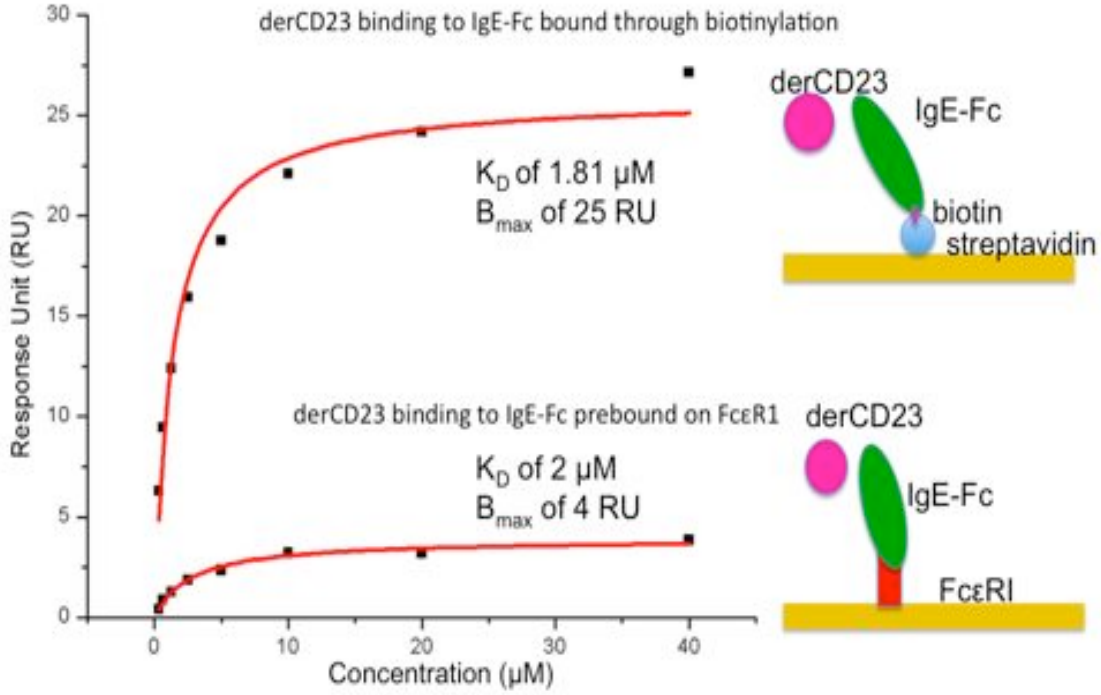

Figure 4.63: The binding of derCD23 on different IgE immobilisations.
The top binding curve shows the binding of derCD23 to IgE bound through biotinylation which showed a K_D value of 1.81 μM. The bottom binding curve shows the binding of derCD23 binding to IgE prebound on FcεR1 which showed a similar K_D value but a much reduced B_{max} at 4 RU. Data fitting was performed using Origin 7.0. (OriginLab Corporation, Northampton, MA)

From the experiment the affinity of both the interaction between derCD23 and IgE-Fc and IgE-Fc bound to FcεRI showed similar values at ~2 μM. However there is a striking difference in terms of the maximum binding capacity (B_{max}) seen in both interactions. The obtained B_{max} value is 25 RU which is approximately similar the calculated predicted value suggests that derCD23 is able to bind to IgE-Fc without any hindrance. However, in the interaction between derCD23 and IgE bound to FcεRI, the B_{max} value is reduced to 4 RU despite the affinity being similar at 2 μM. This suggests a form of a non-competitive inhibition where FcεRI reduces the ability of IgE for binding to derCD23 but not the

affinity of the interaction. Binding of FcεRI may lead to a conformation change of IgE-Fc, which reduces the population of IgE capable of binding to derCD23.

4.7.4 Mast cell degranulation assay to determine the possible biological implications of the observed biophysical phenomena

Mast cell degranulation assays were kindly performed by Heather Bax at the Randall Division (KCL) to examine the role CD23 engagement of IgE in the activation of mast cells. Degranulation measurement is expressed as the percentage of total cellular release of a component of degranulation content, β-hexosaminidase, which is measured through its substrate 4-methylumbelliferyl N-acetyl-β-D-glucosaminide using a fluorometric assay (Heather Bax, personal communication).

In the first experiment, LAD-2 mast cells were incubated with IgE for an hour and then varying amount of derCD23 and trimeric CD23 (0.1 μM, 1.0 μM and 10 μM) were added and incubated for an hour at 37^{o}C. Degranulation measurements indicate that neither derCD23 nor trimeric CD23 triggers IgE-mediated degranulation of mast cells. In contrast, the positive control, an anti-IgE antibody, does efficiently degranulate mast cells (Figure 4.64 (a)).

In the second experiment (Figure 4.64 (b)), a constant concentration of IgE-Fc was premixed with derCD23 and triCD23 in increasing concentrations, incubated for 1 hour at 37^{o}C and then added to the mast cells. An increase of degranulation was observed in both

derCD23/IgE and triCD23/IgE mixtures in a concentration-dependent manner . These observations reflect the avidity effect seen in the SPR experiment in which the CD23 and IgE mixtures form multimeric complexes leading to avidity improved binding to the FcεRI surface (Figure 4.62).

a)

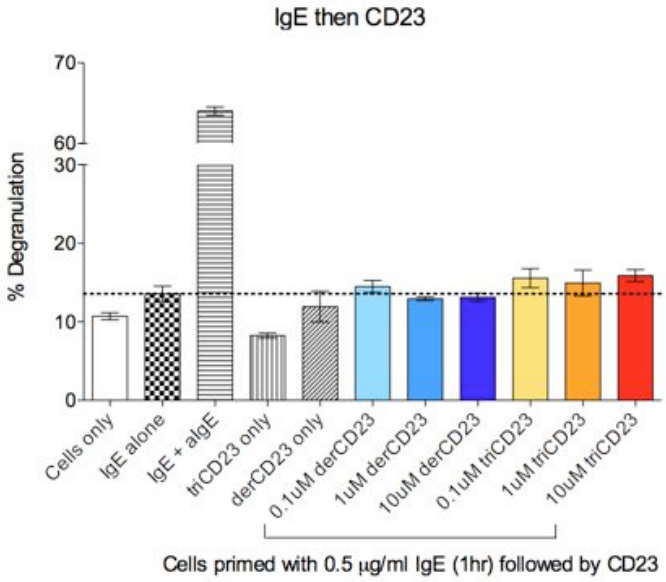

b)

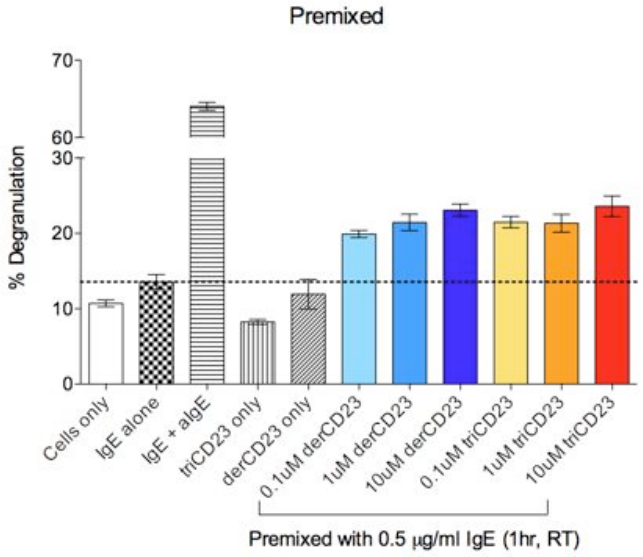

Figure 4.64: Mast cell degranulation assays performed.
a) LAD-2 cells were primed with 0.5 μg/ml IgE for 1 hr and added with derCD23 and triCD23 in an increasing concentration. No significant difference were seen in the degranulation levels. b) A constant concentration of IgE-Fc were mixed with increasing concentration of CD23 and triCD23 and added to the LAD-2 cells. Degranulation was increased in a concentration dependent manner. The experiments were kindly performed by Heather Bax at the at Glaxo Smith Kline Research and Development Unit, Hertforsdshire. Anti-IgE antibody (aIgE) was used as positive control for degranulation (Heather Bax-personal communication).

4.7.5 Discussion

The observation seen in both theSPR experiments as well as the mast cell degranulation assays suggest that there is a possible role of CD23 in the activation of mast cells. It is possible for derCD23 to form a multimeric complex with IgE-Fc leading an increase binding to FcεRI through avidity effect (Figure 4.62). When IgE is bound to FcεRI, derCD23-binding capacity is also reduced although the affinity remained unchanged indicating a non-competitive inhibition, presumably through allosteric mechanisms.

The mast cell degranulation assays indicate that when IgE and CD23 were premixed, an increase of degranulation level is observed, likely through the engagement of FcεRI by the multimolecular complex. In contrast, the addition of CD23 did not degranulate mast ells when IgE was pre-bound to membrane FcεRI, consistent with the SPR data. In the usual mast cell degranulation, allergen crosslinking of IgE is involved but in this study, even in the absence of allergen, IgE-CD23 complexes may degranulate mast cells. It is speculated that the presence of allergen may lead to the formation IgE/CD23/allergen complex that require further studies. CD23 binds to the Cε3 domain of IgE and thus the antigen-binding fragment is accessible for allergen binding.

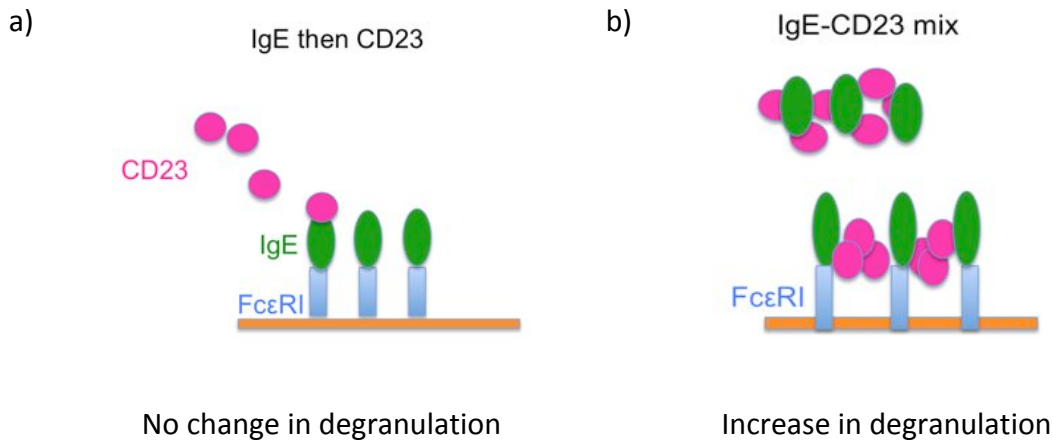

Figure 4.65: The role of CD23 in IgE binding to FcεRI.
a) The binding of CD23 to IgE is reduced by FcεRI b) CD23 form a multimolecular complex with IgE and binds to FcεRI with an added avidity effect.

The CD23 sheddase, ADAM-10 has been identified (Weskamp et al., 2006) and is involved in the upregulation of IgE (Sturgill et al., 2011), presumably by the formation of trimolecular complex with CD21 and membrane IgE as proposed previously by McCloskey et al. (2007).

Recent work has shown that, using a basolateral chamber as a model of the physiological state, CD23 is involved in the transcytosis of IgE/allergen complexes from the airway lumen through the airway epithelial. The IgE/allergen complexes bound to membrane CD23 are transported from the airway lumen and released to subepithelial side. The released IgE/allergen complexes then activate mast cell degranulation in this area (Figure 1.14) (Palaniyandi et al., 2011). One intriguing question would be whether ADAM-10 is present in the sub-epithelial side; this would lead to the release of soluble CD23, which may form a multimeric complex consisting of IgE, CD23 and allergen and activate a higher level of mast cell degranulation through avidity effects. It is not known whether ADAM-10 is present in the subepithelial side of the airway. If it is present it may upregulate mast

cell degranulation through the release of CD23 forming a multimeric complexes with IgE and allergen leading to an increase of binding to mast cells through avidity effect. In this regard, an inhibitor of the IgE/CD23 interaction could be assayed to inhibit CD23-mediated IgE transport in allergen-induced respiratory symptoms.

4.8 Development and optimisation of a differential scanning fluorimetry assay for derCD23.

As described in Chapter 2, differential scanning fluorimetry (DSF) is a fluorescence-based technique primarily utilised to screen compounds and conditions that promote stabilisation of proteins for crystallisation. DSF measures the melting temperature ™, which increases if a protein molecule is more stable in one set of conditions as compared to another. A dye Sypro Orange (Sigma) has its fluorescence intensity excited by light at wavelength of 492 nm and binds to exposed hydrophobic patches during protein denaturation and emits strong fluorescent light at 610 nm, which can be detected by using a quantitative PCR machine (MX3500p, Stratragene).

Initially, to establish the concentration required for the experiment to give a decent, observable signal, experiments were done 5 μM of derCD23 with and without 16 mM EDTA. Cynthia Tso from our laboratory has previously established that under these conditions, 5 μM C3d gives a strong signal and here it is used as a positive control. EDTA was added to derCD23 to see whether removal of calcium might lead to any changes in the signal obtained (Figure 4.66).

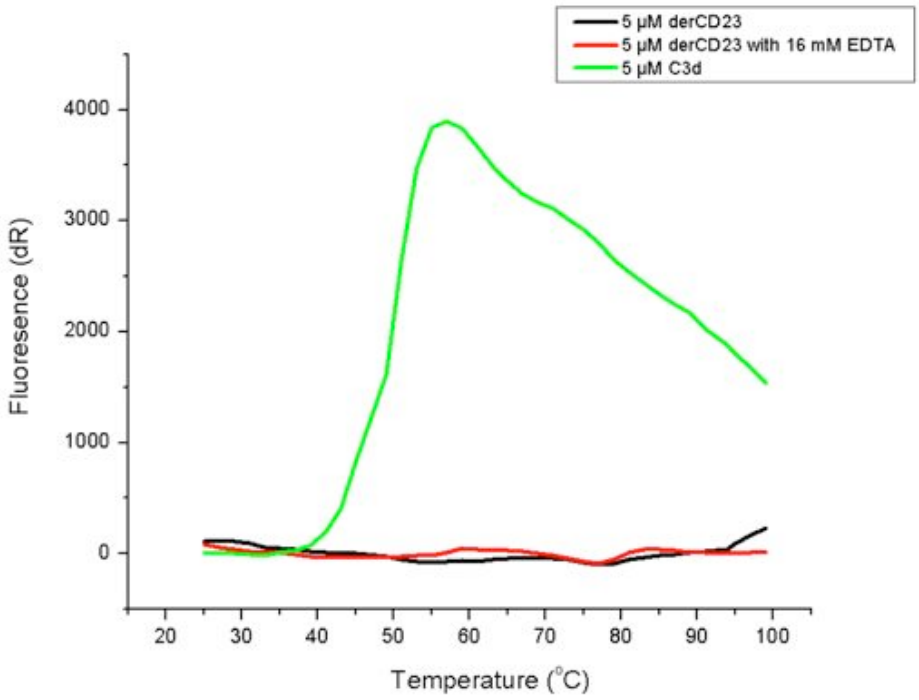

Figure 4.66: Initial DSF experiment with 5 µM C3d (green) and as 5 µM derCD23 with (red) and without (black) 16 mM EDTA.
5 µM C3d gave an observable signal with a T_m of about 48.5°C.

From this experiment C3d show a well-defined T_m of 48.5°C. At a concentration of 5 µM, derCD23 did not show any discernible signal. However upon closer examination of the curves it was seen that the presence of 16 mM EDTA led to a small increase of signal. Therefore concentration of derCD23 was increased at 100 µM and it was shown that the removal of calcium by EDTA has an effect in increasing the signal (Figure 4.67).

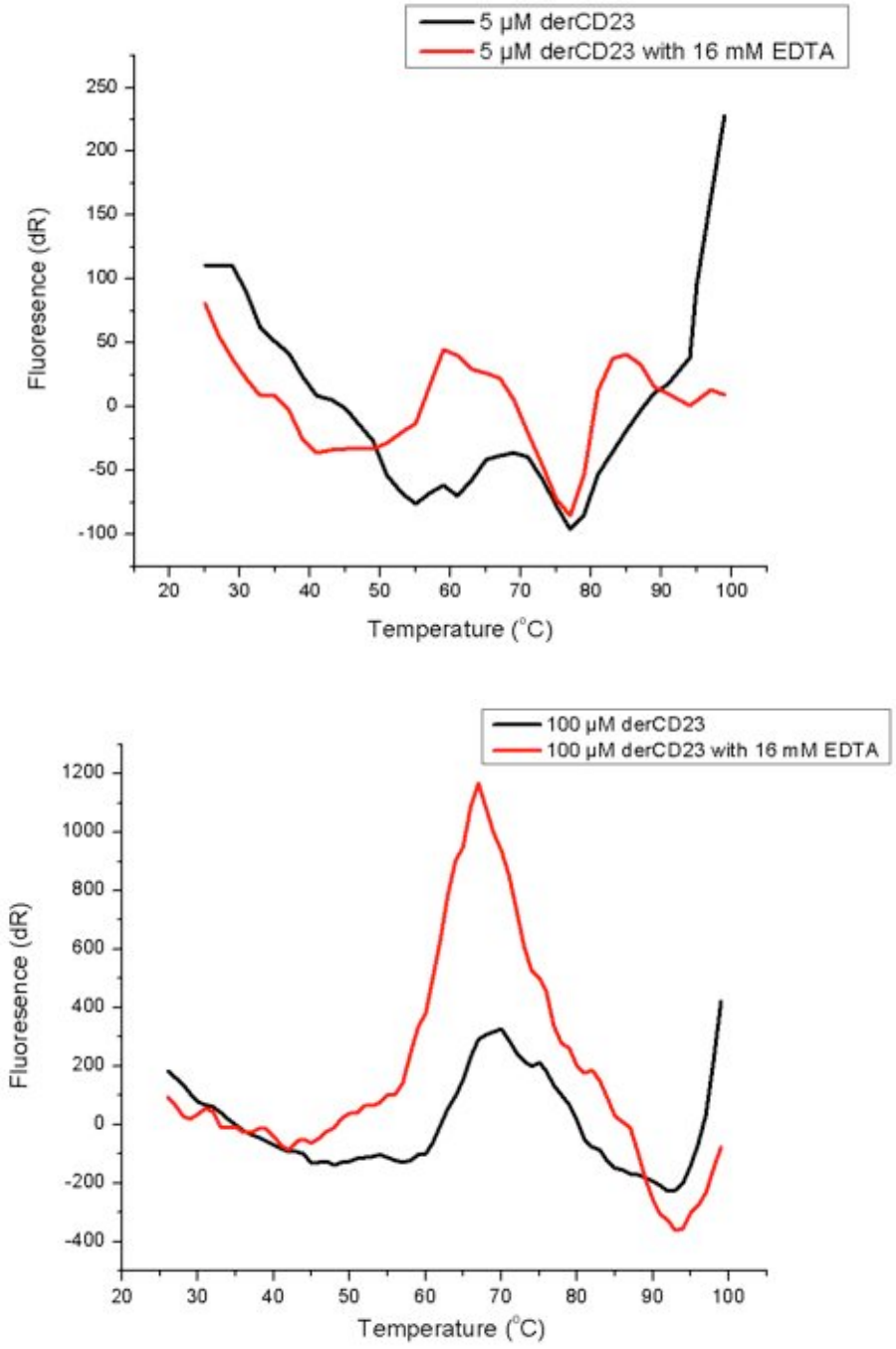

Figure 4.67: The effect of 16 mM EDTA on derCD23 DSF signal.
Close examination of the data revealed that the addition 16 mM EDTA led to a subtle increase of signal (top). The similar experiment was performed at a higher concentration of derCD23 at 100 µM, which led to higher signal. In both cases the addition of 16 mM EDTA, which removes the calcium causing signal increase.

However the signal is still very low for this system to be used for screening of compound. DerCD23 contains four disulfide bonds (C160-C288, C163-C174, C191-C282 and C259-C273), which provide stability to the extent that denaturation by increase of temperature alone may not be sufficient to allow for binding of the dye to exposed hydrophobic patches. Initial experiments showed that increasing the quantity of derCD23 leads to a marked increase of signal (Figure 4.68) but the large amount required make a high throughput screening impractical. Therefore optimization was required to minimize the amount of derCD23 required for this assay.

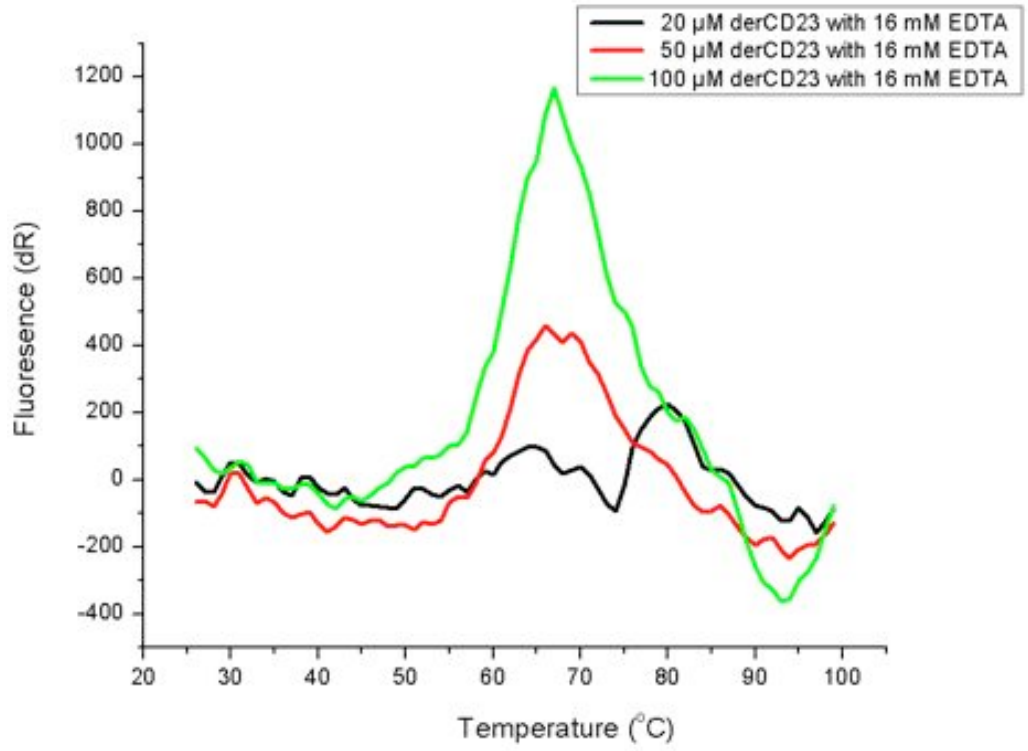

Figure 4.68: The effect of different concentration of derCD23 on the fluorescence signal.
DerCD23 at concentrations 20 µM, 50 µM and 100 µM with 16 mM EDTA. The data shows that the signal obtained increased in a concentration dependent manner. The software Origin 7.0 (Microcal) was used to fit the curves individually using a Boltzmann equation, which gives the midpoint between the minima and the maxima values of the fitted curve, T_m.

The addition of a small quantity of the reducing agent dithiothreitol (DTT) was tested. 10 μM derCD23 with DTT at concentrations of 0 mM, 0.1 mM, 0.25 mM and 0.4 mM were therefore tested. The results showed that addition of DTT not only the increased the signal to a marked degree, but the decrease of T_m was also seen in a concentration dependent manner. The T_m values obtained for 0.1 mM, 0.25mM and 0.5 mM DTT obtained are 59.5 ^oC, 52.0^oC and 48.3^oC respectively, whilst the absence of DTT gave the expected low signal (Figure 4.69). This is therefore a condition that could be used for initial compounds screening for derCD23 using a low concentration derCD23 sample of 10 μM.

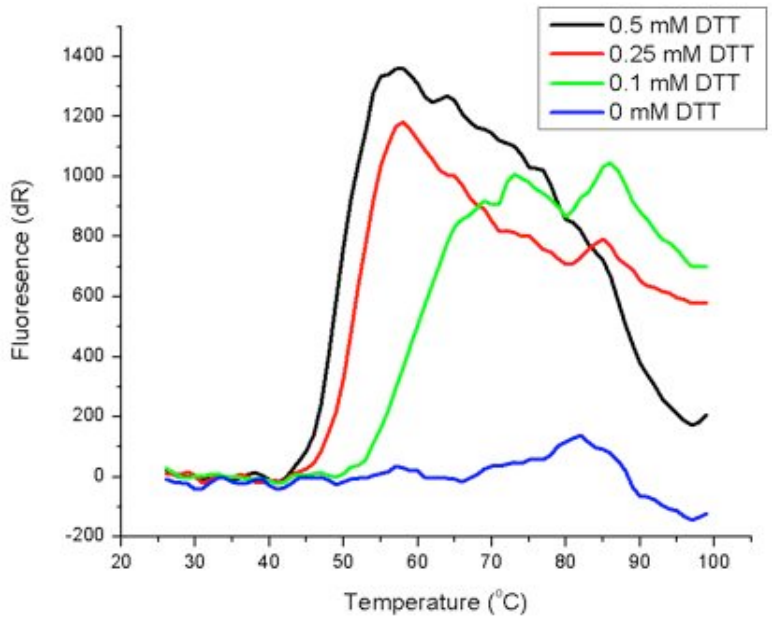

Figure 4.69: The effect of the addition of DTT on the signal obtained with 10 μM derCD23 sample. The software Origin 7.0 was used to fit the curves individually using the Boltzmann equation, which gives the midpoint between the minima and the maxima values of the fitted curve, T_m.

4.8.1 Role of calcium in stabilisation of derCD23 as shown by DSF

DerCD23 is a C-type lectin and requires calcium for its correct function (Richards and Katz, 1990). The binding sites of calcium have been previously determined via crystallography (Wurzburg et al., 2006) as well as NMR (Hibbert et al. 2005) with some differences on the site of calcium occupancy. The presence of calcium affects the affinity of the CD23/IgE interaction, as demonstrated by seven-fold of increase in the presence of calcium (Hibbert et al., 2005). Differential scanning fluorimetry (DSF) experiment was then performed to investigate whether calcium has a role in the stabilisation of the CD23 molecule. DSF is a useful technique to establish the stabilisation of a protein molecule by monitoring the changes of melting temperature, T_m in the presence of various compounds or ligands (Niesen et al., 2007).

A high concentration sample of derCD23 at 1 mM was dialysed into 10 mM HEPES, 150 mM NaCl, 16 mM EDTA pH 7.4 to remove calcium through chelation and dialysed further with the same buffer without EDTA to remove EDTA-calcium complexes and diluted to 100 uM. Previously, Cynthia Tso in our group has established that 5 uM C3d gives good signal and it is used as a positive control

The similar high concentration sample derCD23 at 1mM was also diluted to 100 μM with the same buffer but with 4 mM $CaCl_2$. The experiments were run with three replicates at 15μL each with a final concentration of 2:1000 dilution of Sypro Orange (Sigma) on a 96 well transparent PCR plate with a transparent optical seal, centrifuged and placed into a Stratagene Mx3005P RT-PCR machine with Sypro Orange filter.

An incubation period of 10 minutes at 25°C was employed with 74 cycles of 1°C increment for a period of 90s each to bring to a final temperature of 99°C.

As the profile shows, C3d has a T_m of 50°C. In the presence of 4 mM $CaCl_2$, derCD23 has a T_m of 63°C (Figure 4.70). Removal of calcium lowered the derCD23's T_m to 55°C. This observation showed that that calcium plays a role in stabilising CD23, leading to a higher melting temperature. The fluorescence signal is lower in the presence of calcium, which is probably due to a reduction of dye binding to CD23 in the more stable state (Cummings et al., 2006).

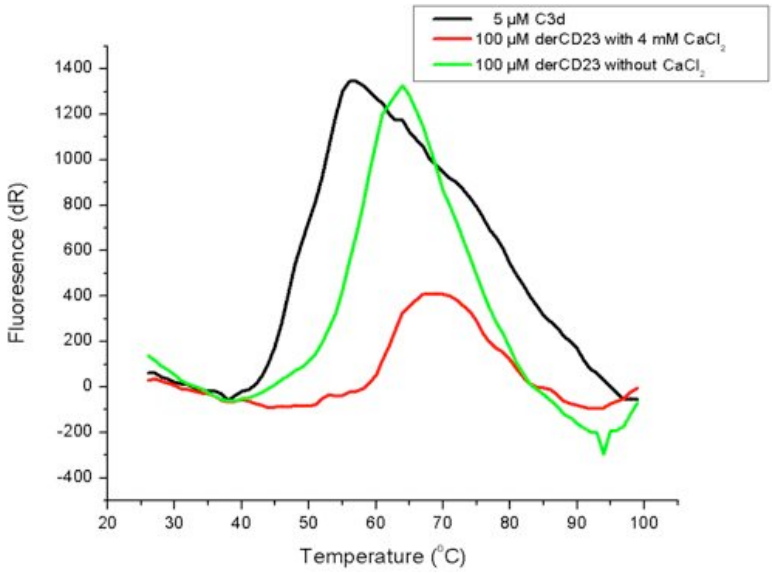

Figure 4.70: The differential scanning fluorimetry experiment performed to established the stabilisation of derCD23 by calcium.
5 µM C3d showed a T_m of 50°C. The presence of 4 mM $CaCl_2$ revealed a T_m of 63°C. The extensive removal of $CaCl_2$ by dialysis in the presence of 16 mM EDTA followed by dialysis in the experimental buffer lead a reduction of T_m by 8°C to 55°C. The software Origin 7.0 was used to fit the curves individually using the Boltzmann equation, which gives the midpoint between the minima and the maxima values of the fitted curve, T_m.

4.9 General discussion

A high-resolution structure of non-mutated derCD23 has been solved to a high resolution at 1.9 Å. The structural alignment shows that CD23 has regions of considerable flexibility at Loop 1 and Loop 4. The mutations H213R and G256S found in the crystal structure solved by Wurzburg et al. (2006) are situated at the trimerisation and IgE binding site, respectively. The G256S mutation, in particular, is in the region that is implicated in IgE binding and may explain the failure of co-crsytallisation of derCD23-IgE-Fc (Cε3-4) initially attempted in the same paper. Using SPR analysis, derCD23 and trimeric CD23 were shown to have different affinities for IgE. Trimeric CD23 has a higher affinity with K_D of 600 nM compared to derCD23 with a K_D of 1.4 μM which is due to avidity effect. Both derCD23 and triCD23 have a propensity to oligomerise, based on a variety of phiophysical measurments by SPR, AUC and NMR. The trimerisation model of the lectin head domain has been proposed previously by Hibbert et al. (2005). The trimerisation site is therefore a potential target for inhibiton as it may disrupt the higher affinity component of CD23 binding. The C-terminus of derCD23 has been established previously to be the CD21 (SCR1-2) binding site. Experiments employing the truncated version of derCD23 lacking the C-terminus were performed to confirm that the binding epitope of CD21 (SCR1-2) lies in the C-terminus alone. However it remains to be seen whether the full length of the C-terminus may be involved in CD21 binding. Binding analysis with the anti-CD23 monoclonal antibody IDEC-152 has shown that it binds to one of the trimerisation sites of CD23, thus having an ability to disrupt oligomerisation of derCD23. Experiments were performed to analyse the trimolecular interation between CD23 with IgE and its high

affinity receptor FcεRI. It was shown that derCD23 may form high molecular complexes with IgE-Fc and bind to membrane-bound FcεRI with a higher affinity due to avidity. DerCD23, however, bind much weaker to IgE bound to FcεRI indicating an unusual non-competitive inhibition of CD23 binding by FcεRI. The biological significance of these SPR-based results was tested in an *in vitro* cellular assay. In a mast cell degranulation system, it was shown that the derCD23/IgE complexes increase mast cell degranulation in a concentration dependent manner, whereas when IgE is bound to the mast cells. This may have an implication in involvement of CD23 in the levels of degranulation. Recently a paper was published defined a new role for CD23 in trancytosis of allergen IgE complexes through the airway epithelia which leads to mast cell degranulation in the sup-epithelial side (Palaniyandi et al., 2011). It is not known as yet whether membrane CD23 proteolysis occurs on the sup-epithelia, which may lead increase of mast cell degranulation. One question that may arise is whether there is an upregulation of ADAM-10, which in turn may increase the cleavage of membrane CD23 into soluble forms. Soluble CD23 may then form a high molecular complex with IgE, and together with allergen, lead to the increase of mast cell degranulation. Differential scanning fluorimetry (DSF) is an assay developed to monitor the thermal stabilisation of protein in the presence of different compounds and conditions. This system was optimised for derCD23 in order to improve the assay signal/noise with the minimum use of protein. Through this assay, it was also confirmed that calcium has a role in stabilising the derCD23 molecule as shown by the increase of T_m in the presence of calcium.

Chapter 5

The interaction between CD21 and C3d

5.1 Introduction

Complement is a key component of the innate immune system that also influences the humoral immune responses. Upon activation, the C3 activation product, C3b, forms covalent bonds with surfaces, thereby generating surface-bound ligands such as C3dg and C3d (a proteolytic fragment of C3) that engage CD21/CD19 B cell co-receptors expressed by mature B cells and follicular dendritic cells. Deficiencies in either C3 or the common gene that generates leukocyte complement receptors 1 (CD35) and 2 (CD21) result in impaired antibody responses in mice (Dempsey et al. 1996). Experiments done with hen egg lysozyme fused to C3d lowered the dose of the antigen required for antibody mediated immune response by 1000-fold in transgenic mice expressing B cell antigen receptor specific for hen lysozyme when compared with the response to lysozyme alone; this experiment indicates that C3d acts as a molecular adjuvant (Dempsey et al., 1996).

In demonstrating the C3d/CD21 involvement in autoimmune disease Del Nagro et al. (2005) immunized $CD19^{-/-}CD21^{-/-}$ mutant mice and wildtype mice, with collagen in a collagen-induced arthritis (CIA) disease model. It was shown that in the absence CD19 and CD21, the mutant mice became unsusceptible to arthritis induction.

5.1.1 Controversy regarding the crystal structure of the CD21 (SCR1-2)-C3d complex

The co-crystal structure of CD21 (SCR1-2)/C3d by Szakonyi et al. (2001) was controversial as it contradicted a large body of evidence from site directed mutagenesis and binding studies. In the crystal structure it is the SCR-2 domain that binds to C3d and SCR1 has no role in the interaction. The area on C3d implicated in CD21 binding was also different to that previously implicated by biochemical analyses, in that it is located on the side of the molecule with residues Gln70 directly implicated. Site-directed mutagenesis and binding studies by Clemenza and Isenman (2000) confirmed that it is a concave region of C3d that consists of mainly negatively charged residues that is mainly involved with binding to CD21.

(a)

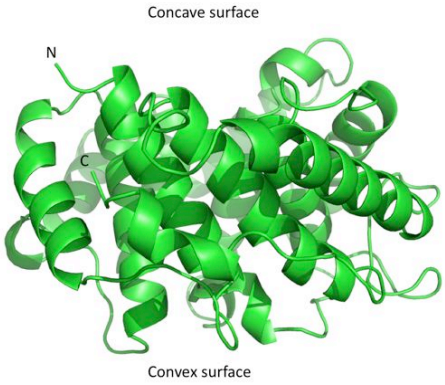

(b)

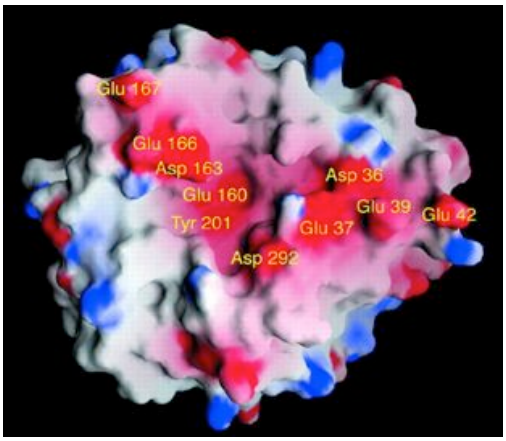

Figure 5.1: The structure of C3d highlighting the surface implicated in ligand binding.
(a) A side view of the crystal structure of C3d indicating the concave and the convex surface b) The main binding site of CD21 on C3d identified by site directed mutagenesis indicating a hydrophobic cleft surrounded by a ring of negatively charged residues. Figures adapted from Nagar et al., (1998) (PDB ID:1C3D) and Clemenza & Isenman (2000).

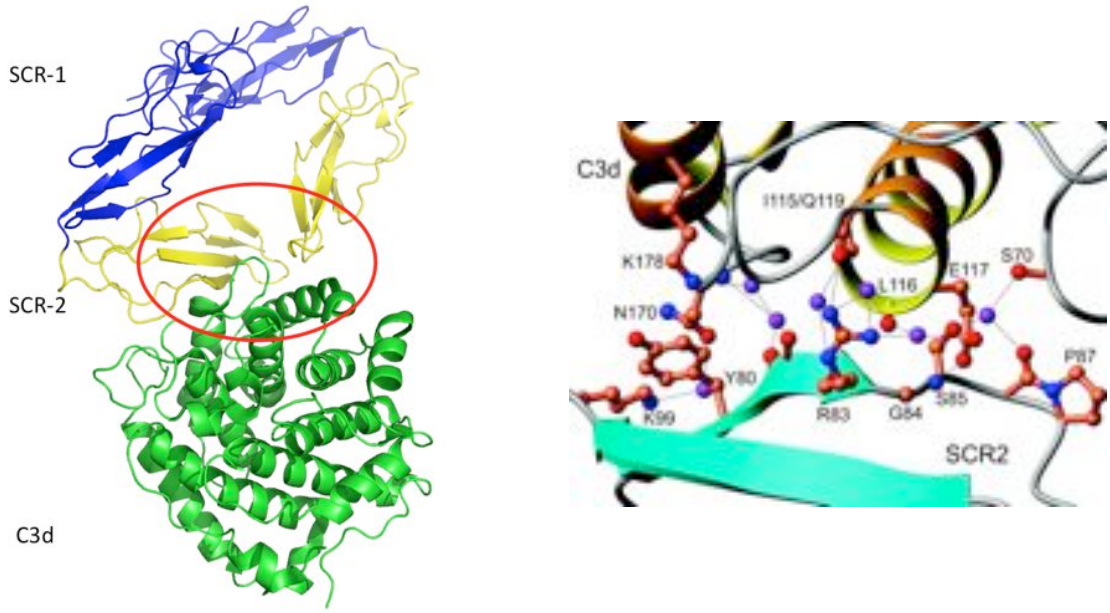

Figure 5.2: The CD21 (SCR1-2)-C3d complex crystal structure as solved by Szakonyi et al. (2001).
Left: The crystal structure showed a dimeric CD21 (SCR1-2) binding to C3d, which suggested that the SCR2 domain was implicated in C3d binding and identified a binding site on C3d different from the region previously implicated in site-directed mutagenesis studies. Right: The close up view of the interaction interface between CD21 with C3d from the crystal structure with the SCR2 domain of CD21 mainly implicated involving residues Y80, R83, G84, and S85 as proposed Hannan et al. (2005) (PDB ID: 1GHQ). The dimeric form of CD21 was later shown to be physiologically irrelevant by Prota et al. (2002).

Hannan et al. (2005) performed mutations on the acidic groove residues of C3d, including residues E117, D122, D128, and D147. They also performed mutation on SCR-2 of CD21: R83A, R83E, G84Y and were found to disrupt the binding to C3dg. In addition to these SCR-2 residues, they also performed mutations on SCR1 residues: (R28A, R28E, R36A, R36E, K41A, K41E, K50A, K50E, K57A, K57E, K67A and K67E). However they proposed that these residues were involved mainly in a pseudospecific interaction.

Isenmen et al. (2010) performed binding experiments between CD21 (SCR1-2) and the C3d mutants to assess residues implicated by Hannan et al. (2005) as well as assessing the residue N170 implicated in the crystal structure by Szakonyi et al. (2001). It was shown by

SPR that these acidic residues are indeed involved in CD21 (SCR1-2) binding. It was also shown that, in their hands, mutating N170 did not lead to any effect, thus contradicting the crystal structure. However all of the experiments in Isenman et al. (2010) were done at a single concentration of C3d at 2.5μM, which allows only a semi-quantitative analysis of binding characteristics. This study did, however, confirm that it is the concave surface of C3d that is mainly involved in binding to CD21.

To map the binding site of C3d on CD21, NMR titration experiments were previously performed by Dr Martine Bomb (Martine Bomb, DPhil thesis, University of Oxford, 2008). Assignment of the NMR resonances in the ^{1}H, ^{15}N-HSQC spectrum was performed by applying both the triple resonance CBCA approach (Grzesiek and Bax, 1993) and NOE-based assignment strategies (Zuiderweg 2002). High resolution interaction site mapping was performed using chemical shift perturbation in the ^{1}H,^{15}N-HSQC experiments. Unlabelled C3d was titrated against the ^{15}N-labelled CD21 (SCR1-2) sample under a variety of buffer conditions.

A titration performed at near physiological ionic strength ([NaCl] = 150 mM) reveals a single contiguous binding site comprised of residues from strands B, C and E of SCR 1 of CD21, including residues 13-18, 21-31 and 42-45 (Figure 5.3). Under these conditions, the interaction shows intermediate exchange characteristics, where peaks from interaction site residues disappear due to line broadening upon ligand binding (Figure 5.3). In addition to the peaks showing line broadening, a small number of residues experience fast exchange kinetics. The residues showing fast exchange characteristics map to the interface between SCR1 and SCR2 as well as the inter-domain linker residues Tyr64,

Phe65 and Asn66. This suggests that the binding of C3d to SCR1 may also perturb the relative orientation between SCR1 and SCR2. The same titrations performed at low ionic strengths ([NaCl]<50 mM) begin to show additional resonances affected at high concentrations of C3d, but these residues do not indicate any contiguous binding site and appear instead to represent non-specific electrostatic interactions (Figure 5.4). Kovacs et al. (2010) performed NMR chemical shift mapping of C3d on CD21 (SCR1-2) and seemed to suggest that there are two binding events involving both SCR2 and SCR1. By utilising NMR chemical shift mapping, residue Arg83 in SCR2 was shown to undergo chemical shift perturbations as well as Arg13 in SCR1. However these experiments were performed at low ionic strength (50mM NaCl) and taking into consideration that the interaction between C3d and CD21 is largely mediated by electrostatics (Morikis and Lambris, 2004) it is likely that some of the residues they predict are involved in C3d binding are a result of non-specific electrostatic interactions.

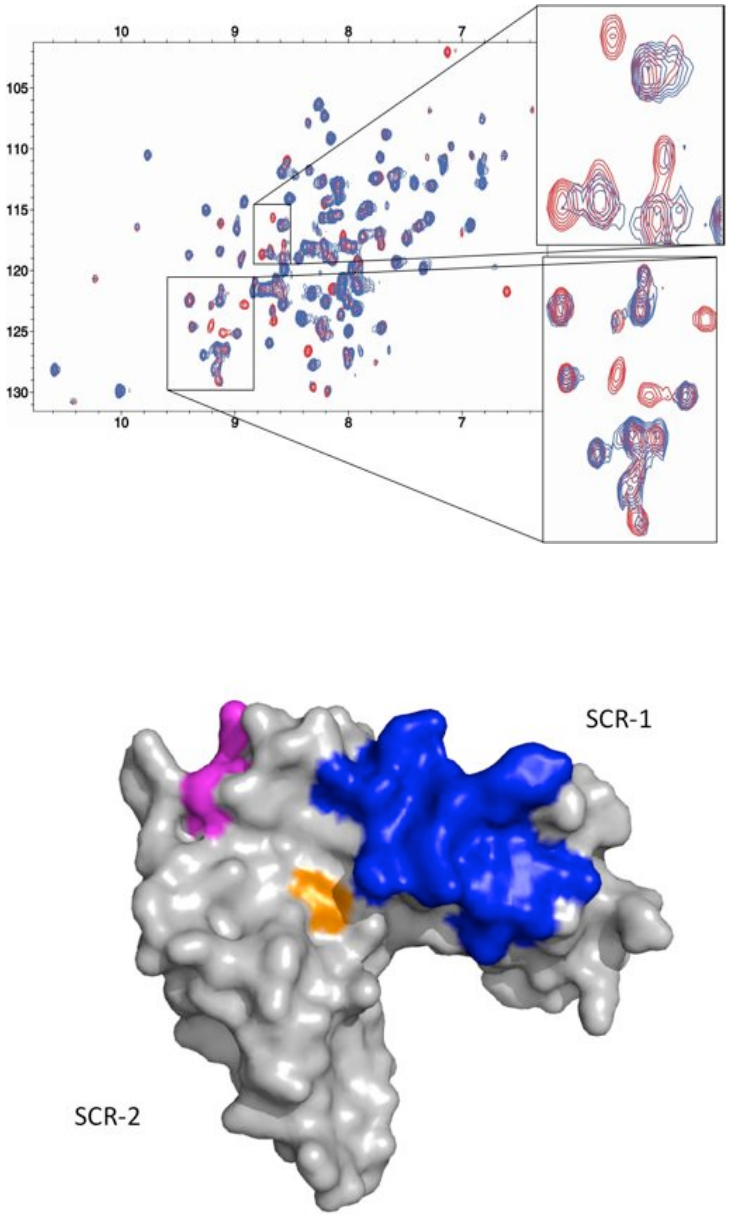

Figure 5.3: The chemical perturbation mapping of C3d binding site on CD21 (SCR1-2).
The chemical shift perturbation observed on the $^{1}H,^{15}N$-HSQC spectrum during the titration of unlabelled C3d into ^{15}N-labelled CD21 (SCR1-2) (top) were mapped on to the CD21 (SCR1-2) structure to reveal a contiguous surface on SCR-1 domain while the interdomain linker region showed chemical shift perturbation on residues Tyr64, Phe65 and Asn 66 (magenta). The side-chain of the interface residue Trp111 (orange) also showed chemical shift perturbation.

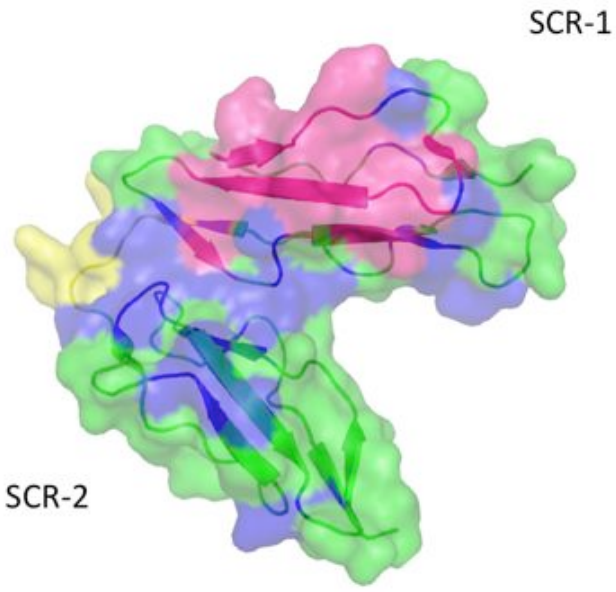

Figure 5.4: Additional chemical perturbations observed at low ionic strength with [NaCl]< 50 mM. The titration of unlabelled C3d into ^{15}N-labelled CD21 (SCR1-2) performed at low ionic strength showed additional chemical shift perturbations that are discontiguous and indicate a non-specific interaction (blue). The interdomain linker residues (yellow) were also perturbed in the titration performed at low ionic strength. The contiguous binding site on SCR1 is highlighted in pink.

Following the NMR chemical shift mapping, binding experiments were performed to assess the NMR mapping as well as to establish the important residues in the CD21/C3d interaction (Martine Bomb, DPhil thesis, 2008). Site-directed mutagenesis was performed on both CD21 (SCR1-2) and C3d, based on previously performed NMR titration on CD21 (Bomb et al., manuscript submitted) as well earlier site-directed mutagenesis studies on C3d (Clemenza and Isenman, 2000). Mutations performed on SCR2 residues implicated in the crystal structure (Arg83 and Gly 84) did not show any differences with the wildtype interactions. Several mutations were performed on the SCR1 domain of CD21 and it was shown that residues Ser32, Arg28 and Lys41 are important in binding. On the C3d side,

alanine mutations performed on C3d residues implicated in the crystal structure, L116 and and E117 (Figure 5.2) in particular, did show any difference to that of wild type interaction. Several other mutations were also performed on C3d and confirmed that it is a ring of negatively charged residues on C3d (Figure 5.5) that is mainly involved in CD21 binding, consistent with previous site-directed mutagenesis studies by Clemenza and Isenman (2010). The binding data for both CD21 and C3d mutations are summarized in Table 5.1 and Figure 5.5.

Table 5.1: Affinities and thermodynamic parameters of CD21 (SCR1-2) and C3d mutants

CD21	K_D (μM)	ΔG (kJmol^{-1})	ΔΔG (kJ mol^{-1})	ΔH (kJ mol^{-1})	TΔS (kJ mol-^{1})
Wildtype	0.19±0.02	-38.3±0.2	---	+58.5±0.5	+96.8
R83A	0.21±0.02	-38.1±0.2	+0.2	+51.2±0.7	+89.3
S32E	0.50± 0.07	-36.0±0.2	+2.3	+15.4±0.6	+51.3
R28A/S32E	1.01±0.10	-34.2±0.2	+4.1	+21.9±0.8	+56.1
K41E	no binding	-----	-----	-----	-----
G84Y	0.32±0.03	-37.0±0.2	+1.3	+47.2±1.8	+84.2
R83E/G84Y	0.28±0.04	-37.4±0.3	+0.9	+53.3±0.8	+90.7
R122E	0.19±0.02	-38.0±0.2	+0.3	+56.8±0.7	+94.8
C3d	K_D (μM)	ΔG (kJmol^{-1})	ΔΔG (kJ mol^{-1})	ΔH (kJ mol^{-1})	TΔS (kJ mol^{-1})
Wildtype	0.19±0.02	-38.3±0.2	---	+58.5±0.5	+96.8
C17A	0.20±0.02	-38.2±0.1	+0.1	+53.0±0.3	+91.2
E36A	0.59±0.03	-35.5±0.3	+2.8	+28.2±0.4	+63.7
E37A	0.80±0.05	-34.8±0.2	+3.5	+46.3±0.3	+81.1
E39A	0.59±0.06	-35.5±0.2	+2.8	+36.5±0.5	+72.0
E37A/E39A	2.72±0.10	-31.7±0.2	+6.6	+38.4±0.4	+70.2
E42A	0.11±0.03	-39.7±0.4	-1.4	+49.8±0.6	+89.5
L116A	0.19±0.03	-38.3±0.4	+0.0	+47.6±0.7	+85.6
E117A	0.22±0.04	-38.0±0.4	+0.3	+48.1±0.6	+86.1
E160A	0.75±0.05	-34.9±0.2	+3.4	+38.1±0.7	+73.0
D163A	1.15±0.09	-33.8±0.2	+4.5	+31.3±0.6	+65.2
E166A	0.96±0.03	-34.3±0.1	+4.0	+24.3±0.4	+58.6
D163A/E166A	4.03±0.13	-30.8±0.1	+7.5	+25.9±0.5	+49.4
N170A	0.16±0.03	-38.7±0.4	-0.4	+44.8±0.8	+83.6
K232A	0.24±0.02	-37.8±0.2	+0.5	+47.4±0.3	+85.2
E265A	0.27±0.03	-37.5±0.3	+0.8	+58.8±0.7	+96.2
D292A	1.73±0.08	-32.9±0.3	+5.4	+40.6±0.3	+73.3

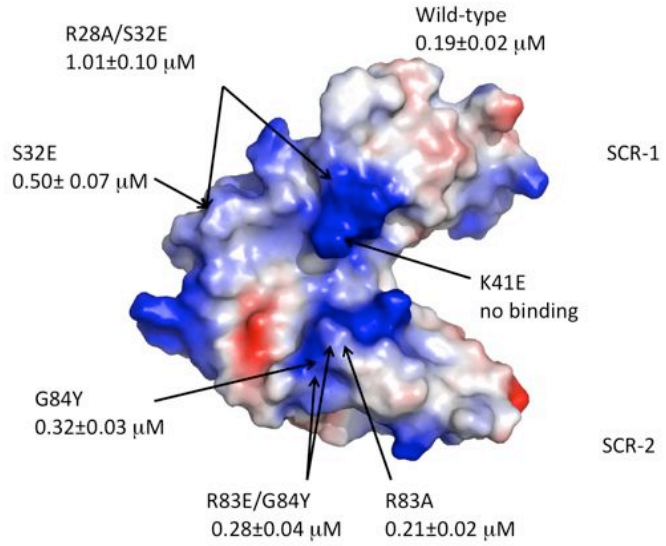

CD21 (SCR1-2)

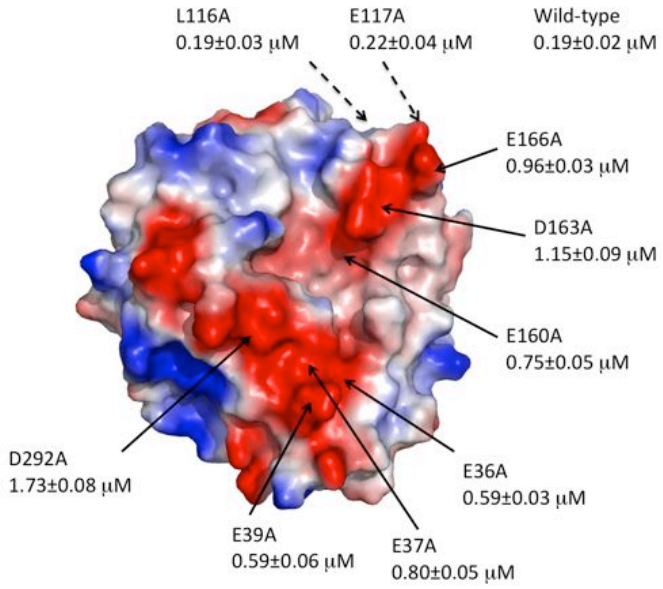

C3d

Figure 5.5: The site directed mutagenesis-binding affinities of C3d and CD21 (SCR 1-2).
The surface representation of CD21 (SCR1-2) and C3d with the affinity values of mutants as previously performed (Martine Bomb, DPhil thesis, 2008). Dashed arrows indicate residues obscured in the presented orientation.

This chapter describes the subsequent work, which was performed to expand the understanding of these interactions. With the knowledge that electrostatics play a central role in the interaction, experiments were subsequently performed under different ionic strength conditions to identify the primary binding site of the C3d/CD21 (SCR1-2) interation. NMR titration experiments were performed to delineate the binding site of C3d on CD21 (SCR1-2) using various ionic strengths emphasizing the ionic strength dependence of this interaction. Several further mutations were performed on SCR1 domain of CD21 to provide a more complete pictue of the interaction. Double mutant cycles were then performed to identify potential salt bridges between CD21 (SCR1-2) and C3d. Using the binding information obtained altogether, a manual docking exercise using PyMol was performed to provide a model of the interaction.

5.2 Purification of CD21 and C3d

5.2.1 Purification of CD21 (SCR1-2)

CD21 (SCR1-2) contains four disulfide bonds and the reducing environment of bacterial cytoplasm leads to difficulty in obtaining soluble protein from bacterial expression systems. Therefore this construct is over-expressed into inclusion bodies (Stewart, 1998). Extensive washing of inclusion bodies is needed to remove impurities that may lead to the aggregation of the protein (Maachupalli-Reddy et al., 1997). The expression and expression of CD21 (SCR1-2) is described in detail in Section 2.3.3. After solubilisation of inclusion bodies with denaturing agent, the protein was refolded in a buffer containing a mixture of oxidising and reducing agents that facilitate in folding. The refolding protocol for CD21 (SCR1-2) has been adapted from a previously established refolding protocol for CR1-3 of the human CR1 (White et al., 2004). The CD21 (SCR1-2) construct contains a histidine tag at the C-terminus. CD21 (SCR1-2) can therefore be purified using a nickel column followed by a size exclusion purification. A typical yield of around 10 mg of labelled protein per litre culture is achieved (Figure 5.6).

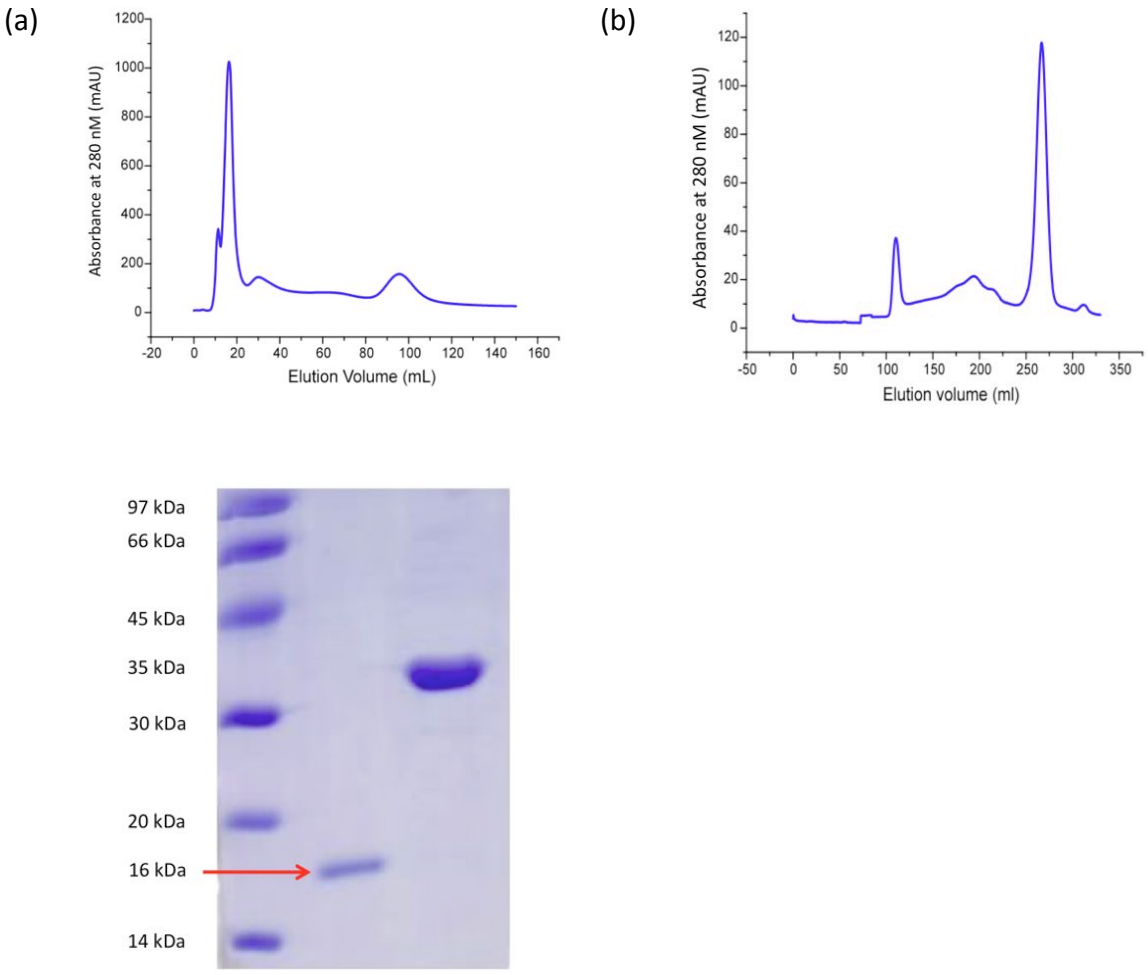

Figure 5.6: Purification of CD21.
(a) Nickel column purification trace, the second peak corresponds to CD21 while the first peak is a non-protein contaminant (b) gel filtration trace, the second dominant peak corresponds to CD21 while the first peak is a contaminant (c) gel electrophoresis indicates a pure CD21 sample is obtained indicated by 16 kDa size.

5.2.1.1 ^{1}H NMR of CD21 and mutants

^{1}H-NMR spectroscopy was employed to ascertain the foldedness of CD21. Well-resolved resonances in the upfield shifted methyl peak region (between 0 and -1.0 ppm) are characteristic of a well-folded protein (Rehm et al., 2002). A correctly folded CD21 shows upfield shifted methyl peaks on the ^{1}H-NMR spectrum (Figure 5.7). The CD21 mutants

described in this chapter also showed the typical ^{1}H spectrum indicating foldedness. (Figure 5.8).

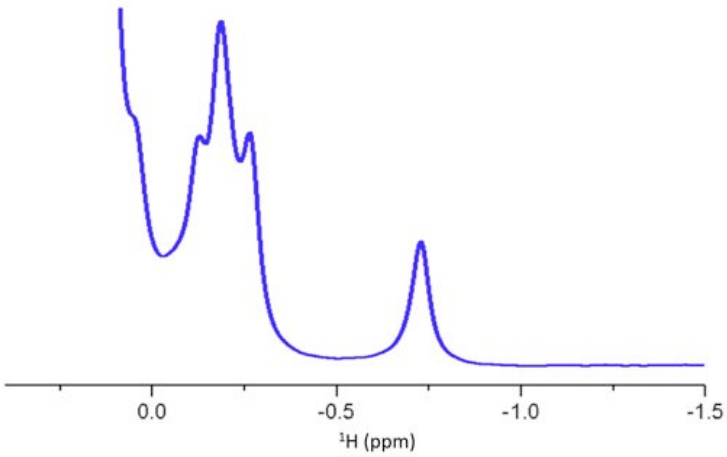

Figure 5.7 A distinct pattern of upfield shifted methyls confirms a correctly folded CD21.

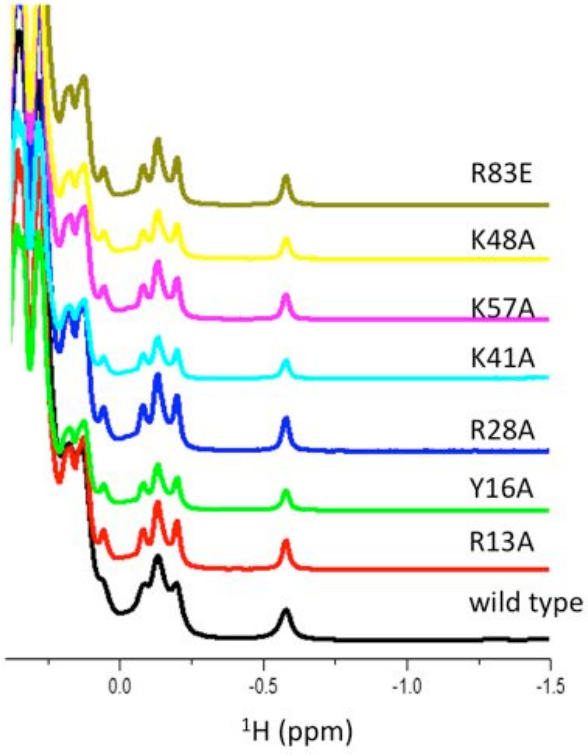

Figure 5.8: ^{1}H-NMR spectra of the refolded wild type CD21 and the mutant proteins used in this study.

5.2.2 Purification of C3d

C3d was cytoplasmically expressed in soluble form (as described in Section 2.3.4) and was purified using three columns, a weak cation exchange column CMFF, a strong anion exchange column Mono Q and finally gel filtration to further resolve and purify the protein from cytoplasmic contaminants (Figure 5.9).

5.2.2.1 ^{1}H NMR experiment of C3d and mutants.

^{1}H-NMR experiments were performed to determine whether the mutations performed have an effect on the foldedness of the C3d protein. It can be seen that the wild type C3d as well as the mutations performed in this study showed well-dispersed upfield shifted methyl peaks on the ^{1}H spectrum indicating foldness (Figure 5.10).

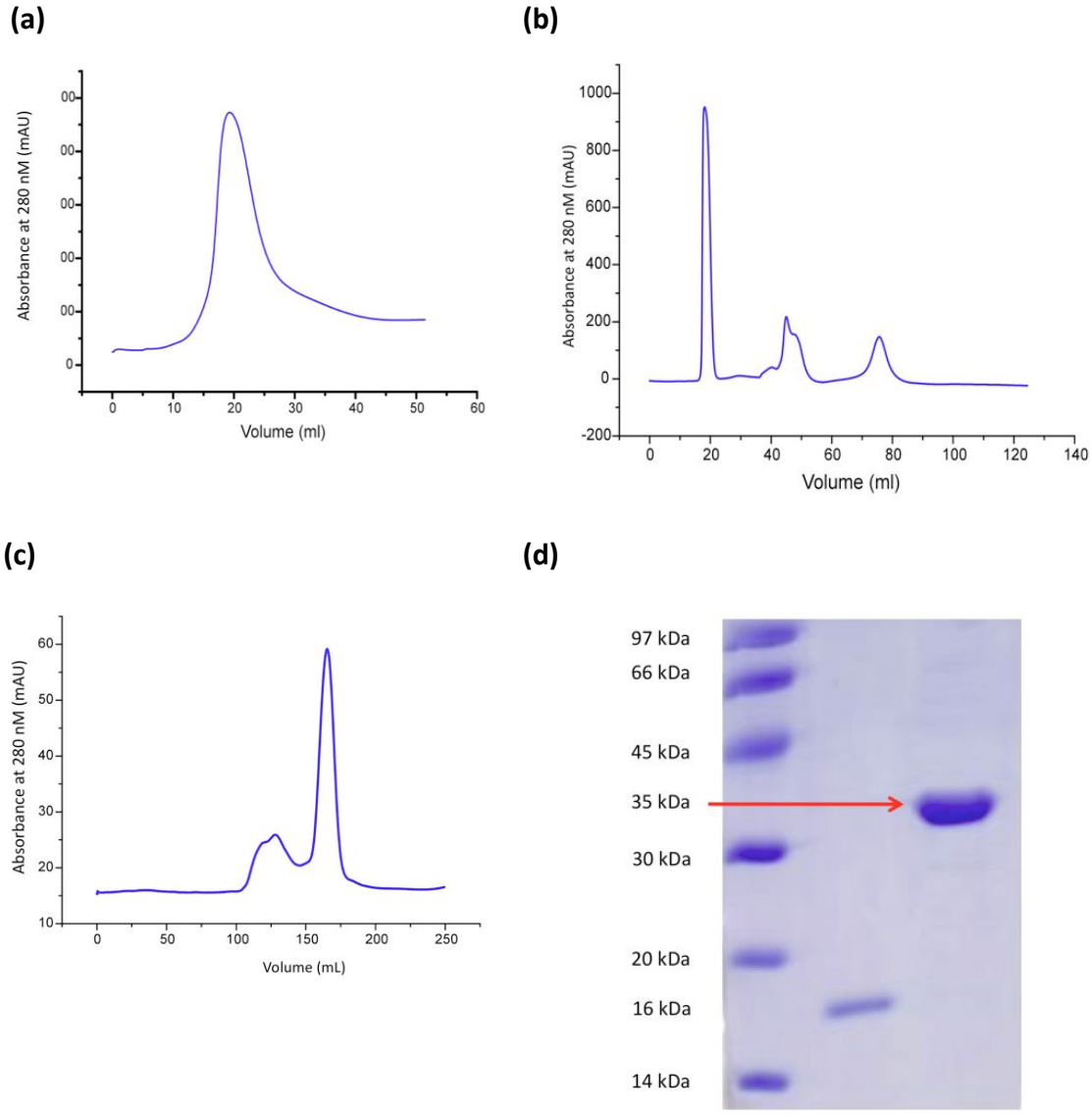

Figure 5.9: Purification of C3d.
(a) CMFF column; (b) MonoQ column purification: the first peak indicates C3d while the others are impurities; (c) gel filtration purification: the dominant peak indicates correctly folded C3d while the first peak indicates incorrectly folded C3d; (d) Gel electrophoresis indicates a pure C3d sample of 35 KDa is obtained.

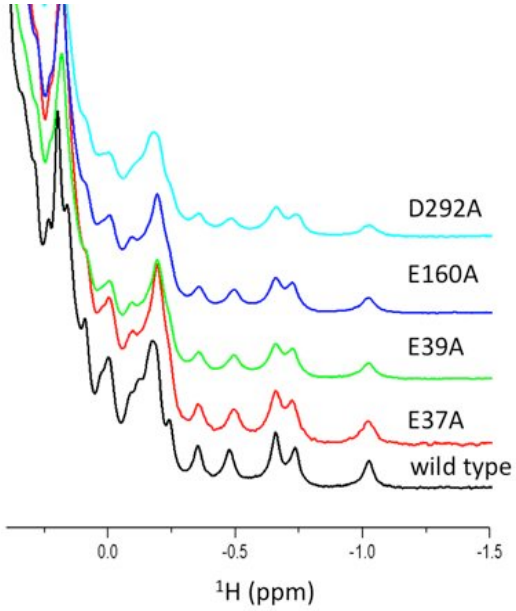

Figure 5.10: ^{1}H-NMR spectra of the wildtype and mutant C3d used.

5.3 Binding analysis of the CD21 (SCR1-2)/C3d interaction

The characterisation of the SCR2 (SCR1-2)/C3d interaction was performed using ITC and SPR. In an ITC experiment, a sample of CD21 (SCR1-2) was titrated in small aliquots against C3d, at a concentration of 14 μM, until a >3-fold molar excessed was achieved. The CD21 (SCR1-2)/C3d interaction has a K_D of 190 ± 20 nM. The interaction is enthalpically unfavourable with ΔH being positive (ΔH = +58.5 ± 0.5 kJ/mol) but is entropically driven by a large favourable entropy change of TΔS = -96.8 kJ/mol (Figure 5.11). These likely results from the displacement of ordered solvent molecules, water or ions, bound to the surface of C3d or CD21 (SCR1-2). The C3d interaction surface consists of a hydrophobic cleft on the concave face of C3d and is surrouded by a ring of negatively charged residue (Nagar et al., 1998). Conversely CD21 (SCR1-2), has a protruding

positively charged surface, which may have lead to the entropically driven interaction seen (Figure 5.12). The interation shows the expected 1:1 stoichiometry (N=0.96 ± 0.05).

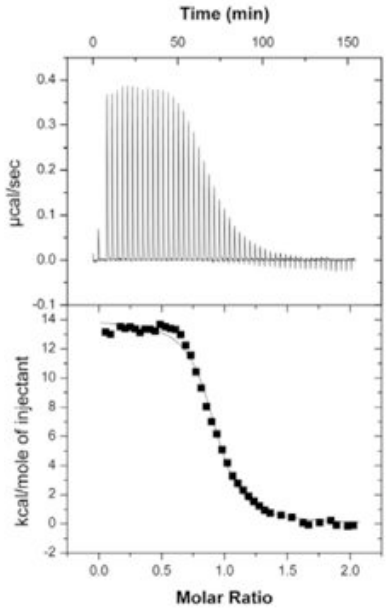

Figure 5.11: A representative figure of CD21 (SCR1-2)/C3d interaction as measured by ITC.
The K_D obtained was 0.19 μM (0.19 ± 0.02) in 150 mM NaCl. The thermodynamic values obtained were ΔG =-38.4 ± 3.8, ΔH = +58.5 ± 0.5, and TΔS = +96.8 (all in kJ/mol).

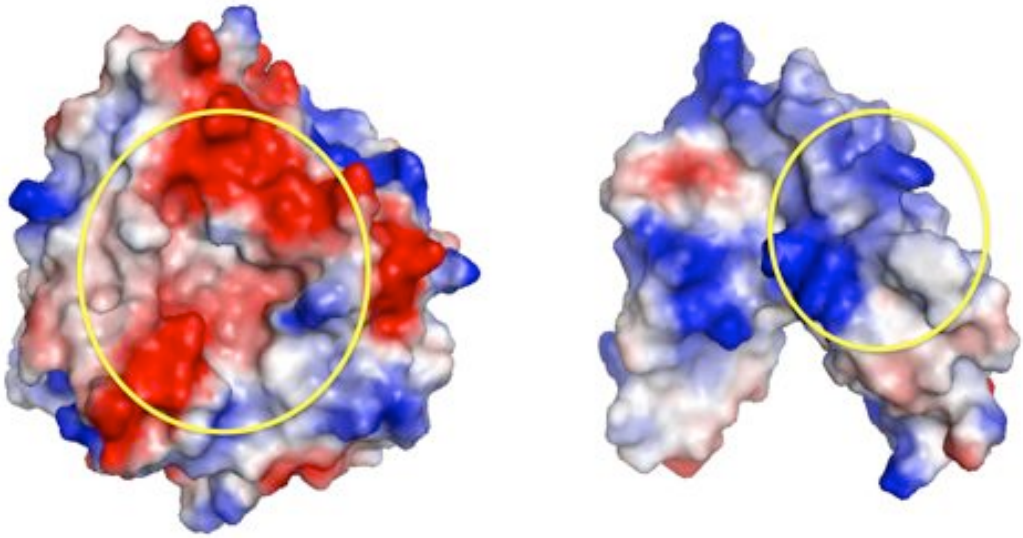

Figure 5.12: Surface charge representation of C3d and CD21 (SCR1-2).
(Left) The surface charge representation of C3d with the hydrophobic cleft surrounded by negatively charged residues. (Right) The protruding side chains of SCR1 domain residues of CD21 (SCR1-2) surrounded by positively charged residues.

As previously reported, the affinity of the CD21/C3d interaction shows a very strong dependence on the ionic strength of the buffer (Morikis and Lambris, 2004). SPR experiments of CD21/C3d binding were performed and the binding affinities of the interaction were measured over a range of ionic strenghts. These SPR experiments were performed using a version of C3d with the residue Ala17 mutated to Cys17. The available thiol group was utilised to immobilise C3d through thiol coupling methods (Schasfoort, 2008). Figure 5.13 shows a plot of log(K_A) versus log(ionic strength). This is a typical experiment used to assess the relative contribution of electrostatics to a molecular interaction; interactions that have no contribution from electrostatics would be expected to have a slope of zero in this plot. The log-log plot of the C3d/CD21 interaction results in a straight line (R = 0.98) with a slope of -1.6 units. This is an unusually high value for a

protein-protein interaction, indicating that electrostatics play a dominant role in interaction binding energy. ITC experiments were also performed at different ionic strengths and show the same pattern, with a K_D values of 190nM at 50 mM NaCl, 920 nM at 150mM NaCl and 5.2 µM at 400 mM NaCl (Figure 5.13); the value for the ITC-derived log-log plot is also -1.6.

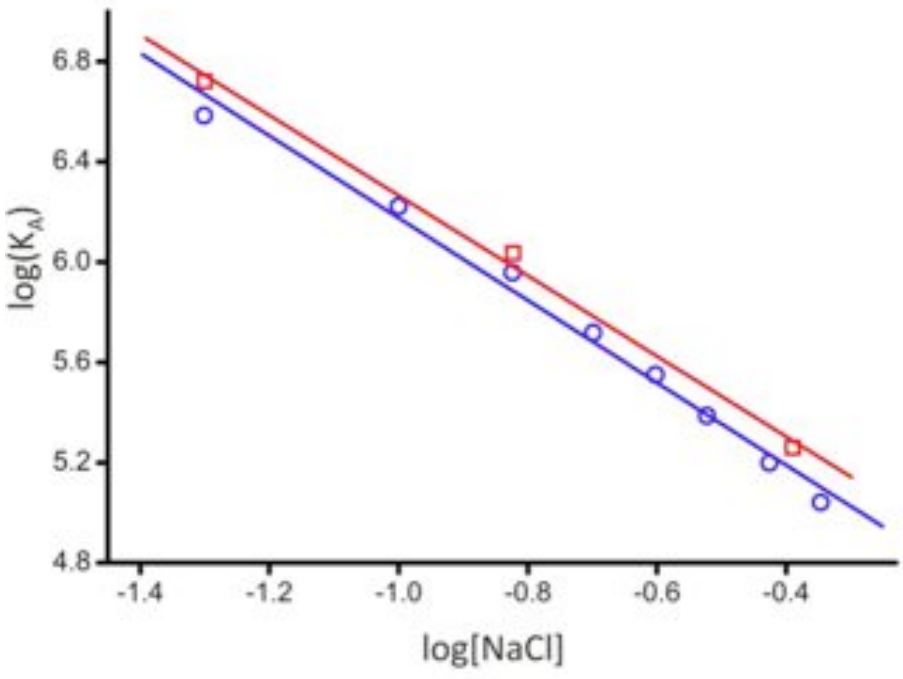

Figure 5.13: The effect of the ionic strength on the CD21 (SCR1-2)/C3d interaction, plotted as log (K_A) vs log (ionic strength).
Data from the SPR measurements are in blue and ITC measurements are in red. Experiments were performed at a range between 50-400 mM NaCL.

5.4 Identification of C3d binding sites on CD21 (SCR1-2) by NMR chemical shift mapping

NMR is a powerful technique for identifying protein-ligand interactions. As discussed in the earlier section, the chemical shift perturbations observed upon addition of a ligand can be be used to map the ligand binding site on a protein. The ^{15}N,^{1}H-HSQC spectrum of CD21 (SCR1-2) was assigned previously by Dr Martine Bomb (Martine Bomb, DPhil thesis, University of Oxford, 2008) and is used to assist in the identification of binding sites in NMR titration experiments. As demonstrated in Section 5.3, electrostatics plays a dominant role in the interaction. Therefore NMR mapping was done at various ionic strengths to map the interaction site on CD21 (SCR1-2) under different conditions.

5.4.1 NMR titration of ^{15}N-labelled CD21 (SCR1-2) with unlabelled C3d.

C3d was titrated into ^{15}N-labelled CD21 at physiologic ionic strength of 150 mM NaCl. The residues Gly12, Arg13, Ile14, Ser15, Tyr16, Tyr17, Ile21, Ala22, Gly24, Thr25, Val26, Ile27, Arg28, Tyr29, Ser30, Cys31, Lys41 and Leu44, Cys45 show chemical shift perturbations. These residues are all localized on the SCR1 domain (Figure 5.14). It is known that the interaction between CD21 and C3d is strongly electrostatic in character (Morikis and Lambris, 2004). Therefore it was thought that the titration experiment done at higher ionic strength (400 mM NaCl) would reveal the specific residues in CD21 that are involved in binding to C3d.

Unlabelled C3d was titrated at concentrations of 0 µM, 12.5µM, 25µM, 37.5µM and 50µM (0:1, 0.25:1,0.5:1,0.75:1. 1:1) into the ^{15}N-labelled obtained CD21 (SCR1-2) sample

at an ionic strength of 400 mM NaCl. Under these conditions, a smaller subset of residues on SCR1 are perturbed (residues Tyr16, Tyr17, Gly24, Thr25, Val26, Ile27, Arg28, Tyr29, Leu44 and Cys45) (Figure 5.14).

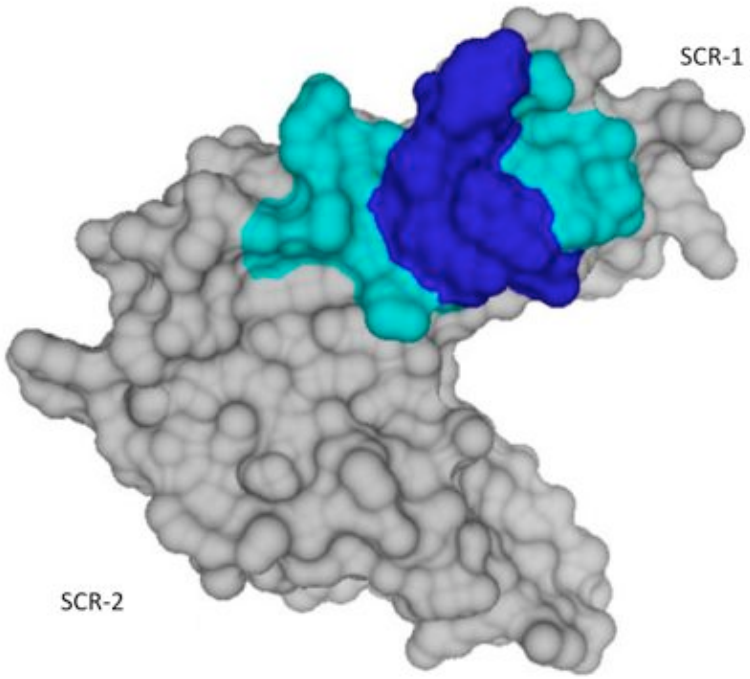

Figure 5.14: Surface representation of residues perturbed by addition of C3d by NMR chemical shift perturbation .
Residues that are perturbed at high salt (400 mM NaCl are highlighted in dark blue. Residues that are perturbed at physiological salt (150 mM NaCl) are highlighted in cyan. Residues in grey are unperturbed by the binding event in the NMR spectra.

At physiological ionic strength the binding binding on SCR1 can be described, as a central core of hydrophobic residues surrounded by a ring of postively charged residues. At high ionic strength (400mM NaCl), the binding site is mapped mostly to the central hydrophobic core (Fig. 5.14).

Arg83 and Gly84 in SCR2 were implicated as binding residues in the crystal structure (Szakonyi et al., 2001) and their role supported by later studies of the same group (Hannan et al., 2005). These residues were not affected in any of the NMR titrations we performed (Fig 5.15), even under low ionic strengths (data not shown). This supports the earlier site-directed mutagenesis studies and our data indicate no direct role for SCR2 in binding to C3d. Our studies clearly indicate that the crystal structure represents a non-physiological complex.

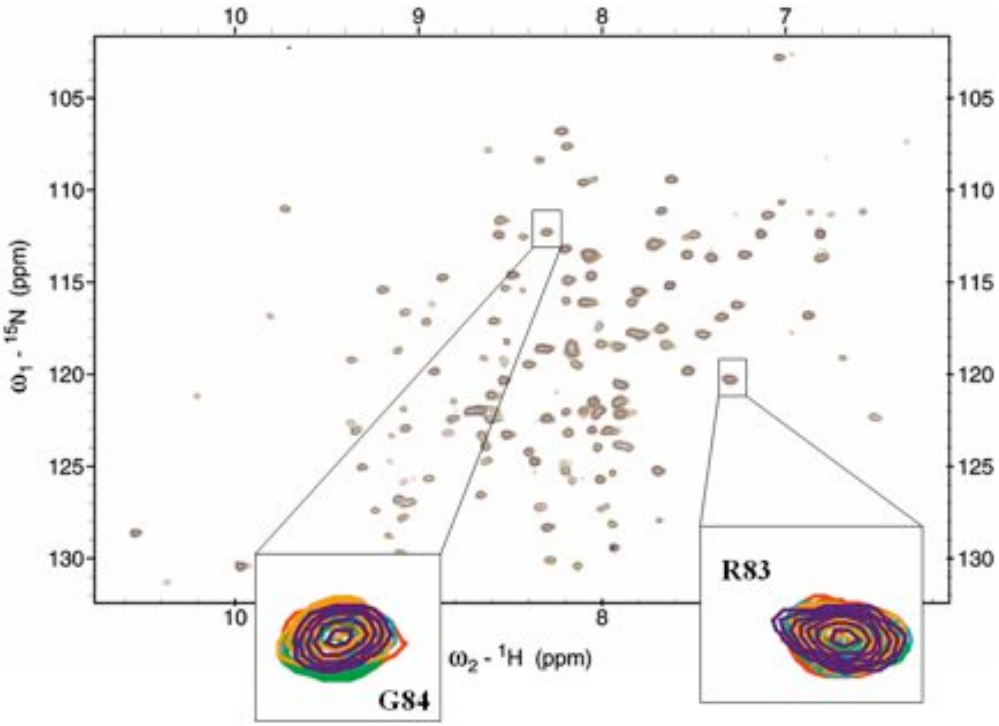

Figure 5.15: Residues Arg83 and Gly84 in SCR2 domain implicated in the crystal structure did not show any changes in the titration.

5.5 Site-directed mutagenesis studies

Based on the NMR mapping, site-directed mutagenesis was performed on the CD21 (SCR1-2) to assess the involvement of those residues implicated in the NMR titration

experiments and to determine the SCR domain that is important in C3d binding. Previously Dr Martine Bomb from our laboratory performed site directed mutagenesis on the following residues: R28A/S32E, K41E, R83A, G84Y, R83E/G84Y and R122E (Martine Bomb, DPhil thesis, 2008). As part of my thesis work, I made an additional series of mutations, including R13A, Y16A, R28A, K41A, K57A and R83E. The binding analysis is summarised in Table 5.2. The K57A and Y16A mutations on SCR1 lead to a dramatic reduction of affinity with K_D values of 1.53±0.20 μM and 3.90±0.35 μM, respectively, compared to the wild type interaction at 0.19±0.02 μM. Y16 is a central residue of the hydrophobic cluster in SCR1, we predict this residue inserts into a hydrophobic surface on the concave groove of C3d. The mutation R28A on SCR1 had a small effect on the interaction with a K_D of 0.61±0.08 μM. The K41A mutation had a large effect on the affinity with a K_D of 3.75±0.05 μM. A non-conservative mutation of this amino acid to a residue of opposite charge, K41E, led to a complete abrogation of C3d binding. The CD21(SCR1-2) mutant K41E has been used as a negative control in their evaluation of a recombinant technetium-labelled CD21 as an *in vivo* complement imaging tool (Badar et al. (2011)).

On the SCR2 domain, residues R83 and G84 were implicated to be important in the CD21 (SCR1-2)/C3d crystal structure (Szakoyi et al. 2001). Mutations were made on these residues to assess their involvement in C3d binding. The R83A mutant showed no affect on binding with a K_D of 0.21±0.02 μM. The non-conservative R83E mutation reduced the affinity to 0.57±0.06 μM, a small but significant effect that is possibly due to a reduction of overall positive charge on the protein surface and hence indirectly alters the

interaction between the oppositely charged interaction between CD21 and C3d molecules. Another non-conservative SCR2 mutant, G84Y, also did not show much difference with a K_D of 0.32±0.03 μM. To emphasize the non-involvement of these two residues R83 and G84, the double mutant R83E/G84Y were made and the binding analysis showed no significant change in affinity as compared to wildtype with a K_D of 0.28±0.04 μM. Finally the mutant R122E, which is distal from the predicted binding surface, showed no difference in affinity with a K_D of 0.19±0.02 μM. Taken together this site-directed mutagenesis confirms that it is the SCR1 that is predominantly important for C3d binding and not SCR2 as suggested by the CD21 (SCR1-2)/C3d crystal structure.

Table 5.2: Summary of the binding experiments performed between various CD21 mutants and wild type C3d

CD21	K_D (μM)	ΔG ($kJmol^{-1}$)	ΔΔG ($kJ\ mol^{-1}$)	ΔH ($kJ\ mol^{-1}$)	TΔS (kJ mol-1)
Wildtype	0.19±0.02	-38.3±0.2	---	+58.5±0.5	+96.8
Y16A	3.90±0.35	-30.9±0.2	+7.4	+7.8±0.6	+38.7
R28A	0.61±0.08	-35.5±0.3	+2.8	+24.1±0.3	+60.6
K41A	3.75±0.05	-31.0	+7.3	+25.6±0.2	+50.1
K57A	1.50±0.20	-33.2±0.3	+5.1	+15.5±0.4	+48.7
R83E	0.57 ±0.06	-34.1±0.3	+4.2	+20.2±2.3	+90.9
Performed previously by Dr. Martine Bomb					
R83A	0.21±0.02	-38.1±0.2	+0.2	+51.2±0.7	+89.3
S32E	0.50± 0.07	-36.0±0.2	+2.3	+15.4±0.6	+51.3
R28A/S32E	1.01±0.10	-34.2±0.2	+4.1	+21.9±0.8	+56.1
K41E	no binding	-----	-----	-----	-----
G84Y	0.32±0.03	-37.0±0.2	+1.3	+47.2±1.8	+84.2
R83E/G84Y	0.28±0.04	-37.4±0.3	+0.9	+53.3±0.8	+90.7
R122E	0.19±0.02	-38.0±0.2	+0.3	+56.8±0.7	+94.8

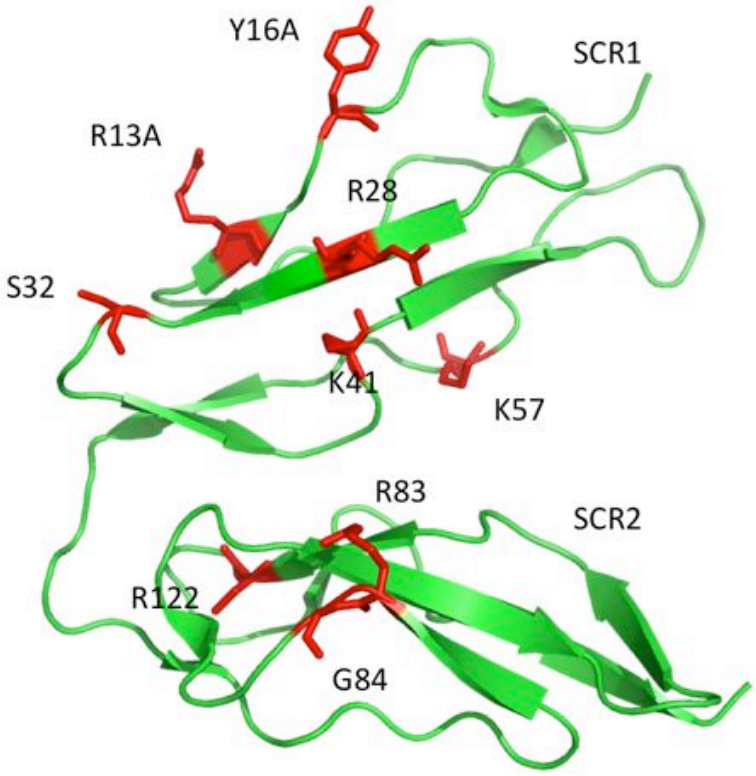

Figure 5.16: The mutations performed on CD21 (SCR1-2).

5.6 Identification of salt bridges

In protein-protein interactions salt bridges are often formed between the anionic carboxylate group ($RCOO^-$) of either aspartic acid or glutamic acid and the cationic ammonium group (RNH_3^+) from lysine or the guanidium group ($RNHC(NH_2)_2^+$) of arginine residues (Xu et al., 1997). Salt bridge pairings can be identified when the alanine mutation on both purported residues in both interacting molecules does not differ in terms of affinity and thermodynamic parameters with the interaction of the mutants and the respective wild type binding partner (Wells, 1990).

Protein1 Protein 2

A -------- B
A^* -------- B
A^* -------- B^*

In this illustration, A and B are wild type molecules. A* and B* are residue knockout in each of the molecules. If the affinity between A* and B and A* and B* do not differ, they can be said to form an exclusive salt bridge between them as no other residues would otherwise be implicated in the binding between the two molecules.

In the results that follow, binding experiments between the various constructs of CD21 (SCR1-2) and C3d were done using ITC, which reveals the affinity values as well as thermodynamic parameter (Table 5.3). Mutations were performed using site directed mugenesis and the protein expressed and purified.

Table 5.3: The overall values of affinity, ΔG and ΔΔG values obtained for the interaction between CD21 and C3d and the mutants.

CD21	C3d	K_D (μM)	ΔG (kJ/mol)	ΔΔG (kJ/mol)
WT	WT	0.19	-38.3	--
WT	E39A	0.59	-35.4	+ 2.8
R13A	WT	3.60	-31.1	+7.2
R13A	E39A	3.51	-31.1	+7.2
WT	E37A	0.78	-34.8	+3.5
R13A	E37A	3.47	-31.1	+7.2

CD21-R13 forms a bifurcated salt bridge with C3d E39 and E37

Table 5.4: The values of affinity, ΔG, ΔΔG and expected ΔΔΔG obtained to highlight a possible salt bridge pairing between CD21 Arg13 and C3d Glu39.

CD21	C3d	K_D (μM)	ΔG (kJ/mol)	ΔΔG (kJ/mol)	Expected ΔΔΔG if the two mutants are independent
WT	WT	0.19	-38.3	--	
WT	E39A	0.59	-35.35	+ 2.8	
R13A	WT	3.60	-31.1	+7.2	
R13A	E39A	3.51	-31.1	+7.2	+10.0

From the data above if C3d E39A and CD21 R13A were independent from each other, the expected ΔΔΔG would be +10.0 kJ/mole. However the value obtained for CD21 Arg13A/C3d Glu39A interaction is +7.2 kJ/mole, which is lower than the value otherwise expected if those residues are independent. This therefore suggests that that CD21 Arg13 and C3d Glu39 form a salt bridge.

Table 5.5: The values of affinity, ΔG, ΔΔG and expected ΔΔΔG obtained to highlight a possible salt bridge pairing between CD21 Arg13 and C3d Glu37.

CD21	C3d	K_D (μM)	ΔG (kJ/mol)	ΔΔG (kJ/mol)	Expected ΔΔΔG if the two mutants are independent
WT	WT	0.19	-38.3	--	
R13A	WT	3.60	-31.1	+7.2	
WT	E37A	0.78	-34.8	+3.5	
R13A	E37A	3.47	-31.1	+7.2	+10.7

Arg13A also appears to form a salt bridge with Glu37, as the double mutation binding yielded a ΔΔΔG value of +7.2 kJ/mole as opposed to the predicted ΔΔΔG of +10.7 kJ/mole. These possible pairings between CD21 Arg13 and residues C3d Glu37 and C3d Glu39

suggest a bifurcated salt bridge between CD21 Arg13 and C3d Glu37 and C3d Glu39 (Fig. 5.15).

5.6.1 Manual docking of CD21 (SCR1-2) with C3d

The binding analysis as well as the double mutant cycling analyis performed so far has assisted in the identification of potential contacts residues between CD21 and C3d. Using the information gathered a manual docking of the CD21/C3d interaction was performed using PyMol. The residues primarily involved in the SCR1 domain and on the C3d side shown below revealed the highest effect in the knock out studies. A potential salt bridge has been identified so far using the ITC based double mutant cycle analysis. Arg13 on CD21 (SCR1-2) forms a bifurcated salt bridge with Glu37 and Glu39 on C3d and is used to anchor the interaction between CD21 (SCR1-2) and C3d to provide a model of the interaction.

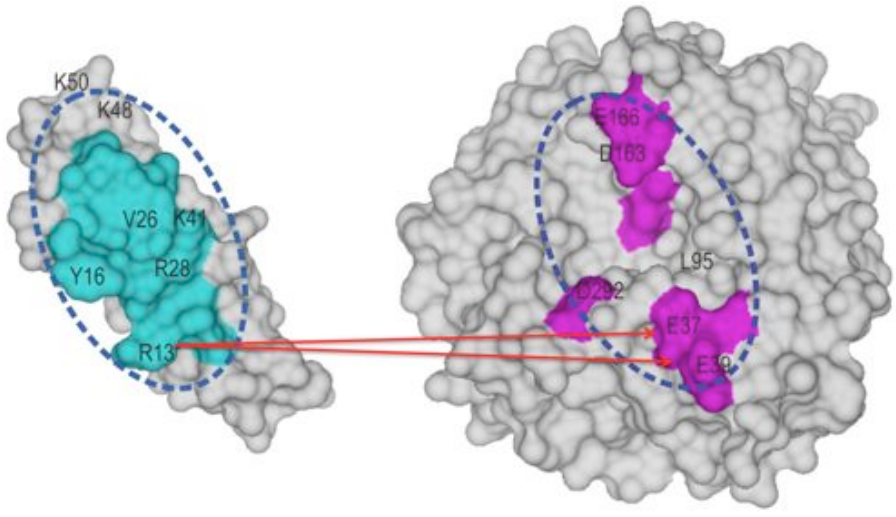

CD21 (SCR 1-2) C3d

Figure 5.17: The proposed binding interaction interface between CD21 (SCR1-2) and C3d.
Residues K41 forms a salt bridge with C3d-D292 and CD21-R13 forms a bifurcated salt bridge with E37 and E39.

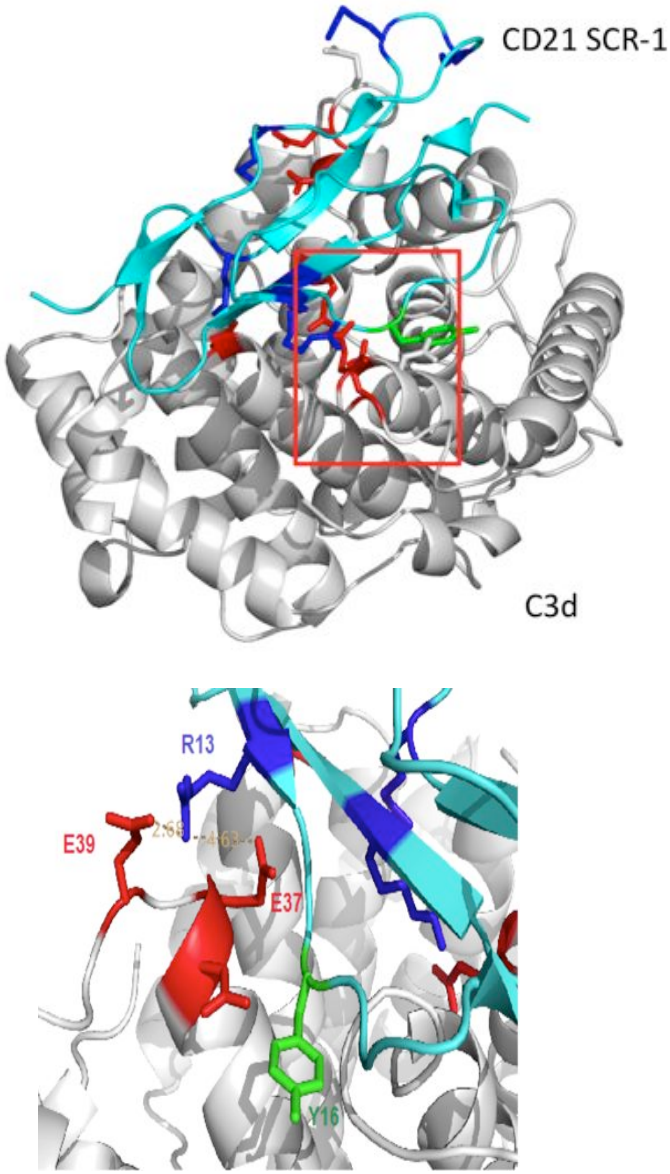

Figure 5.18: Manual docking of C3d and CD21 (SCR 1-2) based on ITC results.
Top: C3d and CD21 (SR 1-2) were manually docked against each other using Pymol and the possible salt bridge was modelled (inset). Below: The positively charged CD21 Arg13 forms a bifurcated salt bridge with Glu39 and Glu37.

5.7 The CD21/C3d binding site: a possible explanation for chemical exchange?

A look at the ^{1}H NMR slices of some of the important residues in the NMR titration experiments revealed an interesting phenomenon in the chemical environment of those residues during the NMR titration. Titrations done in different salt concentrations (50mM, 150 mM and 400 mM NaCl) showed different exchange regimes. As shown in Figure 5.19, both Tyr17 and Ala22 showed intermediate exchange character when titrated with C3d at lower salt concentration, but at higher salt concentration they show shifts to that are more typically observed in slow exchange (gradual loss of binding signal). The increase of ionic strength leads to a reduction in binding affinity (Figure 5.15) and therefore it would be expected that the fast exchange kinetics would be observed. One possible explanation is that the intermediate exchange character observed at lower ionic strength results not from the exchange kinetics between bound and unbound states but instead from the exchange kinetics of different bound states. This "chemical exchange" phenomenon is uncommon but not unheard of for small molecules bound to protein (Stites, 1997) but is very unusual for protein-protein interaction.

Higher ionic strenghs drives the binding event between CD21 (SCR1-2) and C3d to become more specific, and more focused towards a hydrophobic cluster in SCR1 of CD21. Residue Gly84, implicated by the crystal structure (Szakonyi et el., 2001) did not show any changes when the titration was done in either low or higher salt concentration (Figure 5.15).

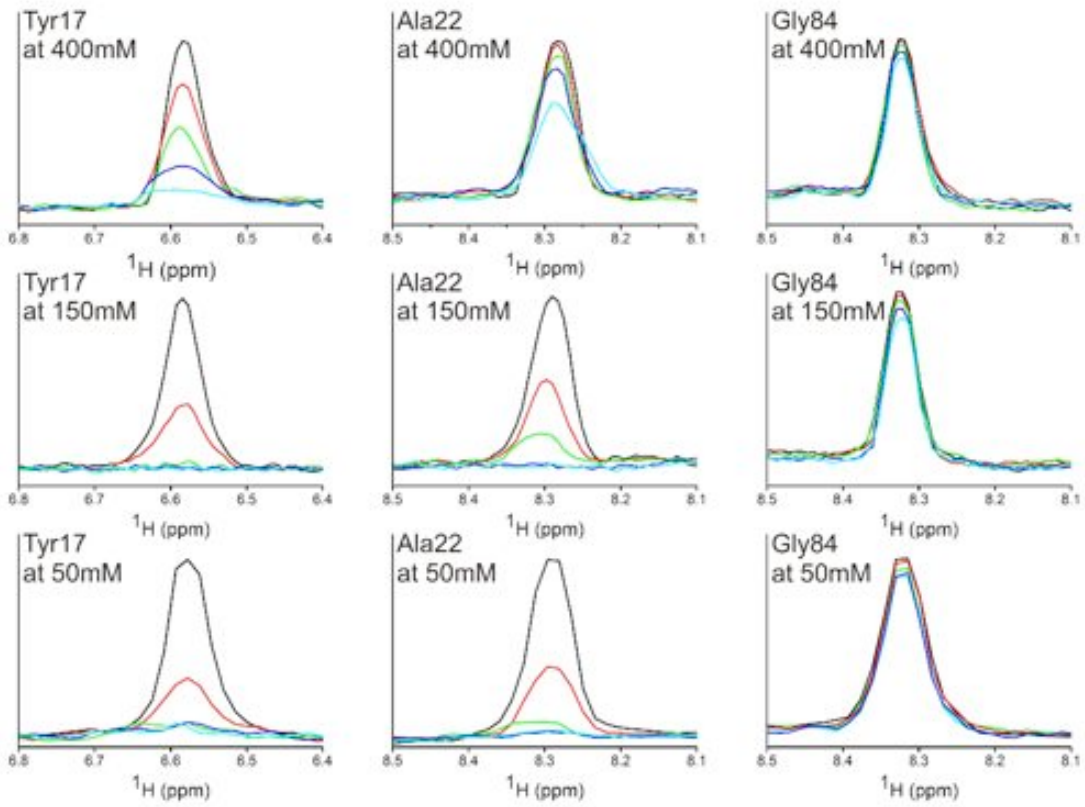

Figure 5.19: One-dimensional ^{1}H-NMR slices of titration of C3d-WT into CD21 at 50mM, 150 mM and 400 mM NaCl for three residues, Tyr17, Ala22 and Gly84.
Both SCR1 residues, Tyr17 and Ala22, implicated in binding in our studies showed a change of exchange behaviour from intermediate to that of a slow exchange at increasing salt concentration while Gly84, a SCR2 domain residue implicated by the crystal structure did not show any discernible changes (black: 0:1, red: 0.25:1, green:0.75:1, blue:1:1, cyan: 1.25:1 molar ratio of C3d:^{15}N-labelled CD21 (SCR1-2).

The interaction of CD21/C3d is mainly electrostatic in nature, as shown by the work performed in this lab and others (Nagar et al., (1998); Clemenza and Isenman, (2000); Morikis and Lambris, (2004)). This is illustrated by the positively charged patch on SCR1 domain of CD21 and the negatively charged ring on the concave region of C3d (Figure 5.12). The SCR1 domain contains a patch of protruding hydrophobic side chains from a tyrosine and leucine residues, which are surrounded by the positively charged residues.

On C3d, it has been established that the binding site is localised on a hydrophobic cleft that is surrounded by the negatively charged residues (Nagar et al., 1998) (Figure 5.18).

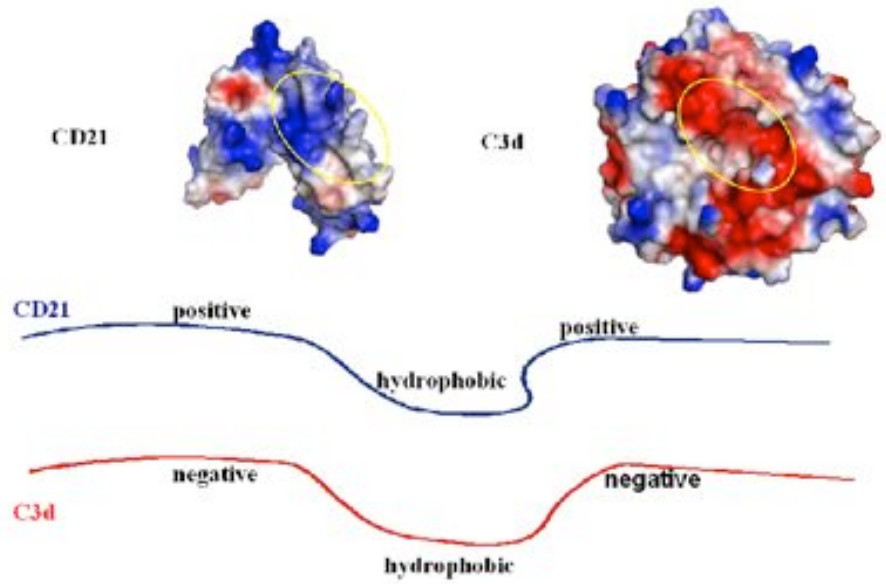

Figure 5.20: The binding sites of CD21/C3d interactions show a complimentary region of oppositely charged areas that fit each other.

It is therefore proposed that the binding occurs in a dynamic fashion in which the hydrophobic knob on SCR1 of CD21 would fit into the hydrophobic cleft of C3d with the oppositely charged interfaces form electrostatic interactions (Figure 5.20).

5.6 Discussion

The work presented in this chapter essentially supports the notion that the controversial crystal structure of the CD21/C3d complex published previously (Szakonyi et al. 2001) to be physiologically irrelevant. NMR experiments conducted indicate that the binding site of C3d is entirely localized on the SCR1 domain rather than SCR2, in contrast to the binding observed in the crystal structure. Binding experiments at different ionic strengths

have revealed that the interaction is highly dependent on electrostatics. Extensive site-directed mutagenesis presented in this work as well as previously done in our lab also confirmed that the binding of C3d is mainly localised on the SCR1 domain of CD21. A bifurcated salt bridge formed between CD21 Arg13 and C3d Glu37/Glu39 has been identified thus far. The knowledge obtained from the site directed mutagenesis based binding studies was used to obtain a model of the interaction. Analysis of the chemical exchange behaviour of this interaction provides a possible multiple binding event of CD21/C3d interaction. The NMR resonance assignment of C3d is currently being performed by Cynthia Tso, which if followed by further titration experiments will lead to detailed definition of the CD21 binding site on C3d. This will then assist in the discovery of compounds that may inhibit this interaction thus having a potential for the development of autoimmune therapeutics.

Summary and future direction

CD23 is a multifunctional molecule. It exists in different forms and structures and exerts its complex biological functions through interaction with various ligands. In its monomeric form it inhibits IgE synthesis. In trimeric form it is proposed to co-ligate both CD21 and membrane IgE on the surface of B cells to stimulate IgE synthesis. Inhibition of CD23, therefore, is an attractive target for reducing IgE synthesis. Current therapeutics target IgE, such as the anti-IgE antibody Omalizumab. An anti-CD23 monoclonal antibody has also been tested in clinical trials for treating allergy and was shown to reduce IgE levels in a dose dependent manner. However, the administration of antibodies is complicated and expensive, and therefore low molecular weight inhibitors would be preferable as therapeutic agents. Dr Ho Ann Chen from our laboratory previously performed phage display screening for CD23 binding peptides and several peptides were derived and tested. It was shown that one of the peptides (12_3C) showed the highest affinity binding and was further characterized. It was shown to inhibit IgE binding to CD23 and inhibits IgE synthesis in IgE-committed primary B cells. It aso inhibited IgE-GFP binding to CD23 on $CD23^+$ 8866 cells, demonstrating its potential in inhibiting the CD23/IgE interaction on the cell surface. Crystallisation of derCD23 with 12_3C peptide was attempted and was unsuccessful. The truncated version of the peptide retaining the consensus NWP motif found in the phage display screen was obtained and shown to bind to CD23, albeit at lower affinity than longer peptides. Crystal soaking was attempted with the NWP peptide but even though it was not successful, it resulted in the highest resolution structure of wild-type CD23 obtained thus far. It was noted that the construct of CD23 used in the

CD23 crystal structure obtained previously by Wurzburg et al. (2006) contains two mutations (H213S and G256S) and may have led to their initial co-crystallisation with IgE to fail, because it may compromise the binding of those two interactants. Various other crystallisation projects were also carried out and at the time this thesis has been written, no other suitable crystals have been found. Lin Dao Peng and Wen Pin Kao at King's College London are continuing these efforts.

The state of oligomerisation of CD23 was also studied, comparing the largely monomeric derCD23 protein and an engineered trimeric CD23 construct. It was shown using SPR that both derCD23 and trimeric CD23 can oligomerise under certain conditions. A crystal structure of derCD23/IgE-Fc (Cε3-4) has been recently solved by Dr. Balvinder Dhaliwal at the Randall Division, KCL, and was used to assess the previously described binding interface of the IgE/CD23 complex, determined using NMR chemical shift mapping by Dr Richard Hibbert and Dr Susmita Borthakur in our lab. However, despite the fact that the crystal structure is still under refinement, several contact residues were identified and these observation are in agreement with the NMR chemical shift mapping, as well as the previously performed biochemical analyses performed by others (Chrétien et al., 1988; Vercelli et al., 1989; Nissim et al., 1993; Sayers, 2004). The C-terminus of CD23 has been previously established through NMR chemical shift mapping as the binding site of CD21. A truncated version of the construct, lacking the C-terminus, was made and an NMR titration with CD21 was performed. It was shown that in the absence of the tail, CD21 (SCR1-2) could not bind to CD23. Immobilisation of CD21 (SCR1-2) was attempted in order to perform a quantitative comparison of the binding of various version of C-terminally

truncation mutants. However, the immobilisation achieved was not ideal and resulted in greatly reducing ligand binding for CD21 (SCR1-2); further optimization is required in order to allow an assay to be developed for quantitative CD21 binding. Co-crystallisation of the derCD21/CD21 (SCR1-2) complex was also attempted; preliminary crystals have been obtained and will be characterised further.

The interaction of CD23 with the antibody IDEC-152 was also characterized using structural and biophysical methods; these studies showed that the antibody may inhibit IgE expression by disrupting the trimerisation interface of CD23. Again this analysis was assisted by the CD23/IDEC-152 crystal structure determined by Dr Balvinder Dhaliwal.

A comparison of the IgE-Fc/derCD23 complex and the IgE-Fc/sFcεRIα complex (Garman et al., 2000) showed that IgE may be able to bind to both its receptors simultaneously, as the two binding site are distal to each other. Thefore several SPR experiments were performed to explore the possible regulatory effects of these two bnding interactions on IgE activities. It was shown that CD23 was able to form high molecular weight complexes with IgE and and that the complexes bind with higher apparent affinity to surface bound FcεRIα than monomeric IgE alone. This may suggest a role for CD23 in modulating mast cell degranulation. However, when IgE was prebound to FcεRI, CD23 bound with the same affinity but with lower apparent binding capacity (B_{max}), which suggests a form of non-competitive inhibition of CD23 binding to IgE by FcεRI. Mast cell degranulation assays showed that premixing IgE with CD23 may induce mast cell degranulation in a concentration dependent manner; in contrast, IgE prebound mast cells could not be triggered by the addition of CD23. These observations are in agreement with the

biophysical analysis and indicate a possible role of CD23 in the regulation of mast cell degranulation. Recently CD23 has been implicated in transcytosis of IgE/allergen complexes, from the epithelial side of lung epithelium to the sub-epithelium side and the release of those immune complexes leads to the increase of mast cells degranulation (Palaniyandi et al., 2011). If the protease ADAM-10 is present in this area then the release of CD23 may form complexes with IgE, leading to mast cell degranulation. It is not known whether ADAM-10 is present in this area. If it does then this may play a role in chronic asthma. In the same paper by Palaniyandi et al. (2011), IDEC-152 was shown to inhibit the trancytosis of the immune complex, which leads to the reduction of mast cell degranulation. Therefore the 12_3C peptide, which inhibits the IgE/CD23 interaction, should also be tested for the same effect.

In keeping with the long-term goal of discovering small molecule inhibitors of CD23, a differential scanning fluorimetry assay was optimised for derCD23. DerCD23 was used because it retains the lectin head domain, which is the main ligand-binding domain. The system was optimised to allow for a detectable spectroscopic signal to be achieved while minimising the amount of derCD23 required for the assay. It was also shown that calcium has a role in stabilising derCD23, or the lectin head domain as it increased the melting temperature of CD23.

The interaction between C3d and CD21 is believed to bridge the innate and the adaptive immune system (Dempsey et al., 1996). Szakonyi et al. published a crystal structure of the C3d/CD21 (SCR1-2) complex in 2001. However it was a controversial structure because it contradicted a large body of biochemical data. The X-ray structure seemed to indicate

that it was the SCR2 domain of CD21 bound to C3d, as opposed to SCR1 domain which previous studies had implicated. Therefore we performed site-directed mutagenesis and NMR chemical shift mapping to determine the true binding site. Taking into consideration the unusual electrostatically mediated interaction of CD21/C3d, different ionic strengths were used in SPR and ITC binding experiments and in NMR titration experiments. It was shown that at physiological ionic strengths, the binding site on CD21 is localised on SCR1, and residues from SCR2 were shown not to be involved in C3d binding. The unexpected chemical exchange behaviour found in the NMR titration also suggest that the interaction between CD21 and C3d may involve multiple binding states, which may make co-crystallisation of the physiological complex impossible. Currently Cynthia Tso from our laboratory is performing a fragment-based screen against C3d, which may lead to the development of a small molecular weight inhibitor of this interaction.

In summary, a peptide that inhibits CD23/IgE interaction has been characterized and showed potential activity in reducing IgE levels. This peptide may be developed further as a structural basis for future inhibitors, with potentially high affinity and activity. This peptide can also be tested for other biological function, such as to inhibit the trancytosis of allergen/IgE complexes across the airway epithelia. The oligomerisation of CD23 has been characterized and this provides a potential target for inhibition by smaller molecule. The crystallisation of complexes between proteins in the IgE network in the future may not only help in obtaining detailed knowledge on these interactions but also inform in the design of potential inhibitors. The interaction between CD23 and CD21 has been characterized further, with the C-terminus of CD23 being confirmed to be the binding site

of CD21. Further characterisation is required to explore the role of the longer C-terminus in binding to CD21. In this regards, the entire C terminal peptide can be synthesized and tested for binding to CD21. CD23 was shown to indicate a role in mast cell degranulation based on the different binding phenomena. An inhibitor of the IgE/CD23 interaction can be tested to assess its effect in mast cell degranulation. The interaction between the antibody IDEC-152 and CD23 has been characterized. The inhibitory mechanism of IDEC-152 can be used for the design of potential inhibitors by mimicking IDEC-152's mode of action, potentially by targeting the trimerisation site of CD23. The interaction between CD21 and C3d has been characterised further, and further drug discovery efforts will be required to obtain a potential inhibitor that could be of therapeutic use.

Bibliography

Ahearn, J. M., Hayward, S. D., Hickey, J. C. and Fearon, D. T. (1988) 'Epstein-Barr Virus (EBV) Infection of Murine L Cells Expressing Recombinant Human EBV/C3d Receptor', *Proceedings of the National Academy of Sciences of the United States of America*, **85**, 9307-9311.

Andrew, S. M. (2002) 'Enzymatic Digestion of Monoclonal Antibodies'. In *Protein Protocols Handbook, The*, New Jersey, Humana Press, 1047-1052.

Arkin, M. R. and Wells, J. A. (2004) 'Small-molecule Inhibitors of Protein–protein Interactions: Progressing Towards the Dream', *Nature Reviews Drug Discovery*, **3**, 301-317.

Ashraf, S. S., Benson, R. E., Payne, E. S., Halbleib, C. M. and Grøn, H. (2004) 'A Novel Multi-affinity Tag System to Produce High Levels of Soluble and Biotinylated Proteins in Escherichia Coli', *Protein Expression and Purification*, **33**, 238-245.

Aubry, J. P., Pochon, S., Graber, P., Jansen, K. U. and Bonnefoy, J. Y. (1992) 'CD21 Is a Ligand for CD23 and Regulates IgE Production', *Nature*, **358**, 505-507.

Badar, A., DeFreitas, S., McDonnell, J. M., Yahya, N., Thakor, D., Razavi, R., Smith, R., Sacks, S. and Mullen, G. E. D. (2011) 'Recombinant Complement Receptor 2 Radiolabeled with [99mTc(CO)3]+ : A Potential New Radiopharmaceutical for Imaging Activated Complement', *PLoS ONE*, **6**, e18275.

Barrington, R. A., Schneider, T. J., Pitcher, L. A., Mempel, T. R., Ma, M., Barteneva, N. S. and Carroll, M. C. (2009) 'Uncoupling CD21 and CD19 of the B-cell Coreceptor', *Proceedings of the National Academy of Sciences*, **106**, 14490-14495.

Beavil, A.J., Edmeades, R. L., Gould, H.J. and Sutton, B J. (1992) 'Alpha-helical Coiled-coil Stalks in the Low-affinity Receptor for IgE (Fc Epsilon RII/CD23) and Related C-type Lectins', *Proceedings of the National Academy of Sciences of the United States of America*, **89**, 753-757.

Bergmann-Leitner, E. S., Leitner, W. W. and Tsokos, G. C. (2006) 'Complement 3d: From Molecular Adjuvant to Target of Immune Escape Mechanisms', *Clinical Immunology* , **121**, 177-185.

Bettler, B., Maier, R., Rüegg, D. and Hofstetter, H. (1989) 'Binding Site for IgE of the Human Lymphocyte Low-affinity Fc Epsilon Receptor (Fc Epsilon RII/CD23) Is Confined to the Domain Homologous with Animal Lectins', *Proceedings of the National Academy of Sciences of the United States of America*, **86**, 7118-7122.

Bokisch, V. A., Dierich, M. P. and Mūller-Eberhard, H. J. (1975) 'Third Component of Complement (C3): Structural Properties in Relation to Functions', *Proceedings of the National Academy of Sciences of the United States of America*, **72**, 1989-1993.

Bomb, M. (2008) 'Characterising the Interaction of CD21 with Multiple Ligands', *DPhil Thesis, University of Oxford.*

Borthakur, S. (2010) 'Structural Flexibility and Immunoglobulin Constant Domains: Role of the Intrinsic Flexibility of the Cε3 domain of Immunoglobulin E', *DPhil Thesis, University of Oxford.*

Bricogne, G., Blanc, E., Brandl, M., Flenburg, C., Paciorek, W., Roversi, P., Smart, O., Vonrhein, C. and Womack, T. (2010) 'BUSTER Version 2.9', *Global Phasing Limited, Cambridge, United Kingdom.*

Brünger, A. T. (1992) 'Free R Value: A Novel Statistical Quantity for Assessing the Accuracy of Crystal Structures', *Nature*, **355**, 472-475.

Buck, E. and Wells, J. A. (2005) 'Disulfide Trapping to Localize Small-molecule Agonists and Antagonists for a G Protein-coupled Receptor', *Proceedings of the National Academy of Sciences*, **102**, 2719-2724.

Byrd, J. C., Kipps, T. J., Flinn, I. W., Castro, J., Lin, T. S., Wierda, W., Heerema, N., Woodworth, J., Hughes, S., Tangri, S., Harris, S., Wynne, D., Molina, A., Leigh, B. and O'Brien, S. (2010) 'Phase 1/2 Study of Lumiliximab Combined with Fludarabine, Cyclophosphamide, and Rituximab in Patients with Relapsed or Refractory Chronic Lymphocytic Leukemia', *Blood*, **115**, 489-495.

Campbell, K. A., Studer, E. J., Kilmon, M. A., Lees, A., Finkelman, F. and Conrad, D.H. (1997) 'Induction of B Cell Apoptosis by Co-cross-linking CD23 and sIg Involves Aberrant Regulation of C-myc and Is Inhibited by Bcl-2', *International Immunology*, **9**, 1131-1140.

Capron, A., Dombrowicz, D. and Capron, M. (1999) 'Regulation of the Immune Response in Experimental and Human Schistosomiasis: The Limits of an Attractive Paradigm', *Microbes and Infection*, **1**, 485-490.

Carel, J. C., Myones, B. L., Frazier, B. and Holers, V. M. (1990) 'Structural Requirements for C3d,g/Epstein-Barr Virus Receptor (CR2/CD21) Ligand Binding, Internalization, and Viral Infection', *The Journal of Biological Chemistry*, **265**, 12293-12299.

Carroll, M. C. (2004) 'The Complement System in Regulation of Adaptive Immunity', *Nature Immunology*, **5**, 981-986.

Carter, R. H. and Fearon, D. T. (1992) 'CD19: Lowering the Threshold for Antigen Receptor Stimulation of B Lymphocytes', *Science*, **256**, 105-107.

Carter, R. H., Spycher, M. O., Ng, Y. C., Hoffman, R. and Fearon, D. T. (1988) 'Synergistic Interaction Between Complement Receptor Type 2 and Membrane IgM on B Lymphocytes', *Journal of Immunology*, **141**, 457-463.

Cavanagh, J., Fairbrother, W. J., Palmer III, A. G. and Skelton, M. R. (2006) *Protein NMR Spectrocopy: Principles and Practice*, Academic Press.

Chomarat, P., Briolay, J., Banchereau, J. and Miossec, P. (1993) 'Increased Production of Soluble CD23 in Rheumatoid Arthritis, and Its Regulation by Interleukin-4', *Arthritis and Rheumatism*, **36**, 234-242.

Chrétien, I., Helm, B. A., Marsh, P. J., Padlan, E. A., Wijdenes, J. and Banchereau, J. (1988) 'A Monoclonal anti-IgE Antibody Against an Epitope (amino Acids 367-376) in the CH3 Domain Inhibits IgE Binding to the Low Affinity IgE Receptor (CD23)', *Journal of Immunology* , **141**, 3128-3134.

Clarkson, J. and Campbell, I. D. (2003) 'Studies of Protein-ligand Interactions by NMR', *Biochemical Society Transactions*, **31**, 1006-1009.

Clemenza, L. and Isenman, D. E. (2000) 'Structure-guided Identification of C3d Residues Essential for Its Binding to Complement Receptor 2 (CD21)', *Journal of Immunology*, **165**, 3839-3848.

Conrad, D.H., Gibb, D.R. and Sturgill, J. (2010) 'Regulation of the IgE Response', *F1000 Biology Reports*.

Conrad, D. H, Ford, Jill W, Sturgill, Jamie L and Gibb, David R (2007) 'CD23: An Overlooked Regulator of Allergic Disease', *Current Allergy and Asthma Reports*, **7**, 331-337.

Cookson, W. (1999) 'The Alliance of Genes and Environment in Asthma and Allergy', *Nature*, **402**, B5-11.

Cummings, M. D., Farnum, M. A. and Nelen, M. I. (2006) 'Universal Screening Methods and Applications of ThermoFluor(R)', *Journal of Biomolecular Screening*, **11**, 854-863.

Davis, A. M., Teague, S. J. and Kleywegt, G. J. (2003) 'Application and Limitations of X-ray Crystallographic Data in Structure-based Ligand and Drug Design', *Angewandte Chemie (International Ed. in English)*, **42**, 2718-2736.

Davis, I. W., Leaver-Fay, A., Chen, V. B., Block, J. N., Kapral, G. J., Wang, X., Murray, L. W., Arendall, W. B., Snoeyink, J., Richardson, J. S. and Richardson, D. C. (2007) 'MolProbity: All-atom Contacts and Structure Validation for Proteins and Nucleic Acids', *Nucleic Acids Research*, **35**, W375-W383.

Del Nagro, C. J., Kolla, R. V. and Rickert, R. C. (2005) 'A Critical Role for Complement C3d and the B Cell Coreceptor (CD19/CD21) Complex in the Initiation of Inflammatory Arthritis', *The Journal of Immunology*, **175**, 5379-5389.

Delespesse, G., Hofstetter, H. and Sarfati, M. (1989) 'Low-affinity Receptor for IgE (FcERII, CD23) and Its Soluble Fragments', *International Archives of Allergy and Applied Immunology*, **90 Suppl 1**, 41-44.

Dempsey, P. W., Allison, M. E. D., Goodnow, C. C., Akkaraju, S., Goodsnow, C. C. and Fearon, D. T. (1996) 'C3d of Complement as a Molecular Adjuvant: Bridging Innate and Acquired Immunity', *Science*, **271**, 348-350.

Derewenda, Z. S. (2010) 'Application of Protein Engineering to Enhance Crystallizability and Improve Crystal Properties', *Acta Crystallographica Section D Biological Crystallography*, **66**, 604-615.

Devereux, G. (2006) 'The Increase in the Prevalence of Asthma and Allergy: Food for Thought', *Nature Reviews Immunology*, **6**, 869-874.

Dierks, S. E., Bartlett, W. C., Edmeades, R. L., Gould, H.J., Rao, M. and Conrad, D.H. (1993) 'The Oligomeric Nature of the Murine Fc Epsilon RII/CD23. Implications for Function', *Journal of Immunology* , **150**, 2372-2382.

Emsley, P. and Cowtan, K. (2004) 'Coot: Model-building Tools for Molecular Graphics', *Acta Crystallographica Section D Biological Crystallography*, **60**, 2126-2132.

Evans, P. and McCoy, A. (2007) 'An Introduction to Molecular Replacement', *Acta Crystallographica Section D Biological Crystallography*, **64**, 1-10.

Fingeroth, J.D., Clabby, M. L. and Strominger, J. D. (1988) 'Characterization of a T-lymphocyte Epstein-Barr virus/C3d Receptor (CD21)', *Journal of Virology*, **62**, 1442-1447.

Fishelson, Z., Pangburn, M. K. and Müller-Eberhard, H. J. (1984) 'Characterization of the Initial C3 Convertase of the Alternative Pathway of Human Complement', *Journal of Immunology* , **132**, 1430-1434.

Ford, J.W., Kilmon, M. A., Haas, K. M., Shelburne, A. E., Chan-Li, Y. and Conrad, D.H. (2006) 'In Vivo Murine CD23 Destabilization Enhances CD23 Shedding and IgE Synthesis', *Cellular Immunology*, **243**, 107-117.

Gallop, M. A., Barrett, R. W., Dower, W. J., Fodor, S. P. and Gordon, E. M. (1994) 'Applications of Combinatorial Technologies to Drug Discovery. 1. Background and Peptide Combinatorial Libraries', *Journal of Medicinal Chemistry*, **37**, 1233-1251.

Garman, S. C., Wurzburg, B.A., Tarchevskaya, S.S., Kinet, J. P. and Jardetzky, T.S. (2000) 'Structure of the Fc Fragment of Human IgE Bound to Its High-affinity Receptor Fc epsilonRI Alpha', *Nature*, **406**, 259-266.

Gill, S. C. and von Hippel, P. H. (1989) 'Calculation of Protein Extinction Coefficients from Amino Acid Sequence Data', *Analytical Biochemistry*, **182**, 319-326.

Goddard, T. D. and Kneller, D. G. 'SPARKY 3 (University of California San Francisco)'.

Gould, H.J. and Sutton, B.J. (2008a) 'IgE in Allergy and Asthma Today', *Nature Reviews Immunology*, **8**, 205-217.

Gould, H.J., Sutton, B.J., Beavil, A., Beavil, R.L, McCloskey, N., Coker, H. A., Fear, D. and Smurthwaite, L. (2003) 'The Biology of IgE and the Basis of Allergic Disease', *Annual Review of Immunology*, **21**, 579-628.

Grzesiek, S. and Bax, A. (1993) 'Amino Acid Type Determination in the Sequential Assignment Procedure of Uniformly 13C/15N-enriched Proteins', *Journal of Biomolecular NMR*, **3**, 185-204.

Hannan, J.P., Young, K.A., Guthridge, J.M., Asokan, R., Szakonyi, G., Chen, X.S. and Holers, V.M. (2005) 'Mutational Analysis of the Complement Receptor Type 2 (CR2/CD21)-C3d Interaction Reveals a Putative Charged SCR1 Binding Site for C3d', *Journal of Molecular Biology*, **346**, 845-858.

Helmy, K. Y., Katschke, K. J., Jr, Gorgani, N. N., Kljavin, N. M., Elliott, J. M., Diehl, L., Scales, S. J., Ghilardi, N. and van Lookeren Campagne, M. (2006) 'CRIg: A Macrophage Complement Receptor Required for Phagocytosis of Circulating Pathogens', *Cell*, **124**, 915-927.

Henchoz, S., Gauchat, J. F., Aubry, J. P., Graber, P., Pochon, S. and Bonnefoy, J. Y. (1994) 'Stimulation of Human IgE Production by a Subset of anti-CD21 Monoclonal Antibodies: Requirement of a Co-signal to Modulate Epsilon Transcripts', *Immunology*, **81**, 285-290.

Hibbert, R. G., Teriete, P., Grundy, G.J., Beavil, R.L., Reljic, R., Holers, V.M., Hannan, J.P., Sutton, B. J., Gould, H.J. and McDonnell, J.M. (2005) 'The Structure of Human CD23 and Its Interactions with IgE and CD21', *The Journal of Experimental Medicine*, **202**, 751-760.

Hjelm, F., Carlsson, F., Getahun, A. and Heyman, B. (2006) 'Antibody-Mediated Regulation of the Immune Response', *Scandinavian Journal of Immunology*, **64**, 177-184.

Hogan, A. (1997) 'Markers of Mast Cell Degranulation', *Methods*, **13**, 43-52.

Hourcade, D., Holers, V.M. and Atkinson, J. P. (1989) 'The Regulators of Complement Activation (RCA) Gene Cluster', *Advances in Immunology*, **45**, 381-416.

Janeway, C. (2005) *Immunobiology : The Immune System in Health and Disease*, New York, Garland Science.

Kaiserlian, D., Lachaux, A., Grosjean, I., Graber, P. and Bonnefoy, J. Y. (1993) 'Intestinal Epithelial Cells Express the CD23/Fc Epsilon RII Molecule: Enhanced Expression in Enteropathies', *Immunology*, **80**, 90-95.

Kantardjieff, K. A. and Rupp, B. (2003) 'Matthews Coefficient Probabilities: Improved Estimates for Unit Cell Contents of Proteins, DNA, and Protein-nucleic Acid Complex Crystals', *Protein Science*, **12**, 1865-1871.

Karagiannis, S. N., Warrack, J. K., Jennings, K. H., Murdock, P. R., Christie, G., Moulder, K., Sutton, B. J. and Gould, H. J. (2001) 'Endocytosis and Recycling of the Complex Between CD23 and HLA-DR in Human B Cells', *Immunology*, **103**, 319-331.

Kato, F., Nomura, M. and Nakamura, K. (1996) 'Arthritis in Mice Induced by a Single Immunisation with Collagen', *Annals of the Rheumatic Diseases*, **55**, 535-539.

Kikutani, H., Inui, S., Sato, R., Barsumian, E. L., Owaki, H., Yamasaki, K., Kaisho, T., Uchibayashi, N., Hardy, R. R. and Hirano, T. (1986) 'Molecular Structure of Human Lymphocyte Receptor for Immunoglobulin E', *Cell*, **47**, 657-665.

Kilmon, M. A., Ghirlando, R., Strub, M. P., Beavil, R.L, Gould, H.J. and Conrad, D.H (2001) 'Regulation of IgE Production Requires Oligomerization of CD23', *The Journal of Immunology*, **167**, 3139-3145.

Kilmon, M. A., Shelburne, A. E., Chan-Li, Y., Holmes, K. L. and Conrad, D.H. (2004) 'CD23 Trimers Are Preassociated on the Cell Surface Even in the Absence of Its Ligand, IgE', *The Journal of Immunology*, **172**, 1065-1073.

Kinet, J. P. (1999) 'The High-affinity IgE Receptor (Fc Epsilon RI): From Physiology to Pathology', *Annual Review of Immunology*, **17**, 931-972.

Kleinau, S., Martinsson, P., Gustavsson, S. and Heyman, B. (1999) 'Importance of CD23 for Collagen-induced Arthritis: Delayed Onset and Reduced Severity in CD23-deficient Mice', *Journal of Immunology*, **162**, 4266-4270.

Kovacs, J. M., Hannan, J. P., Eisenmesser, E. Z. and Holers, V. M. (2009) 'Mapping of the C3d Ligand Binding Site on Complement Receptor 2 (CR2/CD21) Using Nuclear Magnetic Resonance and Chemical Shift Analysis', *Journal of Biological Chemistry*, **284**, 9513-9520.

Ladner, R. (2004) 'Phage Display-derived Peptides as Therapeutic Alternatives to Antibodies', *Drug Discovery Today*, **9**, 525-529.

Lemieux, G. A., Blumenkron, F., Yeung, N., Zhou, P., Williams, J., Grammer, A. C., Petrovich, R., Lipsky, P. E., Moss, M. L. and Werb, Z. (2007) 'The Low Affinity IgE

Receptor (CD23) Is Cleaved by the Metalloproteinase ADAM10', *The Journal of Biological Chemistry*, **282**, 14836-14844.

Liszewski, M. K., Post, T. W. and Atkinson, J. P. (1991) 'Membrane Cofactor Protein (MCP or CD46): Newest Member of the Regulators of Complement Activation Gene Cluster', *Annual Review of Immunology*, **9**, 431-455.

Liu, F.-T., Goodarzi, H. and Chen, H.-Y. (2011) 'IgE, Mast Cells, and Eosinophils in Atopic Dermatitis', *Clinical Reviews in Allergy & Immunology*.

Lo, M. (2004) 'Evaluation of Fluorescence-based Thermal Shift Assays for Hit Identification in Drug Discovery', *Analytical Biochemistry*, **332**, 153-159.

Maachupalli-Reddy, J., Kelley, B. D. and De Bernardez Clark, E. (1997) 'Effect of Inclusion Body Contaminants on the Oxidative Renaturation of Hen Egg White Lysozyme', *Biotechnology Progress*, **13**, 144-150.

Matthews, B. (1968) 'Solvent Content of Protein Crystals', *Journal of Molecular Biology*, **33**, 491-497.

McCloskey, N., Hunt, J., Beavil, R. L., Jutton, M. R., Grundy, G. J., Girardi, E., Fabiane, S. M., Fear, D. J., Conrad, D. H., Sutton, B. J. and Gould, H. J. (2007) 'Soluble CD23 Monomers Inhibit and Oligomers Stimulate IgE Synthesis in Human B Cells', *Journal of Biological Chemistry*, **282**, 24083-24091.

McCoy, A. J., Grosse-Kunstleve, R. W., Adams, P. D., Winn, M. D., Storoni, L. C. and Read, R. J. (2007) 'Phaser Crystallographic Software', *Journal of Applied Crystallography*, **40**, 658-674.

McDonnell, J.M., Calvert, R., Beavil, R.L, Beavil, A.J, Henry, A.J, Sutton, B.J., Gould, H.J. and Cowburn, D. (2001) 'The Structure of the IgE Cepsilon2 Domain and Its Role in Stabilizing the Complex with Its High-affinity Receptor FcepsilonRIalpha', *Nature Structural Biology*, **8**, 437-441.

Mcelroy, H., Sisson, G., Schoettlin, W., Aust, R. and Villafranca, J. (1992) 'Studies on Engineering Crystallizability by Mutation of Surface Residues of Human Thymidylate Synthase', *Journal of Crystal Growth*, **122**, 265-272.

Medek, A., Olejniczak, E. T., Meadows, R. P. and Fesik, S. W. (2000) 'An Approach for High-throughput Structure Determination of Proteins by NMR Spectroscopy', *Journal of Biomolecular NMR*, **18**, 229-238.

Moore, M. D., Cooper, N. R., Tack, B. F. and Nemerow, G. R. (1987) 'Molecular Cloning of the cDNA Encoding the Epstein-Barr virus/C3d Receptor (complement Receptor Type 2) of Human B Lymphocytes', *Proceedings of the National Academy of Sciences of the United States of America*, **84**, 9194-9198.

Morikis, D. and Lambris, J. D. (2004) 'The Electrostatic Nature of C3d-complement Receptor 2 Association', *Journal of Immunology*, **172**, 7537-7547.

Morrow, W. J., Williams, D. J., Ferec, C., Casburn-Budd, R., Isenberg, D. A., Paice, E., Snaith, M. L., Youinou, P. and Le Goff, P. (1983) 'The Use of C3d as a Means of Monitoring Clinical Activity in Systemic Lupus Erythematosus and Rheumatoid Arthritis', *Annals of the Rheumatic Diseases*, **42**, 668-671.

Mossalayi, M.D., Arock, M. and Debré, P. (1997) 'CD23/Fc Epsilon RII: Signaling and Clinical Implication', *International Reviews of Immunology*, **16**, 129-146.

Müller, K. M., Arndt, K. M., Bauer, K. and Plückthun, A. (1998) 'Tandem Immobilized Metal-ion Affinity Chromatography/immunoaffinity Purification of His-tagged Proteins--evaluation of Two anti-His-tag Monoclonal Antibodies', *Analytical Biochemistry*, **259**, 54-61.

Munoz, O., Brignone, C., Grenier-Brossette, N., Bonnefoy, J. Y. and Cousin, J. L. (1998) 'Binding of Anti-CD23 Monoclonal Antibody to the Leucine Zipper Motif of Fcepsilon RII/CD23 on B Cell Membrane Promotes Its Proteolytic Cleavage. Evidence for an Effect on the Oligomer/monomer Equlibrium.', *Journal of Biological Chemistry*, **273**, 31795-31800.

Murshudov, G.N., Vagin, A. A. and Dodson, E. J. (1997) 'Refinement of Macromolecular Structures by the Maximum-likelihood Method', *Acta Crystallographica. Section D, Biological Crystallography*, **53**, 240-255.

Nagar, B., Jones, R. G., Diefenbach, R. J., Isenman, D. E. and Rini, J. M. (1998) 'X-ray Crystal Structure of C3d: A C3 Fragment and Ligand for Complement Receptor 2', *Science*, **280**, 1277-1281.

Niesen, F. H., Berglund, H. and Vedadi, M. (2007) 'The Use of Differential Scanning Fluorimetry to Detect Ligand Interactions That Promote Protein Stability', *Nature Protocols*, **2**, 2212-2221.

Nissim, A., Schwarzbaum, S., Siraganian, R. and Eshhar, Z. (1993) 'Fine Specificity of the IgE Interaction with the Low and High Affinity Fc Receptor', *The Journal of Immunology*, **150**, 1365 -1374.

Oswald, C., Smits, S. H. J., Bremer, E. and Schmitt, L. (2008) 'Microseeding – A Powerful Tool for Crystallizing Proteins Complexed with Hydrolyzable Substrates', *International Journal of Molecular Sciences*, **9**, 1131-1141.

Otwinowski, Z. and Minor, W. (1997) 'Procesing of X-ray Diffraction Data Collected in Oscilliation Mode', *Methods in Enzymology*, **276**, 307-329.

Palaniyandi, S., Tomei, E., Li, Z., Conrad, D.H. and Zhu, X. (2011) 'CD23-Dependent Transcytosis of IgE and Immune Complex Across the Polarized Human Respiratory Epithelial Cells', *Journal of Immunology*, **186**, 3484-3496.

Pasqualini, R., Koivunen, E. and Ruoslahti, E. (1995) 'A Peptide Isolated from Phage Display Libraries Is a Structural and Functional Mimic of an RGD-binding Site on Integrins', *The Journal of Cell Biology*, **130**, 1189-1196.

Pathan, N. I., Chu, P., Hariharan, K., Cheney, C., Molina, A. and Byrd, J. (2008) 'Mediation of Apoptosis by and Antitumor Activity of Lumiliximab in Chronic Lymphocytic Leukemia Cells and CD23+ Lymphoma Cell Lines', *Blood*, **111**, 1594-1602.

Perkins, S. J., Gilbert, H. E., Aslam, M., Hannan, J., Holers, V.M. and Goodship, T. H. (2002) 'Solution Structures of Complement Components by X-ray and Neutron Scattering and Analytical Ultracentrifugation', *Biochemical Society Transactions*, **30**, 996-1001.

Pierce, S. K. (2002) 'Lipid Rafts and B-Cell Activation', *Nature Reviews Immunology*, **2**, 96-105.

Plater-Zyberk, C. and Bonnefoy, J. Y. (1995) 'Marked Amelioration of Established Collagen-induced Arthritis by Treatment with Antibodies to CD23 in Vivo', *Nature Medicine*, **1**, 781-785.

Pochon, S., Graber, P., Yeager, M., Jansen, K., Bernard, A. R., Aubry, J. P. and Bonnefoy, J. Y. (1992) 'Demonstration of a Second Ligand for the Low Affinity Receptor for Immunoglobulin E (CD23) Using Recombinant CD23 Reconstituted into Fluorescent Liposomes', *The Journal of Experimental Medicine*, **176**, 389-397.

Poole, J. A., Meng, Jianfeng, Reff, M., Spellman, M. C. and Rosenwasser, Lanny J. (2005) 'Anti-CD23 Monoclonal Antibody, Lumiliximab, Inhibited Allergen-induced Responses in Antigen-presenting Cells and T Cells from Atopic Subjects', *The Journal of Allergy and Clinical Immunology*, **116**, 780-788.

Potterton, L., McNicholas, S., Krissinel, E., Gruber, J., Cowtan, K., Emsley, P., Murshudov, Garib N, Cohen, S., Perrakis, A. and Noble, M. (2004) 'Developments in the CCP4 Molecular-graphics Project', *Acta Crystallographica. Section D, Biological Crystallography*, **60**, 2288-2294.

Prota, A. E., Sage, D. R., Stehle, T. and Fingeroth, Joyce D (2002) 'The Crystal Structure of Human CD21: Implications for Epstein-Barr Virus and C3d Binding', *Proceedings of the National Academy of Sciences of the United States of America*, **99**, 10641-10646.

Ramachandran, G. N., Ramakrishnan, C. and Sasisekharan, V. (1963) 'Stereochemistry of Polypeptide Chain Configurations', *Journal of Molecular Biology*, **7**, 95-99.

Rambert, J., Mamani-Matsuda, M., Moynet, D., Dubus, P., Desplat, V., Kauss, T., Dehais, J., Schaeverbeke, T., Ezzedine, K., Malvy, D., Vincendeau, P., Mossalayi, M. Djavad and Hartl, D. (2009) 'Molecular Blocking of CD23 Supports Its Role in the Pathogenesis of Arthritis', *PLoS ONE*, **4**, e4834.

Ravelli, R. and Garman, E. (2006) 'Radiation Damage in Macromolecular Cryocrystallography', *Current Opinion in Structural Biology*, **16**, 624-629.

Rehm, T., Huber, R. and Holak, T. A. (2002) 'Application of NMR in Structural Proteomics: Screening for Proteins Amenable to Structural Analysis', *Structure*, **10**, 1613-1618.

Richards, M. L. and Katz, D. H. (1990) 'The Binding of IgE to Murine Fc Epsilon RII Is Calcium-dependent but Not Inhibited by Carbohydrate', *Journal of Immunology*, **144**, 2638-2646.

Rogentine, G. N. and Gerber, P. (1969) 'HL-A Antigens of Human Lymphoid Cells in Long-term Tissue Culture', *Transplantation*, **8**, 28-37.

Rosenwasser, L. (2003) 'Allergic Asthma and an anti-CD23 mAb (IDEC-152) Results of a Phase I, Single-dose, Dose-escalating Clinical Trial', *Journal of Allergy and Clinical Immunology*, **112**, 563-570.

Rosenwasser, L.J. and Meng, J. (2005) 'Anti-CD23', *Clinical Reviews in Allergy & Immunology*, **29**, 061-072.

Rosloniec, E. F., Brand, D. D., Myers, L. K., Whittington, K. B., Gumanovskaya, M., Zaller, D. M., Woods, A., Altmann, D. M., Stuart, J. M. and Kang, A. H. (1997) 'An HLA-DR1 Transgene Confers Susceptibility to Collagen-induced Arthritis Elicited with Human Type II Collagen', *The Journal of Experimental Medicine*, **185**, 1113-1122.

Sarfati, M., Rector, E., Wong, K., Rubio-Trujillo, M., Sehon, A. H. and Delespesse, G. (1984) 'In Vitro Synthesis of IgE by Human Lymphocytes. II. Enhancement of the Spontaneous IgE Synthesis by IgE-binding Factors Secreted by RPMI 8866 Lymphoblastoid B Cells', *Immunology*, **53**, 197-205.

Sayers, I., Housden, J.E., Spivey, A.C. and Helm, B.A. (2004) 'The Importance of Lys-352 of Human Immunoglobulin E in FceRII/CD23 Recognition', *Journal of Biological Chemistry*, **279**, 35320-35325.

Schasfoort, R. (2008) *Handbook of Surface Plasmon Resonance*, Cambridge, Royal Society of Chemistry.

Schulz, O., Laing, P., Sewell, H. F. and Shakib, F. (1995) 'Der P I, a Major Allergen of the House Dust Mite, Proteolytically Cleaves the Low-affinity Receptor for Human IgE (CD23)', *European Journal of Immunology*, **25**, 3191-3194.

Schwarzmeier, J., Hubmann, R., Düchler, M., Jäger, U. and Shehata, M. (2005) 'Regulation of CD23 Expression by Notch2 in B-cell Chronic Lymphocytic Leukemia', *Leukemia & Lymphoma*, **46**, 157-165.

Shi, J., Ghirlando, R., Beavil, R. L., Beavil, A. J., Keown, M. B., Young, R. J., Owens, R. J., Sutton, B J and Gould, H. J. (1997) 'Interaction of the Low-affinity Receptor CD23/Fc epsilonRII Lectin Domain with the Fc Epsilon3-4 Fragment of Human Immunoglobulin E', *Biochemistry*, **36**, 2112-2122.

Spiegelberg, H. L. (1989) 'Biological Role of Different Antibody Classes', *International Archives of Allergy and Applied Immunology*, **90**, 22-27.

Stanworth, D. R. (1993) 'The Discovery of IgE', *Allergy*, **48**, 67-71.

Stewart, E. J. (1998) 'Disulfide Bond Formation in the Escherichia Coli Cytoplasm: An Invivo Role Reversal for the Thioredoxins', *The EMBO Journal*, **17**, 5543-5550.

Stites, W. E. (1997) 'Protein Interactions: Interface Structure, Binding Thermodynamics, and Mutational Analysis', *Chemical Reviews*, **97**, 1233-1250.

Strunk, R. C. and Bloomberg, G. R. (2006) 'Omalizumab for Asthma', *The New England Journal of Medicine*, **354**, 2689-2695.

Sturgill, J.L., Mathews, J., Scherle, P. and Conrad, D.H. (2011) 'Glutamate Signaling Through the Kainate Receptor Enhances Human Immunoglobulin Production', *Journal of Neuroimmunology*.

Szakonyi, G., Guthridge, J. M., Li, D., Young, K., Holers, V. M. and Chen, X. S. (2001) 'Structure of Complement Receptor 2 in Complex with Its C3d Ligand', *Science,* **292**, 1725-1728.

Tack, B. F., Harrison, R. A., Janatova, J., Thomas, M. L. and Prahl, J. W. (1980) 'Evidence for Presence of an Internal Thiolester Bond in Third Component of Human Complement', *Proceedings of the National Academy of Sciences of the United States of America*, **77**, 5764-5768.

Trakhanov, S., Kreimer, D. I., Parkin, S., Ames, G. F. and Rupp, B (1998) 'Cadmium-induced Crystallization of Proteins: II. Crystallization of the Salmonella Typhimurium Histidine-binding Protein in Complex with L-histidine, L-arginine, or L-lysine', *Protein Science: A Publication of the Protein Society*, **7**, 600-604.

Tu, Y., Salim, S., Bourgeois, J., Di Leo, V., Irvine, E. J., Marshall, J. K. and Perdue, Mary H (2005) 'CD23-mediated IgE Transport Across Human Intestinal Epithelium: Inhibition by Blocking Sites of Translation or Binding', *Gastroenterology*, **129**, 928-940.

Van der Merwe, P. A. (2001) *Surface Plasmon Resonance. In Protein-Ligand Interactions: Hydrodynamics and Calorimetry S. Harding, and P. Z. Chowdhry 1st Edition*, Oxford University Press.

Velázquez-Campoy, A., Ohtaka, H., Nezami, A., Muzammil, S. and Freire, E. (2004) 'Isothermal Titration Calorimetry', *Current Protocols in Cell Biology*, **Chapter 17**, Unit 17.8.

Vercelli, D., Helm, B., Marsh, P., Padlan, E., Geha, R. S. and Gould, H. (1989) 'The B-cell Binding Site on Human Immunoglobulin E', *Nature*, **338**, 649-651.

Verstappen, S. M. M., Poole, A. R., Ionescu, M., King, L. E., Abrahamowicz, M., Hofman, D. M., Bijlsma, J. W. J. and Lafeber, F. P. J. G. (2006) 'Radiographic Joint Damage in Rheumatoid Arthritis Is Associated with Differences in Cartilage Turnover and Can Be Predicted by Serum Biomarkers: An Evaluation from 1 to 4 Years After Diagnosis', *Arthritis Research & Therapy*, **8**, R31.

Volanakis, J. (1998) *The Human Complement System in Health and Disease*, New York, M. Dekker.

Vouldoukis, I., Riveros-Moreno, V., Dugas, B., Ouaaz, F., Bécherel, P., Debré, P., Moncada, S. and Mossalayi, M.D. (1995) 'The Killing of Leishmania Major by Human Macrophages Is Mediated by Nitric Oxide Induced After Ligation of the Fc Epsilon RII/CD23 Surface Antigen', *Proceedings of the National Academy of Sciences of the United States of America*, **92**, 7804-7808.

Wallis, R., Mitchell, D. A., Schmid, R., Schwaeble, W. J. and Keeble, A. H. (2010) 'Paths Reunited: Initiation of the Classical and Lectin Pathways of Complement Activation', *Immunobiology*, **215**, 1-11.

Wan, T., Beavil, R.L., Fabiane, S.M., Beavil, A.J., Sohi, M. K., Keown, M., Young, R.J., Henry, A.J., Owens, R.J., Gould, H.J. and Sutton, B. J. (2002) 'The Crystal Structure of IgE Fc Reveals an Asymmetrically Bent Conformation', *Nature Immunology*, **3**, 681-686.

Watt, P. M. (2006) 'Screening for Peptide Drugs from the Natural Repertoire of Biodiverse Protein Folds', *Nature Biotechnology*, **24**, 177-183.

Weis, J. J., Toothaker, L. E., Smith, J. A., Weis, J. J. and Fearon, D. T. (1988) 'Structure of the Human B Lymphocyte Receptor for C3d and the Epstein-Barr Virus and Relatedness to Other Members of the Family of C3/C4 Binding Proteins', *The Journal of Experimental Medicine*, **167**, 1047-1066.

Wells, J. A. (1990) 'Additivity of Mutational Effects in Proteins', *Biochemistry*, **29**, 8509-8517.

Weskamp, G., Ford, J.W., Sturgill, J., Martin, S., Docherty, A. J. P., Swendeman, S., Broadway, N., Hartmann, D., Saftig, P., Umland, S., Sehara-Fujisawa, A., Black, R. A., Ludwig, A., Becherer, J. D., Conrad, D.H. and Blobel, C. P. (2006) 'ADAM10 Is a Principal "sheddase" of the Low-affinity Immunoglobulin E Receptor CD23', *Nature Immunology*, **7**, 1293-1298.

White, J., Lukacik, P., Esser, D., Steward, M., Giddings, N., Bright, J. R., Fritchley, S. J., Morgan, B. P., Lea, S. M., Smith, G. P. and Smith, R. A. G. (2004) 'Biological Activity, Membrane-targeting Modification, and Crystallization of Soluble Human Decay Accelerating Factor Expressed in *E. Coli*', *Protein Science*, **13**, 2406-2415.

Wiesner, S., Wybenga-Groot, L. E., Warner, N., Lin, H., Pawson, T., Forman-Kay, J. D. and Sicheri, F. (2006) 'A Change in Conformational Dynamics Underlies the Activation of Eph Receptor Tyrosine Kinases', *The EMBO Journal*, **25**, 4686-4696.

Wilcock, L. K., Francis, J. N. and Durham, S. R. (2006) 'IgE-facilitated Antigen Presentation: Role in Allergy and the Influence of Allergen Immunotherapy', *Immunology and Allergy Clinics of North America*, **26**, 333-347, viii-ix.

Williams, R. O. (2004) 'Collagen-induced Arthritis as a Model for Rheumatoid Arthritis', *Methods in Molecular Medicine*, **98**, 207-216.

Woo, D. L., Clark-Lewis, I., Chait, B. C. and Kent, S. (1989) 'Chemical Synthesis in Protein Engineering: Total Synthesis, Purification and Covalent Structural Characterization of a Mitogenic Protein, Human Transforming Growth Factor-alpha', *Protein Engineering*, **3**, 29-37.

Wurzburg, B.A, Trachevskaya, S. S. and Jardetzky, T.S. (2006) 'Structural Changes in the Lectin Domain of CD23, the Low-Affinity IgE Receptor, Upon Calcium Binding', *Structure*, **14**, 1049-1058.

Wüthrich, K. (1986) *NMR of Proteins and Nucleic Acids*, New York, Wiley-Interscience.

Xu, D., Tsai, C. J. and Nussinov, R. (1997) 'Hydrogen Bonds and Salt Bridges Across Protein-protein Interfaces', *Protein Engineering*, **10**, 999-1012.

Yang, P. C., Berin, M. C., Yu, L. C., Conrad, D. H. and Perdue, M. H. (2000) 'Enhanced Intestinal Transepithelial Antigen Transport in Allergic Rats Is Mediated by IgE and CD23 (FcepsilonRII)', *The Journal of Clinical Investigation*, **106**, 879-886.

Zuiderweg, E. R. P. (2002) 'Mapping Protein-protein Interactions in Solution by NMR Spectroscopy', *Biochemistry*, **41**, 1-7.